Sarkar, Pabak, Studies on solvent induced fluorescence properties of styryl dye, LDS 798, to develop *in* vitro and *in* situ assay techniques. March, 2011, 100 pp., 2 tables, 32 illustration, bibliography

The styryl group of dyes has been used in cellular studies for over 50 years because of their solvatochromic and/ or electrochromic properties. Here we report characterization of solubility and solvatochromic properties of a near infra-red amiophenylstyrylquinolinum dye, styryl 11 or LDS 798. We have extended our studies to small unilamellar vesicles, lipid based nanoparticles and live cells. Our cellular studies show that LDS 798 preferentially localizes in mitochondria and its fluorescence lifetime changes with change in mitochondrial membrane potential. We have used this change in lifetime as an early marker for mitochondria-dependent apoptosis. We also found that solvatochromic properties of this dye, used in tandem with fluorescence correlation spectroscopy, can be used to efficiently determine the diffusion coefficient and hence the size of the submicron lipid based particles. This dye has the potential to provide essential information about liposomal structures and mitochondrial potential changes *in vitro* and *in situ* respectively.

STUDIES ON SOLVENT INDUCED FLUORESCENCE PROPERTIES OF STYRYL DYE, LDS 798, TO DEVELOP *IN VITRO* AND *IN SITU* ASSAY TECHNIQUES

DISSERTATION

Presented to the Graduate Council of the

Graduate School of Biomedical Science

University of North Texas

Health Science Center at Fort Worth

In Partial Fulfillment of the Requirements

For the Degree of

Doctor of Philosophy

By

Pabak Sarkar, M.S

Fort Worth, Texas

February/ March 2011

ACKNOWLEDGEMENT

This is the very first time I am acknowledging people in print and gazillions of names are coming up in my mind. Mentioning all the names will just make the work look bulkier, but there are some names I need to mention that have brought me to this position. I still cannot believe that I am writing my dissertation and it might take me a few pinches to convince that it is for real. First of all, I would like to mention my mother. I still do not know why she wanted me to pursue higher studies, but her persuasion worked. Next would be my mentors, Professors Zygmunt and Ignacy Gryczynski. They introduced me to this colorful world of fluorescence and taught me nuts and bolts of this wonderful phenomenon. They also gifted me an environment where I could ask questions and look for their answers. Moreover, through them I met people from various fields of science. Interacting with so many people with varied field of expertise was a real experience. In addition to that, all members of Center for Commercialization of Fluorescence Technologies (CCFT) made me feel like home at work place.

Throughout this exercise, I was also mentored by various committees. I would specially like to thank Professor Andras G. Lacko, who served in all of my committees. I would never forget his concept of 'Friday afternoon experiments'. Professor Lacko's lab was very helpful in nanoparticle and cell based studies. Especially, I would like to mention Dr. Nirupama Sabnis who taught me cell based assays and also helped me with thesis writing. Professor Julian Borejdo is one of the faculties who have been in my dissertation as well as qualifying committee. He is one of the prominent members of CCFT and we have interacted a lot on projects, course-works and various presentations. He always comes up with very basic questions regarding the field and drove me to look for the basic concepts of fluorescence to understand its bigger perspective. My University member, Dr. Harold Sheedlo, helped me to understand the biomedical perspective of

the research. Thoroughness and patience of my dissertation committee helped me to be thorough in my work a. I had a few graduate advisors during my course work and everyone guided me whenever I asked for help. I would also like to thank other members of my qualifying and grant writing committee. They helped me to understand the broader aspects of biomedical science and ingrained the concept of integrative science. Lectures, presentations and 'on-the corridor' discussions with faculties, senior researchers and peers were a few other things that helped me understand the vastness of this field.

Throughout this study, I have learned a lot about the techniques and approaches to answer questions. I was grateful to have Dr. Rafal Luchowski as a lab member. He guided me as an elder brother throughout the study; helping me when needed, questioning me when necessary and cautioning me when it was absolutely essential. Other graduate students in the lab, Dr. Shashank Bharill and Sangram Raut were phenomenal company. They came up with ideas, helped me performing the experiments and constructively critiqued the results. Our long hours in lab and free conversations have built camaraderie between us. Visiting scholars; Dr. Thomas Sorenson, Dr. Badri Prasad Maliwaal and Dr. Valeriya Trusova; were a big help in understanding the chemistry of the fluor and its response in different conditions. Dr. Rafal Fudala, who joined the lab later, was very helpful in performing FLIM experiments.

This work would not have been possible without the help of collaborating labs. Dr. Jamboor K. Vishwanatha's lab, especially Sanjay Thamake, helped me a lot with cell cultures, SUV preparation and dynamic light scattering measurements. Sanjay was instrumental in starting the cell culture studies and has been extremely enthusiastic about the application of the fluorescent probe. He also proof read one of the significant chapters in the thesis as well as a few write-ups related to this work. I am grateful to Dr. Alakananda Basu and her lab. Her expertise in studying

apoptotic pathways in cancer cells was invaluable for this study. It was upon her advice that we started looking at mitochondrial membrane depolarization on TNF treatment. Savitha Sridharan, of Dr. Basu's lab helped me with "nuts and bolts" of the TNF based mitochondrial depolarization experiments. Savitha and Deepanwita Pal, from the same lab, helped me by reading parts of this thesis and other write-ups too. A special thanks to Dr. Mariana Jung and Vishal Shinde. Dr. Jung gifted me the mitochondrial inhibitors required and Vishal isolated the mitochondria on Dr. Jung's instruction, for this study.

In addition to these people, I would like to thank Dr. Navin Rauniyar, Dr. Sheetal Bodhankar, Dr. Mallika Valapala and Dr. Subbhamoy Dasgupta for those extended discussions on science, practice of science and scope of our works.

The Department of Molecular Biology and Immunology and UNT Health Science Center campus has been my home for last four and half year. I would like to thank everyone that I have interacted with and wish to say that I have been humbled by their friendship and hospitality. It was a great experience. This community has become my home away from home.

Thank you.

Pabak Sarkar

TABLE OF CONTENTS

APPENDIX A – PUBLISHED ARTICLES ON LDS 798 BY AUTHOR

#	TITLE	JOURNAL
1	Studies on solvatochromic properties of aminophenylstyryl-quinolinum dye, LDS 798, and its application in studying submicron lipid based structure	J. Biophys Chem (2010)
2	Instrument response standard in time-resolved fluorescence	Rev Scien Instru (2009)
3	Fluorescence polarization standard for near infrared spectroscopy and microscopy	App Opt (2008)

APPENDIX B – OTHER FIRST AUTHOR PUBLICATIONS

#	TITLE	JOURNAL
1	Photophysical properties of a new DyLight 594 dye	J. Photochem Photobio B (2010)
2	Photophysical properties of Cerulean and Venus fluorescent proteins	J. Biomed Opt (2009)
3	Binding of 8-anilino-1-naphthalenesulfonate to lecithin:cholesterol acyltransferase studied by	J. Photochem Photobio B

LIST OF TABLES

LIST OF ILLUSTRATIONS

CHAPTER -1

INTRODUCTION: MEMBRANE POTENTIAL MEASUREMENTS AND THEIR FUNCTIONAL RELEVANCE

1.1 Biological membranes

Biological membranes are the bilayered structures that separate a biological system from its surrounding. Cell membrane can be considered as a selectively permeable barrier that separates the cellular contents from outside[1]. In addition to the cell/plasma membrane subcellular structures such as mitochondria, endoplasmic reticulum and nucleus have their own membranes which serve a similar purpose[2]. Though membranes were primarily thought be physical barriers, studies of the last 50 years infer that membranes are one of the most complex, dynamic and functionally active moieties of the cellular architecture[1, 23]. Their functions during cellular communication and signal transduction have been a prime area of interest for several years now. Their amphipathic nature and extensive weak interactions are essential for maintaining thermodynamic stability as well as dynamics in the living cell. A major part of biophysical studies deal with understanding the membrane organization and dynamics in light of thermodynamic laws of nature.

The predominant components of the biological membrane are the amphipathic lipid molecules. These amphipathic molecules are primarily phospholipids, sphingolipids and cholesterols[1]. All of these molecules comprise of a polar and a non-polar component. Non-covalent hydrophobic interactions of non-polar modules result in formation of micelles and bilayered membrane

structures through an entropy-driven process[1]. These structures create 'boundary conditions' and thermodynamically separate a system from its environment. Polar/charged moieties of these amphipathic molecules interact with the polar aqueous environment and keep these structures soluble in that environment through other non-covalent interactions (hydrogen bonding and electrostatic interaction).

In addition to lipid moieties, biological membranes have proteins and sugars associated with them. The proteins, lipids and sugar moieties can act as transducers of information along with some lipid molecules and allow the internal environment of cells adjust to the changes in external environments.

1.2 Understanding biophysics of the membrane

The biological functions of membranes are highly correlated with their fundamental physicochemical properties. These properties govern the processes including membrane transport and energetic [4, 5]. Properties such as the electrostatic potential, phase state and hydration of lipids, proteins and sugar in the membrane ultimately determine the membrane structure and control the trafficking of molecules and ions across the membrane. Electrostatic interactions play a crucial role in biomembrane processes such as membrane stability, flexibility and fusion[5]. Monitoring these properties *in situ* is area of interest in membrane biophysics as these properties eventually lead to altered function and effect the functionality or viability of the cell.

At the beginning of 21st century biological membranes still generate lot of challenges. The fluid –mosaic model[6], that states motion and aggregation of lipids in the membrane is random, is being revisited and reconsidered with new findings indicating that biological lipid membranes are more mosaic than fluid [7, 8]. Examples indicate that lipid composition can influence the incorporation of

proteins in the membrane [3, 9, 10]. The factors controlling the fluid and rigid domains of membranes still remain unclear but their relevance in processes like signal transduction has been demonstrated. The functional role of lipid asymmetry is currently not well understood[11]. This asymmetry leads to non-homogenous distribution of charges and surface potential is created by it. Maintenance and modulation of this distribution impact key cellular mechanisms. This is prominent in phenomena like apoptosis, where cellular disintegration is indicated by appearance of phospholipid phosphatidylserine (PS) on the outer leaflet of the cell membrane[10]. There are other phenomena like protein sorting, where membrane lipid composition and surface charge has an integral role that are yet to be elucidated. Transport of lipophilic cations and peptides without any specific channel has also drawn some attention of late[5]. The factors mentioned above are critical for basic knowledge of membrane organization and are critical for improving drug efficacy and early prognosis of diseases.

1.3 Membrane potential

Some of the phenomena, notably the electrical changes in the membranes of excitable tissues and cells, have been studied in depth by electrophysiological techniques[12]. Though these measurements can give information about distribution of ions between two compartments separated by biological membrane, it is an invasive approach that ultimately leads to unwanted alteration of system under investigation[13]. Traditional experimental methods, like microelctrode techniques, of studying biomembrane electrostatics also do not allow the nanoscopic level of detection[5]. They lack sufficiently low spatial resolution and do not allow the profile of the electrostatic gradient across the membrane to be obtained. The surface potential, as determined by the ζ-potential technique, also lacks high structural resolution, and, cannot be improved further[5, 13]. The cell electrophoresis method, which directly measures membrane surface potential

in the aqueous phase adjacent to the membrane, has been extensively used to study the electrokinetic properties of monodispersed suspensions of erythrocytes [14] and other blood cells [15, 16]. As most of the mammalian cell types are adherent rather than free, for monodispersity they have to be treated by enzymatic, chemical, or mechanical means. Such treatment will affect the surface potential. Another complication in these electrophoresis measurements is that they determine the ζ -potential at an idealized plane of shear at some distance from the membrane surface. Only when this distance is known can it be used to estimate the true surface potential[13]. Monitoring dynamic changes in cell membrane physiology would also be difficult with ζ-potential measurements as they represent an ensemble value rather than a defined value at microscopic level. Therefore, there is an evident need for methods that allow membrane electrostatics to be studied at the nanoscopic level. Of other physicochemical assays that have been used most notably NMR, FTIR and EPR; fluorescence based techniques have emerged as the default choice for non-invasively measuring the electrostatic potential based changes in the biological membranes of intact cells. Unique features of fluorescence techniques are their ultimate sensitivity up to a single-molecule level and their ability to operate in biological systems of varying complexity, up to the level of living cells and tissues.

1.4 Mitochondrial membrane potential and its measurement

Elctrophysiological studies of intracellular structure, mitochondria, have a huge impact on cellular functions. Mitochondria, generally known as ‘powerhouse of the cell’, generates the ‘power’, i.e. ATP, coupling redox potential to molecular phosphorylation[1]. Mitochondrial inner membrane has a crucial role in generating and maintaining the redox potential (commonly known as proton-motive force designated as ψ). The potential maintained by mitochondria is ~-120 mV which is greater than the potential generated at the cell membrane of most of the

excitable cells[17-19]. This is a very interesting electrochemical situation as in this case a very highly charged environment is maintained due to hydrophobic membrane barrier. Though the core of the membrane is hydrophobic, the polar and charged heads of the amphipathic lipids interact with the highly localized distribution of ions (mainly protons). Mitochondria are one of the favorite systems for electrophysiologists as various manipulation techniques can be used to study the potential change. Change in mitochondrial potential is relevant in processes like bioenergetics, aging and apoptosis. Though microelectrode techniques have been used for studying MMP, absorption and fluorescence based techniques have been predominant lately in this field[12, 20-22]. Fluorescence detectors are useful for both qualitative and quantitative studies of MMP [18].

Most of the fluorescence detection techniques depend on fluorescence intensity signal. Fluorescence intensity, though very sensitive to the changes in local environment, gets affected by local concentration of the fluorophore as well. As determination of local concentration of fluorophore inside an intact cell is very challenging and not yet been done, it is impossible to avoid the artifact. Technique(s) that are not dependent on the fluorophore concentration can circumvent the concentration issue. In this study we focus to test one of the techniques, fluorescence lifetime - that is independent of local concentration, for measuring changes in mitochondrial membrane potential. The fluorophore we used for this study is a styryl dye LDS 798. The solvatochromic and potentiometric properties of this dye were characterized in this study. Also, various tests have been performed to characterize its compatibility to live cell imaging.

CHAPTER – 2

MOLECULAR BASIS OF SOLVENT EFFECT

2.1 Molecular basis of fluorescence phenomenon

To understand how some fluorescence indicators can sense and detect changes in ionic distribution, principle of fluorescence phenomenon and fluorophore-solvent interaction need to be reviewed. Fluorescence can be described as a spontaneous emission of photon(s) by a molecule after the molecule is excited with electromagnetic radiation of ultra violet, visible or near- infra red range (UV/Vis/NIR)[23]. The phenomenon of fluorescence can be explained by basic molecular orbital theory. After absorbing the electromagnetic radiation that can supplement the energy band gap of the molecules, the molecule goes to a higher energy state (or excited state) and ultimately returns back to the ground state by losing the energy[24]. This loss of energy is in form of light waves (radiative loss) and other processes (non-radiative loss). The radiative fraction is a photon emitted during the process. If the emission of photon is associated with the transition from singlet excited energy state (shown in Figure – 2.1) to ground state, it is termed as fluorescence[23]. In some cases, the excited molecule can transit to a triplet state. Transition from triplet to ground state is forbidden and the photon ultimately is released microseconds or milliseconds after the initial absorption of energy. This phenomenon is termed as phosphorescence[25]. Variety of dynamic processes, that occurs following light absorption, lead to partial loss of absorbed energy by non-radiative processes. Thus, the emitted photon has less energy than the photon absorbed. This is evident in the emission spectra where number of

photons (collectively called intensity) are plotted as a function of energy. Generally energy of the wave is represented by wavenumber (υ) or wavelengths (λ)as

$E = h\upsilon = hc/\lambda$

Where, h is the Planck's constant.

Traditionally, fluorescence emission spectrum is plotted as intensity vs wavelength. So, decrease in energy of photon emitted results in shift of the distribution to longer wavelengths. This phenomenon was first described by Sir George Gabriel Stokes[26] and is called 'Stokes shift'.

2.2 Solvent relaxation

The fluorophores interact with their environment during the short time they stay in the excited state and are eventually affected by environment. This process of interaction with the surrounding environment is called solvent relaxation.

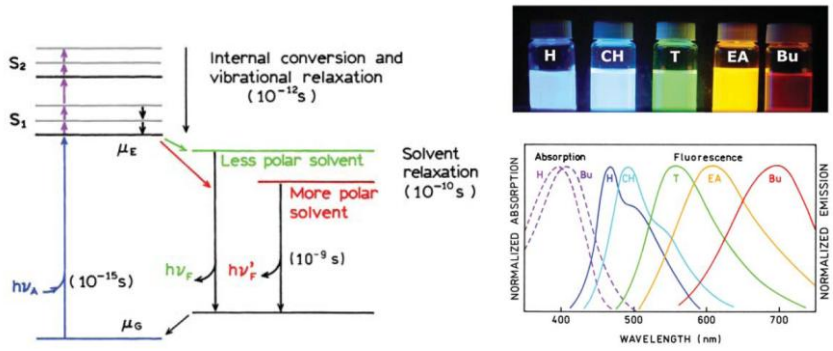

Figure 2.1 – Energy level representation (Jablonski diagram) of solvent relaxation (left). Solvent relaxation result in change of spectral response which is represented in right. The shift of emission to longer wavelengths with solvents of smaller dielectric constants of DNS, a solvent sensitive fluorophore, can be seen in photograph (top right) as well in spectral recording (bottom

right). The diagram is from *Principles of Fluorsccence Spectroscopy (2006); third edition; by Lakowicz J. R.*

Spectral and radiative profiles of fluorphores are strongly influenced by the ionic or polarity of local environment [27]. Solvent polarity is the major phenomenon responsible for Stokes shift. Solvent polarity can have a dramatic effect on emission spectra (Figure 2.1) and due to this reason, spectral analysis of fluorophore's emission spectra in different solvents has been performed regularly. For application in biological system fluorophore's interaction with proteins, membranes, and nucleic acids have also been studied to understand how a particular fluorophore behaves in a complex and dynamic system where effect of polarity is not uniform[28]. Figure 2.2 shows some examples where effect of solvent polarity on fluorophore is successfully employed to understand biologically relevant physical properties of biomolecules. Absorption spectroscopy is less sensitive to solvent polarity than emission/fluorescence spectroscopy. Absorption of light occurs in about 10^{-15} s, a time too short for motion of the fluorophore or solvent and so the molecule is exposed to the same local environment in the ground and excited states during absorption of photon.

Upon absorption of photon, the fluorophore transits (excited) to the first singlet energy state (S1), usually to one of the excited vibrational level within S1. Vibrational relaxation leads to rapid loss of energy. If the fluorophore is excited to the second singlet state (S2), it rapidly decays to the S1 state in 10^{-12} s due to internal conversion[25]. After this quick non-radiative loss of energy, the fluorophore stays at lowest excited energy state for a time period ranging up to few nanoseconds. During its stay in excited state,

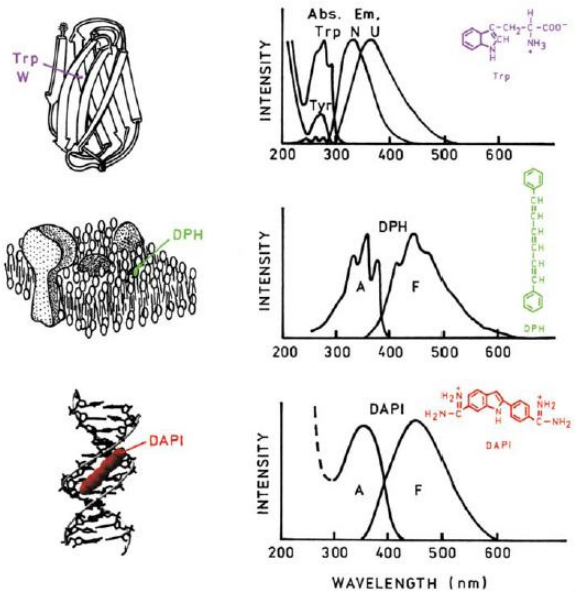

Figure 2.2 –Application of solvent sensitive fluorophore in biological system. Tryptophan ;Trp, W; (top) the amino acids found in most of the proteins, is a solvent sensitive fluorophore. Protein unfolding-refolding can be studied by measuring the spectra and intensity of tryptophan at various stages of protein folding. DPH (middle) is another solvent sensitive fluorophore that is used to measure fluidity of biological membranes. DAPI (bottom) the fluorophore that is used in fluorescence microsopy to visualize nucleus, intercalates to the nuclear DNA and due to loss of solvent relaxation, produces fluorescence signal.

Fluorophore induces and experiences change in the polarity of the surrounding environment with solvent molecules trying to orient them around the dipole moment of the excited state fluorophore. This results in some non radiative energy loss and the extent of this loss depends on the polarity of the environment (Figure 2.1). The emitting fluorophore is exposed to this changed local environment and the transition to ground state is from a lower energy level. So emission from fluorophores generally occurs at wavelengths that are longer than absorption wavelength. The time fluorophore spends at excited state (1–10 ns) are usually much longer than the time

required for solvent relaxation as solvent relaxation occurs in 10–100 ps in fluid solvents[29, 30]. For this reason, the emission spectra of fluorophores are representative of the solvent relaxed state. There are many situations where fluorophore can emit during the solvent relaxation process. In these cases emission spectrum represents an average of partially relaxed excited states[23].

Typically, the fluorophore has a larger dipole moment in the excited state (μ_E) than in the ground state (μ_G). In general, only fluorophores that are themselves polar display a large sensitivity to solvent polarity[23]. Nonpolar molecules, such as unsubstituted aromatic hydrocarbons, are much less sensitive to solvent polarity. One common use of solvent sensitive probes is to determine the polarity of binding site on the macromolecule. This is accomplished by comparison of the emission spectra and/or quantum yields when the fluorophore is bound to the macromolecule or dissolved in solvents of different polarity[27, 31, 32]. However, there are many additional instances where solvent effects are used. The effects of solvent and environment on fluorescence spectra are complex, and are due to several factors in addition to solvent polarity. The factors that affect fluorescence emission spectra and quantum yields include:

- Solvent polarity and viscosity
- Rate of solvent relaxation
- Probe conformational changes
- Rigidity of the local environment
- Internal charge transfer
- Proton transfer and excited state reactions
- Probe–probe interactions

These multiple effects provide many opportunities to use these fluorophores as indicators of change in solution and large molecular assemblies[23].

2.3 Molecular theory of solvent relaxation

Most of the fluorophore molecules have permanent or induced dipole. These molecules can be represented as point dipole with electric field (R). Thus the energy of the dipole (E_{dipole}) will be

$$E = -\mu R \qquad (2.1)$$

The electric field R is the relative reactive field induced by the dipole and μ is the dipole moment. R is parallel and opposite to the direction of dipole and its magnitude is proportional to magnitude of dipole moment, polarizability of the solvent (f) and inversely related to the third power of Önsager radius[23, 31, 32] a (the distance between the dipole entities). Thus R is given by

$$R = \frac{2\mu}{a^3} f \qquad (2.2)$$

Polarizability of the solvent is the result of

a. mobility of electrons of the solvent that depends on the square of refractive index (n).

$$f(n) = \frac{n^2-1}{2n^2+1} \qquad (2.3)$$

b. orientation of solvent molecule's dipole moment that depends on dielectric constant (ε).

$$f(\varepsilon) = \frac{\varepsilon-1}{2\varepsilon+1} \qquad (2.4)$$

The first factor is comparatively faster than the second as electrons can reorient themselves much faster than the whole molecule[24, 29, 30, 32]. The difference of these two factors is termed as orientation polarizability (Δf) and is given by

$$\Delta f(n, \varepsilon) = \frac{\varepsilon - 1}{2\varepsilon + 1} - \frac{n^2 - 1}{2n^2 + 1} \quad (2.5)$$

A fluorophore is in constant interaction with its solvent during absorption and emission. And can have two distinct dipole moments while it is in

A. ground state (μ_G)
B. excited state (μ_E)

The electric fields experienced by both the dipoles can be categorized as :

A. Field due to electronic motion R_{el} given by, $R_{el} = \frac{2\mu}{a^3} f(n)$ (2.6)
B. Field due to molecular dipole motion (orientation) R_{or} given by, $R_{or} = \frac{2\mu}{a^3} \Delta f$ (2.7)

At both excited state and ground state these interactions occur and result in deviation from ideal energy state seen in vapor phase[23, 32]. Thus during absorption,

ground state energy of the fluorophore (E^G_{abs})

$$= E^G_{(vap)abs} - \mu_G R^G_{or} - \mu_G R^G_{el} \quad (2.8)$$

And excited state energy of the fluorophore (E^E_{abs})

$$= E^E_{(vap)abs} - \mu_E R^G_{or} - \mu_E R^E_{el} \quad (2.9)$$

Due to the very fast transition of the fluorophore from ground state to the excited state the molecular reorientation of solvent is not possible and the ground state electric field due to molecular orientation persist at excited state of the fluorophore during the transition[24, 30, 32].

Thus the energy barrier the molecule has to cross to go to the excited state level can be given as the difference of Eq 2.9 and Eq 2.8.

$$\Delta E_{abs} = E^{E}_{abs} - E^{G}_{abs} \quad (2.10)$$

Similarly, the energy barrier that molecule has to cross when it returns from relaxed excited state to ground state can be given as

$$\Delta E_{fl} = E^{E}_{fl} - E^{G}_{fl} \quad (2.11)$$

Where,

$$E^{E}_{fl} = E^{E}_{(vap)fl} - \mu_E R^{E}_{or} - \mu_E R^{E}_{el} \quad (2.12)$$

$$E^{G}_{fl} = E^{G}_{(vap)fl} - \mu_G R^{E}_{or} - \mu_G R^{G}_{el} \quad (2.13)$$

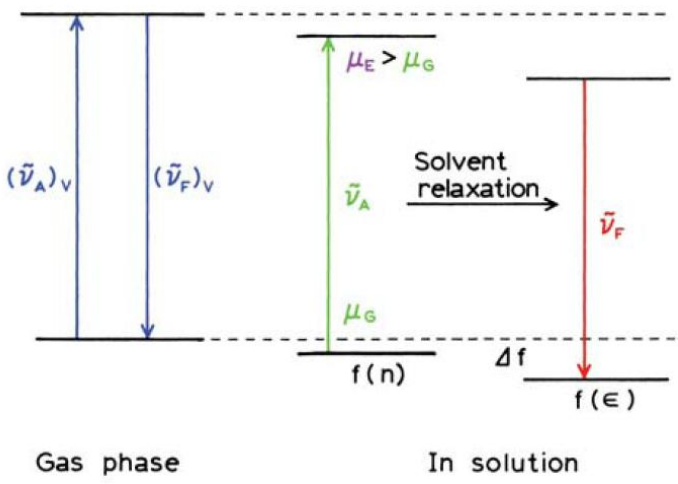

Figure 2.3 – Deviation in energy level of fluorophore in solution from that of the vapor phase (indicated as gas phase). Effect of solvent relaxation on the energy diagram is also depicted and physical meaning of the terms f (n), f (ε) and Δf are shown. The diagram is from *Principles of Fluorsccence Spectroscopy (2006); third edition; by Lakowicz J. R.*

As the energy barrier crossed during transition from one state to other corresponds to the energy of absorbed or emitted photon, we can write, $\Delta E = hc\upsilon$ (2. 14)

So, Eq 2.10 and 2.11 can be written as

$$hc\upsilon_{abs} = E^{E}_{abs} - E^{G}_{abs} \quad (2.15)$$

$$hc\upsilon_{fl} = E^{E}_{fl} - E^{G}_{fl} \quad (2.16)$$

Subtracting equation 2.15 from 2.10 we get,

$$hc\left(\upsilon_{abs} - \upsilon_{fl}\right) = E^{E}_{abs} - E^{G}_{abs} - E^{E}_{fl} + E^{G}_{fl} \quad (2.17)$$

As Stokes shift is defined as the difference between frequency of light absorbed by the molecule and frequency of light emitted by the molecule,

$$\left(\upsilon_{abs} - \upsilon_{fl}\right) = \frac{1}{hc}(E^{E}_{abs} - E^{G}_{abs} - E^{E}_{fl} + E^{G}_{fl}) \quad (2.18)$$

Substituting the values of energy levels in Eq. 2.18 with the expressions derived in Eqs. 2.8, 2.9, 2.12 and 2.13 and considering the energy of the any given fluorophore in vapor state is constant (resulting in all the E_{vap} expressions to be considered as constant) we can express Eq. 2.18 as[23]

$$\left(\upsilon_{abs} - \upsilon_{fl}\right) = -\frac{1}{hc}\,(\mu_E - \mu_G)\,(R^{G}_{or} - R^{E}_{or}) + \text{constant} \quad (2.19)$$

Using Eq 2.7 we can substitute R_{or} expressions in terms of μ, Δf and a. The new expression thus will be

$$\left(\upsilon_{abs} - \upsilon_{fl}\right) = -\frac{2\Delta f}{hca^3}\,(\mu_E - \mu_G)^2 + \text{constant} \quad (2.20)$$

As the onsager radius, a, is supposed to be constant during the event of absorption and emission, Stokes shift depends upon the square of the difference of ground state and excited state dipole moment and orientation polarity (which in turn depends on dielectric permittivity and refractive index of the environment).

2.4 Effect of excimer formation on solvent relaxation

In addition to molecular relaxation phenomena, other factors also can contribute to changes in fluorescence spectral and radiative properties. These factors augment the effect of molecular relaxation in some cases. One of the most studied factors is the isomerism of the fluorophore during excited state. Some fluorophore can form excited state isomers known as excimers when they absorb energy[33]. The formation of excimer might be favorable in certain environment. Mostly these isomeric states arise due to intramolecular charge or proton transfer known respectively as ICT (intramolecular charge transfer) and ESIPT (Excited state intramolecular proton transfer)[23, 33]. Formation of these excimers result in an altered excited state energy level and the molecular transition occurs from that altered state. The extent of excimer formation depends on many variable, of them in physiological conditions, ionic strength, phase transition and pH are crucial.

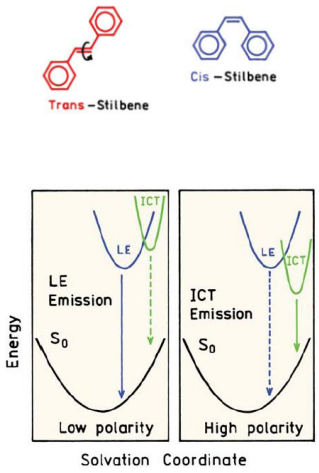

Figure 2.4 – Excited state isomers of stilbene (top) and the effect of intermolecular charge transfer (ICT, bottom). Electronic reorientation of various fluorophore leads to ICT. The solvent polarity has a crucial role in determining extent of ICT and the energy level of ICT (bottom). The spectral and radiative response of the fluorophore is indicator of the transition.

Phenomena like ICT and ESIPT effect both spectral and radiative rate of fluorescence and can be detected by spectral changes, intensity changes and changes in fluorescence decay profile. The characteristic feature of these phenomena is that, in most of the cases, two distinct isomers have two distinct patterns that can be mathematically resolved after analysis of the spectral or the decay profile.

CHAPTER 3

SOLVATOCHROMIC RESPONSE OF POTENTIOMETRIC DYES

3.1 Potentiometric dyes

Potentiometric membrane dyes are employed to study cell physiology. The size of the voltage-dependent signal, although certainly important, is by no means the only factor to be considered in choosing a dye. The initial approach of finding good potentiometric dye was by trial and error. Large number of dyes, with no or little correlation in their structures, was screened by Cohen and his group on the squid axon [12, 34-36]. This exhaustive study led to the availability of a large number of organic dyes whose spectral properties are sensitive to changes in membrane potential. Also, this exhaustive study pioneered to identify the important parameters of dye chemistry that enable the dye to be a useful and practical indicator of potential. A simple yet practically applicable classification that emerged from these studies[12] is based on the speed of their response to voltage changes. The dyes that can respond the voltage changes that occur in excitable cells or tissues are regarded as 'fast dyes'. These dyes respond fluorescently to voltage changes within a millisecond due to intramolecular rearrangement in its chemical structure. 'Slow dyes' responds to slow, but sustained changes in voltage which, may be due to hormonal responses in nonexcitable cells or the change in activity of energy transducing organelles. These slow dyes have electrostatic charges and their response is based upon the rearrangement of distribution of the molecules in response to altered electric field[37].

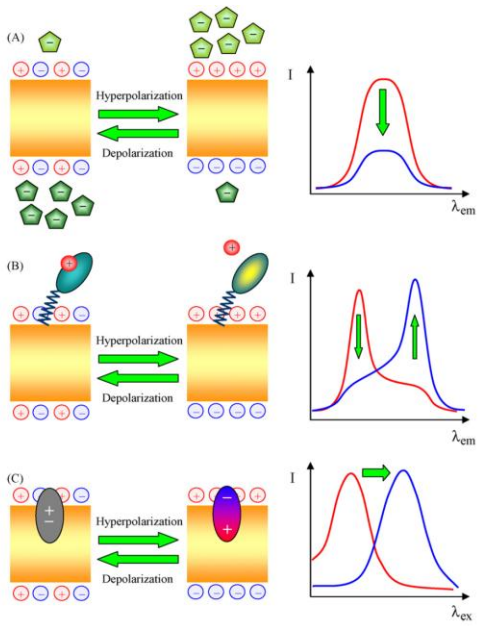

Figure 3.1 Mechanism of action of 'slow' potentiometric dyes (A) and fast potentiometric dyes (B and C) are shown. The slow dyes work in Nernstian way as they distribute themselves along the membrane according to the membrane potential. Fast dyes either go through a protonation-deprotonation cycle in response to change in potential (B) or an electronic reorientation (C) due to change in potential. In case of slow dyes, response can be detected by change of fluorescence intensity (radiative change) while for fast dyes the response accompanies spectral changes along with radiative change. (Adapted from Demchenko and Yesylevskyy; *Chemphyslip* 2009):

Interestingly, in addition to identifying the range of applications accessible to potentiometric indicators, this classification also divides the existing potentiometric indicators into realms of mechanism and sensitivity. Electrochromic and Nernstian redistribution of the dye to electric field is the molecular basis of fast and slow potentiometric dyes respectively. Electrochromism results in intramolecular rearrangement of charges while Nernstian distribution leads to physical

distribution of the fluorophore molecules along the electric field[5]. Thus, Electrochromic dye are efficient in sensing fast and high threshold changes in electric field while Nernstian dyes are more sensitive to detect sustained but slow changes in electric field[5].

3.2 Factors quantitatively effecting electrochromism

The electrochromic dye senses the integrated electric field[38]. Whenever an electric field is produced, some averaging and integration of the electric field takes place ultimately resulting in reorientation of the charges in the fluorophore molecule. The mesoscopic approach[5] that considers the dye π-electronic system as a point dipole, the electric field as a vector $\overrightarrow{F}$ that averages all the fields influencing this system and its surrounding, with effective dielectric constant of the medium being ε_{ef}, can be used for the description of electrochromism in the simplest dipole approximation. The direction and magnitude of the shift, Δobs, is proportional (in this approximation) to the electric field vector $\overrightarrow{F}$ and the change of dipole moment associated with the spectroscopic transition $\overrightarrow{\Delta\mu}$:

$$h\Delta\upsilon_{obs} = -\frac{1}{\varepsilon_{ef}}|\vec{\mu}|\left|\vec{F}\right|\cos\theta \qquad (3.1)$$

Where, θ is the angle between the dipole moments and the electric field. This equation indicate that for maximal sensitivity to electrostatic potential, the probe dye should exhibit substantial change of its dipole moment $\overrightarrow{\Delta\mu}$ on electronic excitation, which implies a substantial redistribution of the electronic charge density[4, 5, 5, 37]. Furthermore, the dye should be located in low-polar environment (low ε_{ef}) and oriented parallel (cos θ = 1) or anti-parallel (cos θ =−1) to the electric field[4]. It is also important that the correlation between the electric field strength and the spectroscopic effect within the applied approximation is linear, which allows, in principle,

easy calibration of this effect in absolute values. Such electrochromic mechanism allows obtaining very fast response, which can be understood from its electronic nature that does not require re-location of molecules or of their groups. Electrochromism allows detecting the response to the changes in electric field in any medium[23].

3.3 Styryl dyes

Styryl dyes and particularly 4-dialkylaminostyrylpyridinium derivatives with electron-donor and electron-acceptor substituent at the opposite ends of their rod-shaped aromatic conjugated moieties are among the best known electrochromic dyes [5, 39, 40]. When excited, these dyes show one of the most dramatic changes in dipole moment. They exhibit efficient excited-state re-location of electronic charge. In the excited state a partial positive charge is reversed by electronic intramolecular charge transfer (ICT) from dialkylamino group to aminophenyl moiety[4, 5]. An external electric field, as seen in membranes of excitable tissue or mitochondrial inner membrane, along the extended π-electron system can modulate electronic polarization of these compounds[5]. Therefore these dyes can exhibit detectable spectral shifts, and these shifts can be modulated by the external electric fields operating on a molecular scale [40]. These spectral shifts can be recorded (in either excitation or emission spectra)[41] and can be correlated with the extent of the electric field. The ratio of these intensities provides ratiometric response, which ideally should not depend on the probe concentration. Regarding the sensitivity to transmembrane potential, the magnitude of this two wavelength intensity ratio is still not very large, about 7–10% per 100mV[4]. These values are influenced by membrane composition.

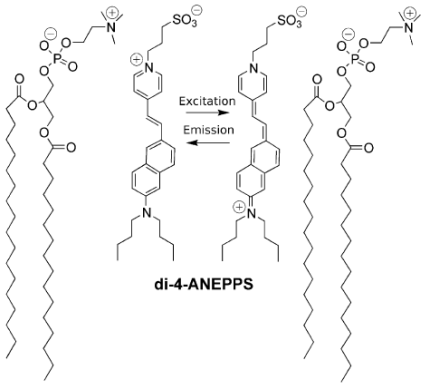

Figure 3.2 – Electronic reorientation of electrochromic styryl dye 4-Dialkyl aminostyrylpyridinium Di-4-ANEPPS upon excitation. This orientation gives rise to an ICT excimer and the extent of formation depends upon the local electric field too.

Most of the styryl dyes used for fluorescence studies with biological samples are have been aminostylyl pyridinium (ASP) derivatives. Typically, their lipophililic alkylaminophenyl 'tail' is connected to electron withdrawing pyridinium 'head' group through conjugate bond(s). The tail, to which usually two aliphatic hydrocarbon chain is linked, is responsible for its membrane binding. Increased number of carbons in that hydrocarbon chain increases the hydrophobicity of the tail region ensuring that the tail will be embedded to the membrane and not dissociate easily. Though this feature is useful, inclusion of longer chain impedes its solubility in water and thus complicates the staining protocol. Styryl dyes used for plasma membrane staining have 7-14 carbon chains. While dyes used for monitoring transport or mitochondrial activity have 1-2 carbon attached to the tail. The head group determines its membrane permeability. Dyes with small alkyl group and only one cation generally stains the mitochondria. While dyes with one cation and one anion at their head group are largely amphoteric. These dyes are ideal to measure membrane potential of excitable cells. For studying processes like endocytosis, styryl dyes with more than one cations are useful. Presence of excess of positive charge decreases its probability

of diffusing through the membrane. The spectral properties are determined by fluorophore nucleus. This generally, is guided by the number of aromatic rings and the conjugate bonds that join head and tail region [42]. Figure 3.3 shows the structure of some aminophenylstryrl pyridinum dyes that are commercially available and whose structures play significant role in its cellular localization.

A) FM 4-64 (staining exocytosis/endocytosis in active cells)

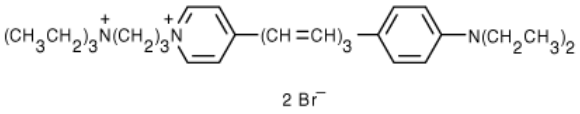

B) RH- 421(Recording electrical potential of excitable cells/ tissue)

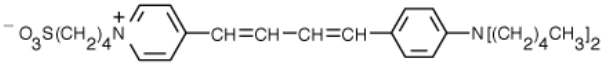

C) DASPMI (Recording mitochondrial membrane potential)

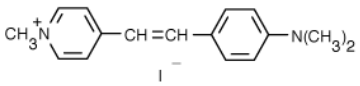

Figure 3.3 – Structures of commercially available aminophenylstyryl pyridinium dyes (taken from Invitrogen'/molecular probes website). The common feature of all these dyes are the aminophenyl moiety (in the right) and pyridinium moiety (in the left) are connected via conjugate double bond found typically in styrene like molecule. This connected structure is the core responsible for fluorescence properties. The 'head' region at pyridinium end is modulated for restricting/ allowing cellular permeability, the aliphatic group at aminophenyl 'tail' region

confers solubility in water and lipid membrane. FM 4-64 (A) is used as a marker to study endocytosis or exocytosis . Divalent cations are introduced in head to make it impermeable to membrane. RH-421(B) is used to measure action potential. Introduction of an anion makes the head region zwitterionic at neutral pH. Long aliphatic group at the tail ensures that its partition coefficient is very high and thus its poorly soluble in water and segregates to membrane lipids. DASPMI (C) is monocationinc molecule with a short aliphatic tail. It permeabilizes through cell membrane and segregates to mitochondria due to high negative mitochondrial potential.

In an aqueous environment, the dielectric properties of water induce high non-radiative decay rates and thus render the molecule non-fluorescent. The free movement of the dye can also lead to increase in non-radiative decay [23]. Once the polarity decreases, the radiative decay becomes substantial and this results in a detectable fluorescence signal. Though there are other factors, including aggregation of the dye in water and charge shift of the dye in the excited state that may contribute to the spectral characteristics of the dye, the solvatochromism still exerts a major impact on the dye's spectral properties [43, 44].

3.4 LDS 798 or Styryl -11

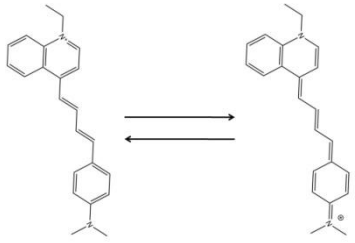

Figure 3.4 – Structure of LDS 798 or styryl -11 and possible excited state isomer. The structure resembles to that of DASPMI. The major difference is the presence of quinolinum moiety instead of pyridinum moiety in DASPMI.

Styryl-11 or LDS 798 (*1-Ethyl-4-(4-(p-Dimethylaminophenyl)-1,3-butadienyl)-quinolinum percholate*) is a styryl compound that contains monocationic quinolinum group instead of the pyridinium group of ASP dyes and has a rather short dialkylaminophenyl 'tail' region [44]. In ethanol its peak absorption is at 580 nm and peak emission is at 770 nm making it a useful near infra-red dye. Near infra-red solvatochromic dyes have been shown to be used for studying tissues in-vivo [45] and are specially useful for imaging as the contribution from autofluorescence is minimal.

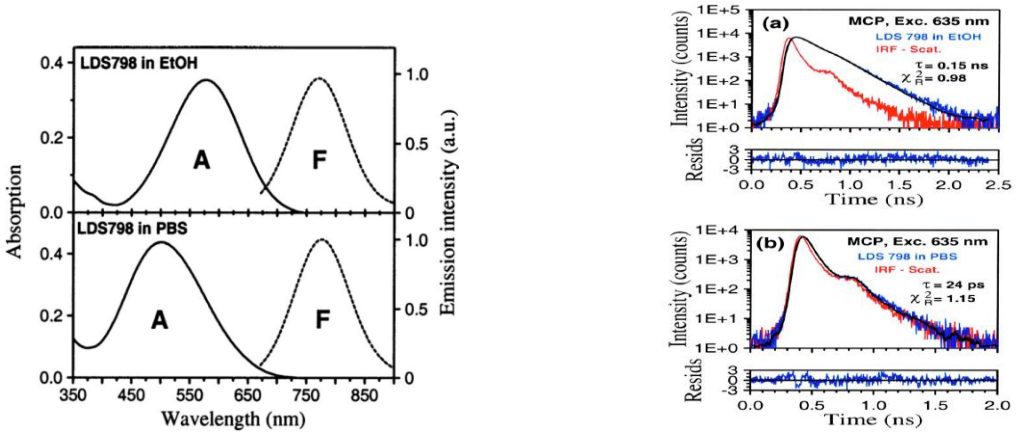

Figure 3.4 – Spectral (left) and decay (right) profile of LDS 798 in water and methanol. The profiles show an indication that LDS 798 might demonstrate electrochromic properties as other styryl dyes. (Figures taken from Luchowski R *et. al.* (2009), *Rev. Sci. Instrum.*

LDS 798 has been used as a laser dye and has a very weak fluorescence in aqueous solution (quantum yield of 0.002) [46, 47]. Previous studies have shown that LDS798 has a very short fluorescence lifetime in water (<20 psec) while its lifetime increases in ethanol and in polymer films[47]. Stoke's shifts have been found to be higher in water than that in ethanol. The purpose of this study was to characterize the solvatochromic properties of this aminophenyl styryl quinolinum (ASQ) dye and compare these features with those of established (well studies) ASP

dyes. Recent studies on the structure and fluorescence properties of ASQ dyes indicate that their quinolinum group acts as the electron acceptor while the aminophenyl group acts as the electron donor[48].

Chapter -4

FLUORESCENCE BASED APPROACHES TO MEASURE MITOCHONDRIAL MEMBRANE POTENTIAL

4.1 Mitochondrial membrane potential and its relation to cellular health

Mitochondrion is the organelle that is primarily known as the powerhouse of the cell. Recent studies on mitochondria reveal that the organelle plays important roles in redox homeostasis, lipid modification, calcium homeostasis, and cell death processes[49]. ATP synthesis, the classical function of mitochondria occurs mainly at inner membrane where a transmembrane gradient of ions is maintained. This gradient that generates mitochondrial potential is indispensable for ATP production through oxidative phosphorylation. Figure 4.1 provides a schematic representation of the electron transport chain in the inner mitochondrial membrane and how it results in the transmembrane ionic gradient.

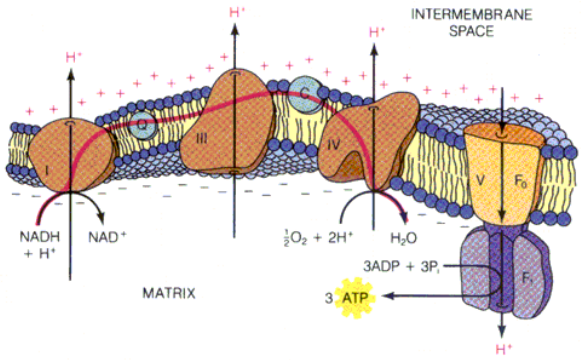

Figure 4.1 – Schematic diagram showing the distribution of ions around the inner membrane of an active mitochondrion. The asymmetric distribution of protons along the membrane generates

a potential. Diagram from *Biochemistry; 2nd edition* by Mathews C.K. and van Holde K. E.*; Benjamin Cummings publication.*

In conditions where mitochondrial membrane integrity is compromised, the membrane potential is lost and ATP synthesis through electron transport chain is disrupted. Hence, mitochondrial potential[50], can be an indicator of mitochondrial integrity and functionality. Mitochondrial potential can be used as a marker for various physiological processes[51]. Apoptotic processes involve mitochondria in most of the cases [2]. Activation of some pro-apoptotic molecules lead to disruption of mitochondrial integrity and release of some other downstream pro-apoptotic factors like cytochrome c[52]. Disruption of mitochondrial membrane integrity leads to decrease in ψ_m and that can be used as indicator of apoptosis[19]. Also, mitochondrial damage in healthy cells leads to their autophagy known as mitophagy. During the process of aging, mitophagic activity slows down and cells accumulate damaged mitochondria that lack mitochondrial potential[51]. Determining the relative number of depolarized mitochondria in a cell can indicate aging of the cell. The ubiquitin-ligase Parkin, whose loss-of-function causes Parkinson's disease, is selectively recruited to dysfunctional mitochondria and causes their autophagy-mediated degradation [53]. This suggests that Parkinson's disease may be at least in part associated with failure to eliminate dysfunctional mitochondria and monitoring abundance of dysfunctional mitochondria can help in disease prognosis [51].

4.2 Early studies on mitochondrial membrane potential

Early studies with isolated mitochondria have characterized mitochondrial potential changes. These studies were done by measuring concentrations of radioactive tracer ions in response to applied electric field or various ionophores. Also, K^+ ion influx was measured by using patch

clamp techniques. These studies, though significant, reported conflicting results from various groups and there was high contribution of artifact during the processing. Also, they did not report mitochondrial potential in its physiological environment. This generated interest in measuring membrane potential of mitochondria in intact cells. Available micro-electrode techniques were supplemented with microscopy for achieving micron-range spatial resolution. Initial mitochondrial stains were saffranin, Anilino-naphthalene sulfonamide (ANS) and Di-o-C_5 [22]. Most of these dyes were actually solvent sensitive in nature and were not specific for mitochondria. This resulted in very high noise-signal ratio. Cyanine dyes were one of the first groups of dyes that were found to have some specificity for mitochondria. Dyes like DiS-C_2-5 and DiO-C_6 were used for isolated mitochondria and intact cell mitochondrial membrane potential. Discoveries that confirmed rhodamine based dyes are selectively localized in mitochondria [20, 54] were pivotal in fluorescence based studies of ψ_m. It was also found that distribution of these dyes in the cell depends on mitochondrial potential.

4.3 Mitochondrial targeting of 'mito-tracker' compounds

Careful studies in the fields of fluorescence and photodynamic therapy field reported that several cationic molecules distribute electrophoretically into the mitochondrial matrix in response to the electrical potential across the inner mitochondrial membrane [17, 20, 21, 55]. The accumulation takes place as a consequence of their charge and of their solubility in both or either inner membrane lipids and the matrix aqueous space[18]. Due to which molecules with lipophilic cationic group and fluorescence properties have been extensively employed to measure the mitochondrial electrical potential exploiting their spectroscopic properties[18, 21, 49, 56].

4.4 Fluorescence based approaches to measure mitochondrial potential

Three types of dyes have been used to measure $\Delta\psi_m$. In all the techniques ratiometric changes in fluorescence intensity have been used to achieve the results[5, 18]. But the basic mechanisms that lead to change in intensities at different wavelengths are distinctly different. For dyes like rhodamine 123, fluorescence quenching is monitored[18, 49]. For proton dependent dyes like JC-1, change in fluorescence spectra is monitored[5]. And for styryl-based dyes, change in excitation spectra is monitored[5]. A diagrammatic representation of dye's response to potential changes have been shown in Figure 3.1.

Proper calibration of fluorescence intensity changes using defined potential across mitochondria allow to estimate the change in magnitude of proton gradient, ψ [50, 56, 57]. Figure 4.2 depicts a classical example where ratio of fluorescence intensities at two different wavelengths is correlated to mitochondrial membrane potential. Without calibration, changes in fluorescence signal can be used to monitor the qualitative response of $\Delta\psi$ to perturbation by external chemical or physical agents.

In case of isolated organelles the potential-dependent uptake induces fluorescence quenching. Quenching is probably seen due to aggregation or stacking of the dye after accumulation [56]. Incidentally, the fact that dye accumulation induces fluorescence quenching in isolated mitochondria suggests that the fluorescence enhancement observed in intact cells is due to relatively low accumulation of the dye in intact cell[18]. The use of such 'potentio-metric' probes with fluorescence microscopy and spectroscopy allows estimation of $\Delta\psi_m$ in individual living cells and big cellular population. These approaches of $\Delta\psi_m$. are valuable for understanding basic energy metabolism and its dysfunction in pathologic cells. But intensity based measurements still

do not indicate the exact photophysical changes happening in the dye and its environment. The effect of local concentration is not very well understood with intensity changes.

Fluorescence lifetime measurements provide an alternate and more direct approach to understand fluorescence photophysics. Lifetime is not dependent upon the local concentration[23], but responds very specifically to internal quenching as well as solvatochromic changes.

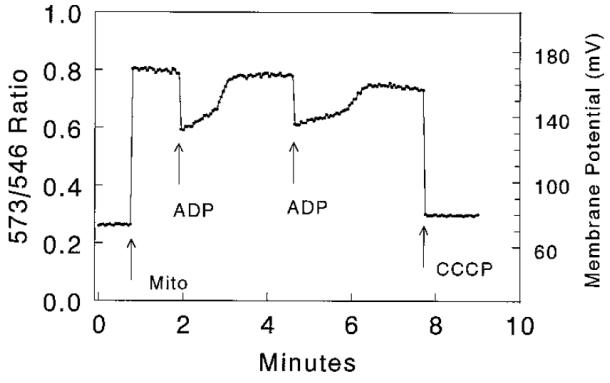

Figure 4.2 – A classical case where ratiometric fluorescence method was used for determination of mitochondrial membrane potential. Isolated mitochondria were used for the study and Tetramethyl rhodamine (derivative of Rh 123) was used as the fluorescence indicator. TMR fluorescence was calibrated to membrane potential. Figure from Solaini *et. al.* Biosci Rep. 2007.

4.5 Fluorescence Spectroscopy

Fluorescence spectroscopy has been applied to investigate membrane potential for more than 40 years[22]. The cells or the isolated mitochondrial extracts are suspended in a cuvette and analyzed in a relatively inexpensive fluorometer[22]. It can detect $\Delta\psi_m$ of the whole population but not of individual cells or mitochondria. Change in spectra or signal is due to the potential change of the whole ensemble and individual details are lost.

Rhodamine group of dyes have been used regularly for spectroscopic approach. In cells or isolated organelles, $\Delta\psi$ with rhodamine dyes can be monitored by two approaches called ‘‘quench mode’’ and ‘‘non-quench mode’’[18]. Non-quench mode has not been despite its considerable sensitivity to detect small changes in mitochondrial potential (few mV). Intensity changes observed during this mode may become non-linear to $\Delta\psi_m$ if the local concentration of dye reaches ‘quench threshold’ or the dye specifically binds to some components in one of the mitochondrial compartments[18]. Therefore, for intensity based spectroscopic measurements, the quench mode is widely used, as it can monitor relevant changes in $\Delta\psi$, with a good level of reliability.

4.6 Fluorescence microscopy and laser-scanning confocal fluorescence microscopy

Optical microscopic techniques can provide spatially resolved suggestive images of mitochondria in an intact cell. These microscopic techniques are widely used due to the possibility of observing even single mitochondrion, their distribution and their organization as reticular networks or single organelles in a cell. This is particularly important also because it allows evaluation of the heterogeneity of the $\Delta\psi_m$ within single cells [54, 58]. In addition, these techniques monitor co-localization of molecules and associated phenomena within single cells. Recent advances in confocal microscopy technique offers better spatially resolved results by controllable depth of field[59, 60]. This eliminates the out-of-focus information that degrades image quality and enables serial collection of optical sections (z-sections) from thick specimens[60]. Confocal microscopy has been extremely popular in recent years due, to the relative ease with which extremely high-quality images can be obtained from specimens prepared for conventional optical microscopy[18, 59, 61]. However, this high resolution has a shortcoming since the imaging field is rather limited. It is difficult to obtain reliable $\Delta\psi$ estimates in cell populations.

Among the most significant technical challenges for performing successful live-cell imaging experiments is to maintain the cells in a functional and healthy state on the microscope stage while imaging[61]. Quantitative three-dimensional imaging in fluorescence microscopy is often complicated by artifacts due to specimen preparation (coverslip thickness, quantum efficiency, and the specimen embedding medium), controllable and uncontrollable experimental variables (bleaching artifacts, inner filter phenomena), or configuration problems with the microscope, including laser system, optical component and alignment immersion oil[50].

4.6 Flow cytometry

This technique offers the advantage of being able to estimate the intracellular fluorescence of cells in the culture media and to evaluate heterogeneity of a cell population due to the different levels of the mitochondrial membrane potential in single cells. Therefore, flow cytometry is conveniently used when one wishes to compare $\Delta\psi$ in two populations of cells [57, 62, 63]. This technique is especially suitable for non-adherent cells. The adherent cells are required to be in suspension, and require either scraping or trypsinization, which induces oxidative stress, therefore affecting the membrane structure and function[18]. Reliable data are obtained particularly when analyzing intact cells. Plasek et al. (2005)[64] developed a flow-cytometric method for monitoring mitochondrial membrane polarization using TMRM and expressed the results in millivolt range.

4.7 Advanced microscopic techniques

The ratio of fluorescence intensity between the mitochondria and adjacent mitochondria-free cytoplasm can in theory be put into the Nernst equation to derive $\Delta\psi$. In practice, the resolution

of the confocal microscope is insufficient to image just the mitochondrial matrix[50] (Nicholls and Ward 2000). More advanced imaging techniques are being developed to achieve nanometer resolution. With this technology, mitochondrial sub-compartments can be resolved. Recent studies with these nanometer-scale imaging approaches have focused on fixed cellular preparations to look into compartments of mitochondria[65] (Figure 4.3). Though, live cell imaging of mitochondrial potential have not yet been reported, theoretically it is possible.

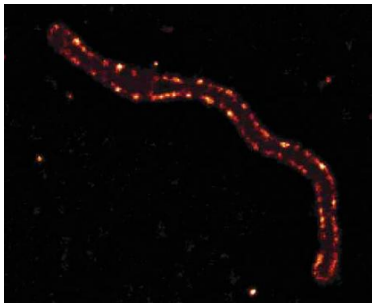

Figure 4.3 – Mitochondria ultra-structure imaged by Stimulated Emission depletion (STED) microscopy. From Schmidt *et.al.* Nature Methods, 2008.

In the last decade, various efforts have been made to integrate advanced fluorescence spectroscopic methods to confocal microscopy. These efforts have made single molecule studies possible and allowed to measure fluorescence phenomenon like fluorescence lifetime in a femto-liter volume[66]. Also, by applying confocal configuration processes like fluctuation correlation have been developed. These new confocal microscopy based techniques have facilitated sub-resolution studies even before the advent of super-resolution microscopy. Fluorescence lifetime imaging microscopy (FLIM) has been extensively used to detect protein-protein interaction in live intact cells[23]. This technique measures fluorescence lifetime of the fluorophores visualized in the cells. Fluorescence lifetimes of potentiometric fluorophores are affected by their environment. But FLIM is not popular for measuring lifetimes of the potentiometric dyes. In this

study, we focus on application of FLIM for measuring $\Delta\psi_m$ in intact live cells. As lifetime approach is independent of the local concentration it will be more informative about the local environment of the dye[23]. Also average lifetime is a statistical parameter unlike fluorescence intensity. Thus, minor changes in lifetime parameter actually indicate significant changes in dye's local environment.

CHAPTER - 5

GOAL AND SPECIFIC AIMS OF THE STUDY

Studies on solvent induced fluorescence properties of styryl dye LDS 798 to develop *in vivo* and *in vitro* assay techniques.

Styryl compounds have been used as dyes in measuring live cell activity due to their solvent sensitive fluorescence (solvatochromic) properties. Their use in measuring action potential is well documented. They have also been used to study vesicle trafficking and to measure mitochondrial functionality. The feature that makes styryl dyes attractive for membrane studies is their spectral and radiative response to local environment polarity.

Styryl-11 or LDS 798 is a styryl compound. Its near infra red (NIR) fluorescence properties make it a powerful candidate for in-vivo fluorescence imaging.

With the recent advent of fluorescence based technologies, like fluctuation correlation spectroscopy, fluorescence lifetime imaging and other techniques, styryl dye's response can be used to obtain detailed information on complex phenomenon. We propose to investigate how LDS798 solvatochromism can be used with the modern fluorescence techniques to probe systems of biomedical significance.

The Goal of the study is to apply solvatochromic properties of styryl dye, LDS 798, in biomedically relevant assay techniques.

Specific Aim 1: To characterize the solubility profile and solvatochromism photophysics of LDS 798.

Initial studies indicate that stokes shift and fluorescence lifetime of LDS 798 is dependent on polarity and viscosity of the environment. LDS 798 is found to be very weakly fluorescent in water, but its fluorescence increases in less polar solvent like ethanol. These changes in fluorescence are generally attributed to its induced dipole. Thus characterizing the photophysics can provide some insights about its behavior in heterogeneous cellular environment.

Specific Aim 2: To study applicability of LDS 798 in cellular staining.

Styryl dyes have been found to label various cellular organelles like the plasma membrane, endocytic and exocytic vesicles and active mitochondria. LDS 798, with its near IR spectral property, can be an ideal fluorophore for subcellular staining due to high signal-to-noise ratio. We would like to study cellular localization of LDS 798 and evaluate its toxicological effects in cultured cell lines.

Specific Aim 3: To apply lifetime-based imaging techniques and fluctuation based correlation techniques with LDS 798 staining for *in vitro* and *in vivo* studies.

Traditionally, change in fluorescence intensity has been used to quantify cellular changes. Fluorescence lifetime has an edge over intensity as it is not dependent on the concentration of the fluorophore and is used in direct determination of environmental changes. For analyzing effects of solvatochromic dye like LDS 798 in a cellular environment, lifetime approach will be more efficient than intensity imaging.

Techniques like correlation spectroscopy provides more information about dynamics associated with molecular movement. Combination of these techniques accompanied by solvatochromic effect of LDS 798 will be used to determine whether LDS 798 fluorescence can be used for functional imaging of cells.

Significance: Cellular activities like calcium efflux, pH changes and potential changes have been measured using fluorescence intensity of various environment sensitive dyes. These measurements need to be ratiometric in most of the cases to avoid the effect of fluorophore concentration. This creates complexity in the data collection scenario and finer spatiotemporal details are lost.

Techniques like FCS and FLIM are insensitive to dye concentration and provide information from structures beyond optical limits. Thus, spatiotemporal analysis of the finer structures is simplified. Application of these techniques for biomedical studies with polarity sensitive NIR probe, LDS 798, will provide a novel tool to understand polarity dependent processes *in vivo* and *ex vivo*.

CHAPTER - 6

MATERIALS AND METHODS

LDS 798 was purchased from Exciton (Dayton, OH) and used without any further purification. 1,4- dioxane, ethyl acetate, dichloromenthane (DCM), 1-octanol, ethanol, methanol, N,N-dimethyl formammide (DMF), dimethyl sulfoxide (DMSO) were purchased from Sigma-Aldrich or Fluka (St. Louis, MO). 1-Butanol, 2-propanol, acetonitrile and chloroform were purchased from Fisher Scientific (Pittsburgh, PA). All the solvents were spectrophotometric grade. Deionized water used for the experiments was from Milipore distillation system. 1,2-dimyristoyl-*sn*-glycero-3-phospho-(1'-rac-glycerol) (DMPG), 1,2-dimyristoyl-*sn*-glycero-3-phosphocholine (DMPC) was purchased from Avanti polar lipids (Alabaster, AL). Sodium dodecyl sulfate (SDS) powder and Triton X- 100 was from Sigma-Aldrich (St. Louis, MO).

6.1 Preparation of phosopholipid bilayers and High density lipoprotein-like nanoparticles

For SUV preparartion, stock solution of lipids was prepared in chloroform. Lipid films were prepared by evaporating the chloroform in inert environment under steady flow of Argon gas. Lipid films were then hydrated with phosphate buffered saline supplemented 500 μM EDTA. After hydration, the samples were sonicated till clarity with 2 minute pulses of sonication with ultrasonic processor UP200H system (Hielscher Ultrasonics GmbH, Germany) followed by resting phase in ice.

The cholate dialysis procedure used was based on the procedures described for discoidal rHDL particles [67-69]. A mixture of Egg yolk phosphatidyl choline (15 mg), free cholesterol (0.35 mg) and cholesterol oleate (0.15mg) all in chloroform were dried down under nitrogen. Apo A-1 (5

mg) or ApoA1-mimetic 5A peptide (1mg) and 3% DMSO were mixed. 14 mg sodium cholate was added and volume was made up to 2 ml with buffer (10mM Tris, 0.1M KCl, 1mM EDTA pH 8.0). The mixture was incubated overnight at 4^0C.

The mixture was then dialyzed against 2 liters of 1X phosphate buffered saline for 48 hours with change of buffer every 2 hours on the first day, 3 times on the second day and later kept overnight. The mixture was centrifuged for a quick spin and then sterilized by passing through 0.45μM filter (Millipore, MA).

The hydrodynamic volume of these SUVs and nanoparticles was estimated using dynamic light scattering Nanotrac Particle Size Analyzer (Nano Track; ISee imaging systems, Raleigh, NC).

6.2 Cell culture techniques and staining protocol

For imaging, the cell cultures were performed in 35 mm radius glass bottom dishes that had 10 mm size 0 coverslips (Mat-tek Corporation; Ashland MA). NIH 3T3 and HEK 293T cell lines were maintained in DMEM / high glucose medium (Invitrogen, Carlsbad CA). MDA MB -231 cells were maintained in DMEM low glucose medium (Invitrogen, Carlsbad CA). MCF-7 and SKOV-3 cell lines were maintained in RPMI 1640 medium supplemented with 2 mM glutamine. All the culture media were supplemented with 10% heat-inactivated fetal bovine serum (Invitrogen Carlsbad) and 1% antibiotic antimicrobial (ABAM) solution (Invitrogen, Carlsbad CA) and kept in a humidified incubator at 37°C with 95% air and 5% CO_2.

For staining with LDS 798, a stock solution of 10 -30 mM of LDS 798 in DMSO was prepared. The stock was diluted in the media used to maintain the cell culture to prepare 5nM – 3μM working concentration. For initial experiments to check whether LDS 798 can be used for imaging, cells were incubated in the dye containing media for 30 minutes in humidified

incubator mentioned before and then culture media with the dye was replaced by the same media with no dye and were immediately used for imaging. For experiments with mitochondrial uncoupler, 1-3 μM of FCCP (p-trifluoromethoxy carbonyl cyanide phenyl hydrazone) was added to the culture while the LDS stained cells were kept in imaging chamber.

6.3 *In vitro* cytotoxicity study by MTT Assays:

In vitro cytotoxicity of LDS 798 was determined on Ovarian cancer cells SKOV-3 and non malignant cells, human embryonic kidney cells (HEK-293) by standard MTT assays. Cells were seeded on a 96 well plate at a density of 7,000 cells per well. Once cells were attached to the plates (18-24 hrs), they were washed with 1X phosphate buffered saline (PBS). A serum free medium containing different concentrations of LDS 798 (0.6 nM to 6μM) was added in the wells. In one row LDS 798 was not added and in another, DMSO was added (as LDS 798 used was dissolved in DMSO). These two rows were used as controls. The plates were incubated at 37^0C and 5% CO_2 for 24 hours. The MTT compound (3-(4,5-Dimethylthiazol-2-yl)-2,5-diphenyltetrazolium bromide) was then added in each well at 0.125 mg/ml. The plates were incubated at 37°C for 3 hours and centrifuged at 1200 rpm for 5 minutes. The supernatant from each well was removed and was replaced with 200 μL DMSO. The absorbance at 570nm was measured on a Bio Rad Microplate reader model 3550. Each drug concentration was tested with at least 6 replicates.

6.4 Spectroscopic studies and mathematical models

Extinction coefficient of LDS 798 in ethanol was reported by the manufacturer [44]. Equal amount of LDS 798 was dissolved in equal volume of ethanol, octanol and water. Then, samples were diluted to various concentrations and optical densities were measured in Cary 50 Bio (Varian

Inc., Australia) spectrophotometer. The absorptions were plotted as a function of concentration calculated using extinction coefficient of LDS 798 in ethanol.

Partition coefficient (log P) was measured by shake-flask method [70]. In brief, supersaturating the mixture of 1:1 water: octanol with LDS 798 was shaken vigorously at room temperature (~20°C) overnight and 500 ul aliquots were taken from both water and octanol phase. The aliquots were diluted with their respective solvents and absorption was measured.

For steady state fluorescence spectroscopic measurements, Cary Eclipse spectrofluorometer (Varian Inc., Australia) was used. In most of the measurements the samples were excited with 530 nm light and a 570 nm long pass filter was used before the detector to minimize the effect due to scattering. For fluorescence spectra measurement of small unilamelar vesicles (SUV)s in aqueous solution of LDS 798, excitation of 470 nm was used and 530 long-pass filter was used at observation in those cases. Absorption values of the samples at 530 or 470 nm were used to correct the difference in fluorescence intensity due to variable excitation. All the samples used had an optical density less than 0.2, but greater than 0.02 at 530 nm. For absorption measurements with SUVs, the scattering due to SUVs was measured with the samples in PBS without LS 798. These values were then subtracted from the absorption values of the SUV samples in LDS 798 solution.

Quantum yield was calculated using cresyl violet in ethanol (quantum yield 0.54) as reference solution. The expression used for the calculation was

$$Q = Q_R \frac{I * abs_R n^2}{I_R * abs\ n_R{}^2} \qquad (6.1)$$

Where, Q and Q_R are quantum yields of the sample and reference, I and I_R are the fluorescence intensities area under the curve for the sample and reference, abs is the absorption of the samples at the wavelength that was used to excite the samples and n is the refractive index of the solvents.

For measuring the effect of solvent relaxation Lippert – Mataga (LM) expression was used. According to LM orientation polarizability, Δf, was calculated as.

$$\Delta f_{LM} = \frac{\varepsilon - 1}{\varepsilon + 2} - \frac{n^2 - 1}{2n^2 + 1} \tag{6.2}$$

Where, ε is the bulk dielectric permittivity.

Stokes shift for LDS 798 in solvents with different dielectric constant was plotted as a function of orientation polarizability of those solvents. And the square of the difference in ground state and excited state dipole $(\mu_E - \mu_G)^2$ was calculated as the slope of the linear fit of the plot as depicted in Equation 2. 20.

orientation polarizability according to simplified Bilot - Kawski (BK) equations was also with following equations

$$f_{BK}(\varepsilon, n) = \frac{2n^2 + 1}{n^2 + 2}\left(\frac{\varepsilon - 1}{\varepsilon + 2} - \frac{n^2 - 1}{n^2 + 2}\right) \tag{6.3}$$

$$g_{BK}(n) = 3/2 \frac{n^4 - 1}{(n^2 + 2)^2}$$

$$\Phi_{BK}(\varepsilon, n) = f_{BK}(\varepsilon, n) + g_{BK}(n) \tag{6.4}$$

Difference and sum between the absorption and fluorescence wave frequency was correlated to

$$\tilde{\nu}_A - \tilde{\nu}_F = m_1 \cdot f_{BK}(\varepsilon, n) + const$$
$$\tilde{\nu}_A + \tilde{\nu}_F = m_2 \cdot \Phi_{BK}(\varepsilon, n) + const \qquad (6.5)$$

and the ratio of excited and ground state dipole moment was calculated using the following expression.

$$\frac{\mu_e}{\mu_g} = \frac{m_1 + m_2}{m_2 - m_1} \qquad (6.6)$$

For lifetime measurements, FluoTime 200 (PicoQuant GmbH, Germany) time domain spectrofluorometer was used. This spectrofluorometer contains cooled Multi-channel plate detector (Hamamatsu, Japan) and is accessorized with a monochromator at the observation. A 470 nm laser diode (LDH-PC- 470) was used as the excitation source. This laser diode has a pulse width of <70 psec. The fluorescence decays were fitted with FluoFit version v-4.0 software (PicoQuant GmbH, Germany) using multiexponential deconvolution model

$$I(t) = \int_{-\infty}^{t} IRF(t') \sum_i \alpha_i e^{-\frac{t-t'}{\tau_i}} \qquad (6.7)$$

Where IRF (t′) is the instrument response function at time t′, α is the amplitude of the decay of the ith component at time t and τ_i is the lifetime of the ith component.

Radiative and non radiative rate constants for LDS 798 in different solvents using following equations

$$Q = \frac{\Gamma}{\Gamma + k_{nr}} \qquad (6.8)$$

$$\tau = \frac{1}{\Gamma + k_{nr}} \qquad (6.9)$$

6.5 Imaging and fluorescence lifetime-based microscopy (FLIM)

For imaging live cells, MicroTime 200 confocal fluorescence lifetime microscope system (Picoquant GmBh, Germany) was used. Imaging can be done with both intensity and lifetime modes simultaneously using this system. This system consists of an inverted microscope (Olympus IX -71) with 4 pulsed laser diode for excitation of which, diode with 475 nm excitation and 635 nm excitation were used in this study. Both lasers have a pulse width of < 100 psec and for imaging cells, 10-50 nW of effective laser power (calculated from the calibration curves supplied by the manufacturer) was used. A water objective (60X magnification) and confocal pinhole of 50 μm radius were used for imaging. Glass bottom dishes were placed in custom-made holders to avoid any unwanted movement while maintaining the culture conditions. 650 long pass filters were used to filter the laser excitation as well as the autofluorescence signal. The detectors used were avalanche photodiode (APD) detector from Perkin- Elmer Corp (Germany). The collected data from the instrument was integrated in a time correlated single photon counting system (PicoHarp 300; PicoQuant GmBh, Germany) and was analyzed in SymphoTime (version -4.2) (PicoQuant GmBh, Germany). Average lifetime (τ_{av}) was calculated as

$$\tau_{av} = \frac{\sum_i \alpha_i \tau_i^2}{\sum_i \alpha_i \tau_i} \qquad (6.10)$$

Lifetime histograms (lifetime distribution), that show the frequency of lifetimes in an entire image, were used for analysis. It is determined by contribution of lifetime component on overall intensity of the images.

For colocalization experiment, the emitted light was first filtered with 500 lp long-pass filter and then separated by dichroic mirror DCXR 650 in to two different detectors. Lifetime gated

analysis was done to check contribution of one dye on the other detector (bleeding). The analysis showed that <1% bleeding was seen in detector specific for rhodamine 123 while <0.1% bleeding was seen in detector for LDS 798.

6.6 Fluorescence Lifetime Correlation Spectroscopy studies

The data for Fluorescence Lifetime Correlation Spectroscopy (FLCS) experiments was collected with MicroTime 200 confocal microscope (Picoquant, Germany). The methodology using these studies has been described earlier [46]. Briefly, pulsed light from 470 nm solid state laser was focused 10 µm above the cover-slip surface, but inside the drop of the sample solution. 20 µW laser light power for all the FLCS experiments was used. Separate measurements characterizing microscope/objective alignment and features for the confocal volume was performed. For the purpose of confocal volume characterization, 3D raster scanning of fluorescence nanospheres was applied [71, 72] that yielded a value of 0.16 fl. Olympus IX71 inverted microscope and Olympus UPlanFL N 100x magnification oil objective, NA=1.3 was used for the measurements. The scattered light was filtered with sets of filters (500 long wavelength pass and 473 RazorEdge, Semrock). Filtered light was focused through 30 µm pinhole to single photon avalanche photodiode (SPCM-AQR-14, Perkin Elmer). Data analysis was performed with SymPhoTime (v. 5.0) software (Picoquant, Germany) and autocorrelation function was defined according the formula:

$$G(\tau) = \frac{\langle \delta I(t) \delta I(t+\tau) \rangle}{\langle \delta I(t) \rangle \langle \delta I(t+\tau) \rangle} \qquad (6.11)$$

Where $\delta I(t)$ and $\delta I(t+\tau)$ are the fluorescence intensity fluctuations from the mean at time t and $t+\tau$, respectively. Auto-correlation curves due to translational diffusion through 3-dimentional Gaussian shaped volume were fitted with following formula [2, 3]:

$$G(\tau)=\sum_{i=1}^{n}\rho_i\left(1+\frac{\tau}{\tau_{Di}}\right)^{-1}\left(1+\frac{\tau}{\tau_{Di}\kappa^2}\right)^{-1/2} \qquad (6.12)$$

where ρ_i is a contribution of i-th diffusion species for total autocorrelation function, τ_{Di} is a diffusion time of i-th diffusion species, κ is length (z_o) to diameter (w_o) of the focal volume. On the basis of the fit to the autocorrelation function we determined also the diffusion coefficient D according:

$$D=\frac{w_o^2}{4\tau_D} \qquad (6.13)$$

Styryl dyes have been used extensively for studying membrane dynamics and changes in membrane potential. The aminostyryl pyridinium sub group has also been reported to be successfully used to probe the dynamics of vesicle trafficking in an activity dependent manner [73].

CHAPTER – 7

SOLVATOCHROMIC CHARACTERIZATION OF LDS 798

Specific Aim 1: To characterize the solubility profile and solvatochromism photophysics of LDS 798.

7.1 Rationale

LDS 798 or styryl-11 contains a quinolinum 'head' region which is connected to the dimethylaminophenyl 'tail' via two alternate double bond structures[44, 74]. This structural configuration is quite unique from that of other well known styryl dyes. While the overall configuration of LDS 798 retains the features responsible for its spectral properties, it has a very short (dimethyl) tail and a bulky (quinolinum) and monocationic head region that is similar to just a few known commercially available styryl dyes[73, 75].

Styryl compounds are ideally soluble in non-polar solvents and in a complex system, they preferentially partition in nonpolar medium[42]. This can limit their use in cellular staining as the aqueous medium is predominant in these cases[37, 40]. Thus, it has been seen that the styryl compound with ideal fluorescent properties might not be a good choice for cellular staining as their effective concentration is limited by their partitioning pattern. LDS 798 has a bulky quinolinum core, but relatively small tail and head group. *In silico* simulation of its partition coefficient using *molinspiration property engine* (v2009.01) generated a logP value of 0.611 indicating that it partitions adequately in water. Experimental confirmation for these values was necessary prior to the use of LDS 798 for staining hydrophobic structures.

In ethanol, LDS 798 has peak absorption at 580 nm and peak emission at 770 nm making it useful for NIR measurements. NIR dyes have been shown to be used for studying tissues *in vivo*. LDS 798 has been used as a laser dye and has a very weak fluorescence in aqueous solution (quantum yield of 0.002)[74]. Previous studies have shown that LDS 798 has a very short fluorescence lifetime in water (<20 psec)[46, 47] while its lifetime increases in ethanol and in polymer films[47]. Stoke's shifts have been found to be higher in water than that in ethanol.

The purpose of this specific aim is also to characterize the solvatochromic properties of LDS 798 in bulk environment and liposome microenvironment. Photophysical properties of the dye, like solvent dependent extinction coefficient, quantum yield, average fluorescence lifetime, and other properties, like ground state and excited state dipole moment, are also calculated.

7.2 Results and Discussion

7.2.1 *Solubility profile of LDS 798*

Current studies were initiated with qualitative characterization of LDS798 solubility in solvents of varying polarity and showed that it is weakly soluble or insoluble both in highly hydrophobic solvents like cyclohexane and hydrophilic aqueous solutions. It was noticed that LDS 798 though dissolved slowly in deionized water, it was totally insoluble in cyclohexane even after vigorous overnight shaking.

During the study of spectral properties of LDS 798, the absorption spectrum was blue shifted in water without any significant spectral broadening (Figure 3.4) ruling out the possibility of LDS 798 self-aggregation. The study of the extinction coefficient of LDS 798 in octanol and water (Figure 7.1, left) showed that the extinction coefficient in water deviated significantly from that reported by the manufacturer, using ethanol as a solvent. Partition experiments, using the shake-

flask method and calculated extinction coefficients for LDS in water and octanol, yielded a log P of 0.54 indicating that LDS 798 dissolves in water reasonably well. Images taken after the separation of 2 phases (Figure 7.1, right) give a visual representation of the aforementioned result.

7.2.3 *Spectral changes in LDS 798fluorescence with polarity*

To understand the spectral changes due to solvatochromic properties of LDS 798, absorption and emission spectra were measured in solvents of various polarity and refractive indices (Table-7.1). Next, the Stoke's shift (υ_{abs} - υ_{Em} in cm^{-1}) was plotted for each solvent as a function of their respective polarity function. Both Lippert-Mataga (LM) (Figure 7.2) and simplified Bilot Kawski (BK) (Figure – 7.3) models were used to fit the data and characterize the solvent effect. Both models indicate that the Stokes shift change was correlated with the polarity function in aprotic solvents. However, a major observation from these plots was that protic and aprotic solvents both show completely different patterns of Stokes shifts. This deviation of protic solvents has been associated with their tendency to hydrogen bonding, aggregation or other specific interaction with the fluorophore. Stokes shift of LDS 798 in alkyl halides, chloroform and dichloromethane, could not be fitted with protic or aprotic profile in both LM and BK model, suggesting that there might be some specific interactions taking place between the solute and solvent that cannot be taken in to account by these models. Using Bilot-Kawski model and considering that both ground state and excited state dipole moments are parallel, we calculated the excited state dipole moment as 2.44 fold larger than the ground state dipole moment.

7.2.4 *Radiative changes of LDS 798 fluorescence with polarity.*

For understanding the radiative changes due to solvatochromic fluorescent properties of LDS 798, we measured its quantum yield in different solvents with cresyl violet in ethanol as the reference solution. We also measured the fluorescence lifetime of LDS 798 in different solvents (Figure – 7.4, top left panel). LDS 798 has a maximum quantum yield of ~ 6% in octanol, whereas its quantum yield was lowest in water (< 0.1%). The fluorescence decay profiles (Figure - 7.4, top right) showed that the maximum average lifetime was in the sub-nanosecond range (maximum 814 psec in chloroform and < 25 psec in water). Radiative and non-radiative rate constants calculated from quantum yields and fluorescence lifetime (Figure 7.4 bottom panels) show that the non-radiative rate constants are two orders of magnitude larger than the radiative decay explaining the major Stoke's shift seen with LDS 798. All these parameters were plotted as a function of LM parameter of polarity (Δf_{LM}). The response from protic solvents was distinctly different from that of aprotic solvents and this further indicates that H- bonding might have a significant effect in LDS798 spectra and fluorescence intensity. As observed earlier, LDS 798 fluorescence response was distinctly different in alkyl halide solvents when compared with that of other aprotic solvents.

The spectral properties of LDS 798 determined here are in good agreement with that of reported ASQ dyes[42]. Its absorption spectrum is blue shifted in polar solvent, like water, as seen in other ASQ dyes. The Bilot-Kawski and Lippert Mataga plots for solvent relaxation show that the Stokes shift increases linearly as a function of orientation polarizability. The interesting observation reflected in the plot is the response of aprotic solvents compared with protic solvents. This deviation of Stokes shift especially seen in protic solvents has been attributed to specific interaction between the solute and solvent, observed in other systems[23]. Both Lippert-

Mataga and Bilot-Kawski models failed to explain the effect of the Stoke's shift in alkyl halide solvents and water indicating that there might be some other specific interactions in addition to polarizability. Significant red shift in fluorescence spectra with increase in solvent polarity indicates that the excited singlet state is stabilized in polar solvents.

7.2.5 *Spectral and radiative changes of LDS 798 fluorescence in micelles and liposomes*

After characterizing the spectral and radiative properties of LDS 798 in solvents with different polarity, studies were performed on its fluorescence properties in the presence of amphipathic molecules, dissolved/dispersed in aqueous medium. Amphipathic molecules like detergents and phospholipids create a hydrophobic micro-environment in aqueous solution. These compounds have been used extensively to study fluorescent properties of other styryl dyes and have laid the foundation for their use in studying cellular events [42].

Spectral properties (both absorption and emission) of LDS 798 were measured while titrated with sodium dodecyl sulfate (SDS-an ionic detergent) and Triton-X 100 (a non-ionic detergent) at room temperature (Figure 7.5). These studies reveal that absorption maximum shifts to longer wavelengths upon addition of both SDS and Triton- X100. The fluorescence spectral analysis showed a progressive blue shift with increasing concentration of Triton-X 100 but not with SDS. The intensity of fluorescence increased with addition of detergents (both SDS and Triton- X 100). This increase was found to be phase dependent as the LDS fluorescence signal increased once the critical micellar concentration was attained (8.2 µM for SDS and 200 µM for TritonX-100) and leveled off after stable micellar structure was attained (at higher concentrations of detergent). This observation is consistent with reports based on study of the polymerization of

styryl dyes [76] that have reported spectral shift in fluorescence decreased once nucleation of polymerization was attained.

Study of spectral and radiative properties of styryl dyes in unilamellar vesicles (mean diameter ~ 60 nm), prepared with neutral phospholipids (DMPC) and negatively charged phospholipids (DMPG) showed a red shift in absorption and a blue shift in emission spectra upon addition of unilamellar vesicles to the dye (Figure – 7.6). Two emission peaks (at 550 nm and 720 nm) in presence of SUVs was observed when excited with 530 or 470 nm light (Figure 7.6). When excited with even longer wavelength (620 nm) only one peak at ~ 740 nm was observed while the LDS 798 fluorescence attained saturation at lower concentrations of DMPG than DMPC (Figure 7.6, lower panels).

Finally, polarity dependent changes in LDS 798 fluorescence in reconstituted high density lipoprotein (HDL) nanoparticles (rHDL) were measured to see whether this phenomenon can be applied to characterization of nanoparticles used in drug delivery. Ensemble studies show that amphipathic molecules influence the spectral properties and radiative rates of LDS 798. Most of the amphipathic molecules induced a red shift in absorption spectra while in all the cases the fluorescence spectra was blue shifted and the peak intensity increased by different magnitudes. In reconstituted bilayered structures, always two peaks were observed. This observation is previously unreported. Unpublished initial studies from our laboratory for these samples indicate that there might be two populations with distinct excitation peak. Molecular phenomenon leading to this observation and its significance is not yet clear and would require further study. The saturation profile of LDS798 fluorescence with DMPC and DMPS suggest that fluorescence properties of LDS 798 are enhanced when it interacts with the negatively charged or polar residues or conversely, LDS 798 might not interact effectively with the neutral phospholipids as

compared with polar/negatively charged lipids. Both these possibilities might be true as previous reports have shown that styryl dyes have enhanced fluorescence properties under mildly acidic.

7.3 Table

Table 7.1 - The list of solvents, their dielectric constants and refractive indices, solubility profile and, fluorescence properties (spectral shift, quantum yield and average lifetimes) of LDS 798 when it was dissolved in them.

Solvent	Dielectric Constant	Refractive Index	$\nu_{Abs} - \nu_{Em}$ cm^{-1}	% Quantum Yield	Average Lifetime (psec)
Aprotic					
Dioxane	**2.21**	**1.42**	**4541.56**	**3.06**	**206**
ethyl acetate	**6.02**	**1.37**	**4903.10**	**2.02**	**223**
Acetonitrile	**36.6**	**1.34**	**5265.30**	**0.23**	**85**
DMF	**38.3**	**1.43**	**5243.48**	**0.35**	**126**
DMSO	**47.2**	**1.48**	**5195.84**	**0.42**	**176**
Protic					
1-octanol	**10.3**	**1.43**	**3426.79**	**6.11**	**562**
1-Butanol	**17.85**	**1.40**	**3950.73**	**2.75**	**330**
n-propanol	**21.65**	**1.39**	**4126.76**	**1.34**	**205**
Ethanol	**24.3**	**1.35**	**4427.06**	**0.76**	**147**
Methanol	**33.1**	**1.33**	**4793.78**	**0.30**	**78**
Outlier					
Chloroform	**4.98**	**1.45**	**3108.66**	**3.21**	**815**
DCM	**8.93**	**1.42**	**2807.91**	**3.52**	**712**
Water	**78.3**	**1.33**	**7205.81**	**0.08**	**<50**

7.4 Figures

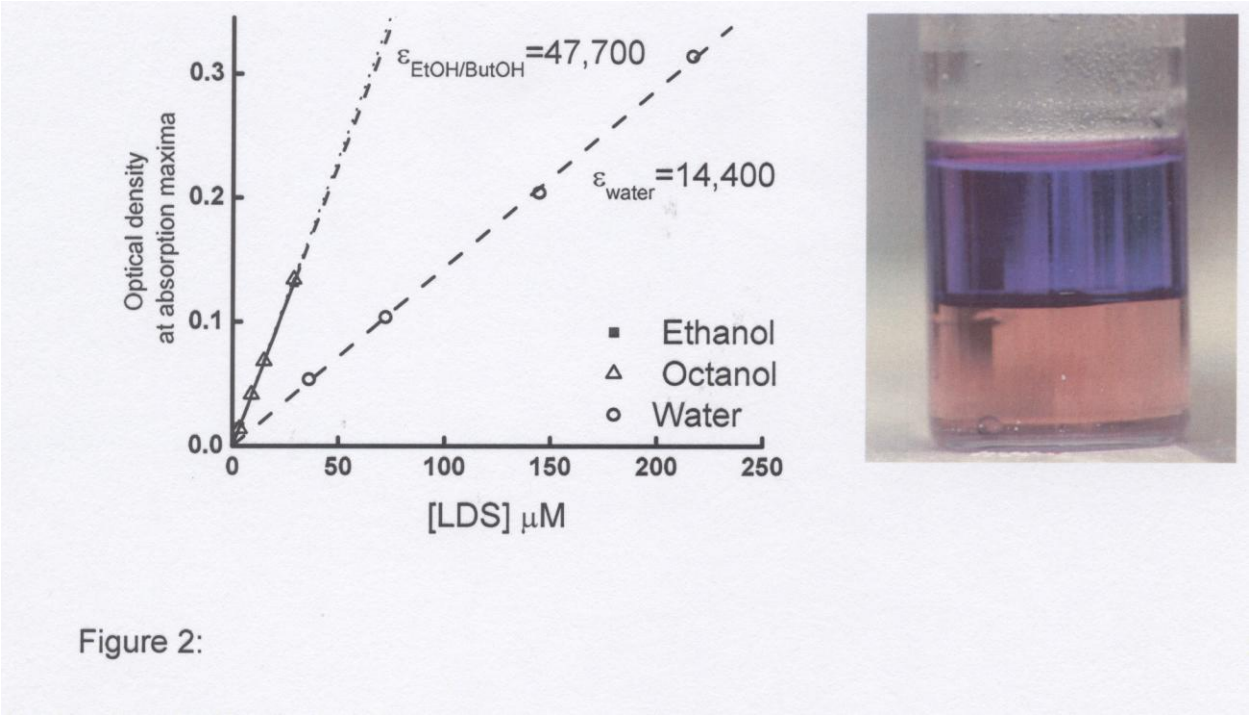

Figure 7.1- Partitioning profile of LDS 798. (left) Extinction coefficient of LDS 798 in octanol and water was calculated using ethanol as standard. (right). Image showing the partitioning of LDS 798 in octanol and water layer after overnight shaking. Concentration of LDS 798 in both layers was calculated using the derived extinction coefficients. Partition coefficient was calculated as the log of the concentration ratio in octanol and water.

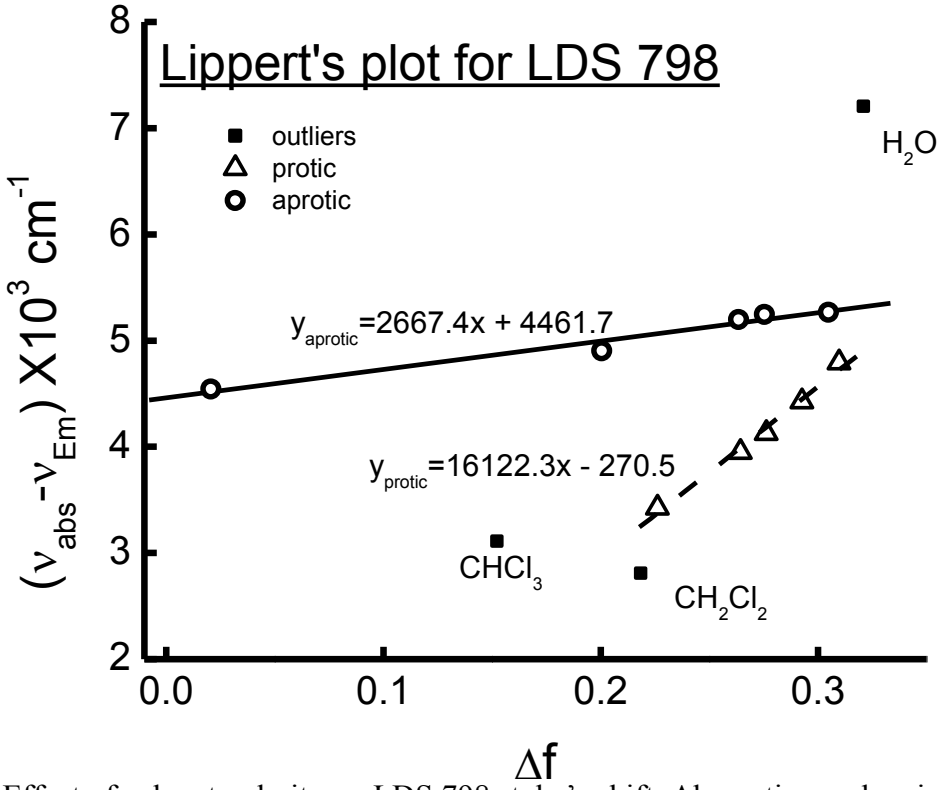

Figure 7.2 - Effect of solvent polarity on LDS 798 stoke's shift. Absorption and emission spectra of LDS 798 in solvents with various dielectric constant values were measured. The difference between the absorption and emission peak was plotted as a function of solvent polarity (Δf is Lippert Mataga function of polarity derived from dielectric constant and refractive index of solvents).

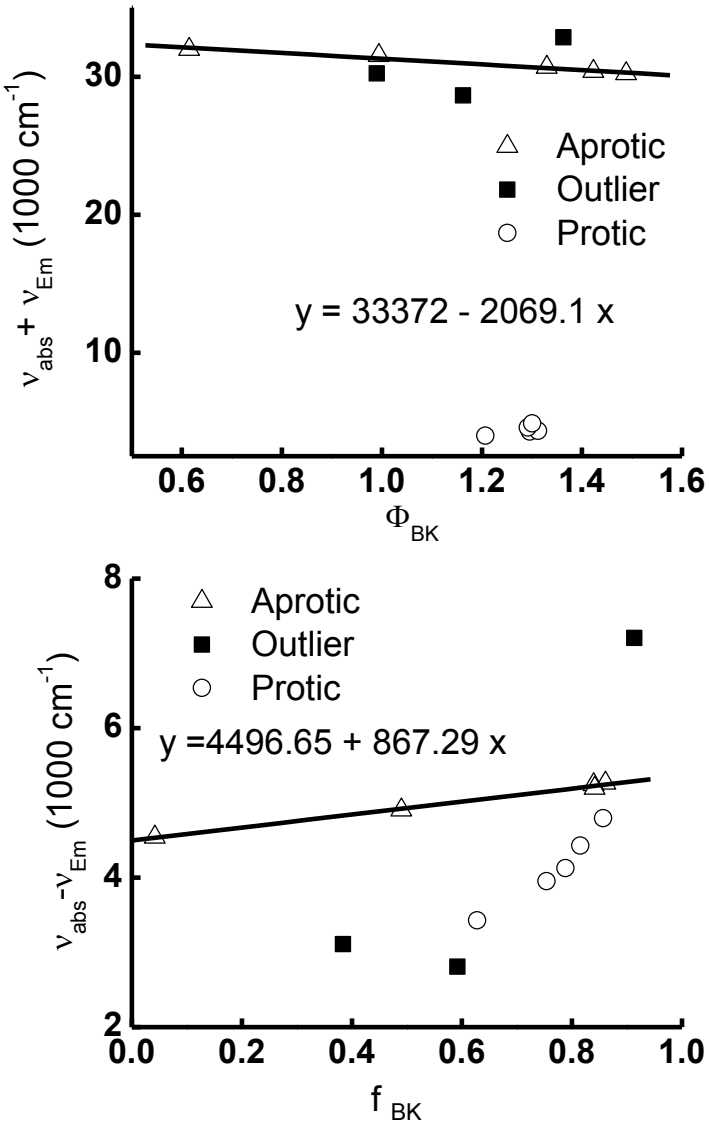

Figure 7.3: Effect of solvent polarity on LDS 798 stoke's shift. Absorption and emission spectra of LDS 798 in solvents with various dielectric constant values were measured. The difference between the absorption and emission peak was plotted as a function of solvent polarity (f_{BK} is Bilot Kawski function of polarity derived from dielectric constant and refractive index of solvents). From this model, the ratio of ground state dipole moment and excited dipole moment was calculated.

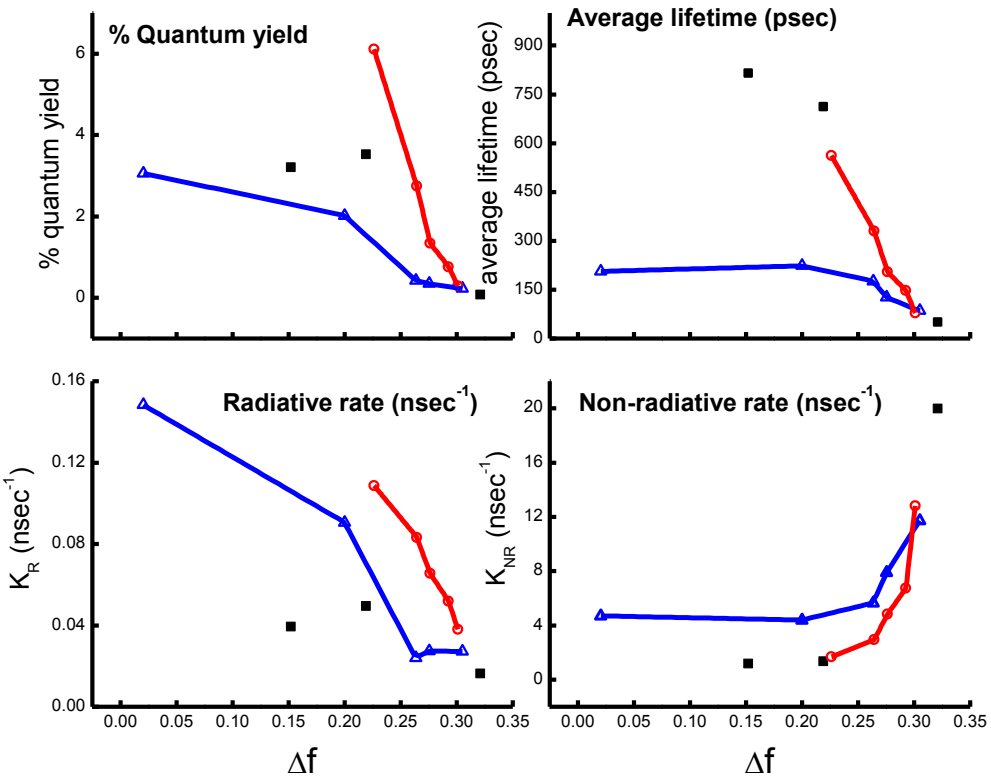

Figure 7.4- Effect of solvent polarity on radiative decay. Quantum yield and fluorescence lifetime of LDS 798 in different solvents was plotted as a function of polarity (Lippert –Mataga function). As the polarity increases, both quantum yield and lifetime values decrease indicating a net increase in non-radiative processes.

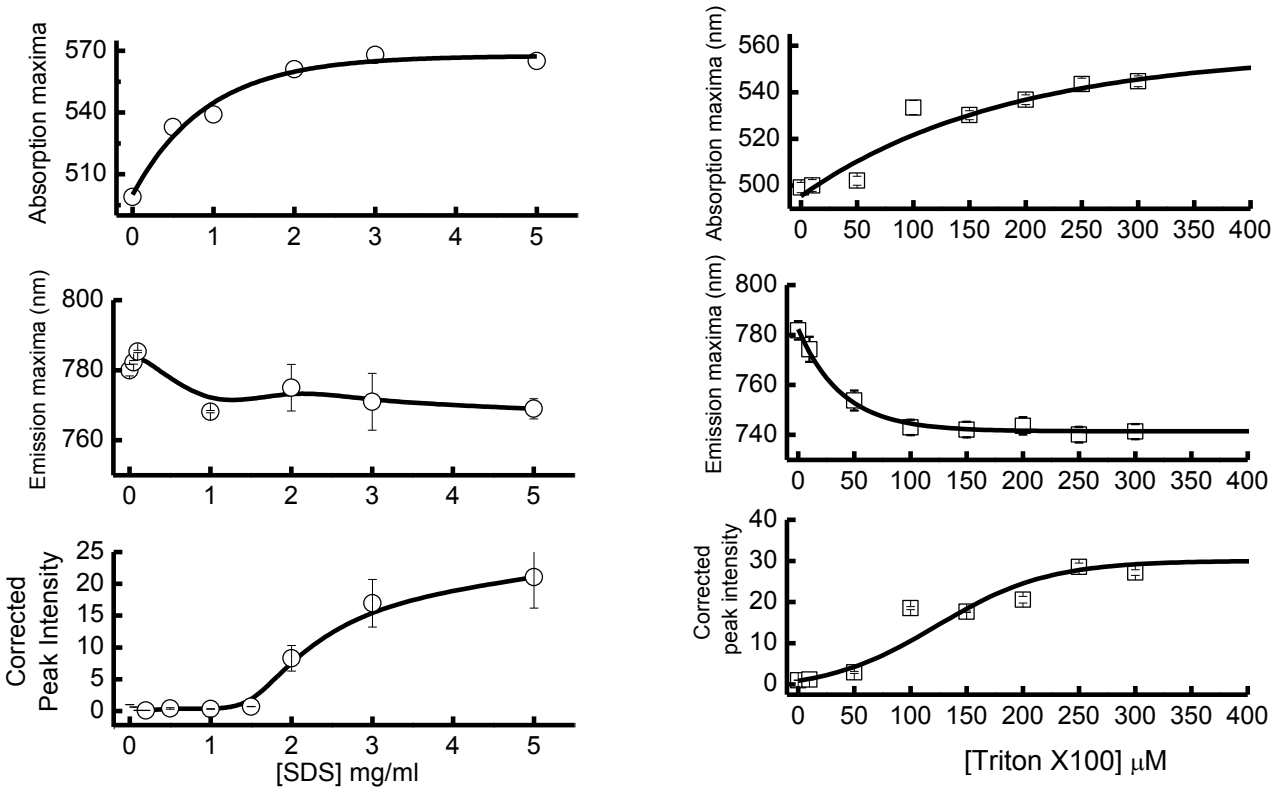

Figure 7.5 - Spectral and intensity changes in LDS 798 fluorescence on addition of detergent to aqueous solution. Aqueous solution of LDS 798 was titrated with two detergents: a) SDS (left), and b) Triton X 100 (right). Absorption and emission spectral results were recorded and absorption maxima (top), emission maxima (middle) and fold increase in peak intensity (bottom) was plotted as a function of detergent concentration. The fluorescence intensity increased around the critical micelle concentration of both the detergents. Spectral shift in emission and absorption maxima also followed the similar pattern indicating the fluorescence pattern responded to decrease in polarity of micellar micro-environment.

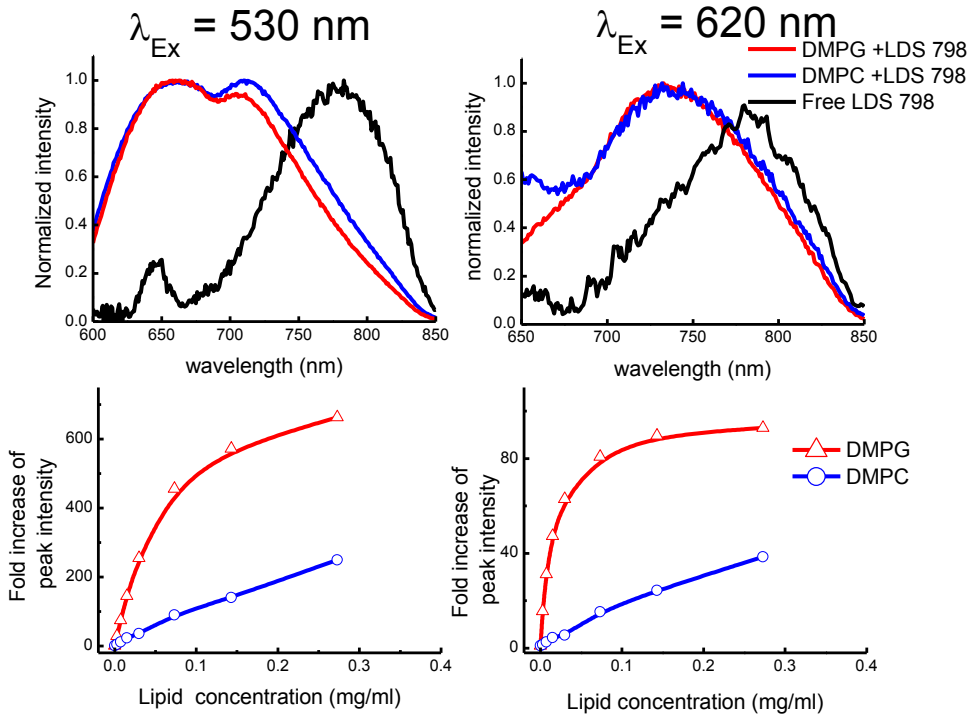

Figure 7.6 - Fluorescence response of LDS 798 with model membrane structures. LDS 798 was titrated with small lamellar vesicles made with pure Dimyristoyl phosphatidylcholine (DMPC) or Dimyristoyl phosphatidylglycerol (DMPG). Fluorescence spectra showed a distinct blue shift when SUVs were added to aqueous solution of LDS 798 (top). Peak intensity of fluorescence increased by few hundred folds in presence of SUVs. Control experiments with no LDS 798 showed that SUVs did not have any inherent fluorescence signal and the change in spectra was due to solvent induced effect on LDS fluorescence. Spectral analysis also indicated that LDS 798 fluorescence signal can be recorded at a range longer than 600nm even if it is excited at wavelengths less than 550 nm.

Chapter – 8

LIVE CELL STAINING WITH LDS 798

Specific Aim 2: To study applicability of LDS 798 in cellular staining and selectivity of staining.

8.1 Rationale

Styryl group of dyes were one of the first group of organic compounds that were used for understanding the excitable properties of cells without having any significant toxicity[37]. Dyes of this group (Di-1,4-ANEPPS and Rh 421) have a big impact in understanding the changes in membrane potential during stimulation[4340]. In early 90's a new sub-group of styryl dyes, called aminophenyl styryl pyridinum (ASP), was characterized [42, 73]and molecules from this group (FM1-43 and FM4-46) are widely used in studying vesicular trafficking[42, 73, 75]. While characterizing these dyes, the investigators were able to postulate the sub-cellular localization of these dyes on basis of their structures.

LDS 798 fluoresces in near infrared (NIR) region[46, 47, 74]. At this region there is considerably less autofluorescence signal [23, 77]. Also, absorption and emission spectra of LDS 798 in water and methanol indicate that there is a huge stoke's shift that makes it easy to filter excitation light [47]. All these features can make LDS 798 a potentially valuable tool for studying cellular activity in live cells. In this specific aim we will test whether LDS 798 can be used for live cell imaging.

Studies performed with small unilamellar vesicles (SUVs), in the last chapter, indicate that the fluorescence spectrum of LDS 798 is blue shifted in membranes. Two distinct peaks (at 650 nm and 720 nm) were seen in the spectra and the excitation spectra from these peaks indicated two

distinct populations. Exciting the fluorophore at longer wavelength (excitation 650 nm) resulted in single peak around 750 nm.

All these results indicate that there might be two major contributing species of LDS 798 in membrane that can result from the orientation of the fluorophores in the membrane. This dimorphic pattern which, shifts when excited with 650 nm light, might also be due to the 'red edge effect'. It has been reported for various fluorophores and generally results in a broad emission peak due to no distinct spectral separation between two interacting species. But in this case, two distinct peaks are visualized.

8.2 Results and Discussion

8.2.1 *Cellular imaging*

The experiments with SUV indicated the excitation and the emission range that was helpful for imaging cells. For the cellular imaging experiments, excitation of 470 nm was used and 650 nm long-pass filter was used before detector, unless otherwise mentioned. Various cell lines were used. These include normal cell lines such as NIH 3T3 and HEK 293T and cancer cell lines such as MDA MB 231, MCF-7 (breast cancer); Hela (cervical cancer); SKOV-3 (ovarian cancer).

Images in Figure – 8.1 show comparison of images of cells stained with LDS 798 and cells treated with DMSO alone. At the settings used to image cells stained with LDS 798, no significant background signal was noticed. LDS 798 emission has been found to shift at least 100 nm towards longer wavelengths from absorption peak in SUV experiments (Figure 7.6). Autofluorescent species in cells that are excited by 470 nm or 635 nm excitation do not have such a huge Stokes shift. Thus, it was expected that settings used for imaging would easily filter both laser line and the autofluorescence from the detected signal without affecting LDS 798

fluorescence. Moreover, the laser power between 50-100 nW was sufficient to excite LDS 798 localized in cells. Low laser excitation is beneficial for live cell imaging as photoproducts are not produced in large amounts in these cases and long-term imaging is feasible.

Labeling cells with LDS 798 gave rise to a punctate pattern with weak staining at the plasma membrane region and no staining in the nuclear region. The punctate pattern of fluorescence signal indicates that LDS 798 might be localized selectively in some intracellular compartment rather than non-specifically distributed throughout the cell. LDS 798 fluorescence was not seen in the nuclear region in any case indicating that this dye does not cross the nuclear membrane.

8.2.2 *Cell viability*

Effect of LDS 798 on cellular viability was checked by MTT assay. The results of cell viability assay showed (Figure – 8.2) that after 24 hours of treatment there is no adverse effect of the dye up to 0.5 μM. Cell viability dropped around 80% in the cells treated with higher concentrations and exposed to LDS 798 for 24 hours.

8.2.3 LDS 798 localization in cells

To check whether the selective staining pattern changes with decrease in concentration of the dye, images with 500 nM LDS concentration were compared with images with 2 nM concentration of LDS 798. Figure – 8.3 shows that there is no apparent change in distribution of signal indicating that the fluorescence pattern is independent of concentration of dye. Thus it can be inferred that the staining pattern observed in these cells is not due to non-specific distribution of LDS 798.

8.2.4 *Correlation of excitation wavelength and cellular fluorescence*

As the experiments with SUVs showed spectral changes upon shifting the excitation towards longer wavelength, it was necessary to check whether the longer wavelength excitation have an effect on localization of LDS fluorescence in cells. The fluorescence image showed a significant signal from the plasma membrane associated fraction which was not seen evidently with 470 nm excitation. This indicates that the LDS 798 subpopulation associated with membrane is more efficiently excited by long wavelength excitation. The basis of this differential signal due to difference in excitation is still not clear, but it has a potential to be studied for understanding membrane dynamics.

Lifetime imaging was also used to understand the punctate distribution of the dye. Lifetime images show that plasma membrane bound fraction and the intracellular fractions have two very distinct average lifetime values. The mean lifetime of plasma membrane bound fraction is around 2.2 nsec, whereas, the intracellular fraction has a lifetime of 1.2 nsec.

8.2.5 *Studying the origin of LDS 798 cellular entry*

To check whether the intracellular fraction of LDS 798 originated from the plasma membrane fraction we blocked membrane endocytosis using actin polymerization inhibitor, cytochalasin D [78, 79]. Treatment of cytochalasin D had no effect on any of the two identified LDS 798 sub-population though the cellular architecture was severely impaired. This suggest that the intracellular sub population of LDS 798 is not associated with membrane trafficking vesicles and LDS 798, most probably, diffuses into the cells rather than being transported due to its association with the cell membrane.

8.3 Figures

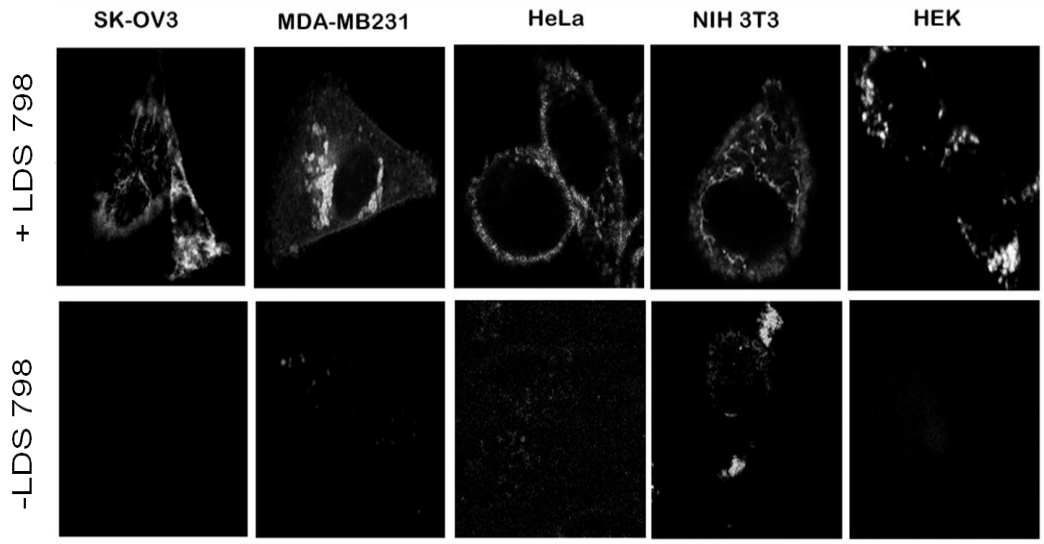

Figure 8.1: Live cell imaging of various cell lines with LDS 798. Live cells retained LDS 798 even after culture media with LDS 798 was replaced by normal media. Retention was in specific regions giving rise to the punctate staining pattern. Cells that were not stained with LDS 798 did not show any significant fluorescence with same imaging set-up indicating the signal - noise ratio of staining was very high.

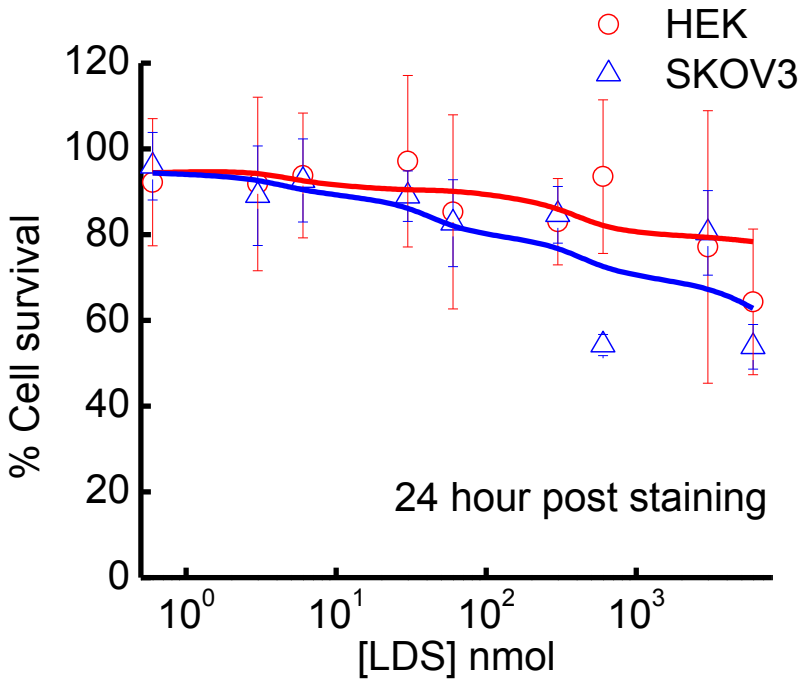

Figure 8.2: Effect of LDS 798 on the cell viability. MTT assay was performed with Human embryonic Kidney (HEK) cells and ovarian cancer (SKOV-3) cell lines. Different concentrations of LDS 798 was added to the cells and incubated for 24 hours. The results indicate that up to 50 nM the effect of the dye on cells were non-lethal.

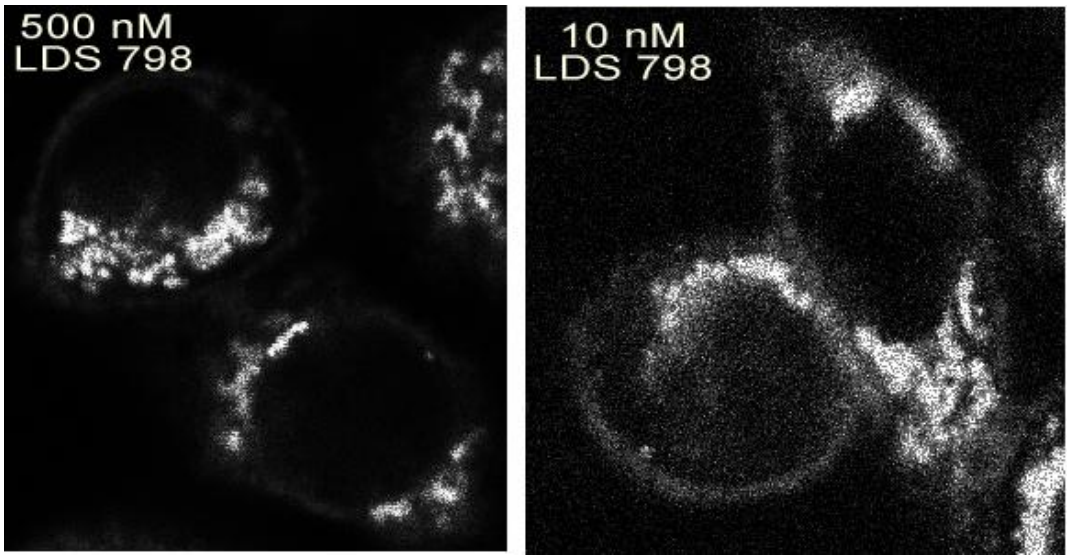

Figure 8.3: Effect of LDS 798 localization on its concentration. Images of MCF-7 cells stained with 500nM of LDS 798 (left) and 10nM of LDS 798 (right). Intracellular and periplasmic localization of LDS 798 can be visualized. These images confirm that imaging with LDS can be successfully performed even with 10nM concentration of the dye. The settings used for imaging ensured that there was no signal from autofluorescent moieties of the cells.

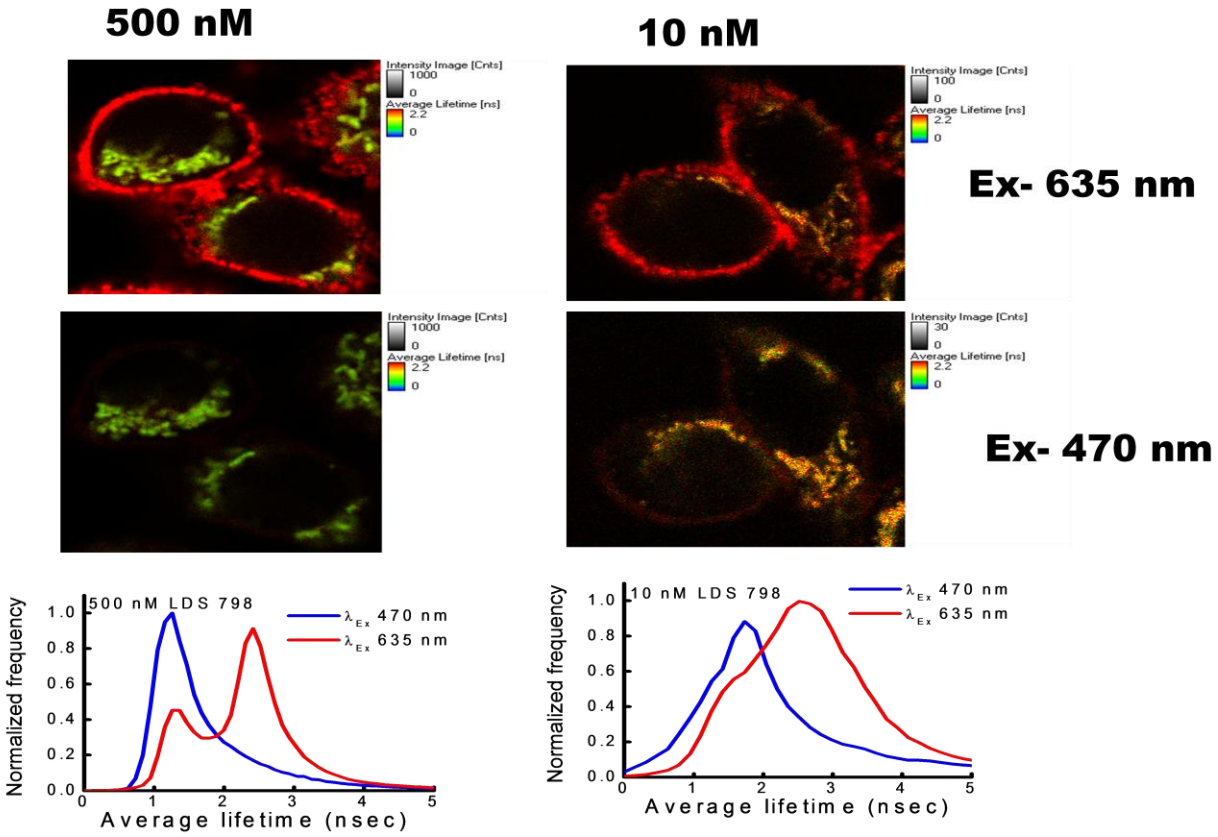

Figure 8.4: Fluorescence lifetime imaging of HeLa cells stained with LDS 798. Lifetime images show two LDS 798 populations with distinct lifetimes a) periplasmic population with average lifetime of 2.2 nsecs and intracellular population with average lifetime of 1.1-1.2 nsec (bottom panel graphs). With excitation 635 nm (red laser), the periplasmic LDS 798 population was easily visualized along with the intracellular punctate population (top panels). Switching to excitation 470 nm minimized the contribution of the periplasmic population (middle panels). Both populations were visualized even when stained with 10 nM LDs 798 (left panels).

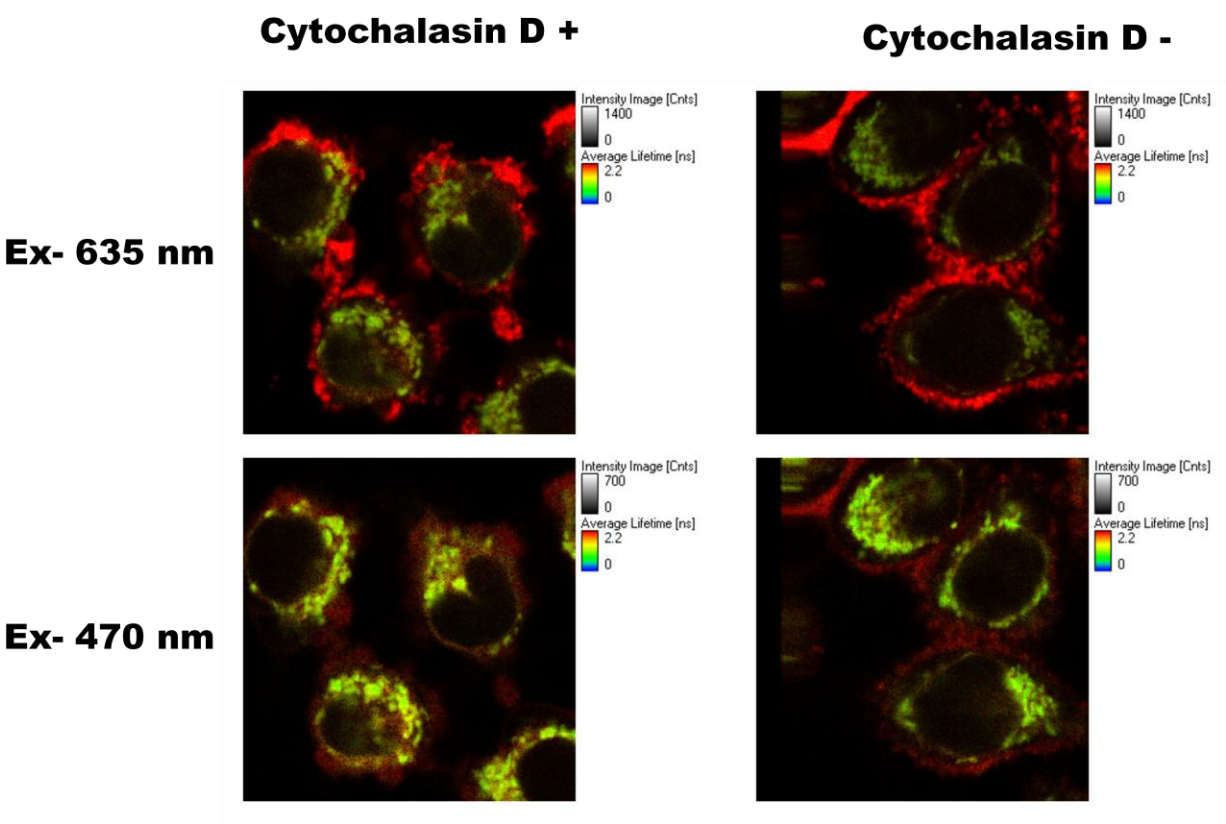

Figure 8.5: Two populations of LDS 798 are not due to membrane recycling. Cytochalasin D, inhibitor of actin assembly and membrane trafficking, treatment to the HeLa cells did not affect the localization of two LDS 798 population (comparing left panels to right panels). This indicates that LDS 798 is not internalized through membrane recycling, but diffuses inside the membrane.

CHAPTER – 9

APPLICATION OF FLIM AND FLCS TECHNIQUES WITH SOLVATOCHROMIC DYES TO DETECT BIOMEDICALLY RELEVANT PROCESSES *IN VITRO* AND *IN SITU*

<u>Specific Aim 3:</u> To apply lifetime-based imaging techniques and fluctuation based correlation techniques with LDS 798 staining for application based studies.

9.1 Rationale

Solvent sensitive fluorescence of LDS 798 can be useful in understanding the local environment around it. With advanced spectroscopic/imaging techniques these changes can be quantified. The goal of this chapter is to evaluate whether LDS 798's solvent sensitivity and compatibility in staining live cells can be useful to address biomedically relevant questions.

Styryl dyes like LDS 798 show change in their fluorescence signal due to solvent effect. Conventionally the change in fluorescence intensity is monitored via ratiometric changes in intensities[5, 20]. However, even in ratiometric studies, where change in intensity is correlated to change of local environment polarity, intensities can also vary due to local changes in fluorophore concentration. Effect of solvent reflects also on the fluorescence decay profile of the fluorophore[23]. In the last decade, fluorescence lifetime imaging microscopy (FLIM) has been applied for studying protein-protein interaction based on Forster Resonance Energy Transfer (FRET) [80-83]. The same instrumentation can be used to study change in lifetime patterns of styryl

dyes in cells. As the cellular environment, especially the membrane polarity, is indicative of various physiological and pathological processes[18, 19], fluorescence lifetime signal from cells stained with styryl dyes can provide depth of information about those processes.

LDS 798 has a very similar structure to ASP dyes; the major difference being the presence of a bulkier quinolinum ring than the pyridinium ring [44, 48]. The quinolinum ring is a part of the core and contributes to the fluorescence properties rather than localization of the dye. In that case, the criteria generated by studying the ASP dyes [42, 73] can be used to predict localization of LDS 798. According to those criteria, LDS 798 should localize in mitochondria. The goal is to test whether LDS can be used as mitochondrial marker. In addition, LDS 798 has high probability of responding fluoremetrically to the electrgenic environment of mitochondrial membrane due to electrochromic nature of styryl group. Thus, the goal is to measure changes in mitochondrial potential via fluorescence lifetime changes of LDS 798 localized in the mitochondria, using FLIM. Mitochondrial depolarization is a early marker for apoptosis. So, the final goal is to test whether lifetime approach with LDS 798 will be useful to measure change in mitochondrial polarization in intact cells during apoptosis.

Hydrophobic nanoparticles are being used heavily for drug delivery purposes [67] and characterization of their size is an important parameter for pharmacokinetics. Usually electron microscopy and scattering patterns are used to measure the particle sizes. But, electron microscopy is an elaborate procedure and requires imaging and statistical expertise, while particle scattering is unreliable when there is minute trace of clumping.

Fluorescence correlation spectroscopy (FCS) has emerged as a reliable technique to estimate the bulk of the nanoparticles under investigation [72, 84]. This technique measures the lateral diffusion

of the unperturbed system with particles of nanometer dimension. Particle size can be estimated and compared if there is prior information about the shape of the particles. FCS analysis of particles stained with LDS 798 can be an alternate method for characterization of particle size.

These assays are rapid and can separate individual particles from aggregated ones due to their diffusion patterns.

9.2 Results and discussion

9.2.1 Application of FLIM approach.

9.2.1.1 *Identifying the intracellular localization*.

To identify the sub-cellular structures where LDS 798 is localized an exhaustive literature search and co-localization experiments were done. It was suggested in the literature that cationic molecules with bulky hydrophobic group and can diffuse the cell membrane are localized in the mitochondria due to its very high negative membrane potential [20, 21, 55]. To check whether LDS 798, that possesses similar chemical features, is localized in mitochondria of the cell we performed colocalization experiments with LDS 798 and known mitochondria specific dye rhodamine 123. Rhodamine 123 and its derivatives like tetra-methyl rhodamine have been frequently used for tracking mitochondria [5, 17, 18]. Rhodamine 123 is very specific for mitochondria and has a partial cationic property with bulky aromatic structure[21]. In cells with active mitochondria it is segregated to mitochondrial matrix. Once mitochondrial potential is lost it partitions out of the matrix and nonspecifically distributed throughout the cell. Ratiometric measurement of Rhodamine 123 intensity has been also used for determining membrane potential.

For the co-localization experiments, 1μM of rhodamine123 and 100nM of LDS 798 were incubated (individually and together) with the cultured cells for 30 minutes. The media containing the dye was replaced with fresh media without any dye and imaging was done. Control experiments showed that the fluorescence intensity overlap of one dye on other dye's detector was less than 1%. For intensity imaging, this was subtracted. For lifetime imaging further filtering was done on the basis of the known lifetime of these fluorophore.

The intensity images of cells co-stained with both the dyes show that rhodamine 123 and LDS 798 co-localize on similar subcellular structures (Figure- 9.1) indicating that LDS 798 might be localized in the mitochondria. The average lifetime analysis of lifetime images further supported the notion (Figure- 9.2). Fluorescence lifetime of rhodamine 123 was much shorter in presence of LDS 798 (mean lifetime of 2.4 nsec, n=14) than in its absence (mean lifetime 3.1 nsec, n=14). This decrease in lifetime is seen during quenching or FRET[23, 81]. The concentration of rhodamine 123 applied for live cell imaging does not lead to its saturation and self-quenching[18]. Moreover, both test and control samples had same concentration of rhodamine 123. This result led to the conclusion that decrease in rhodamine 123 fluorescence lifetimes is not due to self-quenching. No interaction between rhodamine 123 and LDS 798 was observed in cuvette experiments with solution of these dyes. Thus, they are not natural interactors. The only circumstance that can lead to decrease in rhodamine 123 lifetime is through FRET when LDS 798 is in extreme proximity. In cells that might happen between two non-interacting molecules only when these two molecules are in same subcellular compartment.

Another approach was used to further substantiate the sub-cellular localization of LDS 798. Extent of FRET of Rhodamine 123 FRET in presence of unbleached LDS 798 and bleached LDS 798 was measured. LDS 798 was bleached with high intensity (~100 μW power) 635 nm laser.

Rhodamine 123 molecule does not absorb energy of that wavelength and hence it is not excited or photobleached. Average lifetime of rhodamine 123 increased upon bleaching of LDS 798 indicating decrease in FRET (Figure- 9.3 , bottom panel).

Another effect observed during photobleaching experiment was the distribution of rhodamine 123. The dye was distributed throughout the cell body non-specifically (Figure- 9.3, top panel images). Prior literature reveals this pattern of rhodamine 123 localization is seen when mitochondria is depolarized[61]. It appears that, photobleahing of LDS 798 resulted in mitochondrial depolarization. Photobleaching leads to formation of photoproduct radical[61]. These radicals can injure the mitochondria if they are locally produced. Thus, to begin with LDS 798 has to be localized in or around mitochondria to induce mitochondrial depolarization on photobleaching.

9.2.1.2 *LDS 798 lifetime imaging for mitochondrial functional assay*

To further corroborate the co-localization and FRET experiments, functional assays were carried out. Treatments that alter mitochondrial polarization were administered and the effect on LDS 798 fluorescence (distribution, intensity and lifetimes) was observed.

Initially, experiments with isolated functional mitochondria were done and spectral changes and change in intensity of LDS 798 in response to common mitochondrial inhibitors, such as rotenone, carbonyl cyanide p-[trifluoromethoxy]-phenyl-hydrazone (FCCP), and sodium azide (NaN_3) was recorded (Figure 9.4). Upon addition of mitochondrial extract in aqueous solution of LDS 798, both the absorption and emission spectra and fluorescence intensity changed and the change was similar to that seen with SUVs. On addition of inhibitors the LDS 798 intensity dropped, but no effect was seen in the fluorescence spectra (Figure 9.4). None of the inhibitors

affected the LDS 798 fluorescence in absence of mitochondrial extract. These results indicate that LDS 798 responds to mitochondrial membrane potential. Rotenone and NaN_3 are known mitochondrial electron transport chain (ETC) inhibitors whereas FCCP is an uncoupler[1]. Blocking the complex and uncoupling the oxidative phosphorylation eventually results in low proton gradient at inter-membrane space[1]. Our experiments indicate that LDS 798 fluorescence intensity responds to this change.

The next step was to check whether these responses can be replicated in intact cells. This was critical for practical application of LDS 798 based cell staining. Also, another question that needed to be answered was the counter-intuitive response of LDS 798. A decrease in proton concentration can be loosely related to decrease in environment polarity and in this case, it should lead to increase in LDS fluorescence. But, our steady state measurement of intensity showed a drop in intensity. Thus, to check the paradoxical nature of the results, lifetime based imaging was performed.

Lifetime based imaging (Figure 9.5) showed that though intensity of LDS 798 decreases on addition of mitochondrial uncoupler FCCP in cell culture, LDS 798 lifetime distribution shows a change on peak lifetime. Lifetime peak shifted from 1.2 nsec to 1.5 nsec indicating though the fluorescence lifetime of LDS 798 is increasing due to decrease in proton gradient, the low proton gradient also result in decrease of local concentration of LDS 798 that ultimately is indicated by the drop of intensity. The images support these inferences. As the LDS 798 labels the mitochondria of the cells, upon addition of FCCP, the punctate staining pattern is lost and the dye is not selectively located, though it does not cross the nuclear membrane.

To confirm these results similar experiment was performed with an atypical uncoupler, rottlerin[85]. Various studies have used rottlerin to induce autophagy, but some studies indicate that rottlerin acts as an uncoupler[85, 86]. We tested the effect of rottlerin on LDS 798 fluorescence (Figure 9.6). Treatment of rottlerin did not result in diffuse pattern of distribution of LDS 798, but the fluorescence lifetime of the dye was affected. The lifetime distribution histogram showed that treatment of rottlerin to cells result in two peaks. Both these peaks were distinct from that seen in control. The longer peak was at the same as seen with FCCP treatment. The shorter peak might be due to contribution of small highly quenched population of LDS 798. Thus, rottlerin treatment proves that LDS 798 responds to altered mitochondrial potential.

9.2.1.3 *Correlating mitochondrial functional assay to apoptotic pathway*

Apoptosis and various apoptotic agents affect mitochondrial integrity. This has been documented by release of mitochondrial protein cytochrome-c in the cytoplasm that eventually forms apoptosome[19, 52]. Release of cytochrome-c is thought to be due to formation of pores in mitochondrial membrane by pro-apoptotic proteins. These pores also lead to release of ions and thus disrupt the mitochondrial potential[19]. As LDS 798 can sense the change in membrane potential, it was interesting to check whether they respond to an apoptotic signal. Tumor necrosis factor α (TNF-α) is a known apoptotic agent that has been shown to cross-talk with mitochondrial apoptotic pathway[19, 52]. Thus the effect of TNF on LDS 798 lifetime changes was measured.

The lifetime images of MCF-7 cells (sensitive to TNF-α treatment) were recorded at different intervals after TNF-α treatment (Figure 9.7). After 7 hours of treatment, significant number cells had depolarized mitochondria (as seen via LDS 798 staining and lifetime imaging). The

proportion of cells increased with time. At 9 hours post treatment (when cytochrome-c is seen in cytosol) upto 80% cells were identified having depolarized mitochondria. These observations indicate that lifetime imaging of LDS 798 in live cell mitochondria can be used as an early indicator in mitochondria mediated apoptosis.

9.2.2. Application of FLCS

Positive log P value of LDS 798 and manifold increased quantum yield of LDS 798 in non-aqueous solvents prompted to the hypothesis that in an aqueous solution with SUV, LDS 798 fluorescence signal will preferentially be associated with the SUVs. Thus, LDS 798 fluorescence signal can be used to characterize the diffusion profile of these sub-micron particles. The diffusion pattern of the detected LDS 798 molecules, associated with the nanoparticles, can correspond to size of the particles and can be significantly different from those that are free and weakly fluorescent. We decided to test the hypothesis using single point fluorescence lifetime correlation spectroscopy. Figure 9.8 (bottom) and 9.9 (bottom) show the correlation profile and the burst profile of the measurements. Table – 2 shows the average number of particles and the diffusion coefficient of LDS 798 in pure phospholipid vesicles (Figure- 9.8), reconstituted rHDL and nanoparticles with reconstituted 5A peptide (Figure- 9.9).

The FCS results were in agreement with dynamic light scattering results measured independently with the same batch of nanoparticles (Table-2). The traces measured, showed very high fluctuations (Figure 9.8, bottom) corroborating that correlation originated from the phospholipid vesicle bound LDS 798 molecules. The signal from the Free LDS 798 in water was very weak and was characterized by poor correlation and fast diffusion rates typcal of free dyes (Figures – 9.8, bottom and 9.9, bottom).

These nanoparticles were shown to have a mean diameter of <20 nm (Table- 9.1) and contained egg yolk phosphatidyl choline, cholesterol, cholesteryl oleate and either apolipoprotein A-I protein (in rHDL) or an apolipoprotein mimetic peptide (termed as 5A peptide in the Figures). These polypeptide components are required for structural integrity of the synthetic/reconstituted lipoprotein particles. Addition of rHDL, containing either apo A-I or the 5A peptide, in aqueous solution of LDS 798 led to a mild red shift in absorption spectra and strong blue shift in emission spectra (Figure 9.9). The fluorescence intensity increased upon addition of the respective nanoparticles to the dye. The change in fluorescence spectrum of LDS 798 in presence of rHDL and peptide nanoparticles suggest alterations in their surface charge, possibly due to conformational change in the polypeptide components as the lipid ingredients of both preparations were identical. The smaller HDL like particle was observed to have a relatively slow diffusion rate (Table – 9.1). However, this trend was consistent in all 3 sets of experiments performed. This decrease in diffusion may be due to the incorporation of ApoA1 or the mimetic peptide that increases the density of the particle and slows down its Brownian motion. These results indicate that FCS can be used to study the diffusion, and hence size, of the submicron lipid structures using solvatochromic fluorescence properties of LDS 798. Fluorescence correlation studies with LDS 798 dyes indicate that it can be used to study hydrophobic structures with relatively easy staining protocol. Advanced correlation techniques have been developed and can be used to study aggregation pattern inside a cell.

9.3 Table

Table 9.1- Size distribution, Diffusion coefficient and detected concentrations of the lipid based small unilamelar vesicles and nanoparticles.

Sample	Size distribution (nm)	Diffusion coefficient ($\mu m/sec^2$)	Detected concentration (nM)
Free LDS 798	**-**	**199± 25**	
SUVs (pure)			
DMPC	**55.4 (98%)** **2100 (2%)**	**3.28±0.5**	**19.1**
DMPG	**56.4 (96%)** **295 (4%)**	**3.79±1.1**	**0.25**
Nanoparticles (mixed lipids)			
rHDL NP	**43 (100%)**	**2.0± 0.3**	**15.2**
Peptide NP	**34 (100%)**	**3.1±0.5**	**11.1**

9.4 Figures

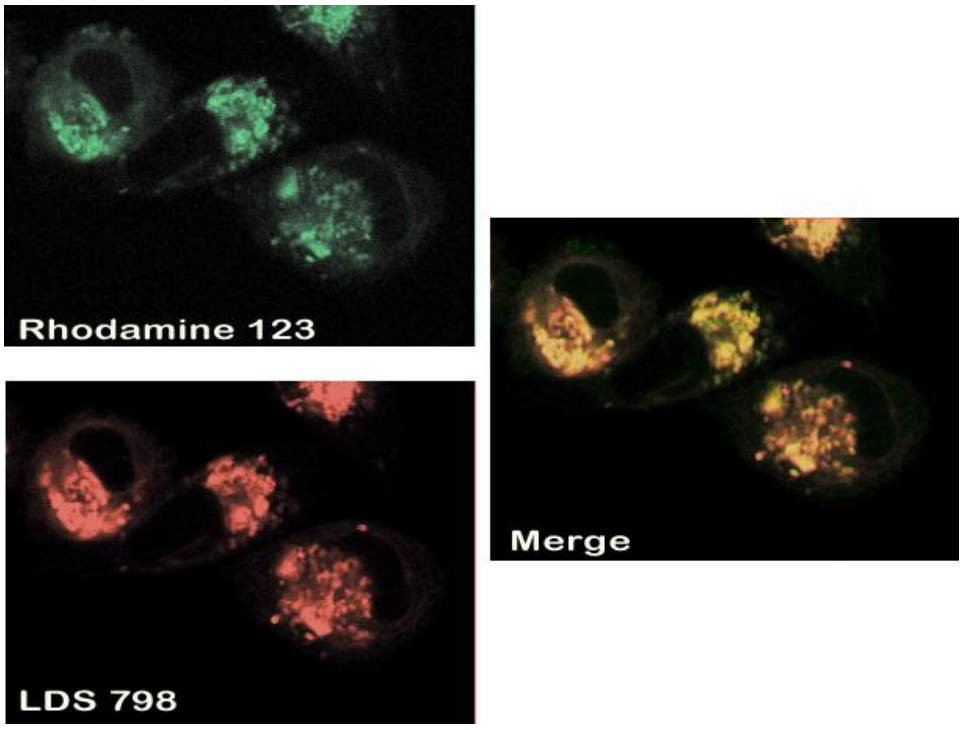

Figure 9.1: Colocolization of LDS 798 with mitochondria specific dye, Rhodamine 123. MDA - MB-231 cells were stained with both LDS 798 and Rhodamine 123 and the fluorescence from the dyes were detected on separate detectors. A bandpass filter, 582 bp75, was placed before the rhodamine detector to detect fluorescence between 545 nm and 620 nm. A longpass 650 filter was placed before LDS 798 detector to detect fluorescence signal of waves more than 650 nm. 470 nm laser was used to excite both the dyes. The intensity signal was collected and a false color image was generated. The merged figure on right was achieved by superposition of the false color images.

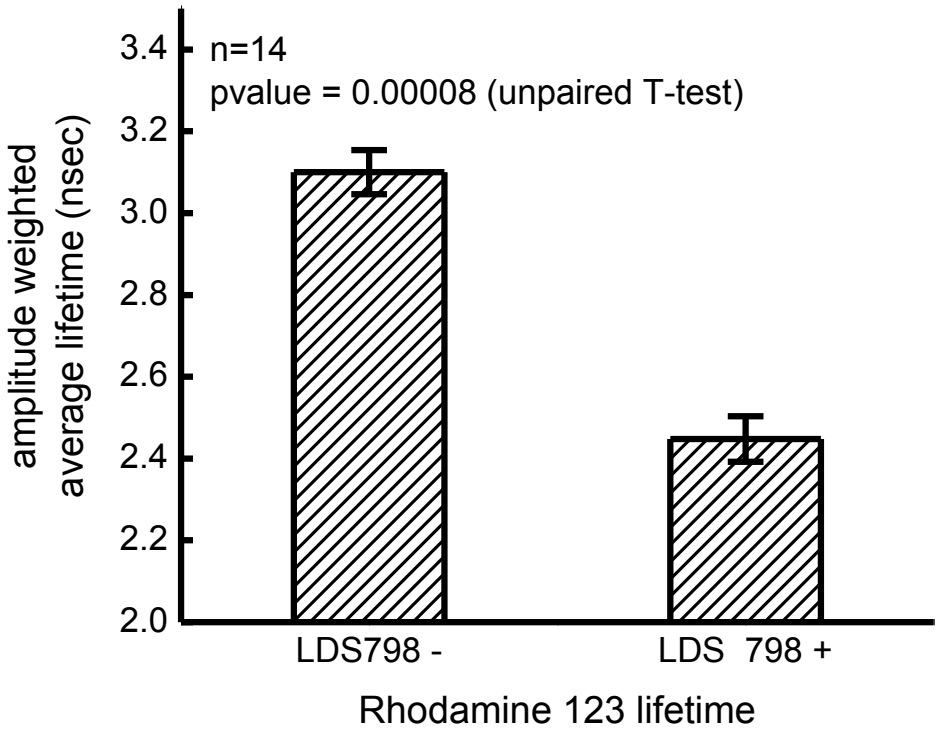

Figure 9.2 – Lifetime tagged images indicate Rhodamine 123 and LDS 798 are in close proximity inside the cells. Lifetime of rhodamine 123 in HeLa cells in presence and absence of LDS 798 were calculated from the images. Average lifetime of rhodamine 123 decreased in presence of LDS 798 indicating that energy transfer is taking place with rhodamine 123 as a donor and LDS 798 as acceptor. As energy transfer can take place when molecules are ~10 nm apart, it can be inferred that two dyes are in close proximity and thus in mitochondrial region.

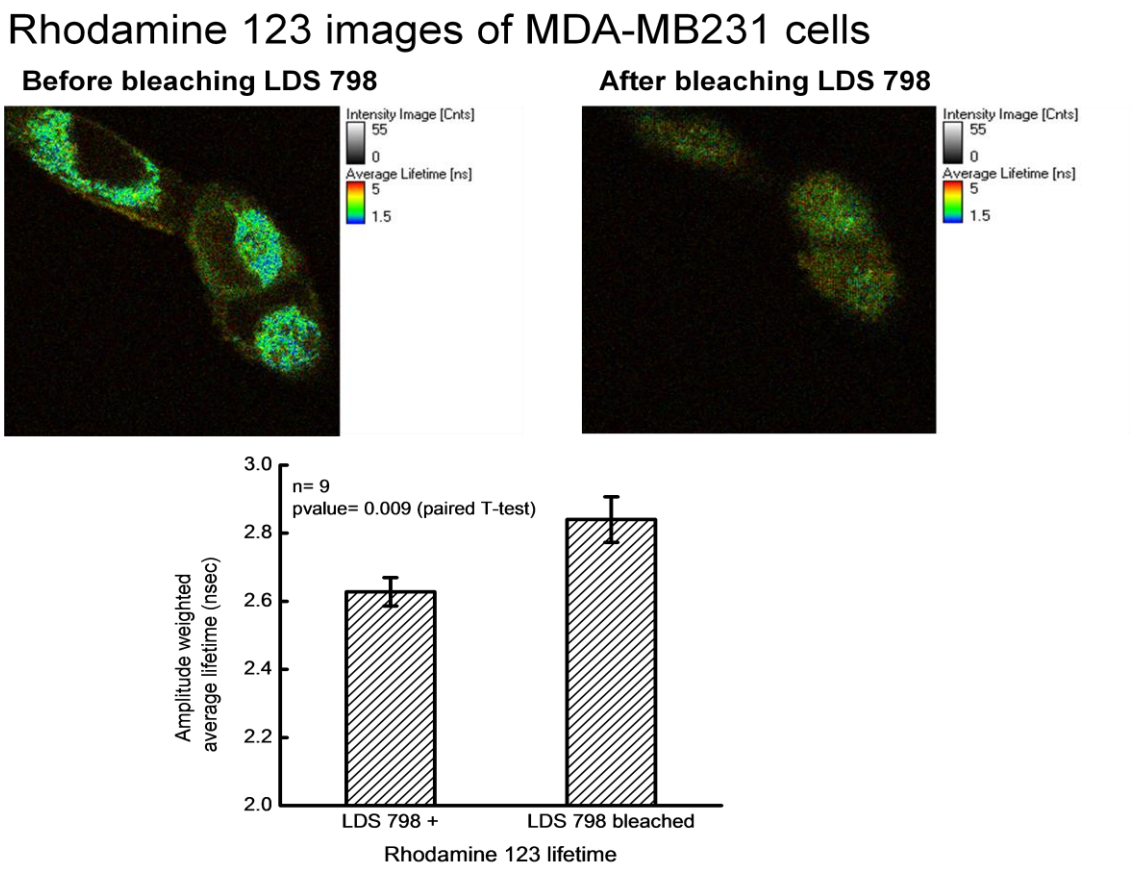

Figure 9.3 – Photobleaching of LDS 798 results in recovery of rhodamine 123 lifetime and loss of mitochondrial membrane potential. Photbleaching LDS 798 in MDA-MB 231 cells co-stained with LDS 798 and rhodamine 123 leads to a) increase in rhodamine 123 lifetime (seen in bottom panel graph) without significant increase in its intensity , and b) nonspecific distribution of rhodamine123 (seen in images of top panels) that is usually observed when mitochondrial potential is lost. These results indicate that photoproduct of LDS 798 locally affects the mitochondria, further supporting the hypothesis that LDS 798 localizes in mitochondria.

A)

B)

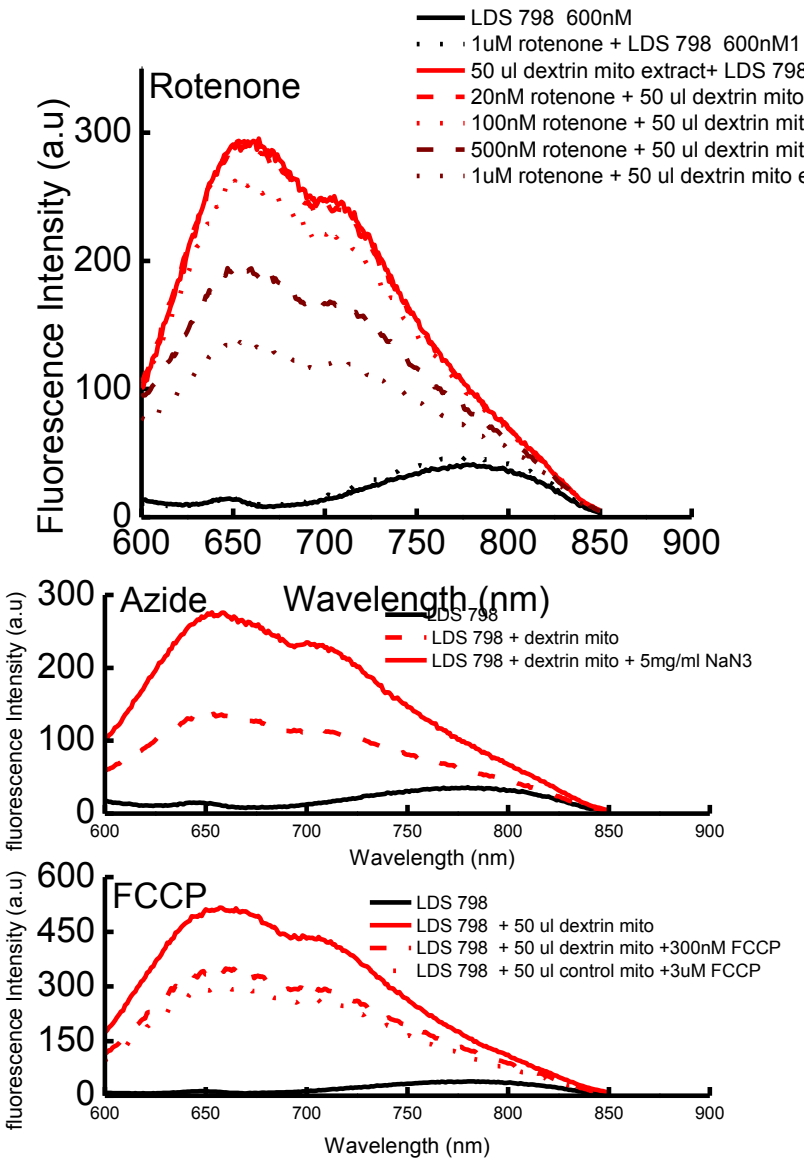

Figure 9.4 – Effect of mitochondrial ETC inhibitor and uncouplers on LDS 798 fluorescence in a mitochondrial suspension. Effect of Rotenone (A) and FCCP and Sodium azide (B) on LDS intensity can be seen. Though the inhibitors do not specifically affect LDS signal, LDS intensity drops when the inhibitors are added in mitochondrial suspension. Indicating LDS 798 actually senses mitochondrial depolarization induced by these inhibitors.

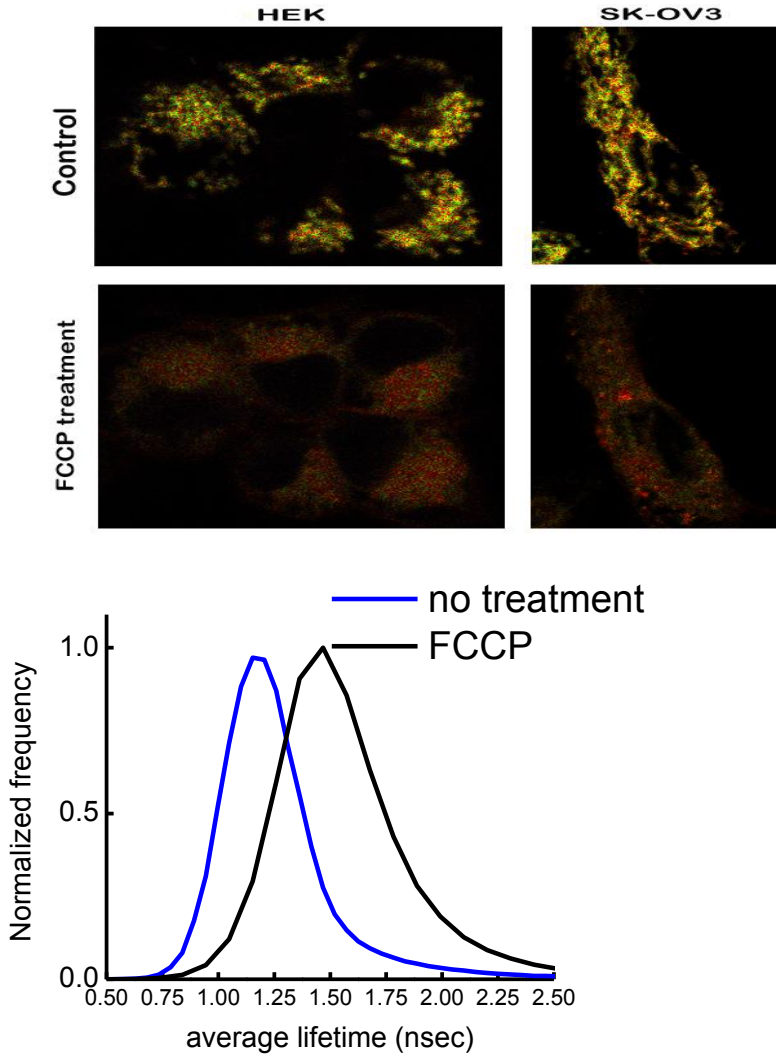

Figure 9.5 - Mitochondrial uncoupler FCCP treatment to cells affect the lifetime distribution of LDS 798. Cells in an optical field were imaged before and after FCCP treatment (termed as 'control' and 'FCCP treatment' respectively and colored according to their average fluorescence lifetime. Average fluorescence lifetime distribution shifted to right indicating increase in fluorescence lifetime, though the intensity dropped. The experiment was done with HEK, SKOV-3 (shown), MDA-MB231 and MCF-7 cells (not shown) and results were reproducible in all the cell lines.

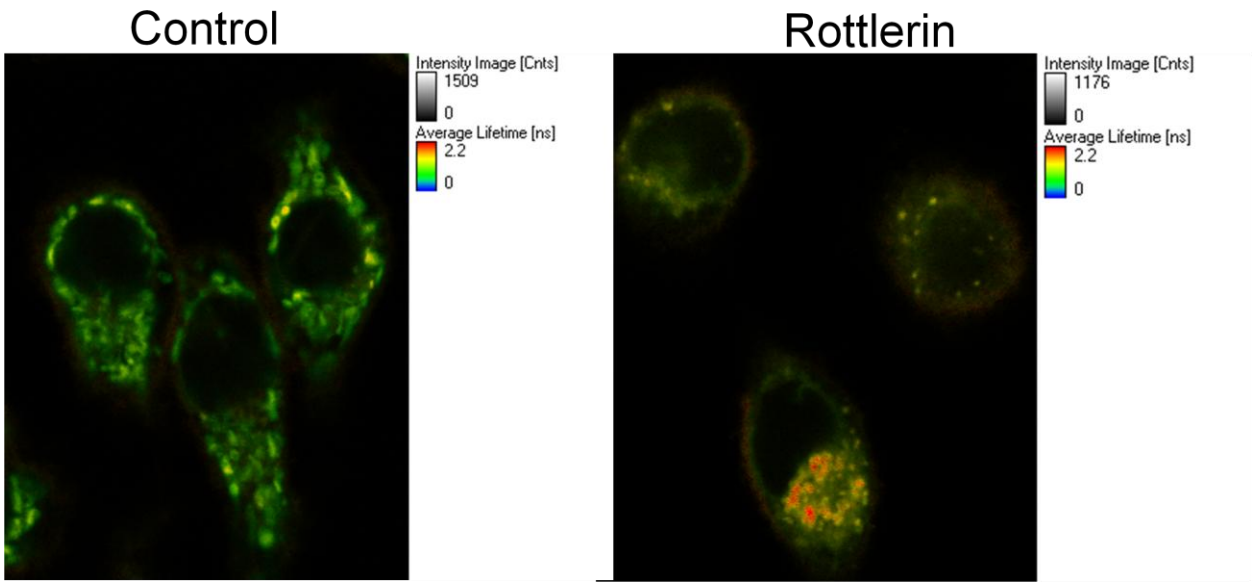

Figure 9.6 –Average lifetime of LDS 798 increased on treatment of cells with rottlerin. This indicates that the response seen with FCCP was not a special case. Mitochondrial uncoupling leads to increase in LDS 798 fluorescence lifetime.

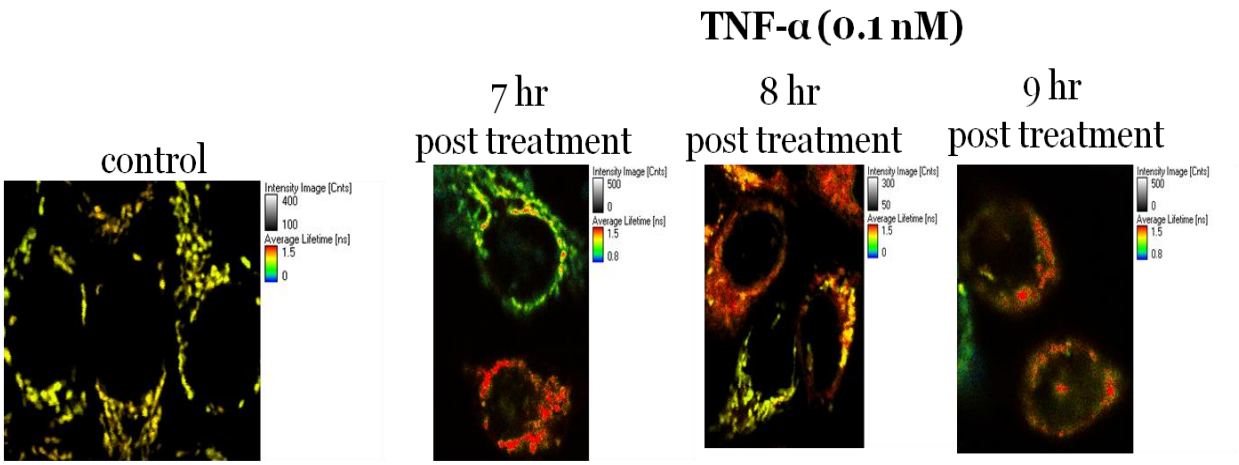

Figure 9.7- Apoptotic signals can be studied by changes in LDS 798 lifetimes in intact live cells. TNF- α treatment amplifies apoptosis in MCF-7 cells via mitochondria apoptotic pathway. Its earliest marker is the release of cytochrome c from mitochondrial interstitial space into the cytosol. Cytochrome c release has been observed 9 hours post-TNF treatment. Here, images of live MCF-7 cells show mitochondrial depolarization as seen by change in LDS 798 lifetimes. The depolarization can be seen in individual cells even at 7 hours post TNF treatment indicating LDS 798 lifetime imaging in intact cells can be an early marker of mitochondria related apoptotic pathways.

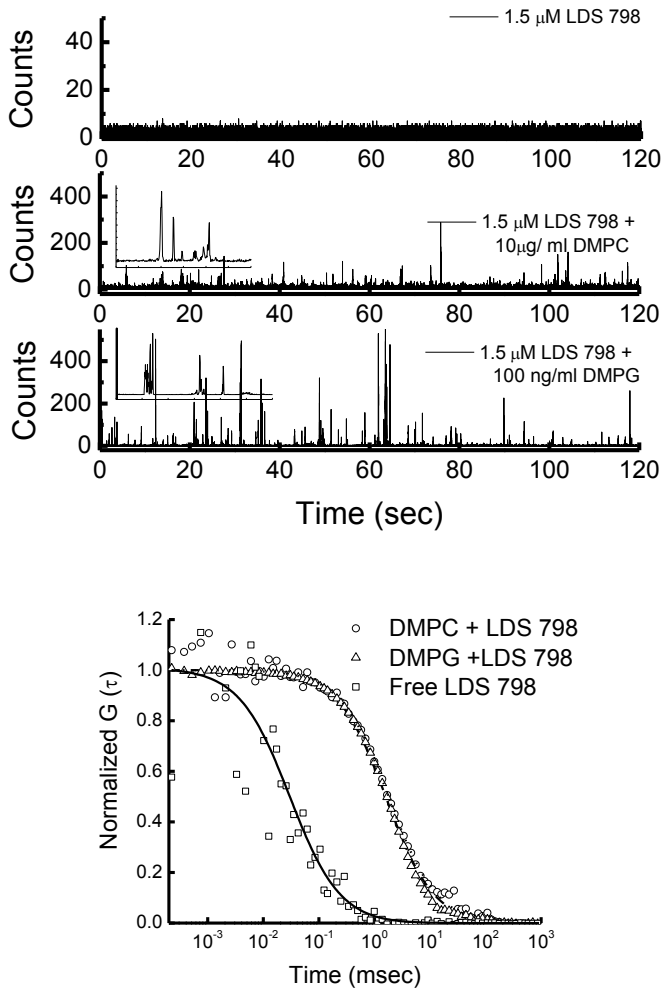

Figure 9.8 - FLCS in identification of SUV using LDS 798 staining. Time trace (top) from aqueous solution of LDS 798 in absence and presence of SUVs (DMPC and DMPG). Correlation patterns (bottom) can be calculated from the time trace data that indicate in presence of SUV the diffusion of LDS 798 resembles a macromolecule.

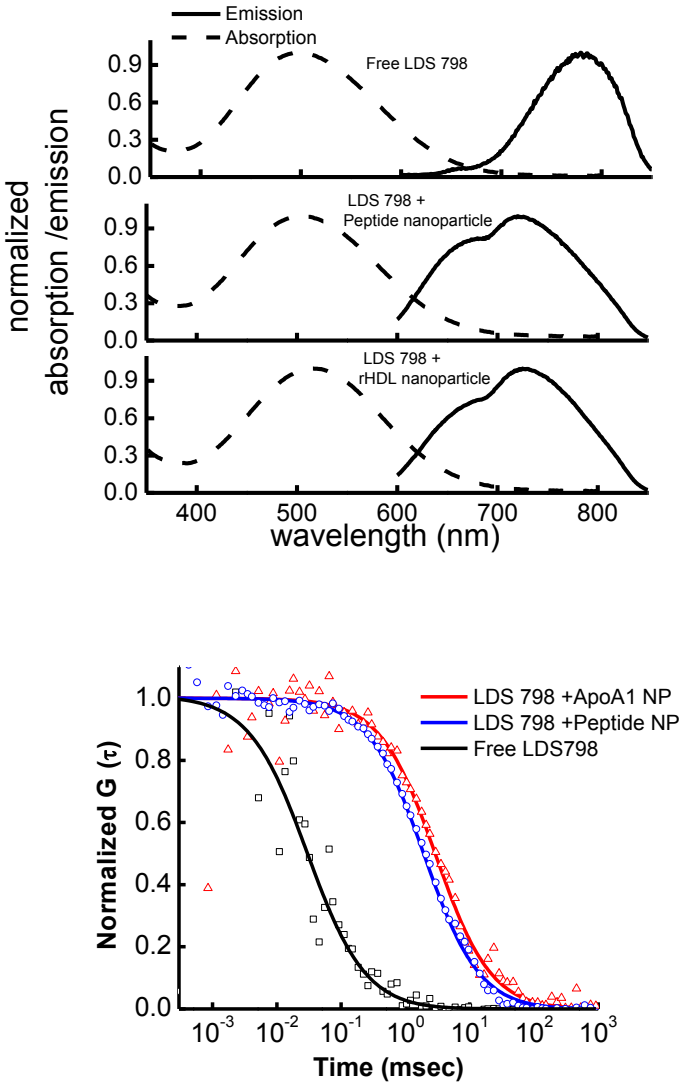

Figure 9.9 – Spectral and aucorrelation profile of LDS 798 bound to lipid nanoparticles rHDL and pep5A nanoparticles (peptide NP). Both measurements indicate that the presence of nanoparticle can be detected by these techniques. Moreover by autocorrelation profile diffusion pattern of the nanoparticles can be calculated. As diffusion coefficient is an index of the volume, change in volume can be estimated by FCS.

CHAPTER 10

CONCLUSION

Solvent sensitive fluorophores have been used to study processes like protein folding, DNA intercalation, action potential and phase state transformation. Our study deals with application of fluorescence in estimating changes in mitochondrial polarization (potential). A near-infra red dye styryl-11 or LDS 798 was used for the study. Solubility and partition of LDS 798 in polar and non-polar solvents was measured. The solvatochromic properties of LDS 798 were characterized and the magnitude change in its dipole moment after excitation was estimated. Effect of solvent polarity on quantum yield and fluorescence lifetime was recorded. Results show increase in fluorescence intensity when amphipathic molecules (detergents and small unilamellar vesicles) were introduced to aqueous solution of LDS 798. All these observation indicate that this NIR dye is solvatochromic, but it also dissolves well in water and aqueous environment. The fluorescence signal is extremely weak in aqueous environment, but increases when amphipathic environment is introduced. Thus change in fluorescence depends upon the dielectric of local environment.

Cellular experiments show that LDS 798 can stain live cells and the signal is beyond 650 nm (near infra-red range). Signal from LDS population in plasma membrane and in mitochondria can be seen. But both populations respond to different excitation wavelength and have a unique fluorescence lifetime profile. Fluorescence lifetime imaging can be used to segregate these two populations. FLIM is also sensitive to change in mitochondrial depolarization and can be used to estimate mitochondrial status in intact cells. As mitochondrial activity status is correlated to

physiological processes like apoptosis and aging, and pathological diseases like alzheimer's, LDS 798 based lifetime imaging of intact cells can be an early marker for these conditions. This approach can provide an alternate detection technique in fields like biotechnology; where evaluating health of cells in continuous or batch bioprocessor is vital; or pharmaceutics; where effect of drug on induction or rescue of mitochondria dependent apoptosis has to be evaluated.

Near infra red dyes have been successfully used for small animal imaging. LDS 798 can be an interesting dye to be used for this type of imaging. Further studies are needed to check LDS 798's applicability in non-invasive whole body imaging of experimental animals.

BIBLIOGRAPHY

1. Nelson DL, Cox MM, Lehninger AL. *Principles of Biochemistry*. Freeman New York; 2008.

2. Alberts, B., Bray,D., Lewis, J., Raff, M., Roberts K., Watson, J.D.,. *Molecular Biology of the Cell.* ; 1994.

3. Bagatolli LA, Ipsen JH, Simonsen AC, Mouritsen OG. An outlook on organization of lipids in membranes: Searching for a realistic connection with the organization of biological membranes. *Prog Lipid Res*. 2010.

4. Demchenko AP, Mély Y, Duportail G, Klymchenko AS. Monitoring biophysical properties of lipid membranes by environment-sensitive fluorescent probes *Biophys J*. 2009;96:3461-3470.

5. Demchenko AP, Yesylevskyy SO. Nanoscopic description of biomembrane electrostatics: Results of molecular dynamics simulations and fluorescence probing. *Chem Phys Lipids*. 2009;160:63-84.

6. Singer SJ, Nicolson GL. The fluid mosaic model of the structure of cell membranes. *Science*. 1972;175:720-731.

7. Vereb G, Szöllősi J, Matko J, et al. Dynamic, yet structured: The cell membrane three decades after the Singer–Nicolson model. *Proc Natl Acad Sci U S A*. 2003;100:8053.

8. Engelman DM. Membranes are more mosaic than fluid. *Nature*. 2005;438:578-580.

9. Nag K. *Structure and Dynamics of Membranous Interfaces*. Wiley; 2008.

10. Leventis PA, Grinstein S. The distribution and function of phosphatidylserine in cellular membranes. *Annual review of biophysics*. 2010;39:407-427.

11. Lindner R, Naim HY. Domains in biological membranes. *Exp Cell Res*. 2009;315:2871-2878.

12. Cohen LB, Salzberg BM. Optical measurement of membrane potential. *Ergeb Physiol*. 1978;83:35-88.

13. Xu C, Loew LM. The effect of asymmetric surface potentials on the intramembrane electric field measured with voltage-sensitive dyes *Biophys J*. 2003;84:2768-2780.

14. Nakano Y, Makino K, Ohshima H, Kondo T. Analysis of electrophoretic mobility data for human erythrocytes according to sublayer models. *Biophys Chem*. 1994;50:249-254.

15. Makino K, Taki T, Ogura M, et al. Measurements and analyses of electrophoretic mobilities of RAW 117 lymphosarcoma cells and their variant cells. *Biophys Chem*. 1993;47:261-265.

16. Vassar PS, Levy EM, Brooks DE. Studies on the electrophoretic separability of B and T human lymphocytes. *Cell Immunol*. 1976;21:257-271.

17. Smith J. Potential-sensitive molecular probes in membranes of bioenergetic relevance. *Biochim Biophys Acta*. 1990;1016:1-28.

18. Solaini G, Sgarbi G, Lenaz G, Baracca A. Evaluating mitochondrial membrane potential in cells. *Biosci Rep*. 2007;27:11-21.

19. Shakibaei M, Schulze-Tanzil G, Takada Y, Aggarwal BB. Redox regulation of apoptosis by members of the TNF superfamily. *Antioxidants & Redox Signaling*. 2005;7:482-496.

20. Chen LB. Mitochondrial membrane potential in living cells. *Annu Rev Cell Biol*. 1988;4:155-181.

21. Rottenberg H. Membrane potential and surface potential in mitochondria: Uptake and binding of lipophilic cations. *J Membr Biol*. 1984;81:127-138.

22. Rottenberg H. The measurement of membrane potential and deltapH in cells, organelles, and vesicles. *Methods Enzymol*. 1979;55:547-569.

23. Lakowicz JR. *Principless of Fluorescence Spectroscopy.* 2nd ed. New York: Kluwer Academic / Plenum Publisher; 1999.

24. Kasha M. Characterization of electronic transitions in complex molecules. *Discuss Faraday Soc*. 1950;9:14-18.

25. Lakowicz J. Fluorescence spectroscopy of biomolecules, in encyclopaedia of molecular biology and molecular medicine. . 1995.

26. Stokes G. On the change of refrangibility of light.--no. II. *Philosophical Transactions of the Royal Society of London*. 1853;143:385-396.

27. Lippert E. Spektroskopische bestimmung des dipolmomentes aromatischer verbindungen im ersten angeregten singulettzustand. *Zeitschrift für Elektrochemie, Berichte der Bunsengesellschaft für physikalische Chemie*. 1957;61:962-975.

28. Slavik J. Anilinonaphthalene sulfonate as a probe of membrane composition and function. *Biochim Biophys Acta*. 1982;694:1-25.

29. McRae E. Theory of solvent effects on molecular electronic spectra. frequency shifts. *J Phys Chem*. 1957;61:562-572.

30. Suppan P. Invited review solvatochromic shifts: The influence of the medium on the energy of electronic states. *J Photochem Photobiol A*. 1990;50:293-330.

31. Mataga N, Kaifu Y, Koizumi M. Solvent effects upon fluorescence spectra and the dipolemoments of excited molecules. *Bull Chem Soc Jpn*. 1956;29:465-470.

32. Kawski A. On the estimation of excited-state dipole moments from solvatochromic shifts of absorption and fluorescence spectra. *ZEITSCHRIFT FUR NATURFORSCHUNG A*. 2002;57:255-262.

33. Rettig W. Charge separation in excited states of decoupled systems-TICT compounds and implications regarding the development of new laser dyes and the primary process of vision and photosynthesis. *Angewandte Chemie International Edition in English*. 1986;25:971-988.

34. Cohen LB, Salzberg BM, Davila HV, et al. Changes in axon fluorescence during activity: Molecular probes of membrane potential. *J Membr Biol*. 1974;19:1-36.

35. Ross WN, Salzberg BM, Cohen LB, et al. Changes in absorption, fluorescence, dichroism, and birefringence in stained giant axons: Optical measurement of membrane potential. *J Membr Biol*. 1977;33:141-183.

36. Gupta RK, Salzberg BM, Grinvald A, et al. Improvements in optical methods for measuring rapid changes in membrane potential. *J Membr Biol*. 1981;58:123-137.

37. Loew LM. Characterization of potentiometric membrane dyes. *Adv Chem Ser*. 1994;235:151.

38. Bublitz GU, Boxer SG. Stark spectroscopy: Applications in chemistry, biology, and materials science. *Annu Rev Phys Chem*. 1997;48:213-242.

39. Clarke RJ, Kane DJ. Optical detection of membrane dipole potential: Avoidance of fluidity and dye-induced effects. *Biochimica et Biophysica Acta (BBA)-Biomembranes*. 1997;1323:223-239.

40. Loew L, Simpson L. Charge-shift probes of membrane potential: A probable electrochromic mechanism for p-aminostyrylpyridinium probes on a hemispherical lipid bilayer. *Biophys J*. 1981;34:353-365.

41. Gross E, Bedlack Jr RS, Loew LM. Dual-wavelength ratiometric fluorescence measurement of the membrane dipole potential. *Biophys J*. 1994;67:208-216.

42. Betz WJ, Mao F, Smith CB. Imaging exocytosis and endocytosis. *Curr Opin Neurobiol*. 1996;6:365-371.

43. Fluhler E, Burnham VG, Loew LM. Spectra, membrane binding, and potentiometric responses of new charge shift probes *Biochemistry (N Y)*. 1985;24:5749-5755.

44. Brackmann U, ed. *Lambdachrome Laser Dyes Data Sheets*; 1994.

45. Berezin MY, Lee H, Akers W, Achilefu S. Near infrared dyes as lifetime solvatochromic probes for micropolarity measurements of biological systems. *Biophys J*. 2007;93:2892-2899.

46. Luchowski R, Kapusta P, Szabelski M, et al. FRET-based picosecond lifetime reference for instrument response evaluation *Measurement Science and Technology*. 2009;20:095601.

47. Luchowski R, Gryczynski Z, Sarkar P, et al. Instrument response standard in time-resolved fluorescence *Rev Sci Instrum*. 2009;80:033109.

48. Jędrzejewska B, Pietrzak M, Pączkowski J. Solvent effects on the spectroscopic properties of styrylquinolinium dyes series *J Fluoresc*. 2010;20:73-86.

49. Scheffler IE. A century of mitochondrial research: Achievements and perspectives. *Mitochondrion*. 2001;1:3-31.

50. Nicholls DG, Ward MW. Mitochondrial membrane potential and neuronal glutamate excitotoxicity: Mortality and millivolts. *Trends Neurosci*. 2000;23:166-174.

51. Mammucari C, Rizzuto R. Signaling pathways in mitochondrial dysfunction and aging. *Mech Ageing Dev*. 2010.

52. Lu D, Huang J, Basu A. Protein kinase Cϵ activates protein kinase B/Akt via DNA-PK to protect against tumor necrosis factor-α-induced cell death. *J Biol Chem*. 2006;281:22799.

53. Narendra D, Tanaka A, Suen DF, Youle RJ. Parkin is recruited selectively to impaired mitochondria and promotes their autophagy. *Science's STKE*. 2008;183:795.

54. Johnson LV, Walsh ML, Chen LB. Localization of mitochondria in living cells with rhodamine 123. *Proc Natl Acad Sci U S A*. 1980;77:990.

55. Dykens JA, Stout AK. Assessment of mitochondrial membrane potential in situ using single potentiometric dyes and a novel fluorescence resonance energy transfer technique. *Methods Cell Biol*. 2001;65:285-309.

56. Emaus RK, Grunwald R, Lemasters JJ. Rhodamine 123 as a probe of transmembrane potential in isolated rat-liver mitochondria: Spectral and metabolic properties. *Biochimica et Biophysica Acta (BBA)-Bioenergetics*. 1986;850:436-448.

57. Juan G, Cavazzoni M, Sáez GT, O'Connor JE. A fast kinetic method for assessing mitochondrial membrane potential in isolated hepatocytes with rhodamine 123 and flow cytometry. *Cytometry*. 1994;15:335-342.

58. Nakayama S, Sakuyama T, Mitaku S, Ohta Y. Fluorescence imaging of metabolic responses in single mitochondria. *Biochem Biophys Res Commun*. 2002;290:23-28.

59. Mitra K, Lippincott-Schwartz J. Analysis of mitochondrial dynamics and functions using imaging approaches. .

60. Jester JV, Andrews PM, Matthew Petroll W, Lemp MA, Dwight Cavanagh H. In vivo, real-time confocal imaging. *J Electron Microsc Tech*. 1991;18:50-60.

61. Mitra K, Lippincott-Schwartz J. Analysis of mitochondrial dynamics and functions using imaging approaches *Curr Protoc Cell Biol*. 2010;Chapter 4:Unit 4.25.1-21.

62. Rottenberg H, Wu S. Quantitative assay by flow cytometry of the mitochondrial membrane potential in intact cells. *Biochimica et Biophysica Acta (BBA)-Molecular Cell Research*. 1998;1404:393-404.

63. Cossarizza A, Baccaranicontri M, Kalashnikova G, Franceschi C. A new method for the cytofluorometric analysis of mitochondrial membrane potential using the J-aggregate forming lipophilic cation 5, 5', 6, 6'-tetrachloro-1, 1', 3, 3'-tetraethylbenzimidazolcarbocyanine iodide (JC-1). *Biochem Biophys Res Commun*. 1993;197:40-45.

64. Plasek J, Vojtiskova A, Houstek J. Flow-cytometric monitoring of mitochondrial depolarisation: From fluorescence intensities to millivolts. *Journal of Photochemistry and Photobiology B: Biology*. 2005;78:99-108.

65. Schmidt R, Wurm CA, Jakobs S, Engelhardt J, Egner A, Hell SW. Spherical nanosized focal spot unravels the interior of cells. *Nature Methods*. 2008;5:539-544.

66. Celli A, Gratton E. Dynamics of lipid domain formation: Fluctuation analysis. *Biochim Biophys Acta*. 2009.

67. Lacko AG, Nair M, Paranjape S, Mooberry L, McConathy WJ. Trojan horse meets magic bullet to spawn a novel, highly effective drug delivery model *CHEMOTHERAPY-BASEL-*. 2006;52:171.

68. Matz C, Jonas A. Micellar complexes of human apolipoprotein AI with phosphatidylcholines and cholesterol prepared from cholate-lipid dispersions. *J Biol Chem*. 1982;257:4535.

69. Jonas A. Reconstitution of high-density lipoproteins *Methods Enzymol*. 1986;128:553-582.

70. Short J, Roberts J, Roberts D, Hodges G, Gutsell S, Ward R. Practical methods for the measurement of log P for surfactants *Ecotoxicol Environ Saf*. 2010.

71. Magde D, Elson E, Webb W. Thermodynamic fluctuations in a reacting system—measurement by fluorescence correlation spectroscopy *Phys Rev Lett*. 1972;29:705-708.

72. Magde D, Elson EL, Webb WW. Fluorescence correlation spectroscopy. II. an experimental realization *Biopolymers*. 2004;13:29-61.

73. Betz WJ, Mao F, Bewick GS. Activity-dependent fluorescent staining and destaining of living vertebrate motor nerve terminals. *J Neurosci*. 1992;12:363-375.

74. Luchowski R, Sarkar P, Bharill S, et al. Fluorescence polarization standard for near infrared spectroscopy and microscopy *Appl Opt*. 2008;47:6257-6265.

75. Jensen KHR, Rekling JC. Development of a no-wash assay for mitochondrial membrane potential using the styryl dye DASPEI. *Journal of Biomolecular Screening*. 2010.

76. Hranjec M, Kralj M, Piantanida I, et al. Novel cyano-and amidino-substituted derivatives of styryl-2-benzimidazoles and benzimidazo (1, 2-a quinolines. synthesis, photochemical synthesis, DNA binding, and antitumor evaluation, part 3 *J Med Chem*. 2007;50:5696-5711.

77. Jameson DM, Croney JC, Moens PD. Fluorescence: Basic concepts, practical aspects, and some anecdotes. *Methods Enzymol*. 2003;360:1-43.

78. Fang Z, Takizawa N, Wilson KA, et al. The Membrane-Associated protein, supervillin, accelerates F-Actin-Dependent rapid integrin recycling and cell motility. *Traffic*. 2010;11:782-799.

79. Mills JW, Falsig Pedersen S, Walmod PS, Hoffmann EK. Effect of cytochalasins on F-actin and morphology of ehrlich ascites tumor cells. *Exp Cell Res*. 2000;261:209-219.

80. Chen Y, Mills JD, Periasamy A. Protein localization in living cells and tissues using FRET and FLIM. *Differentiation*. 2003;71:528-541.

81. Gautier I, Tramier M, Durieux C, et al. Homo-FRET microscopy in living cells to measure monomer-dimer transition of GFP-tagged proteins. *Biophys J*. 2001;80:3000-3008.

82. Harpur AG, Wouters FS, Bastiaens PI. Imaging FRET between spectrally similar GFP molecules in single cells. *Nat Biotechnol*. 2001;19:167-169.

83. Kinnally KW, Tedeschi H, Maloff BL. Use of dyes to estimate the electrical potential of the mitochondrial membrane. *Biochemistry*. 1978;17:3419-3428.

84. Celli A, Gratton E. Dynamics of lipid domain formation: Fluctuation analysis. *Biochim Biophys Acta*. 2009.

85. Soltoff SP. Rottlerin: An inappropriate and ineffective inhibitor of PKC [delta]. *Trends Pharmacol Sci*. 2007;28:453-458.

86. Soltoff SP. Rottlerin is a mitochondrial uncoupler that decreases cellular ATP levels and indirectly blocks protein kinase Cδ tyrosine phosphorylation. *J Biol Chem*. 2001;276:37986.

APPENDIX A

PUBLISHED ARTICLES ON LDAS 798 BY AUTHUR

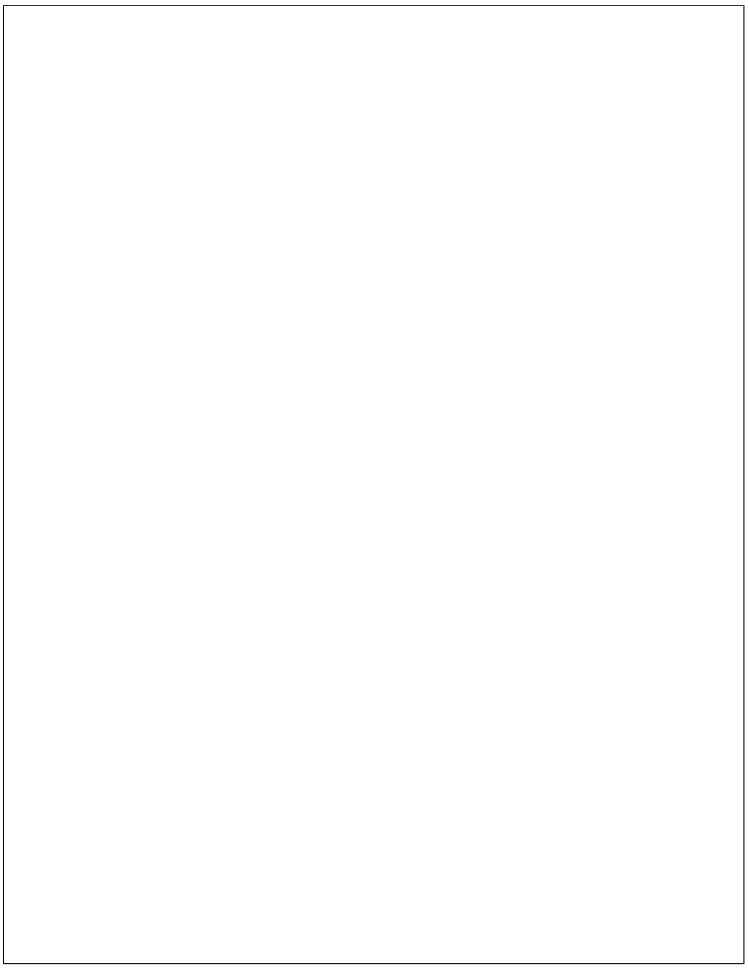

Biophysical Chemistry 153 (2010) 61–69

Contents lists available at ScienceDirect

Biophysical Chemistry

journal homepage: http://www.elsevier.com/locate/biophyschem

Studies on solvatochromic properties of aminophenylstyryl-quinolinum dye, LDS 798, and its application in studying submicron lipid based structure

Pabak Sarkar [a,c,*], Rafal Luchowski [a,c], Sangram Raut [a,b], Nirupama Sabnis [c], Alan Remaley [d], Andras G. Lacko [c], Sanjay Thamake [b], Zygmunt Gryczynski [a,c], Ignacy Gryczynski [a,e,*]

[a] Center for Commercialization of Fluorescence Technologies, University of North Texas Health Science Center, Fort Worth, TX 76107, United States
[b] Department of Biomedical Sciences, University of North Texas Health Science Center, Fort Worth, TX 76107, United States
[c] Department of Molecular Biology and Immunology, University of North Texas Health Science Center, Fort Worth, TX 76107, United States
[d] Department of Laboratory Medicine, National Institute of Health, Bethesda, MD, United States
[e] Department of Cell biology and Anatomy, University of North Texas Health Science Center, Fort Worth, TX 76107, United States

ARTICLE INFO

Article history:
Received 17 September 2010
Accepted 4 October 2010
Available online 13 October 2010

Keywords:
Aminostyryl quinolinum dye
Fluorescence correlation Spectroscopy
Solvatochromism

ABSTRACT

The styryl group of dyes has been used in cellular studies for over 20 years because of their solvatochromic and/or electrochromic properties. Here we report characterization of solubility and solvatochromic properties of a near infra-red styryl dye, styryl 11 or LDS 798. We have extended our studies to small unilamellar vesicles and lipid based nanoparticles and found that solvatochromic properties of this dye used in tandem with fluorescence correlation spectroscopy can be used to efficiently determine the diffusion coefficient and hence the size of the submicron lipid based particles. This technique has the potential to provide essential information about liposomal and vesicular structures and their movement *in vitro* and *in situ*.

Published by Elsevier B.V.

1. Introduction

Styryl dyes have been investigated and used commercially for their solvatochromic/electrochromic properties. Their use as potentiometric dyes is well documented [1,2]. For more than a decade they have also been used to study vesicle trafficking and exocytosis [3,4]. The feature that makes styryl dyes attractive for membrane studies is their spectral response to local electric fields. Also, similar to other solvatochromic dyes, styryl dyes fluoresce strongly in a non-polar environment. They can thus be used as membrane markers in co-localization experiments.

Most of the styryl dyes used for fluorescence studies with biological samples have been aminostylyl pyridinium (ASP) derivatives. Typically, their alkylaminophenyl 'tail' is connected to electron withdrawing pyridinium 'head' group through conjugate bond(s). The tail is responsible for its membrane binding while the cationic head group determines its membrane permeability. The spectral properties are determined generally by the number of aromatic rings and the conjugate bonds that join them [3]. In an aqueous environment, the dielectric properties of water induce high non-radiative decay rates and thus render the molecule non-fluorescent. The free movement of the dye can also lead to increase in non-radiative decay [5]. Once the polarity decreases, the radiative decay becomes substantial and this results in a detectable fluorescence signal. Though there are other factors, including aggregation of the dye in water and charge shift of the dye in the excited state, that may contribute to the spectral characteristics of the dye, solvatochromism still exerts a major impact on the dye's spectral properties [2].

Styryl-11 or LDS 798 (*1-Ethyl-4-(4-(p-Dimethylaminophenyl)-1,3-butadienyl)-quinolinum percholate*) is a styryl compound that contains monocationic quinolinum group instead of the pyridinium group of ASP dyes and has a rather short dialkylaminophenyl 'tail' region [6]. In ethanol its peak absorption is at 580 nm and peak emission is at 770 nm making it a useful near infra-red dye. Near infra-red solvatochromic dyes have been shown to be useful for studying tissues in-vivo [7]. LDS 798 has been used as a laser dye and has a very weak fluorescence in aqueous solution (quantum yield of 0.002 [8]). Previous studies have shown that LDS798 has a very short fluorescence lifetime in water (<20 ps) while its lifetime increases in ethanol and in polymer films [9]. Stoke's shifts have been found to be higher in water than in ethanol. The purpose of this study was to characterize the solvatochromic properties of this aminophenyl styryl quinolinum (ASQ) dye and compare these features with those of established (well studied) ASP dyes. Recent studies on the structure and fluorescence properties of ASQ dyes indicate that their quinolinum group acts as the electron acceptor while the aminophenyl group acts as the electron donor [10]. Our studies show that styryl-11 (LDS 798) retains all the solvatochromic

* Corresponding authors. Sarkar is to be contacted at the Center for Commercialization of Fluorescence Technologies, Department of Molecular Biology and Immunology, University of North Texas Health Science Center, 3500 Camp Bowie Boulevard, Fort Worth, TX 76107, United States. Tel.: +1 11 817 735 0148; fax: +1 11 817 735 2118. Gryczynski, Department of Cell Biology and Anatomy, University of North Texas Health Science Center, 3500 Camp Bowie Boulevard, Fort Worth, TX 76107, United States. Tel.: +1 11 817 735 5471; fax: +1 11 817 735 2118.
E-mail addresses: psarkar@live.unthsc.edu (P. Sarkar), ignacy.gryczynski@unthsc.edu (I. Gryczynski).

0301-4622/$ – see front matter. Published by Elsevier B.V.
doi:10.1016/j.bpc.2010.10.005

properties of ASP and ASQ dyes. The studies described here also indicate that LDS 798 might integrate into the bilayered lipid membrane in multiple orientations due to its bulky aromatic head region and short alkyl tail region.

With the recent advent of advanced fluorescence based technologies, including fluctuation correlation spectroscopy, fluorescence lifetime imaging, generalized polarization microscopy and single molecule detection, styryl dyes can be used to obtain detailed information on complex systems. Solvatochromic dyes, like Lauradan, are being extensively used for correlation spectroscopy and generalized polarization studies of lipid membranes [11] while lifetime based imaging using this group of dyes has a potential to be used for probing excitable cell/tissue samples. One of our goal was to investigate how LDS798 solvatochromism can be used with the modern fluorescence techniques for probing systems of biomedical significance. Thus, we investigated the potential application of LDS 798 to determine the dimensions and movement of submicron lipid-based structures using fluorescence correlation spectroscopy (FCS) that has already been used to study the dynamics of cellular and subcellular structures [11,12]. FCS is markedly more sensitive than similar fluorescence based techniques like fluorescence recovery after photobleaching (FRAP) or fluorescence loss in photobleaching (FLIP). The findings obtained using FCS analysis with LDS 798 fluorescence show that this approach may be particularly appropriate for labeling the lipid based submicron structures and the study of their dynamics.

2. Materials and methods

LDS 798 was purchased from Exciton (Dayton, OH) and used without any further purification. 1,4-dioxane, ethyl acetate, dichloromenthane (DCM), 1-octanol, ethanol, methanol, N,N-dimethyl formammide (DMF), dimethyl sulfoxide (DMSO) were purchased from Sigma-Aldrich or Fluka (St. Louis, MO). 1-Butanol, 2-propanol, acetonitrile and chloroform were purchased from Fisher Scientific (Pittsburgh, PA). All the solvents were spectrphotometric grade. Deionized water used for the experiments was from Millipore distillation system. 1,2-dimyristoyl-*sn*-glycero-3-phospho-(1′-rac-glycerol) (DMPG), 1,2-dimyristoyl-*sn*-glycero-3-phosphocholine (DMPC) was purchased from Avanti polar lipids (Alabaster, AL). sodium dodecyl sulfate (SDS) powder and Triton-X-100 was from Sigma-Aldrich (St. Louis, MO).

2.1. Preparation of phosopholipid bilayers and high density lipoprotein-like nanoparticles

For SUV preparation, stock solution of lipids was prepared in chloroform.

Lipid films were prepared by evaporating the chloroform in inert environment under steady flow of Argon gas. Lipid films were then hydrated with phosphate buffered saline supplemented 500 μM EDTA. After hydration, the samples were sonicated till clarity with 2 minute pulses of sonication with ultrasonic processor UP200H system (Hielscher Ultrasonics GmbH, Germany) followed by resting phase in ice.

The cholate dialysis procedure used, was based on the procedures described for discoidal rHDL particles [13–15]. A mixture of Egg yolk phosphatidyl choline (15 mg), free cholesterol (0.35 mg) and cholesterol oleate (0.15 mg) all in chloroform were dried down under nitrogen. Apo A-1 (5 mg) or ApoA1-mimetic 5A peptide (1 mg) and 3% DMSO were mixed. 14 mg sodium cholate was added and volume was made up to 2 ml with buffer (10 mM Tris, 0.1 M KCl, 1 mM EDTA pH 8.0). The mixture was incubated overnight at 4 °C.

The mixture was then dialyzed against 2 liters of 1X phosphate buffered saline for 48 h with change of buffer every 2 h on the first day, (at least) 3 times and later kept overnight. The mixture was centrifuged for a quick spin and then sterilized by passing through 0.45 μM filter.

The hydrodynamic volume of these SUVs and nanoparticles was estimated using dynamic light scattering Nanotrac Particle Size Analyzer (Nano Track; ISee imaging systems, Raleigh, NC).

2.2. Spectroscopic studies and mathematical models

Extinction coefficient of LDS 798 in ethanol was reported by the manufacturer [6]. Equal amount of LDS 798 was dissolved in equal volume of ethanol, octanol and water. Then, samples were diluted to various concentrations and optical densities were measured in Cary 50 Bio (Varian Inc., Australia) spectrophotometer. The absorptions were plotted as a function of concentration calculated using extinction coefficient of LDS 798 in ethanol.

Partition coefficient (log P) was measured by shake-flask method [16]. In brief, supersaturating the mixture of 1:1 water:octanol with LDS 798 was shaken vigorously at room temperature (~20 °C) overnight and 500 ul aliquots were taken from both water and octanol phase. The aliquots were diluted with their respective solvents and absorption was measured.

For steady state fluorescence spectroscopic measurements, Cary Eclipse spectrofluorometer (Varian Inc., Australia) was used. In most of the measurements the samples were excited with 530 nm light and a 570 nm long-pass filter was used before the detector to minimize the effect due to scattering. For some measurements, like that with small unilamelar vesicles (SUV)s, excitation of 470 nm was used and 530 long-pass filter was used at observation in those cases. Absorption of each sample at 530 or 470 nm were used to correct the difference in fluorescence intensity due to variable excitation. All the samples used had an optical density less than 0.2, but greater than 0.02 at 530 nm. For absorption measurements with SUVs, the scattering due to them was measured and subtracted from the absorption values.

Quantum yield was calculated with cresyl violet in ethanol (quantum yield 0.54) as reference solution, using the equation

$$Q = Q_R \frac{I^* abs_R n^2}{I_R{}^* abs\, n_R^2} \tag{1}$$

Where, Q and Q_R are quantum yields of the sample and reference, I and I_R are the fluorescence intensities area under the curve for the sample and reference, abs is the absorption of the samples at the wavelength that was used to excite the samples and n is the refractive index of the solvents.

For Lippert–Mataga (LM) plot following equations were used to calculate the orientation polarizability, Δf.

$$\Delta f_{LM} = \frac{\varepsilon - 1}{\varepsilon + 2} - \frac{n^2 - 1}{2n^2 + 1} \tag{2}$$

Where, ε is the bulk dielectric permittivity.

Simplified Bilot–Kawski (BK) equations were also used to calculate orientation polarizability and the ratio of excited and ground state dipole moment with following equations

$$f_{BK}(\varepsilon, n) = \frac{2n^2 + 1}{n^2 + 2}\left(\frac{\varepsilon - 1}{\varepsilon + 2} - \frac{n^2 - 1}{n^2 + 2}\right) \tag{3}$$

$$g_{BK}(n) = {}^3/_2 \frac{n^4 - 1}{\left(n^2 + 2\right)^2}$$

$$\Phi_{BK}(\varepsilon, n) = f_{BK}(\varepsilon, n) + g_{BK}(n) \tag{4}$$

$$\begin{aligned} \tilde{\nu}_A - \tilde{\nu}_F &= m_1 \cdot f_{BK}(\varepsilon, n) + const \\ \tilde{\nu}_A + \tilde{\nu}_F &= m_1 \cdot \Phi_{BK}(\varepsilon, n) + const \end{aligned} \tag{5}$$

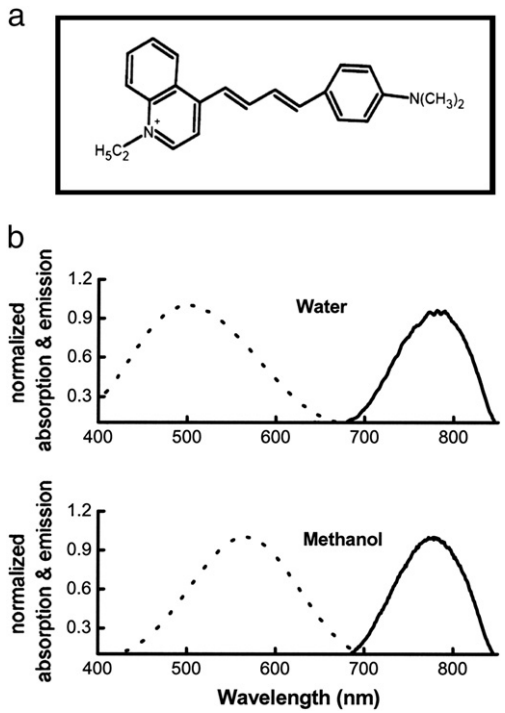

Fig. 1. Initial indications about solvatochromic property of LDS 798. Chemical structure of LDS 798 (styryl-11) (a). Absorption (dotted line) and emission spectra (continuous line) of LDS 798 in ethanol (top) and water (bottom) (b).

$$\frac{\mu_e}{\mu_g} = \frac{m_1 + m_2}{m_2 - m_1} \tag{6}$$

For lifetime measurements, FluoTime 200 (PicoQuant GmbH, Germany) time domain spectrofluorometer was used. This spectrofluorometer contains cooled multi-channel plate detector (Hamamatsu, Japan) and is accessorized with a monochromator at the observation. 470 nm laser diode (LDH-PC-470) was used as the excitation source. This laser diode has a pulse width of <70 ps. The fluorescence decays were fitted with FluoFit version v-4.0 software (PicoQuant GmbH, Germany) using multiexponential deconvolution model

$$I(t) = \int_{-\infty}^{t} IRF(t') \sum_i \alpha_i e^{-\frac{t-t'}{\tau_i}} \tag{7}$$

Where IRF (t′) is the instrument response function at time t′, α is the amplitude of the decay of the ith component at time t and τ_i is the lifetime of the ith component.

Radiative and non-radiative rate constants for LDS 798 in different solvents using following equations

$$Q = \frac{\Gamma}{\Gamma + k_{nr}} \tag{8}$$

$$\tau = \frac{1}{\Gamma + k_{nr}} \tag{9}$$

2.3. Fluorescence lifetime correlation spectroscopy studies

The data for fluorescence lifetime correlation spectroscopy (FLCS) experiments was collected with MicroTime 200 confocal microscope (PicoQuant GmBh, Germany). The methodology using these studies has been described earlier [17]. Briefly, pulsed light from 470 nm solid state laser was focused 10 μm above the cover-slip surface, but inside the drop of the sample solution. 20 μW laser light power for all the FLCS experiments was used. Separate measurements characterizing microscope/objective alignment and features for the confocal volume was performed. For the purpose of confocal volume characterization, 3D raster scanning of fluorescence nanospheres was applied [18,19] that yielded a value of 0.16 fl. Olympus IX71 inverted microscope and Olympus UPlanFL N 100× magnification oil objective, NA = 1.3 was used for the measurements (fluorescence fluctuations). The scattered light was filtered with sets of filters (500 long wavelength pass and 473 RazorEdge, Semrock). Filtered light was focused through 30 μm pinhole to single photon avalanche photodiode (SPCM-AQR-14, Perkin Elmer). Data analysis was performed with SymPhoTime (v. 5.0) software (Picoquant, Germany) and autocorrelation function was defined according the formula:

$$G(\tau) = \frac{\langle \delta I(t) \delta I(t+\tau) \rangle}{\langle \delta I(t) \rangle \langle \delta I(t+\tau) \rangle} \tag{10}$$

Where $\delta I(t)$ and $\delta I(t+\tau)$ are the fluorescence intensity fluctuations from the mean at time t and $t+\tau$, respectively. Auto-correlation curves due to translational diffusion through 3-dimentional Gaussian shaped volume were fitted with following formula [2,3]:

$$G(\tau) = \sum_{i=1}^{n} \rho_i \left(1 + \frac{\tau}{\tau_{Di}}\right)^{-1} \left(1 + \frac{\tau}{\tau_{Di}\kappa^2}\right)^{-1/2} \tag{11}$$

where ρ_i is a contribution of ith diffusion species for total autocorrelation function, τ_{Di} is a diffusion time of ith diffusion species, κ is length (z_o) to diameter (w_o) of the focal volume. On the basis of

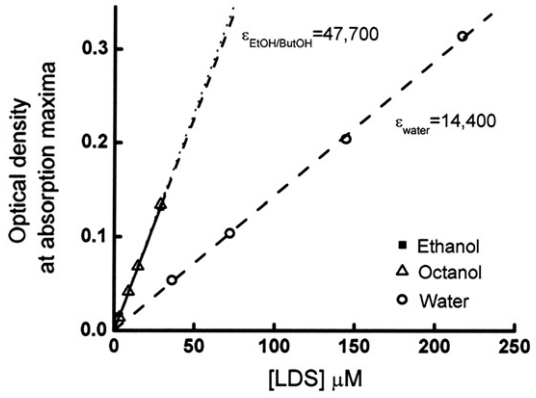

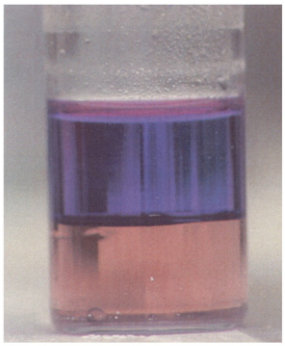

Fig. 2. After factoring its low extinction coefficient in water it was found that LDS 798 partitions adequately in water. Extinction coefficient of LDS 798 in different solvents (a). Partition coefficient of LDS 798 (b).

Table 1
List of solvents, their dielectric constants and refractive indices, solubility profile and, fluorescence properties (spectral shift, quantum yield and average lifetimes) of LDS 798 when it was dissolved in them.

Solvent	Dielectric constant	Refractive index	$\nu_{Abs} - \nu_{Em}$ cm^{-1}	% quantum yield	Average lifetime (ps)
Aprotic					
Dioxane	2.21	1.42	4541.56	3.06	206
Ethyl acetate	6.02	1.37	4903.10	2.02	223
Acetonitrile	36.6	1.34	5265.30	0.23	85
DMF	38.3	1.43	5243.48	0.35	126
DMSO	47.2	1.48	5195.84	0.42	176
Protic					
1-Octanol	10.3	1.43	3426.79	6.11	562
1-Butanol	17.85	1.40	3950.73	2.75	330
n-Propanol	21.65	1.39	4126.76	1.34	205
Ethanol	24.3	1.35	4427.06	0.76	147
Methanol	33.1	1.33	4793.78	0.30	78
Outlier					
Chloroform	4.98	1.45	3108.66	3.21	815
DCM	8.93	1.42	2807.91	3.52	712
Water	78.3	1.33	7205.81	0.08	<50

the fit to the autocorrelation function we determined also the diffusion coefficient D according:

$$D = \frac{w_o^2}{4\tau_D} \tag{12}$$

3. Results and discussion

Styryl dyes have been used extensively for studying membrane dynamics and changes in membrane potential. The aminostyryl pyridinium sub group has also been be successfully used to probe the dynamics of vesicle trafficking in an activity dependent manner [3].

3.1. Solvatochromic characterization of LDS 798

LDS 798 or styryl-11 contains a quinolinum 'head' region which is connected to the dimethylaminophenyl 'tail' via two alternate double bond structures (Fig. 1 top). This structural configuration is quite distinct from that of other well known styryl dyes. While the overall configuration of LDS 798 retains the features responsible for its spectral properties, it has a very short (dimethyl) tail and a bulky (quinolinum) and monocationic head region that is unique to most of the commercially available styryl dyes. In our previously published study, we have observed the difference in Stoke's shift of LDS spectra with ethanol and aqueous medium (Fig. 1 bottom) that led us to study the solvatochromic properties of LDS 798.

Current studies were initiated with qualitative characterization of LDS 798 solubility in solvents of varying polarity and showed that it is weakly soluble or insoluble both in highly hydrophobic solvents like cyclohexane and hydrophilic aqueous solutions. It was noticed that LDS 798, though dissolved slowly in deionized water, was totally insoluble in cyclohexane even after vigorous overnight shaking.

During study of spectral properties of LDS 798, the absorption spectrum was blue shifted in water without any significant spectral broadening (Fig. 1 bottom) ruling out the possibility of LDS 798 self-aggregation. The study of the extinction coefficient of LDS 798 in octanol and water (Fig. 2 left) showed that the extinction coefficient in water deviated significantly from that value reported by the manufacturer (with ethanol as solvent) [6]. Partition experiments, using the shake-flask method and calculated extinction coefficients for LDS in water and octanol, yielded a log P of 0.54 indicating that LDS 798 dissolves in water reasonably well.

To understand the spectral changes due to solvatochromic properties of LDS 798, absorption and emission spectra were measured in solvents of various polarity and refractive indices (Table 1). Next, the Stoke's shift ($\nu_{abs} - \nu_{Em}$ in cm^{-1}) was plotted for each solvent as a function of their respective polarity function. Both Lippert–Mataga (LM) and simplified Bilot–Kawski (BK) models were used to fit the data (Fig. 3) and characterize the solvent effect. Both models indicate that the Stoke's shift change was correlated with the polarity function in aprotic solvents. However, a major observation from these plots was that protic and aprotic solvents both show completely different patterns of Stoke's shifts. This deviation of protic

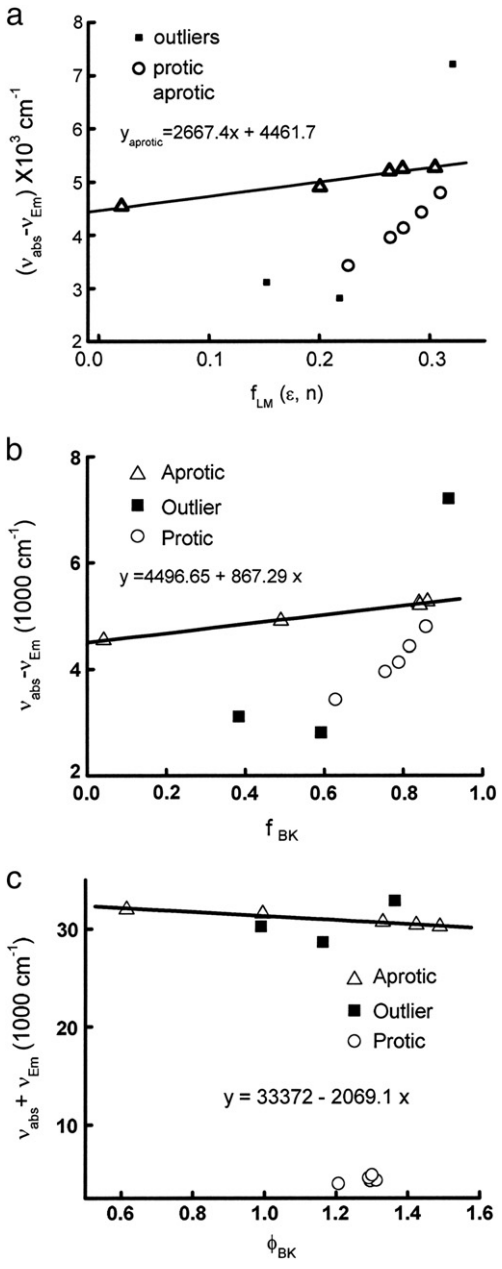

Fig. 3. Solvent relaxation pattern of LDS 798. a) The difference of absorption and emission maxima was plotted as a function of Lippert–Mataga parameter f_{LM} (ε, n). b) The difference of absorption and emission maxima was plotted as a function of Bilot–Kawski parameter f_{BK}(ε, n) and c) the sum of absorption and emission maxima was plotted as function of Bilot–Kawski parameter Φ(ε, n). The protic and aprotic solvent showed a difference in magnitude of solvent relaxation.

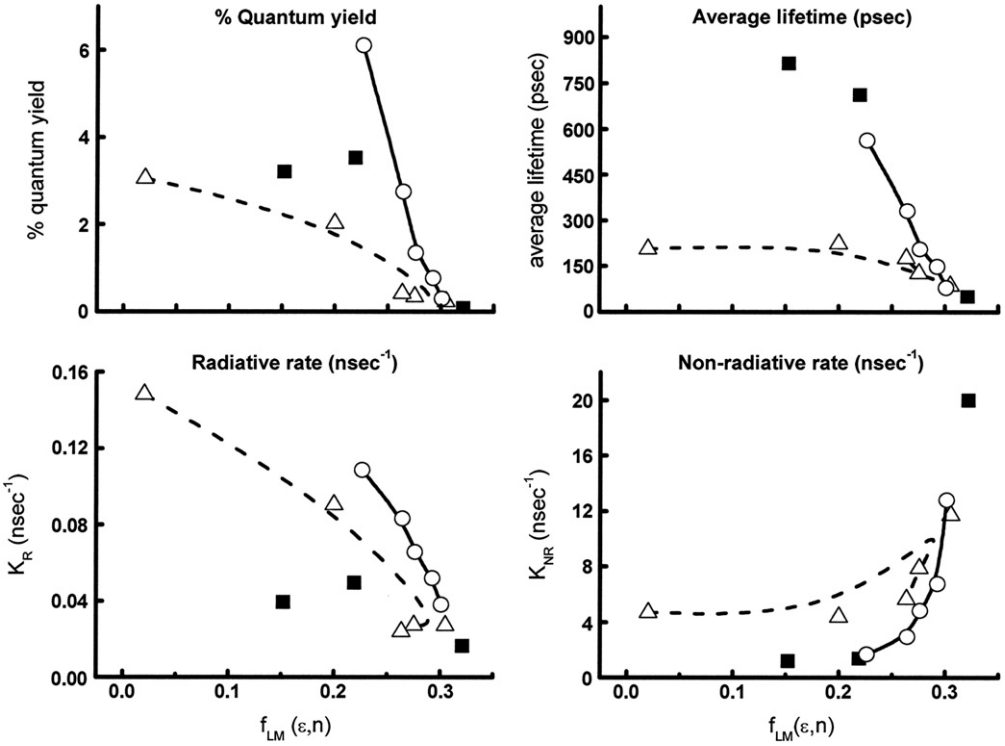

Fig. 4. Solvent induced changes in radiative rates of LDS 798. (Top) The change in quantum yield and fluorescence decay lifetime with change in Lippert's function of dielectric. (Bottom) Non-radiative and fluorescence decay of LDS 798 with change in Lippert's function of dielectric. Δ indicates aprotic solvents, ○ indicates protic solvents and ■ indicates outliers.

solvents has been associated with their tendency hydrogen bonding, aggregation or other specific interaction with the fluorophore [5]. Stoke's shift of LDS 798 in alkyl halides, chloroform and dichloromethane, could not be fitted with protic or aprotic profile in both LM and BK model, suggesting that there might be some specific interactions taking place between the solute and solvent that cannot be taken in to account by these models. Using Bilot–Kawski model and considering that both ground state and excited state dipole moments are parallel, we calculated the excited state dipole moment as 2.44 fold larger than the ground state dipole moment.

For understanding the radiative changes due to solvatochromic fluorescent properties of LDS 798, we measured its quantum yield in different solvents with cresyl violet in ethanol as the reference solution Fig. 4 (top left). We also measured the fluorescence lifetime of LDS 798 in different solvents (Fig. 4 top right). LDS 798 has a maximum quantum yield of ~6% in octanol, whereas its quantum yield was lowest in water (<0.1%). The fluorescence decay profiles showed that the maximum average lifetime was in the sub-nanosecond range (maximum 814 ps in chloroform and <25 ps in water). Radiative and non-radiative rate constants calculated from quantum yields and fluorescence lifetime (Fig. 5 bottom) show that the non-radiative rate constants are two orders of magnitude larger than the radiative decay explaining the major Stoke's shift seen with LDS 798. All these parameters were plotted as a function of LM parameter of polarity (*f*). The response from protic solvents was distinctly different from that of aprotic solvents and this further indicates that H-bonding might have a significant effect in LDS798 spectra and fluorescence intensity (Fig. 5). As observed earlier, LDS 798 fluorescence response was distinctly different in alkyl halide solvents when compared with that of other aprotic solvents.

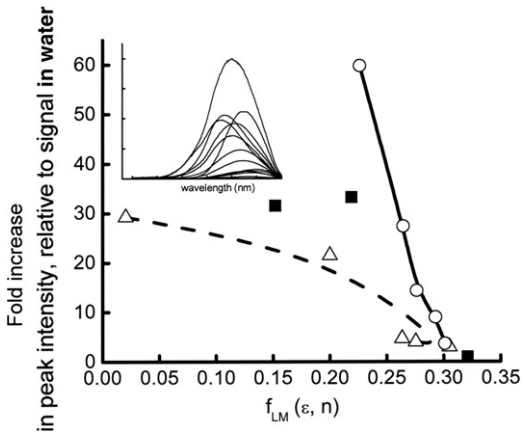

Fig. 5. Effect of polarity on the peak intensity of LDS 798. (Inset) Spectral data of LDS 798 fluorescence in various pure solvents. (Main plot) The peak intensity was plotted with Lippert–Mataga function for protic (o), aprotic (Δ) and other (■) solvents.

The spectral properties of LDS798 determined here are in good agreement with that of reported ASQ dyes [10]. Its absorption spectrum is blue shifted in polar solvent, like water, as seen in other ASQ dyes. The Bilot–Kawski and Lippert–Mataga plots for solvent relaxation show that the Stoke's shift increases linearly as a function of orientation polarizability. The key observation reflected in the plot is the response of aprotic solvents compared with protic solvents. This has been attributed to the formation of hydrogen bonds between the solute and solvent, observed in other systems [5]. Both Lippert–Mataga and Bilot–Kawski models failed to explain the effect of the Stoke's shift in alkyl halide solvents and water indicating that there might be some other specific interactions in addition to polarizability. Significant red shift in fluorescence spectra with increase in solvent polarity indicates that the excited singlet state is stabilized in polar solvents.

3.2. Spectral and radiative changes of LDS 798 fluorescence in micelles and liposomes

After characterizing the spectral and radiative properties of LDS 798 in solvents with different polarity, studies were performed on its

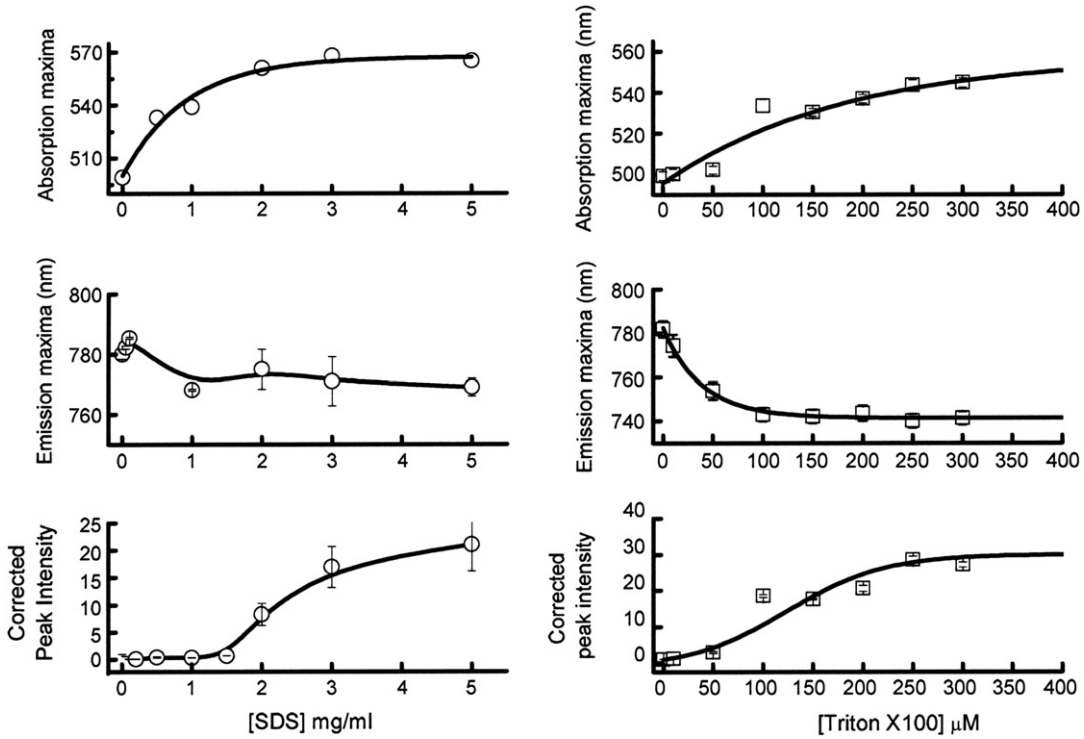

Fig. 6. Effect of detergents on the fluorescence signal of LDS 798 in aqueous solution. Addition of detergent in aqueous solution of LDS 798 resulted in red shift of absorption maxima (top panels), blue shift in emission maxima (middle panel) and increase of fluorescence intensity (bottom panels).

fluorescence properties in the presence of amphipathic molecules, dissolved/dispersed in aqueous medium (Fig. 6). Amphipathic molecules like detergents and phospholipids create a hydrophobic environment in aqueous media. These compounds have been used extensively to study fluorescent properties of other styryl dyes and have laid the foundation for their use in studying cellular events [2].

Spectral properties (both absorption and emission) of LDS 798 were measured while titrated with sodium dodecyl sulfate (SDS—an ionic detergent) and Triton-X 100 (a non-ionic detergent) at room temperature. These studies reveal that absorption maxima shifted to the longer wavelengths upon addition of both SDS and Triton-X100. The fluorescence spectral analysis showed a progressive blue shift with increasing concentration of Triton-X 100 but not with SDS. The intensity of fluorescence increased with addition of detergents (both SDS and Triton-X 100). This increase was found to be phase dependent as the LDS fluorescence signal increased once the critical micellar concentration was attained (8.2 μM for SDS and 200 μM for Triton-X-100) and leveled off after stable micellar structure was attained (at higher concentrations of detergent). This observation is consistent with reports based on the study of the polymerization of styryl dyes [20] that have reported spectral shift in fluorescence decreased once nucleation of polymerization was attained.

Study of spectral and radiative properties of styryl dyes in unilamellar vesicles (mean diameter ~60 nm; Table 2), prepared with neutral phospholipids (DMPC) and negatively charged phospholipids (DMPG) showed a red shift in absorption and a blue shift in emission spectra upon addition of unilamellar vesicles to the dye. Two emission peaks (at 550 nm and 720 nm) in presence of SUVs was observed when excited with 530 or 470 nm light (Fig. 7). When excited with even longer wavelength (620 nm) only one peak at ~740 nm was observed while the LDS 798 fluorescence attained saturation at lower concentrations of DMPG than DMPC (Fig. 7, lower panels).

Finally, polarity dependent changes in LDS 798 fluorescence in reconstituted high density lipoprotein (HDL) nanoparticles (rHDL) were measured to see whether this phenomenon can be applied to characterization of nanoparticles used in drug delivery. These nanoparticles were shown to have a mean diameter of <20 nm (Table 2) and contained egg yolk phosphatidyl choline, cholesterol, cholesteryl oleate and either apolipoprotein A-I protein (in rHDL) or an apolipoprotein mimetic peptide (termed as 5A peptide in the figures). These polypeptide components are required for structural integrity of the synthetic/reconstituted lipoprotein particles. Addition of rHDL (containing either apo A-I or the 5A peptide) in aqueous solution of LDS 798 led to a mild red shift in absorption spectra and strong blue shift in emission spectra (Fig. 8). The fluorescence intensity increased upon addition of the respective nanoparticles to the dye. The change in fluorescence spectrum of LDS 798 in presence of rHDL and peptide nanoparticles suggest alterations in their surface charge, perhaps due to conformational change in the polypeptide components as the lipid ingredients of both preparations were identical.

Ensemble studies show that amphipathic molecules influence the spectral properties and radiative rates of LDS 798. Most of the amphipathic molecules induced a red shift in absorption spectra while in all the cases the fluorescence spectra was blue shifted and the peak intensity increased by different magnitudes. In reconstituted

Table 2
Size distribution, Diffusion coefficient and detected concentrations of the lipid based small unilamelar vesicles and nanoparticles.

Sample	Size distribution (nm)	Diffusion coefficient ($\mu m/s^2$)	Detected concentration (nM)
Free LDS 798	–	199 ± 25	
SUVs (pure)			
DMPC	55.4 (98%)	3.28 ± 0.5	19.1
	2100 (2%)		
DMPG	56.4 (96%)	3.79 ± 1.1	0.25
	295 (4%)		
Nanoparticles (mixed lipids)			
rHDL NP	43 (100%)	2.0 ± 0.3	15.2
Peptide NP	34 (100%)	3.1 ± 0.5	11.1

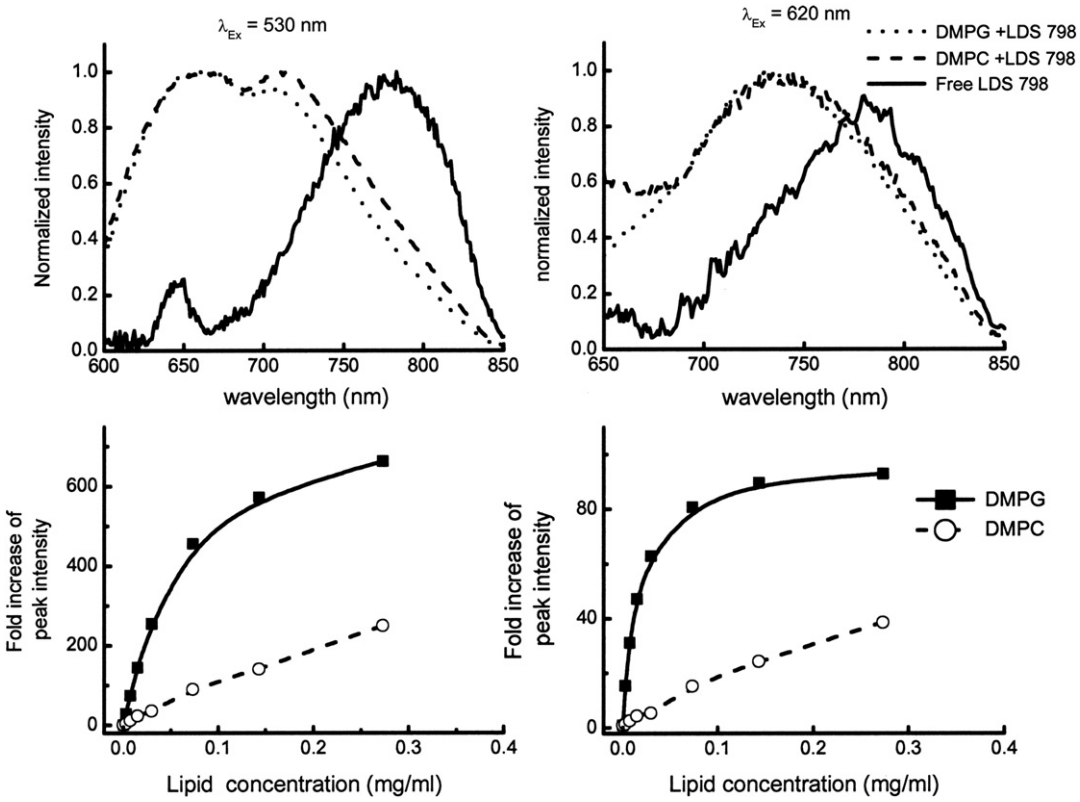

Fig. 7. Spectral and radiative changes in LDS 798 fluorescence on addition of bilayered membrane. (Top) Normalized spectra of free LDS 798 (continuous line) and LDS 798 in presence of DMPC (dashed lines) or DMPG (dotted lines) with 530 nm (left) and 620 nm (right) excitation. (Bottom) Fold change in LDS 798 fluorescence at peak intensities on addition of lipid membranes.

bilayered structures, always two peaks were observed. This observation is previously unreported. Unpublished initial studies from our laboratory for these samples indicate, that there might be two populations with distinct excitation peaks. Molecular phenomenon leading to this observation and its significance is not yet clear and would require further study. The saturation profile of LDS798 fluorescence with DMPC and DMPS suggest that fluorescence properties of LDS 798 are enhanced when it interacts with the negatively charged or polar residues or conversely, LDS 798 might not interact effectively with the neutral phospholipids as compared with polar/negatively charged lipids. Both these possibilities might be true as previous reports have shown that styryl dyes have enhanced fluorescence properties under mildly acidic condition.

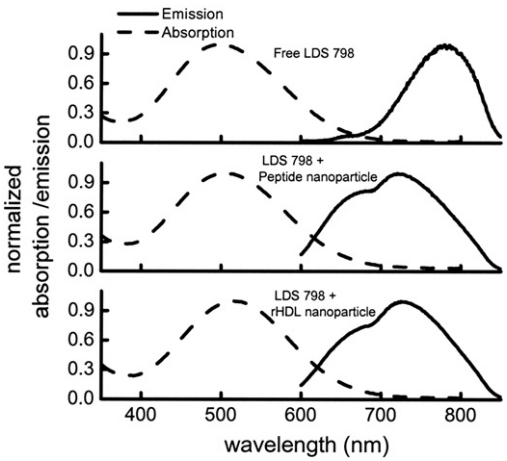

Fig. 8. Effect of HDL and HDL-like nanoparticles on LDS 798 fluorescence. Addition of nanoparticles resulted in slight red shift of absorption maxima and strong blue shift of emission maxima. Two peaks were observed in the fluorescence spectra after addition of nanoparticles to aqueous solution of LDS 798.

3.3. Fluorescence correlation spectroscopy studies on LDS 798

Small log P value of LDS 798 and manifold increased quantum yield of LDS 798 in non-aqueous solvents prompted us to hypothesize that in an aqueous solution with SUV, LDS 798 fluorescence will preferentially be associated with the nanoparticles as the signal generated by these associated LDS 798 molecules will be stronger than the LDS 798 molecules in the aqueous phase. Thus, LDS 798 fluorescence signal can be used to characterize the diffusion of these submicron particles. The diffusion pattern of LDS 798 molecules associated with the nanoparticles will thus correspond to that of the particles themselves and will be significantly different from those that are free (and weakly fluorescent). We decided to test the hypothesis using single point fluorescence lifetime correlation spectroscopy. Figs. 9 and 10 shows the correlation profile and the burst profile of the measurements. Table 2 shows the average number of particles and the diffusion coefficient of LDS 798 in pure phospholipid vesicles (Fig. 9), reconstituted rHDL and nanoparticles with reconstituted 5A peptide (Fig. 10). The FCS results were in agreement with dynamic light scattering results measured independently (Table 2). The traces measured, showed very high fluctuations (Fig. 9, left) corroborating that correlation originated from the phospholipid vesicle bound LDS 798 molecules. The signal from the Free LDS 798 in water was very weak and was characterized by poor correlation and fast diffusion rates typical of free dyes (Fig. 10). The smaller HDL-like particle was observed to have a relatively slow diffusion rate. However, this trend was consistent in all 3 sets of experiments performed. This decrease in diffusion might be due to the incorporation of ApoA-I or the mimetic peptide that increases the density of the particle and slows down its Brownian motion. These results indicate that FCS can be used to study

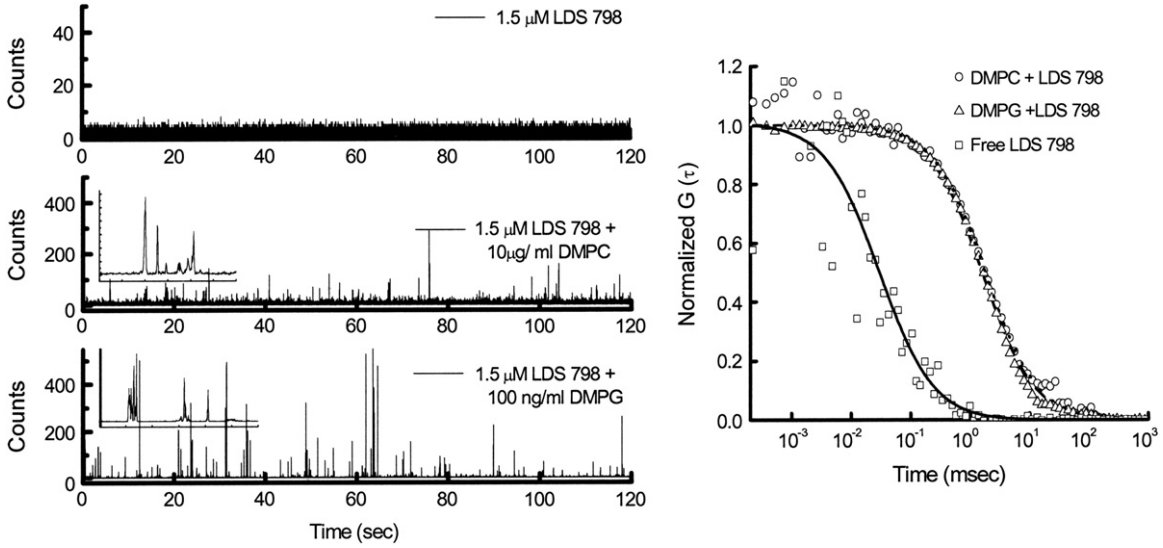

Fig. 9. Fluorescence correlation pattern of pure lipid SUVs. MCS traces of the measurements are shown in the left panels and normalized correlation pattern of LDS 798 fluorescence fluctuations is shown in the left panel.

the diffusion, and hence size, of the submicron lipid structures using solvatochromic fluorescence properties of LDS 798.

Fluorescence correlation studies with LDS 798 dyes indicate that it can be used to study hydrophobic structures with relatively easy staining protocol. Advanced correlation techniques have been developed and can be used to study aggregation pattern inside a cell. On the other hand, styryl dyes have been used to study exocytosis and other vesicle related phenomenon. Hence we anticipate that advanced correlation spectroscopy using styryl dye labeling can play a critical part in understanding the mechanism of vesicular transport dynamics. Long wavelength dyes like LDS 798 have an added advantage as the auto fluorescence background signal is negligible in the near-infra-red range. Though we have not checked the toxic effects of LDS 798, it has been reported for ASP dyes that concentrations below micromoles are not toxic for the cells up to 8–10 h after labeling [4].

Membrane localization and orientation of this subgroup of dyes has been very carefully linked to its structure. The structure of LDS 798 is very similar the ASP dyes. The major difference is in the head region, which contain a quinolinum ring rather than pyridinium. The tail region of LDS 798 is very short and contains dimethyl group. For ASP dyes this short tail generally leads to membrane permeabilization. The log P value and solubility profile of LDS 798 suggests that it can be soluble in aqueous media too. Thus, we believe LDS 798 might be useful in staining intracellular organellar membranes. Its localization in sub-cellular structures can be very interesting.

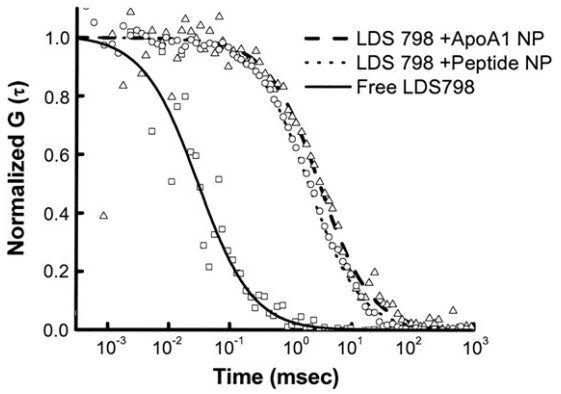

Fig. 10. Characterization of the dimensions of the HDL and HDL-like nanoparticles using FCS.

4. Conclusion

LDS 798 is a styryl group dye with near infra-red fluorescence. Its structure and fluorescence properties indicate that its radiative rate is dependent upon the micro-domain polarity among other factors. Our studies show that this can be conveniently used for FCS measurements of lipid based particles smaller than optical resolution. The concept of studying trafficking patterns of lipid structures using styryl dyes and FCS is novel and can provide insights in vesicle transport and release in cytological studies.

Acknowledgements

This work was supported by the Texas Emerging Technology Funding grant (given to the Center for Commercialization of Fluorescence Technology). ST was funded by a predoctoral fellowship (BC093521) DOD Breast Cancer Research Program (SIT). We would also like to thank Dr. Jamboor K. Viswanatha for allowing us to use the NanoTrack dynamic light scattering instrument and sonication system; Dr. Thomas Just Sørenson, for helping with solvent relaxation studies; and Dr. Badri Prasad Maliwal and Dr. Valeriya Trusova for the SUV preparation.

References

[1] C. Xu, L.M. Loew, The effect of asymmetric surface potentials on the intramembrane electric field measured with voltage-sensitive dyes, Biophys. J. 84 (2003) 2768–2780.
[2] E. Fluhler, V.G. Burnham, L.M. Loew, Spectra, membrane binding, and potentiometric responses of new charge shift probes, Biochemistry (N. Y.) 24 (1985) 5749–5755.
[3] W.J. Betz, F. Mao, G.S. Bewick, Activity-dependent fluorescent staining and destaining of living vertebrate motor nerve terminals, J. Neurosci. 12 (1992) 363–375.
[4] W.J. Betz, F. Mao, C.B. Smith, Imaging exocytosis and endocytosis, Curr. Opin. Neurobiol. 6 (1996) 365–371.
[5] J.R. Lakowicz, Principless of Fluorescence Spectroscopy, 2nd Ed.Kluwer Academic / Plenum Publisher, New York, 1999.
[6] U. Brackmann, Lambdachrome Laser Dyes Data Sheets, 1994.
[7] M.Y. Berezin, H. Lee, W. Akers, S. Achilefu, Near infrared dyes as lifetime solvatochromic probes for micropolarity measurements of biological systems, Biophys. J. 93 (2007) 2892–2899.
[8] R. Luchowski, Z. Gryczynski, P. Sarkar, J. Borejdo, M. Szabelski, P. Kapusta, et al., Instrument response standard in time-resolved fluorescence, Rev. Sci. Instrum. 80 (2009) 033109.
[9] R. Luchowski, P. Sarkar, S. Bharill, G. Laczko, J. Borejdo, Z. Gryczynski, et al., Fluorescence polarization standard for near infrared spectroscopy and microscopy, Appl. Opt. 47 (2008) 6257–6265.
[10] B. Jędrzejewska, M. Pietrzak, J. Pączkowski, Solvent effects on the spectroscopic properties of styrylquinolinium dyes series, J. Fluoresc. 20 (2010) 73–86.
[11] A. Celli, E. Gratton, Dynamics of lipid domain formation: fluctuation analysis, Biochim. Biophys. Acta 1798 (2010) 1368–1376.

[12] S.A. Sánchez, M.A. Tricerri, G. Ossato, E. Gratton, Lipid packing determines protein–membrane interactions: challenges for apolipoprotein AI and high density lipoproteins, Biochim. Biophys. Acta BBA Biomembr. 1798 (2010) 1399–1408.
[13] A.G. Lacko, M. Nair, S. Paranjape, L. Mooberry, W.J. McConathy, Trojan horse meets magic bullet to spawn a novel, highly effective drug delivery model, Chemotherapy (Basel) 52 (2006) 171.
[14] C. Matz, A. Jonas, Micellar complexes of human apolipoprotein AI with phosphatidylcholines and cholesterol prepared from cholate-lipid dispersions, J. Biol. Chem. 257 (1982) 4535.
[15] A. Jonas, Reconstitution of high-density lipoproteins, Meth. Enzymol. 128 (1986) 553–582.
[16] J. Short, J. Roberts, D. Roberts, G. Hodges, S. Gutsell, R. Ward, Practical methods for the measurement of log P for surfactants, Ecotoxicol. Environ. Saf. 73 (2010) 1484–1489.
[17] R. Luchowski, P. Kapusta, M. Szabelski, P. Sarkar, J. Borejdo, Z. Gryczynski, et al., FRET-based picosecond lifetime reference for instrument response evaluation, Meas. Sci. Technol. 20 (2009) 095601.
[18] D. Magde, E. Elson, W. Webb, Thermodynamic fluctuations in a reacting system—measurement by fluorescence correlation spectroscopy, Phys. Rev. Lett. 29 (1972) 705–708.
[19] D. Magde, E.L. Elson, W.W. Webb, Fluorescence correlation spectroscopy. II. An experimental realization, Biopolymers 13 (2004) 29–61.
[20] A. Bajorek, K. Trzebiatowska, B. Jędrzejewska, M. Pietrzak, R. Gawinecki, J. Pączkowski, Developing of fluorescence probes based on stilbazolium salts for monitoring free radical polymerization processes. II, J. Fluoresc. 14 (2004) 295–307.

Instrument response standard in time-resolved fluorescence

Rafal Luchowski,[1,2] Zygmunt Gryczynski,[1] Pabak Sarkar,[1] Julian Borejdo,[1] Mariusz Szabelski,[1] Peter Kapusta,[3] and Ignacy Gryczynski[1,4]
[1]*Department of Molecular Biology and Immunology, Center for Commercialization of Fluorescence Technologies (CCFT), UNTHSC, Fort Worth, Texas 76107, USA*
[2]*Department of Biophysics, Institute of Physics, Maria Curie-Sklodowska University, 20-031 Lublin, Poland*
[3]*PicoQuant GmbH, 12489 Berlin, Germany*
[4]*Department of Cell Biology and Genetics, UNTHSC, Fort Worth, Texas 76107, USA*

(Received 26 December 2008; accepted 16 February 2009; published online 17 March 2009)

The fluorescence of LDS 798 dye in aqueous solution has a very short lifetime of 24ps, independent of excitation wavelength. The time response of common photon counting detectors depends on the wavelength of the registered photon. In lifetime measurements, the instrument response function (IRF) is usually approximated by the temporal profile of the scattered excitation light. Because λ_{Exc} is typically much shorter than λ_{Em}, a systematic error may be present in these measurements. We demonstrate that the fluorescence decay of LDS 798 is a better approximation of IRF, in particular, for avalanche photodiodes used in the near infrared spectral region. © *2009 American Institute of Physics.* [DOI: 10.1063/1.3095677]

I. INTRODUCTION

The instrument response function (IRF) in time-resolved fluorescence measurements is usually obtained by recording the temporal profile of the excitation light. Back reflection or elastic scattering provides a strong, easily obtainable signal, but only observable at wavelengths shorter than the fluorescence emission. Conventional photomultiplier tubes (PMTs) and avalanche photodiodes (APDs) used in time-resolved spectroscopy and microscopy suffer from the so-called color effect: their timing response depends on the energy of the detected photon. This wavelength dependent detector response may seriously distort the results of time-resolved measurements for both frequency and time-domain lifetime determinations. This effect becomes particularly serious when the fluorescence lifetime to be resolved is comparable with the detector response time. A typical example of time-domain data analysis is the iterative reconvolution. The measured instrument response to excitation pulses is convolved with a theoretical model decay function and the result is compared to the recorded fluorescence decay curve. An inherent assumption involved here is that the temporal response of the instrument is the same for excitation pulses and fluorescence photons. However, due to the above-mentioned color effect of detectors, this is rarely the case. Recording the IRF at the spectral range of fluorescence would be more appropriate and often more convenient. For example, changing filters, dichroic mirrors, and altering the detection pathway could be avoided in microscope based setups.

It should be noted that fast microchannel-plate PMTs (MCP-PMTs) are virtually free of color effects.[1–3] Due to their high price, relatively low quantum yield, and low damage threshold, MCP-PMTs are still not standard detectors in this field. Especially in time resolved microscopy, because of very weak signals, the high quantum yield APD is the detector of choice.

The use of reference fluorophores for lifetime measurements has already been reported. Erythrosine B in water solution has a lifetime of about 90 ps and was used as a reference in flavin fluorescence studies.[4,5] Recently, we showed that Erythrosine B and Rose Bengal fluorescence emission can be effectively quenched by potassium iodide, resulting in a lifetime of about 25 ps.[6] Collisional quenching of fluorophores is an easy method of shortening the lifetime. For example, already three decades ago Harris and Lytle were able to reduce the Rhodamine 6G lifetime to about 50 ps,[7] preserving a monoexponential decay. More recently, quenched Rhodamine 6G solutions were used for multipoint calibration of a frequency-domain system.[8] The idea of using short lived reference dyes to avoid the color effect was also proposed by Szabo and co-workers[9] and de Schryver and co-workers.[10] Intramolecular quenching by covalent acrylamide-indole adduct demonstrated by Eftink *et al.*[11] shortened the indole lifetime to about 30 ps. The lifetime of a fluorophore can also be shortened by stimulated emission depletion (STED), as has been demonstrated by Hell *et al.*[12,13]

In the visible (VIS) region of the spectrum, it is easier to find a short lived reference compound, or one can use collisional quenchers. In addition to the above-mentioned dyes and methods, several stilbenes and styrenes display short, picosecond decays.[14–16] Lifetime standards in ultraviolet and VIS regions measured independently by various groups have been recently summarized by Boens *et al.*[17] However, there is a renewed interest in time-resolved microscopy and lifetime imaging (FLIM) in the near infrared (NIR) region. Recently, we characterized the LDS 798 (Fig. 1) dye oriented in poly(vinyl)alcohol films as a polarization standard in the NIR spectral region.[18] Although in a solid polymer matrix this fluorophore displays a lifetime of about 2 ns, we noticed that lifetimes were remarkably shorter in solutions. In this article we report on the ultrashort fluorescence emission of

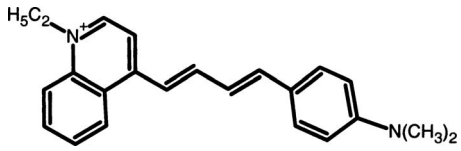

FIG. 1. Chemical structure of LDS 798.

LDS 798 in solution. We demonstrate its advantage over conventional recording of scattering in NIR lifetime measurements when utilizing APDs.

II. MATERIALS AND METHODS

1-ethyl-4-[4-(p-dimethylaminophenyl)-1,3-butadienyl]-quinolinium perchlorate (LDS 798) and pyridine 1 (PY1) in crystalline form were purchased from Exciton, Inc. and used without further purification. Rhodamine 800 (Rh800) was obtained from Lambda Physik (Fort Lauderdale, FL). The purity of Rh800 and LDS 798 were more than 98% and 99%, respectively, as revealed by reversed-phase high-performance liquid chromatography (RP-HPLC) using Kromasil column C-8, 5 μm, 250 mm long, i.d.=4.5 mm, detection at 223, 254, and 500 nm for LDS 798, and 223, 254, and 680 nm for Rh800. The mobile phase was a gradient running from 0% to 100% of B (A=water with an addition of 0.01% trifluoroacetic acid, B=80% acetonitrile in water with an addition of 0.08% trifluoroacetic acid) over 60 min. Acetonitrile for HPLC was obtained from Sigma-Aldrich. Water was deionized using a Milli-Q Synthesis A10 system produced by Millipore.

Stock solutions of LDS 798, PY1, and Rh800 were prepared in spectral grade (99.6%) ethanol (EtOH) from Sigma Aldrich. The phosphate buffered saline (PBS) (20X PBS, pH of 7.4 from AMRESCO, OH) solution of LDS 798 was prepared by 10 min sonication followed by centrifugation for 15 min at 2000$\times$g in order to remove the microcrystals of the dye present in the sample.

A. Spectroscopic measurements

Light absorption measurements were performed on a Cary 50 Bio spectrophotometer (Varian, Inc.). Emission spectra were recorded with a Cary Eclipse (Varian, Inc.) equipped with a red sensitive photomultiplier.

Reference fluorescence lifetimes were measured with a FluoTime200 fluorometer (PicoQuant, GmbH). Our setup is equipped with an MCP detector (Hamamatsu, Inc.), polarizers, monochromator, and proper long-pass filters matched to the excitation lines. LDH470 and LDH635 diode laser heads driven by a PDL800-B driver emitted pulses at 470 and 635 nm with a repetition rate of 40 MHz and an optical pulse duration of about 65 ps. The fluorescence decay curves were analyzed by means of iterative reconvolution using the FLUOFIT software package (version 4.2.1, PicoQuant GmbH). A sum of exponentials,

$$I(t) = \sum_i \alpha_i \exp(-t/\tau_i), \tag{1}$$

where α_i and τ_i are pre-exponential factors and fluorescence lifetimes, respectively, was used to describe the data.

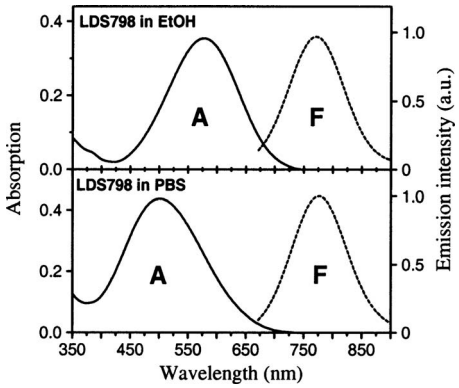

FIG. 2. Absorption and fluorescence spectra of LDS 798 in EtOH (top) and PBS (bottom).

B. Microscopic measurements: Evaluation of the APD detector

We evaluated the timing responses of two Perkin-Elmer SPCM-AQR-14 single photon sensitive APDs incorporated in the MicroTime200 time-resolved confocal microscope (PicoQuant GmbH). LDH-P-C-470B and LDH-P-C-635B pulsed laser diodes (similar to the lasers of the FluoTime200 fluorometer) were used as excitation sources in these experiments. The excitation beam was spectrally cleaned by z463/25x-HT and z636/10x bandpass filters (Chroma Technology Corp.) for 470 and 635 nm lasers, respectively. A drop of sample solution deposited on a glass cover slip (Menzel-Glaser #1) was mounted on an Olympus IX71 inverted microscope stage. An Olympus UPlanSApo (60$\times$ magnification, numerical aperture of 1.2, water immersion) objective focused the laser beam 10 μm above the surface of the cover slip into the sample volume. The same objective collected the fluorescence and/or the scattered excitation light, which was detected by the APD and processed by the PicoHarp300 time-correlated single-photon counting module. For measurements of scattered light, we used a dilute solution of colloidal silica (Ludox, Aldrich, Inc.). Fluorescence emission in the NIR region was observed through combination of a 640 nm long-pass Razor Edge and 775/175 band-pass filters (Semrock). Decay data analysis was performed using SYMPHOTIME (v. 4.7.2.1) software package that controlled the data acquisition as well.

III. RESULTS AND DISCUSSION

A. Spectral properties of LDS 798

LDS 798 (Fig. 1) is a well known styryl dye, which is often used (in a slightly modified form) for staining of biological materials.[19] Figure 2 shows the absorption and fluorescence spectra of LDS 798 in EtOH and PBS. The absorption spectrum of LDS 798 in EtOH solution consists of an unstructured band in the long wavelength region with a maximum at 580 nm. The absorption in water solution (PBS) is shifted to shorter wavelengths and displays a maximum at 500 nm. Such a large shift in the absorption maximum for molecules in water solutions typically results from homoaggregates.[20–22] Dipolar coupling is more likely to lead to delocalized excitonic states for the LDS 798. The ob-

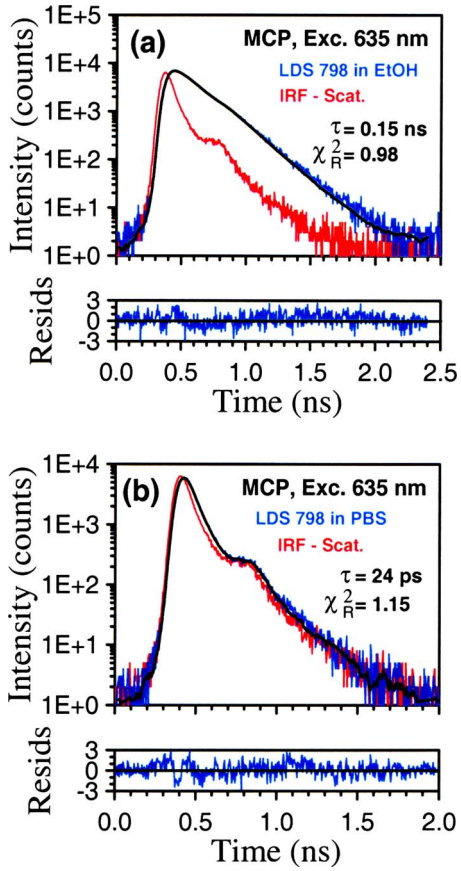

FIG. 3. (Color online) Fluorescence intensity decays of LDS 798 in (a) EtOH and (b) PBS *p*H 7.4.

served hypsochromic shift suggests that the excitonic interactions are associated with a formation of small molecular aggregates with oblique orientation of dipole moments of the neighboring molecules. An alternative explanation is the possibility of cis-isomerization in prolate molecules like stilbenes[23–25] or diphenyloctatriene.[26]

Although LDS 798 has a strong fluorescence emission in a rigid polymeric matrix [quantum yield of 0.48 (Ref. 18)], in liquid solutions, the fluorescence is weaker. Upon 635 nm excitation the fluorescence quantum yield is 0.011 and 0.002 in EtOH and PBS, respectively. The emission maximum is at 770 nm in EtOH solvent and at 777 nm in PBS (see Fig. 2). There is no measurable spectral shift of emission when the excitation wavelength is changed to 470 nm.

Full explanation of the LDS 798 photophysics is out of the scope of this communication. The reproducibility of sample preparation is more important for its use as an IRF standard. We repeated the preparation of LDS 798 in PBS solution several times and checked the consistency of spectral properties. We observed no changes in the position of absorption and fluorescence spectra for a set of samples with maximum absorbances from about 0.02–1.1, corresponding to concentrations of $0.4\times10^{-6}M$ to about $24\times10^{-6}M$.

B. Fluorescence intensity decays of LDS 798 measured with an MCP detector

Figure 3 shows the fluorescence decays of LDS 798 in EtOH and in aqueous PBS, together with the IRF obtained by (Ludox) scattering the 635 nm laser beam used for excitation. The smooth curves are single exponential decay functions convoluted with the IRF. The fitted lifetime values are 0.15 ns and 24 ps for EtOH and PBS, respectively. Including a second exponential term into the model did not improve the goodness of the fit (reduced chi-squared, χ_R^2) parameter significantly. We repeated these measurements using samples with various concentrations of LDS 798 and the fitted lifetimes were found to be constant. Because the weighted residuals are smaller than three standard deviations already for a single exponential decay model, we concluded that the fluorescence decay of LDS 798 is indeed single exponential with lifetimes reported above.

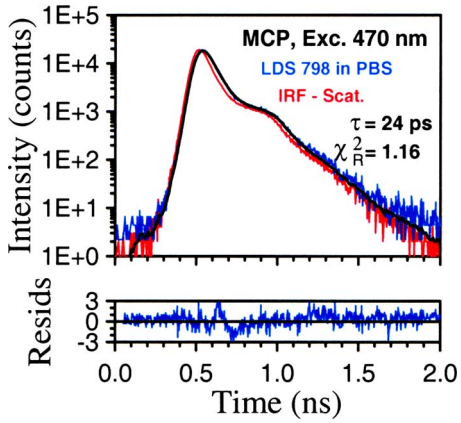

FIG. 4. (Color online) Fluorescence intensity decays of LDS 798 in PBS, *p*H 7.4, excited at 470 nm, observed at 770 nm.

Fluorescence decay measurements of LDS 798 in PBS were performed also using the 470 nm diode laser. The result, a single exponential decay with a lifetime of 24 ps is shown in Fig. 4. Our conclusion is that the decay time of LDS 798 in PBS is independent of the excitation wavelength and the MCP-PMT does not show any discernible color effect. LDS 798 in aqueous buffer solution is an ideal lifetime standard in the NIR region and the very short lifetime gives the opportunity to characterize the IRF of other photodetectors used in NIR time-resolved fluorescence spectroscopy/microscopy.

C. IRF evaluation of an APD detector

The Perkin Elmer SPCM-AQR series detectors are single photon sensitive avalanche photodiodes, very popular in microscopy because of their high quantum efficiency. We evaluated the timing response of this detector as a function of detection wavelength. First, we obtained an IRF with 588 ps full width at half the maximum (FWHM) when the scattered excitation photons with $\lambda=470$ nm were detected. The optical duration of our laser pulses is shorter than 70 ps and the electrical timing resolution of the TCSPC electronics is better than 24 ps FWHM. Therefore the FWHM of the experimentally obtained IRF is entirely dominated by the timing response of the APD. By replacing the Ludox scatterer with a drop of LDS 798 solution in PBS and observing the fluorescence at around 775nm, we obtained an IRF with 470 ps FWHM. This is a very significant difference and Fig. 5 shows the comparison. As expected (data not shown) the

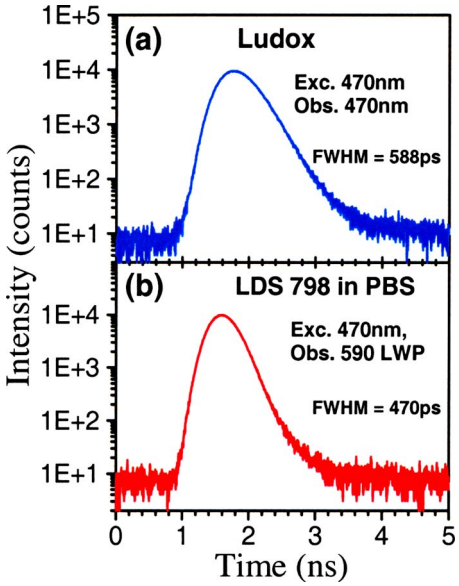

FIG. 5. (Color online) APD (Perkin-Elmer SPCM-AQR-14) responses to the pulsed 470 nm excitation. (a) Scattering from colloidal silica observed at 470 nm. (b) Fluorescence signal from LDS 798 in PBS, *p*H 7.4, observed at longer wavelengths ($\lambda > 590$ nm).

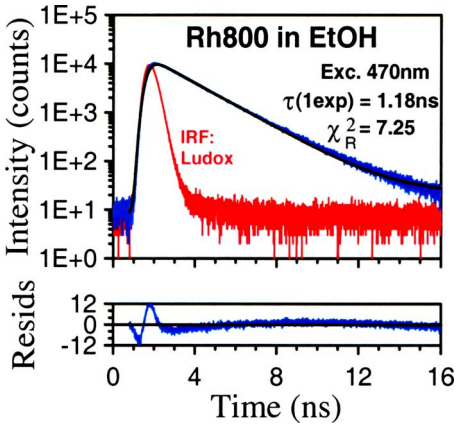

FIG. 6. (Color online) Fluorescence intensity decay of Rh800 in EtOH, detected with Perkin-Elmer SPCM-AQR-14 detector. IRF is approximated by the temporal profile of scattered 470 nm excitation light. The single exponential model (smooth curve) does not match the experimental data.

color effect is weaker for 635 nm excitation. The difference in FWHM value for 635 nm laser and LDS 798 emission at 775 nm is about 30 ps. IRF received from the scatterer still remains broader, despite of a 24 ps lifetime of the dye. Both APDs incorporated in our setup show the same behavior. We conclude that higher energy photons cause secondary photophysical processes in silicon photodiodes upon detection, resulting in broader timing responses in the blue region than in the red. However, this color effect is very critical for precise measurements of fluorescence lifetimes.

D. Lifetime measurements with an APD detector

In order to show how severe the distortion can be, we compared the lifetime analysis results obtained by using either Ludox scatterer or LDS 798 in PBS. Figure 6 shows the fluorescence decay of Rh800 in EtOH solvent (blue) excited at 470 nm and observed through a 590 long pass filter. Using scattered excitation light as the IRF, the decay is not well described with a single exponential model. The χ_R^2 for this evaluation is 7.25 and the residuals in Fig. 6 show systematic deviation. In this case the fitted single exponential lifetime is 1.18 ns, much shorter than that reported in the literature[27] and also obtained by us with the MCP detector based setup. It is possible to achieve an acceptable fit with a χ_R^2 close to unity using the double exponential model with lifetimes of 54 ps and 1.94 ns and relative amplitudes of 0.77 and 0.23, respectively. However, this is contradictory because the decay of Rh800 in EtOH is indeed single exponential. The results of iterative single exponential reconvolution analyses are summarized in Table I. Approximating the IRF by the fluorescence decay of LDS 798 in PBS yields a much better fit with a lifetime of 1.85 ns and an acceptable χ_R^2 value, as shown on Fig. 7.

To further explore the significance of color effect, we recorded the fluorescence decay of PY1 dye in EtOH (Fig. 8). Owing to the relatively short lifetime of PY1 in comparison to Rh800, the impact of the color effect on the analysis is much more pronounced. Using the scattering as an IRF yields a lifetime of 0.28 ns with $\chi_R^2 = 18.41$, an obviously wrong result. Because the temporal profile of scattering is broader than the real IRF, reconvolution fitting leads to an apparent, shorter lifetime value as compared to that in the literature.[28] The proper lifetime of 0.37 ns and acceptable distribution of residuals are obtained when the fluorescence decay of LDS 798 is used as an IRF (Fig. 9). Again, the

TABLE I. The measured lifetimes of LDS 798, Rh800, and PY1 in EtOH and PBS using different detectors and IRFs.

Compound	Exc. (nm)	Detector	IRF	α_1	τ_1 (ns)	χ_R^2
LDS 798 in EtOH	635	MCP	Ludox	1	0.15	0.98
LDS 798 in PBS Buffer	635	MCP	Ludox	1	0.024	1.16
LDS 798 in PBS Buffer	470	MCP	Ludox	1	0.024	1.15
Rh800 in EtOH	470	MCP	Ludox	1	1.86	1.12
Rh800 in EtOH	470	SPAD	Ludox	1	1.18	7.25
Rh800 in EtOH	470	SPAD	LDS 798	1	1.85	1.75
PY1 in EtOH	470	MCP	Ludox	1	0.37	1.11
PY1 in EtOH	470	SPAD	Ludox	1	0.28	18.41
PY1 in EtOH	470	SPAD	LDS 798	1	0.37	1.11

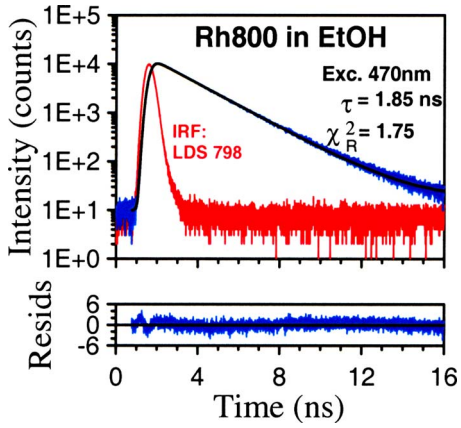

FIG. 7. (Color online) Fluorescence intensity decay of Rh800 in EtOH, the same as in Fig. 6. IRF is approximated by the fast fluorescence of LDS 798 in PBS solution. A single exponential reconvolution fit successfully describes the data and yields the correct lifetime.

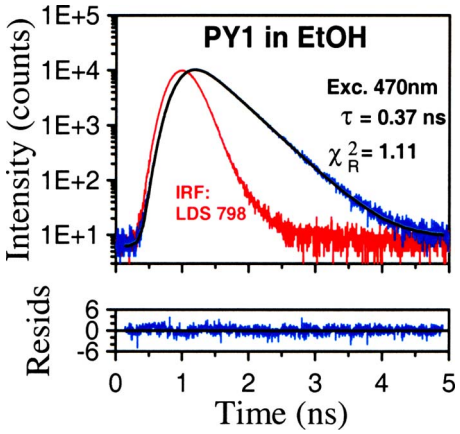

FIG. 9. (Color online) Fluorescence intensity decay of PY1 in EtOH (the same as in Fig. 8). The fast fluorescence of LDS 798 in the PBS solution is included as an IRF approximation. Correct decay parameters are recovered and the quality of the fit is acceptable.

outcome is fully consistent with the reference measurement performed with the MCP detector (see Table I).

IV. CONCLUSIONS

The fast fluorescence decay of LDS 798 fills the NIR spectral gap of fluorescence standards. This reference sample is very easy to prepare, covers extended regions of excitation and emission wavelengths (see Fig. 2), and is relatively bright. The advantage of using short lived fluorescence compounds instead of scattering is evident for APD detectors, especially when the observation is at much longer wavelength(s) than that of the excitation. In this case, an IRF obtained by scattering excitation light hampers the determination of correct lifetimes and may result in false and misleading virtual decay components. Proper IRF approximation is therefore extremely important in FLIM measurements, where these effects can completely distort the picture. Additional benefit of the use of fast lifetime references, like the proposed LDS 798 in water-based solution, is the partially depolarized signal. Microscope based anisotropy measurements typically utilize two detectors with a polarizing beam splitter between them. Simultaneous determination of two IRFs is necessary, which is difficult to accomplish using scattered light. Because weak scattering or back reflection preserves the polarization plane of the excitation beam, the parallel polarized signal is by orders of magnitudes stronger than the perpendicular polarized one, leading to problems with signal to noise ratio.

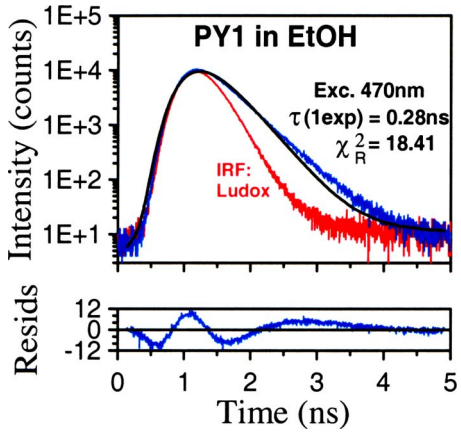

FIG. 8. (Color online) Fluorescence intensity decay of PY1 in EtOH together with the temporal profile of scattered 470 nm excitation light and an unsatisfactory single exponential fit. There are strong, systematic deviations in the distribution of residuals (bottom panel).

ACKNOWLEDGMENTS

This work was supported by Texas ETF (CCFT, Z.G.) and THECB (I.G.) grants and by NSF Grant No. DBI-0649889 (Z.G.). R.L. and M.S. are recipients of a researcher's mobility program from the Polish Ministry of Science and Higher Education.

[1] K. W. Berndt, I. Gryczynski, and J. R. Lakowicz, Anal. Biochem. **192**, 131 (1991).
[2] G. Laczko, I. Gryczynski, Z. Gryczynski, W. Wiczk, H. Malak, and J. R. Lakowicz, Rev. Sci. Instrum. **61**, 2331 (1990).
[3] J. R. Lakowicz, G. Laczko, and I. Gryczynski, Rev. Sci. Instrum. **57**, 2499 (1986).
[4] P. I. Bastiaens, A. van Hoek, W. F. Wolkers, J. C. Brochon, and A. J. Visser, Biochemistry **31**, 7050 (1992).
[5] P. A. van den Berg, S. B. Mulrooney, B. Gobets, I. H. van Stokkum, A. van Hoek, and C. H. Jr Williams, Protein Sci. **10**, 2037 (2001).
[6] M. Szabelski, D. Ilijev, P. Sarkar, R. Luchowski, Z. Gryczynski, P. Kapusta, R. Erdmann, and I. Gryczynski, Appl. Spectrosc. **63**, 363 (2009).
[7] J. M. Harris and F. E. Lytle, Rev. Sci. Instrum. **48**, 1469 (1977).
[8] Q. S. Hanley, V. Subramaniam, D. J. Arndt-Jovin, and T. M. Jovin, Cytometry **43**, 248 (2001).
[9] M. Zuker, A. G. Szabo, L. Bramall, D. T. Krajcarski, and B. Selinger, Rev. Sci. Instrum. **56**, 14 (1985).
[10] M. van den Zegel, N. Boens, D. Daems, and F. C. de Schryver, Chem. Phys. **101**, 311 (1986).
[11] M. R. Eftink, Y. W. Jia, D. E. Graves, W. Wiczk, I. Gryczynski, and J. R. Lakowicz, Photochem. Photobiol. **49**, 725 (1989).
[12] I. Gryczynski, S. W. Hell, and J. R. Lakowicz, Biophys. Chem. **66**, 13 (1997).
[13] I. Gryczynski, J. Kusba, and J. R. Lakowicz, J. Phys. Chem. **98**, 8886 (1994).
[14] A. Kawski, I. Gryczynski, and Z. Gryczynski, Z Naturforsch **48a**, 551 (1992).
[15] A. Kawski, I. Gryczynski, K. Nowaczyk, P. Bojarski, and Z. Lichacz, Z Naturforsch **46a**, 1043 (1991).
[16] J. R. Lakowicz, I. Gryczynski, G. Laczko, and D. Gloyna, J. Fluoresc. **1**, 87 (1991).

[17] N. Boens, W. Qin, N. Basaric, J. Hofkens, M. Ameloot, J. Pouget, J. P. Lefevre, B. Valeur, E. Gratton, M. vandeVen, N. D. Silva, Jr., Y. Engelborghs, K. Willaert, A. Sillen, G. Rumbles, D. Phillips, A. J. Visser, A. van Hoek, J. R. Lakowicz, H. Malak, I. Gryczynski, A. G. Szabo, D. T. Krajcarski, N. Tamai, and A. Miura, Anal. Chem. **79**, 2137 (2007).
[18] R. Luchowski, P. Sarkar, S. Bharill, G. Laczko, J. Borejdo, Z. Gryczynski, and I. Gryczynski, Appl. Opt. **47**, 6257 (2008).
[19] M. Wang, M. Gao, K. D. Miller, G. W. Sledge, G. D. Hutchins, and Q. H. Zheng, Eur. J. Med. Chem. (to be published), available online.
[20] M. Kasha, Radiat. Res. **20**, 55 (1963).
[21] M. Kasha, H. R. Rawls, and M. Ashraf El-Bayoumi, Pure Appl. Chem. **11**, 371 (1965).
[22] R. Luchowski and S. Krawczyk, Chem. Phys. **293**, 155 (2003).
[23] D. Gloyna, A. Kawski, I. Gryczynski, and H. Cherek, Monatsch. Chem. **118**, 759 (1987).
[24] I. Gryczynski, A. Kawski, Z. Gryczynski, and D. Gloyna, J. Chem. Soc., Faraday Trans. 2 **82**, 1879 (1986).
[25] J. Saltiel and J. T. D'Agostino, J. Am. Chem. Soc. **94**, 6445 (1972).
[26] A. Kawski, Z. Gryczynski, I. Gryczynski, and H. Malak, Z Naturforsch **46a**, 621 (1991).
[27] D. Bock, K. Galla, M. Martin, J. Wolfrum, and S. Seeger, Sens. Actuators B **29**, 293 (1995).
[28] B. S. Lin-I Liu, "Time-resolved fluorescence studies of dye-polymers as excited by laser and beta-radiation," Ph.D. thesis, Texas Tech University, 1997.

Fluorescence polarization standard for near infrared spectroscopy and microscopy

Rafal Luchowski,[1,3,*] Pabak Sarkar,[1] Shashank Bharill,[1] Gabor Laczko,[1,4] Julian Borejdo,[1] Zygmunt Gryczynski,[1,2] and Ignacy Gryczynski[1,2,5]

[1]Center for Commercialization of Fluorescence Technologies (CCFT), Department of Molecular Biology & Immunology, University of North Texas Health Science Center, Fort Worth, Texas 76107, USA

[2]Department of Cell Biology and Genetics, University of North Texas Health Science Center, Fort Worth, Texas 76107, USA

[3]Department of Biophysics, Institute of Physics, Maria Curie-Sklodowska University, 20-031 Lublin, Poland

[4]Department of Experimental Physics, University of Szeged, Szeged, Dom ter 9., 6720 Hungary

[5]igryczyn@hsc.unt.edu

*Corresponding author: rluchows@hsc.unt.edu

Received 16 June 2008; revised 9 October 2008; accepted 11 October 2008; posted 21 October 2008 (Doc. ID 97453); published 19 November 2008

We present studies of polarized absorption [linear dichroism (LD)] and fluorescence polarization of the styryl derivative (LDS 798) embedded in oriented poly(vinyl alcohol) (PVA) films. These films were oriented by progressive stretching up to eight folds. Both vertical and horizontal components of absorptions and fluorescence were measured and dichroic ratios were determined for different film stretching ratios. The dichroic ratio and fluorescence anisotropy values were analyzed as a function of PVA film stretching ratio by fitting according to the previously developed theory. For maximum stretching ratios, exceptionally high anisotropy (~0.8) and polarization (~0.9) values have been measured. The stretched films have high polarization values also for isotropic excitation in a wide spectral range (500–700 nm). Such films can be conveniently used as high polarization standards and we envision they will also have applications in near infrared (NIR) imaging microscopy, where they can be used for correcting an instrumental factor in polarization measurements.

OCIS codes: 180.2520, 300.6280.

1. Introduction

Fluorescence spectroscopy is a well recognized tool for probing molecular structures, environment, and studying underlying dynamics of biomolecular systems *in vitro* and *in vivo*. Rapidly growing applications of fluorescence in cellular and tissue imaging stimulated great efforts to develop new water-soluble fluorophores that emit in red and near infrared (NIR) spectral ranges where the background (autofluorescence) from biological samples is minimized. Many of the biological processes like biomolecular transport, ligand binding, and protein-protein interactions can now be monitored on the cellular and tissue level. During the last decade, progress in detector technology also enabled new advanced applications of fluorescence microscopy that now extend to detection and studying even single molecule systems. The biggest obstacles for single molecule studies are background fluorescence, fluorophore photostability, and fluorophore blinking. Today's market offers a wide variety of red and NIR fluorescence labels as well as fluorescence proteins that can be used for labeling biological systems. An ideal fluorescent dye for single molecule spectroscopy should have high photostability, high quantum yield, and minimal blinking.

0003-6935/08/336257-09$15.00/0

Many of the new emerging applications are beginning to use more sophisticated fluorescence measurements in microscopy setups. Fluorescence lifetime imaging (FLIM) [1–3] and/or Förster resonance energy transfer (FRET) [4–7] are frequently used to directly study biomolecular interactions and their colocalization [8,9]. Also measurements of fluorescence polarization and fluorescence correlation spectroscopy (FCS) are becoming more common since they provide useful information regarding macromolecular mobility and flexibility on the cellular level [10–12]. It is becoming more and more evident that many of these advanced applications will benefit from information on basic spectroscopic properties of fluorescent probes. Generally, available information is limited to extinction coefficient, quantum yield, and occasionally fluorescence lifetime of these probes. The fundamental information regarding the number of available transitions, and especially the orientation of transition moments, is almost always not available or unknown for new dyes. This information can be crucial for polarization-based studies or for determination of the orientational factor in FRET (κ^2), and FRET data interpretation [13–16]. Also, knowledge of transition moment orientation may generally helps in rational use of various dyes as labels to study the polarization and flexibility/mobility of biological systems.

Fluorescence polarization (anisotropy) measurements have already proved their value to study macromolecular mobility *in vitro* using protein or other biomolecule solutions in the cuvette system. Presently, more sophisticated applications of fluorescence anisotropy using a microscope configuration provide unique opportunities for characterization and tracking of small subunits of living systems [17,18]. Small confocal volume makes it possible to perform anisotropy even inside the cells, which can allow characterization of the microenvironment of cell interiors [19,20]. Similarly, localized FRET measurements provide information about distance distribution and homo-FRET between green fluorescent proteins (GFPs) expressed in bacteria [21–23]. The sophisticated optics of a typical microscopy system contains multiple optically active elements, and proper interpretation of the details of the measurements will require very precise optical system calibration. This calls for special geometrical conditions and, most importantly, for molecular fluorescence standards to correct for light depolarization by massive numbers of optical elements in an optical path. Over the years many fluorescence standards for polarization measurements in the classic fluorometric configuration (square and front-face) have been developed [24–27]. Such standards are typically used to calibrate optical pathways in standard fluorometers (so called *G*-factor correction). However, microscope configuration is different from configuration of fluorometers and contains multiple optical elements, especially high numerical aperture (NA) objectives that may drastically effect polarization of transmitted light. Unfortunately, today we do not have simple standards that could be used to test and calibrate optical paths for microscope systems.

Here, we have selected a commercially available fluorescent dye LDS 798 (styryl 11) that has very wide visible absorption band from about 450 to 730 nm, with maximum absorption peak at about 600 nm and maximum emission at 750 nm. These are very convenient wavelengths for laser diode excitations at 635 and 650 nm and are generally available with today's microscopy systems. We conducted in-depth spectroscopy studies of the dye and have determined excitation and emission polarizations, fluorescence lifetimes, and transition moment orientation. Linear dichroism (LD) and fluorescence polarization studies in oriented polymer films revealed that low energy absorption transition dipoles and emission transition dipoles are oriented almost along a long molecular axis. Also we have realized that a stretched polymer film with embedded dyes can be conveniently used as high polarization standards for microscopy. Such polymer films are very thin (can be $\sim$100 μm) and are very stable. We also present simple examples of how to use such standard to test and calibrate a typical confocal microscopy system.

2. Materials and Methods

A. Chemicals

All experiments described below were performed using LDS 798 and PVA obtained as powder from Exciton (OH) and Sigma Aldrich, respectively, and used without further purification. All aqueous solutions were prepared from deionized water (Millipore). 10% PVA films were prepared by dissolving PVA in water heated to 100 °C under continuous stirring for 2–3 h. The mixtures of LDS 798 with PVA were poured onto horizontal glass plates and left for 48 h to dry. The films were removed and cut into rectangular pieces ($\sim$30 mm × 20 mm). Such a piece was clamped in a stretching device and progressively stretched up to $\sim$8 times its original length, which was close to its elastic limit. In the stretching procedure, the film was heated and the stretching force adjusted to assure a smooth film elongation. Before stretching we marked a 10 mm diameter circle in the center of a film strip. The stretching ratio has been defined as the ratio between the long and short axis of the ellipsoid formed upon stretching [28–30].

For correctly prepared films, the center area of about (5 mm × 5 mm) is very uniform. The fluorescence signal intensity and polarization measured with laser excitation (beam diameter 0.5 mm) was the same within the entire central region of the stretched film.

We prepared films with various LDS 798 concentrations and did not find any dependence of dichroic ratio on the dye concentration. In the case of LDS 798, the optical densities of prepared films were rather low, not extending 1.0 at 600 nm because of

the dye solubility in the PVA solution. Low concentration of the dye also avoids unwanted crystallization during the drying process.

B. Instrumentation

Absorption, emission, and excitation spectra were recorded using a Cary 50 Bio and a Cary Eclipse fluorescence spectrophotometer (Varian) equipped with manual rotatable polarizers in the light travel path. Polarized components of the fluorescence emission were measured in a front-face configuration on a FluoTime 200 (Picoquant, GmbH) equipped with a 635 nm laser diode that was near the absorption maximum of LDS 798. The fluorescence passed through a long wavelength pass (LWP650) filter, Glan–Taylor (G-T) polarizer and monochromator. The emission intensities were measured alternatively for parallel and perpendicular orientation of polarizer-analyzer. Microscopy measurements were done on a time resolved confocal system, MicroTime 200 (Picoquant, GmbH). This microscope is equipped with avalanche photodiode detectors (APDs) (Perkin Elmer SPCM-AQR-14) and a 60× water immersion NA 1.2 OLYMPUS objective.

C. Theory

The theory for polarized absorption and emission of prolate dyes oriented in stretched PVA films have been previously described in detail [28–34]. Here we only summarize the procedures used previously. The two orthogonal absorption components $A_{\parallel}(\lambda)$ and $A_{\perp}(\lambda)$ measured for light polarized in two orthogonal directions, parallel ($\parallel$) and perpendicular ($\perp$) to the stretching direction, can be expressed by dichroic ratio R_d in the following form:

$$R_d(\lambda) = \frac{A_{\parallel}(\lambda)}{A_{\perp}(\lambda)}. \tag{1}$$

The measured value of dichroic ratio R_d depends on stretching ratio $R_s = a/b$ (defined as the axial semimajor a and the axial minor b axis of an ellipse deformed from a circle of radius that was initially drawn on the film [28–30]). And the absorption anisotropy K [35,36] is given by

$$K(\lambda) = \frac{A_{\parallel}(\lambda) - A_{\perp}(\lambda)}{A_{\parallel}(\lambda) + 2A_{\perp}(\lambda)} = \frac{R_d(\lambda) - 1}{R_d(\lambda) + 2}. \tag{2}$$

The measured wavelength dependent emission anisotropy $r(\lambda)$ is defined as

$$r(\lambda) = \frac{I_{VV}(\lambda) - G(\lambda) I_{VH}(\lambda)}{I_{VV}(\lambda) + 2G(\lambda) I_{VH}(\lambda)}, \tag{3}$$

where $G(\lambda)$ is the wavelength dependent instrumental correction factor (G factor). The first index refers to the orientation of the excitation polarizer (H–horizontal, V–vertical) and the second to the orientation of the emission polarizer.

The limiting value of the anisotropy (polarization) for a single electronic transition is reached when no molecular reorientation occurs during the excited state lifetime. Calculation of theoretical values of absorption and emission anisotropy relies on the assumption that a rigid isotropic solution of fluorophores is excited by linearly polarized light and photoselected molecules conserve the initial distribution. Figure 1 represents an arbitrarily selected molecule in the coordinate system. Angle ω_1 refers to the orientation of the absorption transition moment and angle ω_2 to the orientation of the emission transition moment of the molecule. φ is the angle between long axis (OM) of the molecule and the absorption transition dipole moment $\vec{A}$, and β is the angle between

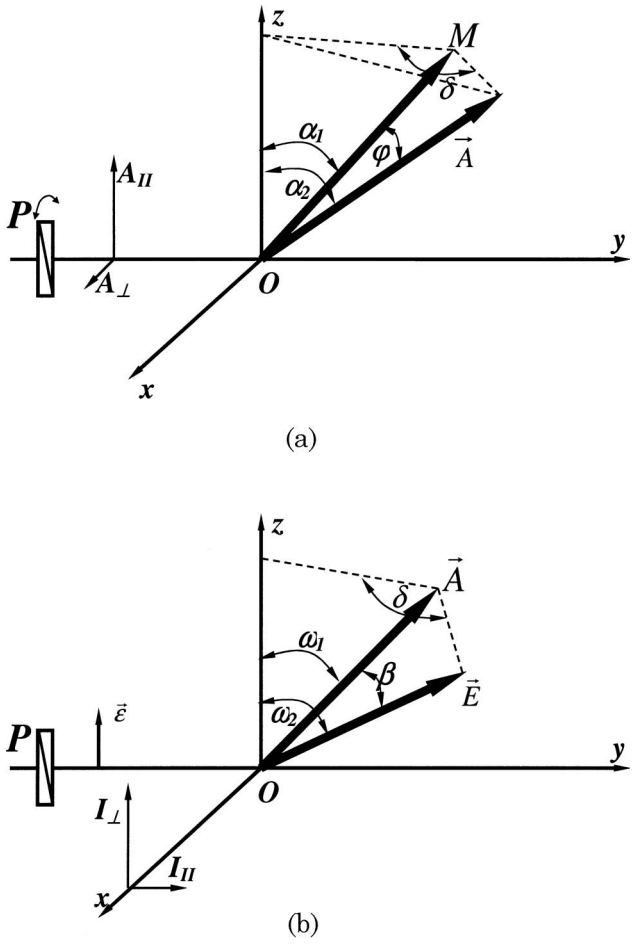

Fig. 1. (a) Geometry of photoselection: P, polarization filter; $A_{\parallel}$ and $A_{\perp}$, absorbances of light measured parallel and perpendicular to stretching direction, respectively; ω_1 and ω, angles between orientation axis z and transition dipole moments for absorption $\vec{A}$ and long axis of molecule OM, respectively; φ, angle between transition dipole moment $\vec{A}$ and molecular axis OM; δ, angle formed by the planes (z, OM) and ($z,\vec{A}$). (b) Geometry of dichroic calculations: $\vec{\varepsilon}$, polarized electric vector of excitation light; P, projection of the polarization filter; $I_{\parallel}$ and $I_{\perp}$, intensities of emission light measured parallel and perpendicular to the incidence polarization, respectively; ω_1 and ω_2, angles between the photoselection axis z and the transition dipole moments for absorption $\vec{A}$ and emission $\vec{E}$, respectively; β, angle between transition dipole moments $\vec{A}$ and $\vec{E}$; δ, angle formed by the planes ($z,\vec{A}$) and ($\vec{E},\vec{A}$).

absorption and emission (E) transition moments. The value of absorption $K(\omega,\varphi)$ and emission anisotropy $r(\omega_1,\beta)$ can be expressed as [30–32]

$$K(\omega,\varphi)=\frac{3\langle\cos^2\omega_1\rangle-1}{2}=\left(\frac{3}{2}\langle\cos^2\omega\rangle-\frac{1}{2}\right)\left(\frac{3}{2}\cos^2\varphi-\frac{1}{2}\right),\quad(4)$$

$$r(\omega_1,\beta)=\frac{3\langle\cos^2\omega_2\rangle-1}{2}=\left(\frac{3}{2}\langle\cos^2\omega_1\rangle-\frac{1}{2}\right)\left(\frac{3}{2}\cos^2\beta-\frac{1}{2}\right),\quad(5)$$

where ω and ω_1 are angles between the z axis of the coordinate system and the long axis of the molecule (ω) and the absorption transition dipole moment $\vec{A}$, respectively. β is the angle between the absorption and emission transition dipole moments, and ω_2 is the angle between the z axis and the emission transition moment. For uniform distribution around the δ angle, the average value of $\cos^2\omega$ or $\cos^2\omega_1$ is given by

$$\langle\cos^2\omega\rangle=\frac{\int_0^{\pi/2}f(\omega)\cos^2\omega\,\mathrm{d}\omega}{\int_0^{\pi/2}f(\omega)\,\mathrm{d}\omega},\quad(6)$$

$$\langle\cos^2\omega_1\rangle=\frac{\int_0^{\pi/2}f(\omega_1)\cos^2\omega_1\,\mathrm{d}\omega_1}{\int_0^{\pi/2}f(\omega_1)\,\mathrm{d}\omega_1},\quad(7)$$

where functions $f(\omega)\mathrm{d}\omega$ and $f(\omega_1)\mathrm{d}\omega_1$ describe the distribution of the long molecular axis (OM) and the distribution of absorption dipole moment, respectively. The orientational distribution function for elongated molecules in a stretched polymer can be described as function of stretching ratio R_S [28,29]:

$$f(\omega)=R_S^2\sin\omega[1+(R_S^2-1)\sin^2\omega]^{-3/2},\quad(8)$$

$$f(\omega_1)=R_S^2\sin\omega_1\cos^2\omega_1[1+(R_S^2-1)\sin^2\omega_1]^{-3/2}.\quad(9)$$

We seek analytical solutions for $K(\omega,\varphi)$ and $r(\omega_1,\varphi)$ presented in Eqs. (4) and (5). To do this we need to put Eq. (8) into Eq. (6) and make substitution for trigonometric function $\cos\omega=x$. This results in

$$\langle\cos^2\omega\rangle=\frac{\int_1^0\frac{R_S^2x^2\mathrm{d}x}{(R^2-1)^{3/2}(a^2-x^2)^{3/2}}}{\int_1^0\frac{R_S^2\mathrm{d}x}{(R^2-1)^{3/2}(a^2-x^2)^{3/2}}},\quad(10)$$

where $a^2=R_S^2/(R_S^2-1)$. An analogical procedure was performed for the solution of the average value of $\cos\omega_1$ in Eq. (7). A combination of Eqs. (9) and (7) gives

$$\langle\cos^2\omega_1\rangle=\frac{\int_0^{\pi/2}R_S^2\sin\omega_1\cos^4\omega_1[1+(R^2-1)\sin^2\omega_1)]^{-3/2}\mathrm{d}\omega_1}{\int_0^{\pi/2}R_S^2\sin\omega_1\cos^2\omega_1[1+(R_S^2-1)\sin^2\omega_1]^{-3/2}\mathrm{d}\omega_1},\quad(11)$$

where both the numerator and the denominator can be simplified to an easier form by substitution of $\cos\omega_1=y$. This enables us to rewrite the integrals as

$$\langle\cos^2\omega_1\rangle=\frac{\int_1^0\frac{R_S^2y^4\mathrm{d}y}{(R^2-1)^{3/2}(a^2-y^2)^{3/2}}}{\int_1^0\frac{R_S^2y^2\mathrm{d}y}{(R^2-1)^{3/2}(a^2-y^2)^{3/2}}}.\quad(12)$$

Finally, one may calculate both anisotropies (K and r) dependent on the stretching ratio and angle φ between the long axis of the molecule and the transition dipole moment for absorption (or the angle between absorption and emission transition dipole moments β for r calculation):

$$K(\varphi,R_S)=\left\{\frac{3}{2}a^2[1-(a^2-1)^{1/2}\arcsin(1/a)]-\frac{1}{2}\right\}\times\left(\frac{3}{2}\cos^2\varphi-\frac{1}{2}\right),\quad(13)$$

$$r(\beta,R_S)=\left[\frac{3}{2}\frac{(a^2-1)^{1/2}+2a^2(a^2-1)^{-1/2}-3a^2\arcsin\left(\frac{1}{a}\right)}{2(a^2-1)^{-1/2}-2\arcsin\left(\frac{1}{a}\right)}-\frac{1}{2}\right]\left(\frac{3}{2}\cos^2\beta-\frac{1}{2}\right).\quad(14)$$

Based on Eqs. (2) and (13) dichroic ratio R_d is given by

$$R_d=2\frac{1+a^2[1-(a^2-1)^{0.5}\arcsin(1/a)](3\cos^2\varphi-1)-\cos^2\varphi}{1-a^2[1-(a^2-1)^{0.5}\arcsin(1/a)](3\cos^2\varphi-1)+\cos^2\varphi}.\quad(15)$$

3. Results and Discussion

The structure of the LDS 798 compound is illustrated in Fig. 2. The chromophore consists of phenyl and quinoline rings with positive charge delocalized across the quinoline ring and the system of five conjugated bonds. This elongated molecule can be efficiently oriented in an anisotropic environment. Normalized absorption and emission spectra of

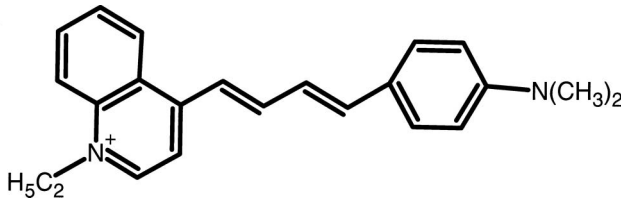

Fig. 2. Chemical structure of NIR fluorophore LDS 798.

LDS 798-doped PVA films in the visible range to NIR are shown in Fig. 3. Maximum absorption spectrum was found at about 600 nm. Both absorption and fluorescence spectra are not structured and display a large Stokes shift. Excitation anisotropy data (Fig. 3, filled circles) at observation of 750 nm reveals that the lowest energy absorption band (electronic $S_0 \rightarrow S_1$ transition) is a single transition that is oriented almost parallel to the long molecular axis. In fact, anisotropy for the whole long wavelength absorption band is high and consistent with a single transition. The emission spectrum shown in Fig. 3 was recorded using an excitation wavelength of 635 nm. As expected, the emission spectrum does not change shape when excited with different wavelengths. Measured fluorescence anisotropy within the emission band slightly decreases for longer wavelengths, suggesting a residual relaxation process.

The strong single electronic transition in the wide (visible–NIR) range of wavelengths and the large Stokes shift make LDS 798 dye a good candidate for the fluorescence standard. We estimated the quantum yield (QY) of LDS 798 in PVA as 0.47 compared with the ethanol solution of nile blue, QY = 0.27 [37]. Figure 4 presents the polarized absorption spectra of PVA films containing LDS 798 as a function of the stretching ratio. In general, the spectra show progressive increase of dichroic ratio with an increase of the stretching ratio, as expected for elongated molecules. This dependence is shown in Fig. 5. Dichroic ratio plotted on this figure progressively increases with the film stretching ratio. The dependence of absorption anisotropy versus stretching ratio is shown in Fig. 6. Based on Eq. (13), an average orientation of the absorption transition dipole moment of LDS 798 chromophore with respect to the long axis of this molecule can be calculated. The theoretical fit to experimental data presented in Fig. 6 as a continuous line is consistent with angle $\varphi = 0$, which means that the transition dipole moment for LDS 798 is practically aligned along the long axis of the molecule.

Highly efficient orientation of the LDS 798 molecule under stretching conditions can be seen in Figs. 7 and 8. Figure 7(a) shows the size and shape of a film used for photographs. Figure 7(b) shows four photographs of fluorescence spots received for highly

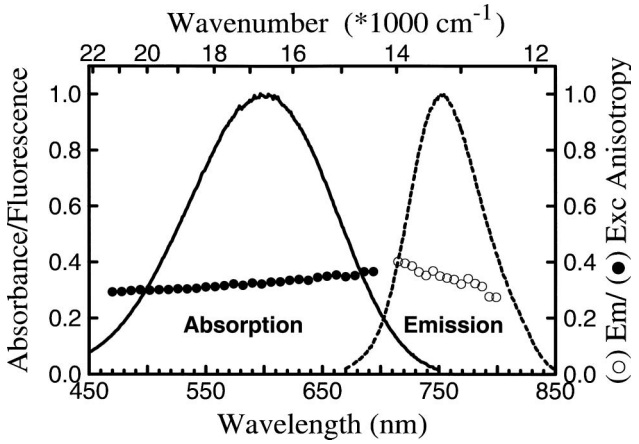

Fig. 3. Normalized absorption and emission spectra LDS 798 in isotropic (unstretched) PVA film shown as solid and dotted line, respectively. Filled and empty points present anisotropy data for excitation (observed at 750 nm) and emission (excitation at 635 nm) fluorescence, respectively.

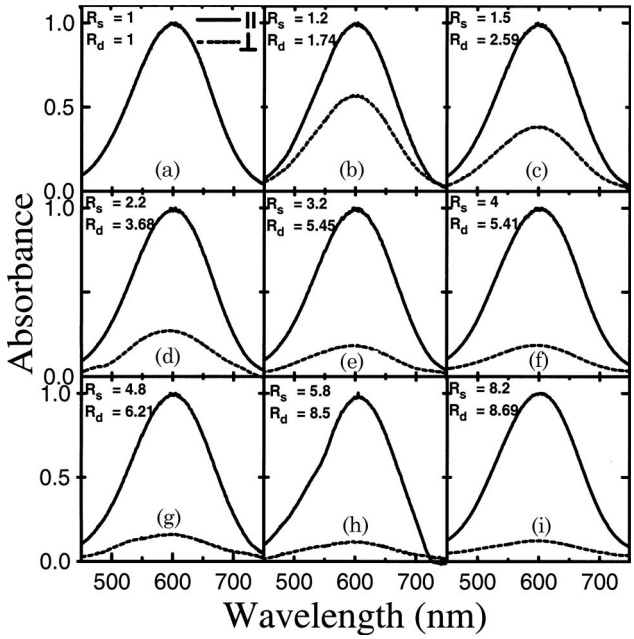

Fig. 4. Parallel (—) and perpendicular (- -) polarized absorption spectra of LDS 798 recorded for different values of stretching ratio R_S.

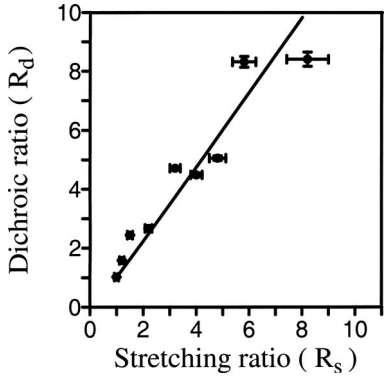

Fig. 5. Dependence of dichroic ratio R_d on stretching ratio R_S for LDS 798-doped PVA films. Symbols correspond to experimental data and the continuous line corresponds to the theoretical values obtained for $\varphi = 0°$ in Eq. (15). The error bars for R_S were estimated with the assumption of 0.2 mm accuracy in the length measurements.

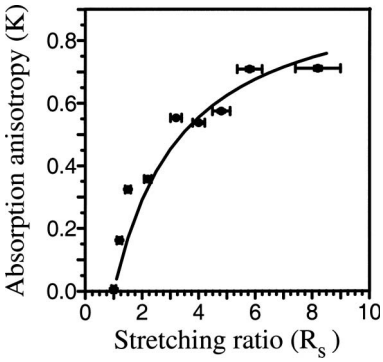

Fig. 6. Experimental points and theoretical prediction for the dependence of the absorption anisotropy $K(R_S, \varphi)$ on the stretching ratio R_S for LDS 798-doped PVA films. The theoretical line was calculated from Eq. (13) with the assumption $\varphi = 0°$.

stretched polymer film illuminated with visible nonpolarized light and observed through an analyzing polarizer with a different orientation relative to the stretching direction. The photographs were taken with a Canon EOS 300D digital SLR camera with 18–55 mm f-stop lens (Canon) through a LWP650 long wavelength pass filter and a polarizer. Different angles give easily recognizable differences in intensity of fluorescence light.

Figure 8 presents image data measured by a CCD camera in microscope configuration for the same stretched film for two orthogonal orientations, perpendicular and parallel relative to the excitation polarizer orientation, respectively. Almost 80% change in intensity was observed by the system when changing the film orientation.

The angular relation between the electronic transition dipole moment for absorption and emission is given by a combination of Eqs. (14) and (15) and is reflected in the plot of fluorescence anisotropy as a function of dichroic ratio (Fig. 9). The maximum value of anisotropy (0.82) was observed for $R_S = 8$. The solid line in Fig. 9 is a theoretical prediction of experimental values (as expected from Eq. (14)) with an assumption of alignment of the transition dipole moment along long axis of molecule ($\varphi = 0$). Although this equation is only an approximation, a very good fit can be observed for the angle between

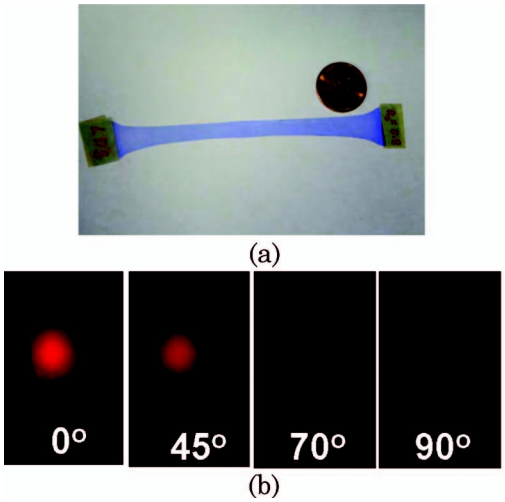

Fig. 7. (a) Photograph of stretched LDS 798-doped PVA film. (b) Intensities of fluorescence emission observed for four different angles (0, 45, 70, and 90°) relative to the stretching direction of the PVA film.

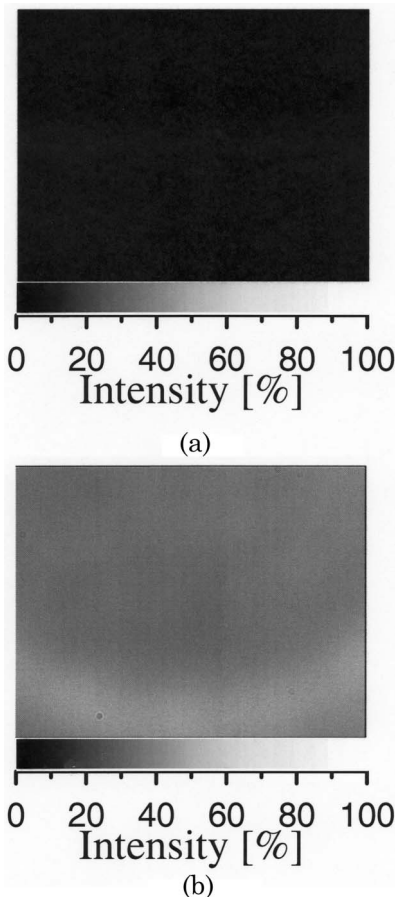

Fig. 8. Images observed for highly stretched PVA film with LDS 798 for two different polarizations, (a) perpendicular and (b) parallel.

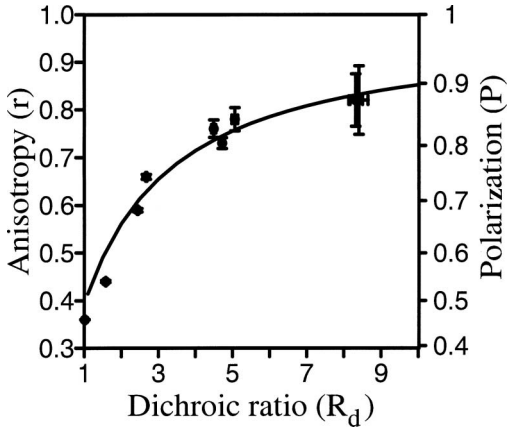

Fig. 9. Dependence of the emission anisotropy r (and polarization P) on the dichroic ratio R_d determined for stretched PVA films doped with LDS 798. Figure presents experimental data (points) and least square fit to them by using Eq. (14).

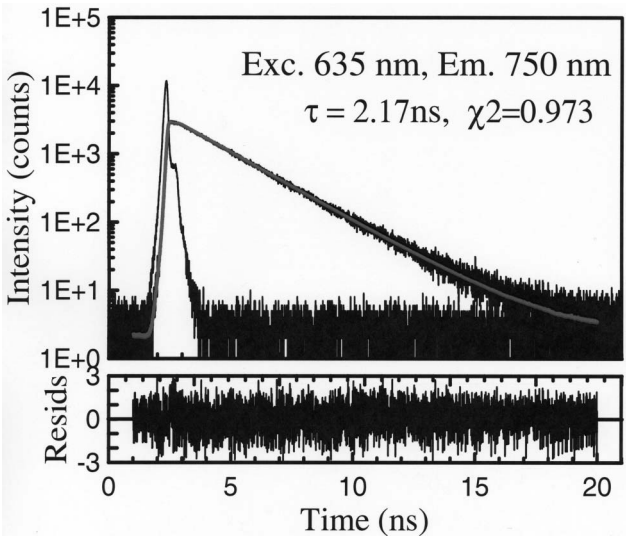

Fig. 10. Fluorescence intensity decay of LDS 798-doped PVA film (isotropic). Excitation was 635 mm, observation was 750 mm.

the absorption and the emission transition dipole moments of about $\beta = 8°$.

Measured fluorescence intensity decay for this chromophore in the isotropic PVA film is presented in Fig. 10. Data were obtained with an excitation pulse at 653 nm and observation at 750 nm. A very good fit with fluorescence decay of the LDS 798 was obtained using a single exponential (χ^2) value equal to 0.973. Analysis of intensity decay reveals a single fluorescence lifetime (2.17 ns) that is also reported in Table 1. The fluorescence lifetime drops significantly for the same probe in organic solvents and water (data not shown).

4. Conclusions

LDS 798 dye has been characterized in PVA films. The dye has a relatively high quantum yield (0.47 in PVA film) and single electronic transition $S_0 - S_1$ in red and NIR regions. Consequently, LDS 798 displays a high degree of linear dichroism and very high fluorescence anisotropy (Figs. 3 and 4) in stretched polymer films. The progressive stretching of the polymeric films is accompanied with a progressive orientation of the dye molecules along the stretching axis. The absorption and fluorescence measurements conducted in a front-face configuration provided the quantitative data on a dichroic ratio, as well as on fluorescence quantum yield, lifetime, and anisotropy. The known values of anisotropy can be used to determine the correction factors in polarization measurements using the microscope. This is important in the case of high numerical aperture objectives that distort polarization [38]. To evaluate this distortion, we rotated the unstretched LDS 798-doped PVA film and observed fluorescence signals through a polarizer oriented parallel or perpendicular to the polarization direction of the excitation laser (Fig. 11).

Table 1. Photophysical Characteristics of LDS 798-Doped PVA Film

Compound	λ^{max} abs (nm)	λ^{max} em (nm)	QY	τ (ns)	r_{max}	φ (deg)
LDS 798 in PVA Film	600	750	0.47	2.17	0.37	8

In the case of an isotropic film, polarized components of fluorescence do not depend on the orientation of the sample. The ratio of parallel to perpendicular emission components remains constant at a value of 2.79. If the polarized components were not distorted, the ratio should be equal to 2.41, which corresponds to the value of anisotropy of 0.32 (see Fig. 3 at 635 nm excitation). To obtain a correct value of anisotropy, the parallel component should be multiplied by a factor of 1.16 (G factor).

We also present another way to find the G factor that does not require prior knowledge of sample anisotropy. This is a more general and accurate approach that only requires a partially oriented sample, such as a stretched polymer film. Figure 12 shows the polarized components while the stretched sample was rotated on the microscope stage. Because of the symmetry of the fluorophores distribution in the stretched film, the maximum intensity of the perpendicular component appears with double frequency (compare Figs. 12(a) and 12(b)). When the film is oriented and excited at 45°, the parallel and perpendicular components must be equal. The ratio of the intensities of polarized components measured with parallel and perpendicular orientation of analyzer–polarizer is equal to the G-factor value. The same ratio was found for different stretched films and does not depend on the stretching ratio. The average value of the G factor estimated from stretched and isotropic films was found to be 1.155. This is very close to the value that was determined from the unstretched film method.

We recommend this simple method for finding the G factor in any spectroscopy/microscopy instrumentation. Note that, using oriented dye-doped films, the

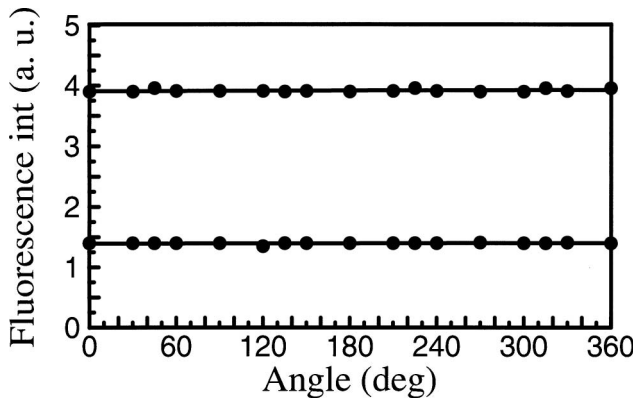

Fig. 11. Fluorescence intensities of polarized components observed for an isotropic sample of LDS 798-doped PVA film. The sample was rotated on the microscope stage and illuminated by high numerical aperture objective 1.2, 60× OLYMPUS. To obtain a correct value of anisotropy (0.32, Fig. 3), the parallel component must be multiplied by a G factor of 1.16.

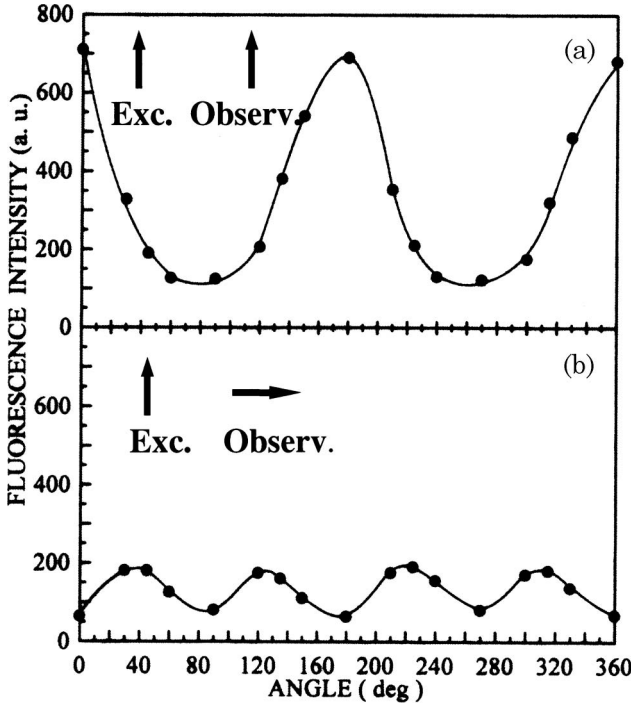

Fig. 12. .a) Fluorescence intensity of a parallel component observed for the 8-fold stretched sample of LDS 798-doped PVA film, b) Perpendicular component of this sample. The sample was rotated on the microscope stage.

investigator does not need to know either anisotropy values or stretching ratio to estimate the instrumental G factor.

This work is supported by the Polish Ministry of Science and Higher Education Grant No.17/MOB/2007/0 (R. L.) and by Texas ETF grant (CCFT). We dedicate this paper to professor Alfons Kawski for his contribution to the field.

References

1. A. Periasamy, M. Elangovan, E. Elliott, and D. L. Brautigan, "Fluorescence lifetime imaging (FLIM) of green fluorescent fusion proteins in living cells," Methods Mol. Biol. **183**, 89–100 (2002).
2. A. Squire, P. I. H. Bastiaens, "Three dimensional image restoration in fluorescence lifetime imaging microscopy," J. Microsc. **193**, 36–49 (1999).
3. G. Mariott, R. M. Clegg, D. J. Arndt-Jovin, and T. M. Jovin, "Time resolved imaging microscopy, phosphorescence, and delayed fluorescence imaging," Biophys. J. **60**, 1374–1387 (1991).
4. T. Förster, "Intermolecular energy migration and fluorescence," Ann. Phys. **2**, 55–75 (1948).
5. S. Hohng, C. Joo, and T. Ha, "Single-molecule three-color FRET," Biophys. J. **87**, 1328–1337 (2004).
6. X. Zhuang, H. Kim, M. J. Pereira, H. P. Babcock, N. G. Walter, and S. Chu, "Correlating structural dynamics and function in single ribozyme molecules," Science **296**, 1473–1476 (2002).
7. D. W. Piston and M. Rizzo, "FRET by fluorescence polarization microscopy," Methods Cell Biol. **85**, 415–430.
8. I. Koyama-Honda, K. Ritchie, T. Fujiwara, R. Iino, H. Murakoshi, R. S. Kasai, and A. Kusumi, "Fluorescence imaging for monitoring the colocalization of two single molecules in living cells," Biophys. J. **88**, 2126–2136 (2004).
9. P. H. Lommerse, H. P. Spaink, and T. Schmidt, "*In vivo* plasma membrane organization: results of biophysical approaches," Biochim. Biophys. Acta **1664**, 119–131 (2004).
10. K. Bacia, I. V. Majoul, and P. Schwille, "Probing the endocytic pathway in live cells using dual-color fluorescence cross-correlation analysis," Biophys. J. **83**, 1184–1193 (2002).
11. N. Kahya, D. Scherfeld, K. Bacia, B. Poolman, and P. Schwille, "Probing lipid mobility of raft-exhibiting model membranes by fluorescence correlation spectroscopy," J. Biol. Chem. **278**, 28109–28115 (2003).
12. J. R. Lakowicz, "Fluorescence correlation spectroscopy," in *Principles of Fluorescence Spectroscopy* (Springer, 2006), pp. 797–840.
13. R. M. Clegg, "Fluorescence resonance energy transfer and nucleic acids," Methods Enzymol. **211**, 353–388 (1992).
14. A. Kawski, "Excitation energy transfer and its manifestation in isotropic media," Photochem. Photobiol. **38**, 487–508 (1983).
15. Z. Gryczynski, I. Gryczynski, and J. R. Lakowicz, "Basics of fluorescence and FRET," in *Molecular Imaging, FRET Microscopy and Spectroscopy*, A. Periasamy and N. R. Day, eds. (Oxford, 2005), pp. 21–56.
16. W. M. Shih, Z. Gryczynski, J. R. Lakowicz, and J. A. Spudich, "A FRET-based sensor reveals large ATP hydrolysis-induced conformational changes and three distinct states of the molecular motor myosin," Cell **102**, 683–694 (2000).
17. J. N. Forkey, M. E. Quinlan, M. A. Shaw, J. E. T. Corre, and Y. E. Goldman, "Three-dimensional structural dynamics of myosin V by single-molecule fluorescence polarization," Nature **422**, 399–404 (2003).
18. S. Syed, G. E. Snyder, C. Franzini-Armstrong, P. R. Selvin, and Y. E. Goldman, "Adaptability of myosin V by simultaneous detection of position and orientation," EMBO J. **25**, 1795–1803 (2006).
19. K. Suhling, J. Siegel, P. M. Lanigan, S. Lévêque-Fort, S. E. Webb, D. Phillips, D. M. Davis, and P. M. French, "Time-resolved fluorescence anisotropt imaging applied to live cells," Opt. Lett. **29**, 584–586 (2004).
20. J. A. Dix and A. S. Verkman, "Mapping of fluorescence anisotropy in living cells by ratio imaging," Biophys. J. **57**, 231–240 (1990).
21. A. H. Clayton, Q. S. Hanley, D. J. Arndt-Jovin, V. Subramaniam, and T. M. Jovin, "Dynamic fluorescence anisotropy imaging microscopy in the frequency domain (rFLIM)," Biophys. J. **83**, 1631–1649 (2002).
22. A. Squire, J. Verveer, O. Rocks, and P. I. Bastiaens, "Red-edge anisotropy enables dynamic imaging of homo-FRET between green fluorescent proteins in cells," J. Struct. Biol. **147**, 62–69 (2004).
23. A. G. Harpur, F. S. Wouters, and P. I. H. Bastiaens, "Imaging FRET between spectrally similar GFP molecules in a single cells," Nat. Biotechnol. **19**, 167–169 (2001).
24. A. P. Demchenko, I. Gryczynski, Z. Gryczynski, W. Wiczk, H. Malak, and M. Fishman, "Intramolecular dynamics in the environment of the single tryptophan residue in staphylococcal nuclease," Biophys. Chem. **48**, 39–48 (1993).
25. Z. Gryczynski and E. Bucci, "A new front-face optical cell for measuring weak fluorescent emissions with time resolution in the picosecond time scale," Biophys. Chem. **48**, 31–38 (1993).
26. Z. Gryczynski, E. Bucci, and J. Kusba, "Linear dichroism study of metalloporphyrin transition moments in view of radiationless interactions with tryptophan in hemoproteins," Photochem. Photobiol. **58**, 492–498 (1993).
27. R. B. Thompson, I. Gryczynski, and J. Malicka, "Fluorescence polarization standards for high-throughput screening and imaging," BioTechniques **32**, 37–38, 40, 42, (2002).
28. Y. Tanizaki, "Dichroizm of dyes in the stretched PVA sheet. II. The relation between the optical density ratio and the stretch

ratio, and an attempt to analyze relative directions of absorption bands," Bull. Chem. Soc. Japan **32**, 75–80 (1959).
29. Y. Tanizaki, "The correction of the relation of the optical density ratio to the stretch ratio to the dichroic spectra," Bull. Chem. Soc. Japan **38**, 1798–1799 (1965).
30. A. Kawski and Z. Gryczynski, "On the determination of transition-moment directions from emission anisotropy measurements," Z. Naturforsch. A **41a**, 1195–1199 (1986).
31. A. Kawski and P. Bojarski, "Photoselection of luminescent molecules in isotropic and anisotropic media by multiphoton excitation. Electronic transition moment directions," Asian J. Spectroscopy **11**, 67–94 (2007).
32. A. Kawski and Z. Gryczynski, "On the determination of transition-moment directions from emission anisotropy measurements," Z. Naturforsch **42a**, 617–621 (1987).
33. A. Kawski and Z. Gryczynski, "Determination of the transition-moment directions from photoselection in partially oriented systems," Z. Naturforsch. A **42a**, 808–812 (1987).
34. A. Kawski and Z. Gryczynski, "Relation between the emission anisotropy and the dichroic ratio for solute alignment in streached polymer films," Z. Naturforsch. A **42a**, 1396–1398 (1987).
35. C. Horcssler, B. Hardy, and E. Fredericq, "Interaction of ethidium bromide with DNA. Optical and electrooptical study," Biopolymers **13**, 1144–1160 (1974).
36. Y. Matsuoka, "Film dichroism. 4. Linear dichroism study of orientation behavior of planar molecules in stretched poly (viny1 alcohol) film," J. Phys. Chem. **84**, 1361–1366 (1980).
37. R. Sens and K. H. Drexhage, "Fluorescence quantum yield of oxazine and carbazine laser dyes," J. Lumin. **24/25**, 709–712 (1981).
38. D. Axelrod, "Carbocyanine dye orientation in red cell membrane studied by microscopic fluorescence polarization," Biophys. J. **26**, 557–573 (1979).

APPENDIX B

OTHER FIRST AUTHUR PUBLICATIONS

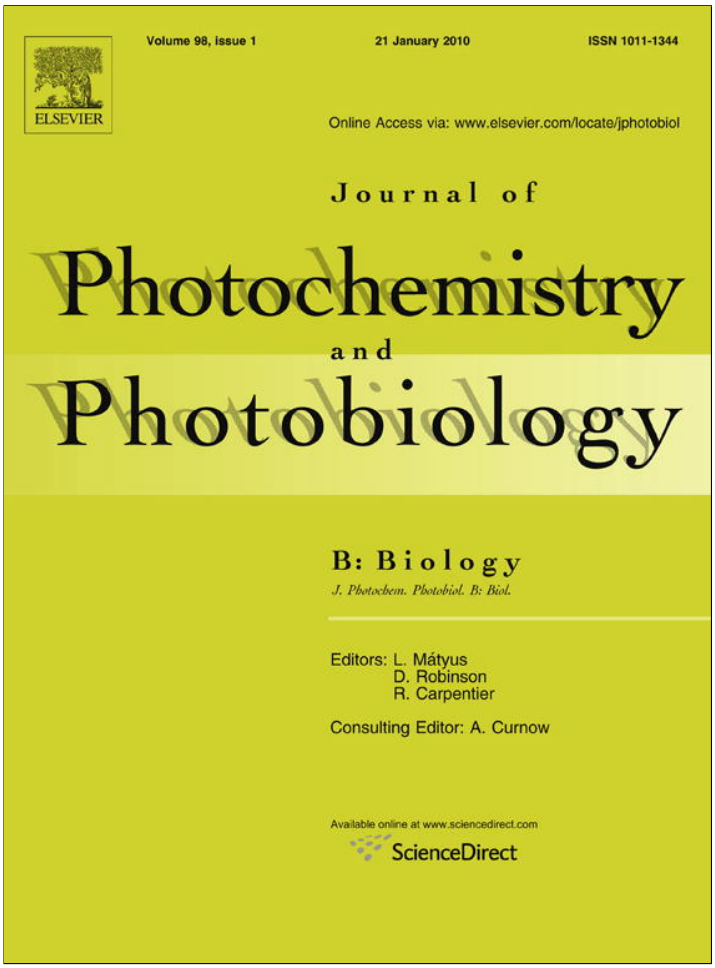

Journal of Photochemistry and Photobiology B: Biology 98 (2010) 35–39

Contents lists available at ScienceDirect

Journal of Photochemistry and Photobiology B: Biology

journal homepage: www.elsevier.com/locate/jphotobiol

Photophysical properties of a new DyLight 594 dye

Pabak Sarkar [a], Savitha Sridharan [a], Rafal Luchowski [a,b], Surbhi Desai [c], Boguslawa Dworecki [c], Marie Nlend [c], Zygmunt Gryczynski [a], Ignacy Gryczynski [a,d,*]

[a] Center for Commercialization of Fluorescence Technologies, Department of Molecular Biology and Immunology, University of North Texas Health Science Center, 3500 Camp Bowie Boulevard, Fort Worth, TX 76107, United States
[b] Department of Biophysics, Institute of Physics, Maria Curie-Sklodowska University, 20-031 Lublin, Poland
[c] Thermo Fisher Scientific, 3747 N. Meridian Road, PO Box 117, Rockford, IL 61105, United States
[d] Department of Cell Biology and Anatomy, University of North Texas Health Science Center, 3500 Camp Bowie Boulevard, Fort Worth, TX 76107, United States

ARTICLE INFO

Article history:
Received 26 August 2009
Received in revised form 12 October 2009
Accepted 29 October 2009
Available online 4 November 2009

Keywords:
Fluorophore
Quantum yield
Anisotropy
Fluorescence lifetime

ABSTRACT

We describe spectral properties of novel fluorescence probe DyLight™ 594. Absorption and fluorescence spectra of this dye are in the region of Alexa 594 fluor spectra. The quantum yield of DyLight 594 in conjugated form to IgG is higher than corresponding quantum yield of Alexa 594 by about 50%. The new DyLight dye also shows slightly longer lifetime and photostability. These favorable properties and high anisotropy value, as well as a high cross-section for two-photon excitation, make this fluorophore attractive as a fluorescence probe in biochemical/biological studies involving fluorescence methods.

Published by Elsevier B.V.

1. Introduction

The fluorescence applications depend on the development of new probes. In recent years there is a constant progress in new fluorescence markers such as quantum dots [1–3] or fluorescent proteins [4–6]. However, these new fluorescence probes cannot always substitute organic fluorophores. Therefore many of new fluorophores and their active forms have been developed and commercially produced. It is now easy to select a fluorescent probe in any spectral region. Despite this enormous progress however, there is still a need for more efficient and photostable dyes. This is due to minimization of used volumes and constant demand for higher sensitivity in high throughput screening and arrays analysis. Also, immunohistology studies demand photostable, long wavelength dyes for detection of less abundant tissue proteins [7]. The major problem for meeting this demand is in the fact that quantum yield of conventional organic fluorophores decreases once it is conjugated to proteins [7]. Though fluorescein based dyes are not quenched to that extent, they are considered to be photolabile [8] and unsuitable for prolonged microscopy experiments. Rhodamine based dyes are known for their photostability but tend to form non-fluorescent derivatives and get self-quenched upon conjugation with proteins [9]. New dyes based on the structure of these dyes, but with modified reactive groups, have been developed by various groups. These dyes have: (a) comparatively high brightness and photostability and (b) are insensitive to temperature and pH changes in the environment.

Other photophysical properties like fluorescence lifetimes and correlation times of fluorophores are also becoming important as techniques like fluorescence lifetime imaging microscopy (FLIM) and anisotropy decay are being used in understanding molecular interactions in intact cells and cell-free extracts in diagnostics. Förster's resonance energy transfer (FRET) measurements using FLIM to confirm macromolecular interactions have gained popularity in last decade. Measurement of these properties in microscopic configuration is challenging if the signal to noise ratio is not adequate. One of the approaches to increase this ratio is to perform the measurements at longer excitation wavelength, where the cellular components do not absorb efficiently. But conventional 'long wavelength fluorophores' generally are not bright and have very low fluorescent lifetime values (~1 ns). Thus, they are inconvenient to be used as donors for FRET experiments. Longer lifetime fluorophores at long wavelength regime are lanthanide elements-based complex compounds [10–12] and transition metal–ligand complexes like ruthenium 2,2′-bipyridyl $[Rubpy)_3]_{2+}$ [13–15]. However, these compounds are too bulky to be conjugated with proteins and cannot be used for immunoassays. Therefore, organic compounds with emission at longer wavelength (>550 nm) and

* Corresponding author. Address: Center for Commercialization of Fluorescence Technologies, Department of Molecular Biology and Immunology, University of North Texas Health Science Center, 3500 Camp Bowie Boulevard, Fort Worth, TX 76107, United States. Tel.: +1 817 735 2036; fax: +1 817 735 2610.
E-mail address: igryczyn@hsc.unt.edu (I. Gryczynski).

1011-1344/$ - see front matter Published by Elsevier B.V.
doi:10.1016/j.jphotobiol.2009.10.005

considerable lifetime values (>2 ns) would be ideal as donors for FRET experiment.

In this manuscript, we describe photophysical properties of a new dye DyLight 594 from Thermo Scientific (Rockford, Il). This fluorophore has a convenient spectral range, high brightness and fluorescence anisotropy, and is very photostable. We compared the properties of DyLight 594 with Alexa 594 Fluor, which is known for its performance as a fluorescent label.

2. Materials and methods

DyLight and Alexa 594 fluors, both NHS esters and immunoglobin G conjugated form, were provided by Fisher Scientific, IL. Solutions of the fluorophores were made in phosphate buffered saline pH 7.4 (the stock solution of PBS was purchased from Amresco, OH).

2.1. Steady-state measurements

Cary 50 Bio® (Varian Inc. Australia) spectrophotometer was used for absorption studies and Cary Eclipse fluorescence spectrophotometer (Varian Inc., Australia) was used for steady-state fluorescence measurements. The Cary Eclipse spectrofluorometer is fitted with peltier system (Quantum Northwest, WA) for temperature control and has polarizers as accessories. The absorption and emission of the samples was measured in a 1 cm × 1 cm cuvette (in case of free dyes) or a 1 cm × 0.4 cm cuvette (in case of conjugated dyes). The fluorescence signal of those samples was measured as a function of emission wavelength using suitable excitation wavelength and emission range (so that the total area under the curve can be recorded). To calculate quantum yield following formula was used:

$$Q = Q_R \frac{I.(OD_R).n^2}{I_R.(OD).n_R^2} \tag{1}$$

where Q is quantum yield, I is the area under curve (AUC) of fluorescence signal, n is the refractive index (the ratio of n^2/n_R^2 always 1 in these calculations). Prefix R is for reference. Cresyl violet in methanol, with a quantum yield of 0.53 [16], was used as reference compound.

We used broad range (UV–VIS) polarizers (Manual Polarizer Accessory, Varian Inc., Australia) for measurements in both visible and ultraviolet region. At 350 nm the polarization was more than 94% whereas in visible region the polarization was ~99%. The mathematical expression used to calculate anisotropy was

$$r = \frac{I_{VV} - GI_{VH}}{I_{VV} + 2GI_{VH}} \tag{2}$$

where I_{VV} and I_{VH} are vertically excited-vertically emitted and vertically excited-horizontally emitted fluorescence components of the proteins, and G is the instrumental G-factor.

We used Perrin equation to calculate the apparent rotational correlation time θ for the dye in free and IgG bound form. Perrin's equation is given by:

$$\theta = \frac{\tau}{r_o/r - 1} \tag{3}$$

where r_o is a fundamental anisotropy for which transition dipole moment for absorption has the same direction like transition dipole moment for emission.

2.2. Time-resolved measurements

Time-resolved fluorescence measurements were carried out on FluoTime200 fluorometer (PicoQuant, GmbH). This fluorometer is equipped with an ultrafast microchannel plate (MPT) and is capable to well-resolve sub-nanosecond decays. A 405 nm pulsed laser diodes LDH-PC-405 (PicoQuant, GmBh) was in low power regime (<70 ps FWHM) with 5 MHz repetition rates. The laser diodes are routinely used to measure fluorescence decays and lifetimes within ±10 ps accuracy. The lifetime data were analyzed by FluoTime Software, Version 4.0 (PicoQuant, GmbH).

For lifetime measurements, a monochromator supported by long wave pass filter on the observation path was used. All the measurements for lifetime decay were performed using magic angle conditions. The decay was fitted with multi-exponential model using the expression

$$I(t) = \sum_{i=1} \alpha_i e^{-\frac{t}{\tau_i}} \tag{4}$$

where $I(t)$ is the intensity at a time t, α_i is the amplitude of ith component and τ_i is the lifetime of the ith component.

2.3. Photobleaching studies

All the experiments were performed with dyes (samples) of absorption less than 0.2 OD at their peak to avoid any inner filter effect.

For each photobleaching experiment, two dye laser cuvettes (0.1 cm × 1 cm dimension) were used. To each one of them 200 μl of sample was added. One of them (Dark) was always exposed to ambient room light, the other (Light) was illuminated by a well collimated 7 W lamp for different intervals of time. To negate the effect of heat generated by the lamp, a water-filter (a cuvette of 1 cm × 1 cm; filled with water) was placed in between the sample and the lamp; neutral density filter of 0.4 OD was used to decrease the photon flux to the sample. The sample cuvette and water-filter were placed in such a way that the lamp uniformly illuminated them.

Intensity from both 'Light' and 'Dark' samples were measured at different time points in Varian eclipse spectrofluorometer using appropriate excitation wavelength. The instrumental parameters were not modulated during measurements. The ratio between 'Light' and 'Dark' samples was plotted against time for each time point. Then the plotted points were fit with mono-exponential decay function using equation:

$$y = y_0 + A_0 e^{x/t} \tag{5}$$

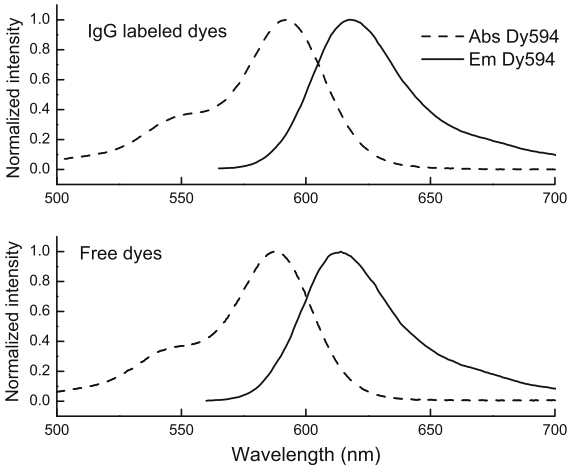

Fig. 1. Absorption (broken line) and emission (solid line) spectra of DyLight 594 dyes. Top panel shows the spectra of immunoglobin (IgG) conjugated dye and the bottom panel shows the spectra of free dye. There is no significant shift in either absorption or emission spectra upon conjugation.

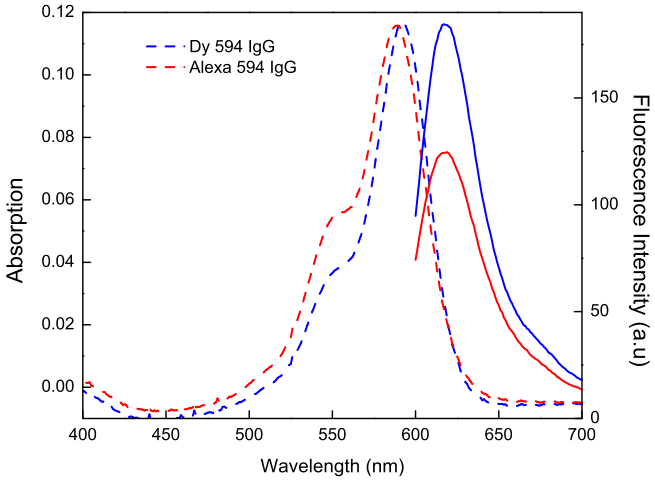

Fig. 2. Comparative analysis of intensities of IgG conjugated DyLight 594 dye and Alexa 594 dye. Absorption spectra (broken lines) show that both molecules absorb similarly at 594 nm wavelength. Emission intensities recorded when both molecule were excited with light of 594 nm wavelength shows that peak intensity of DyLight 594 dye conjugated with IgG was 1.5 times more than that of the IgG conjugated Alexa 594 dye.

where y_0 is the background level, A_0 is the maxima, x is the plotted intensity and t is the average time.

3. Results and discussion

Absorption and fluorescence emission spectra of DyLight 594 free and labeled on IgG are presented in Fig. 1. This dye can be conveniently excited from 530 to 610 nm. Many excitation sources like a green 532 nm, 543 nm and 568 nm lasers, as well as Rhodamine 6G dye laser operate in this spectral region. Most types of photodetectors are sensitive to the range where DyLight 594 emits (600–650 nm). The DyLight 594 emission overlaps with absorption spectra of long wavelength fluorophores like Cy5 dye or Alexa 647 Fluor as well as SETA Biomedical and DyLight red dyes series. This high overlap and great quantum yield (0.83 in free form and 0.64 as conjugated) makes DyLight 594 as an efficient donor of the excitation energy for popular red dyes. For example, the characteristic Förster distance between DyLight 594 and DyLight 647 is 76.1 Å. Whereas R_0 for homotransfer of DyLight 594 is ~57 Å.

We compared the fluorescence emission of IgG conjugated to DyLight 594 and Alexa 594 fluors. The optical densities of both dyes were adjusted to yield the same absorptions at 594 nm, as shown in Fig. 2. The excitation at 594 nm results in about 50% stronger fluorescence of DyLight 594 than Alexa 594 fluor (Table 1). A higher quantum yield of DyLight 594 extends the range of FRET. This has a significant advantage in detection of molecular interactions. In case of FRET experiments using DyLight 594 or Alexa 594 as donor and DyLight 647 as acceptor the characteristic

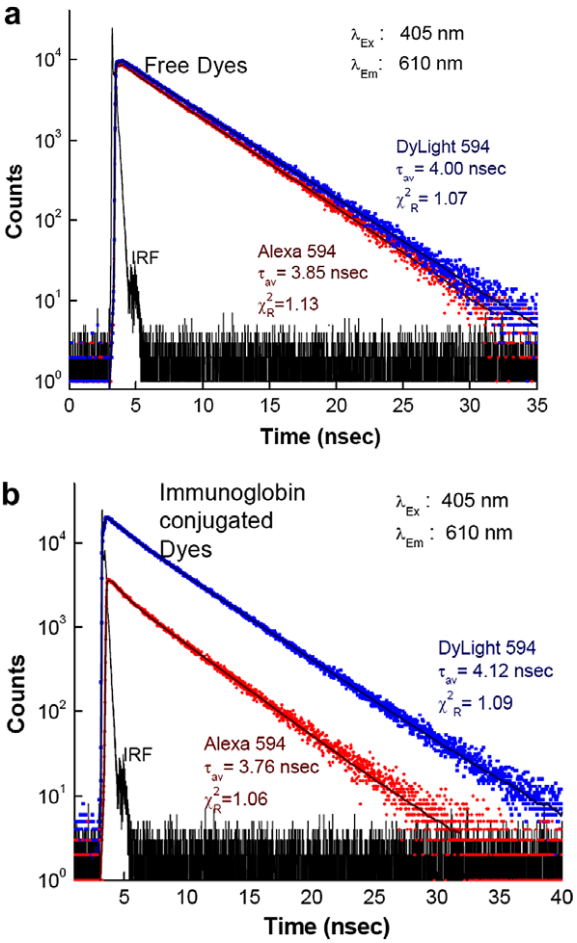

Fig. 3. Fluorescence decay profile of: (a) free and (b) immunoglobin conjugated DyLight 594 (blue) and Alexa 594 (red) dyes. The fluorophores were excited with 405 nm laser diode. The decay of fluorescence intensity was observed at 610 nm wavelength. The measured decays were fitted with deconvoluted multi-exponential decay model using instrument response function; fits are shown in solid lines. Average lifetime (τ_{av}) and goodness-of fit (χ_r^2) of the fit are indicated. (For interpretation of the references to colour in this figure legend, the reader is referred to the web version of this article.)

Förster distances (R_0) will be 70 Å for Alexa 594 and 75 Å for DyLight 594 (the difference is due to the quantum yields). If the apparent distance between donor and acceptor residues in a proteins complex is 75 Å, the energy transfer efficiency will be ~50% in the case of DyLight 594 (easily measurable), and ~40% in the case of Alexa 594 Fluor.

Fluorescence lifetimes are about 10% longer for DyLight 594 when conjugated to immunoglobin (IgG) dye than that for Alexa 594 fluor (Fig. 3, Table 1). A relatively long lifetime in the red spec-

Table 1
Quantum yields and average lifetimes of Alexa 594 and DyLight 594 free form and conjugated to immunoglobin.

Quantum yield	DyLight 594 unlabeled 0.83	DyLight 594 IgG labeled 0.64	Alexa 594 unlabeled 0.83	Alexa 594 IgG labeled 0.42
Lifetime (intensity weighted)	**τ_{av} = 4.04 ns** τ_1 = 4.06 ns α_1 = 0.98 τ_2 = 0.34 ns α_2 = 0.02	**τ_{av} = 4.12 ns** τ_1 = 4.44 ns α_1 = 0.91 τ_2 = 1.48 ns α_2 = 0.07 τ_3 = 0.09 ns α_3 = 0.02	**τ_{av} = 3.89 ns** τ_1 = 3.91 ns α_1 = 0.98 τ_2 = 0.34 ns α_2 = 0.02	**τ_{av} = 3.76 ns** τ_1 = 4.00 ns α_1 = 0.91 τ_2 = 0.90 ns α_2 = 0.09

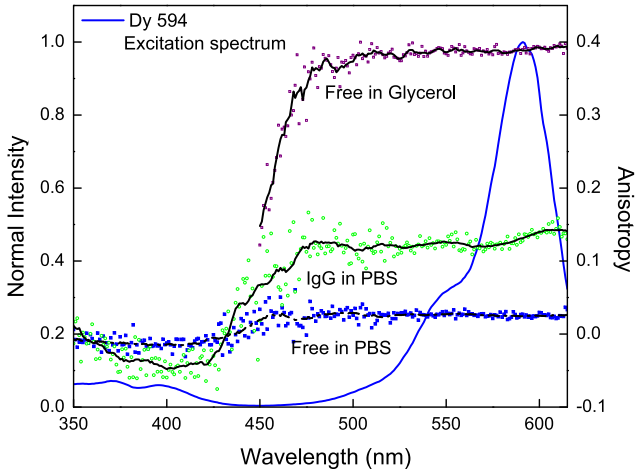

Fig. 4. Excitation anisotropy spectra of free (■, broken line) and IgG conjugated (○, solid line) DyLight 594 dyes at room temperature and in glycerol at 5 °C (free only) (■, solid line). Decreases in anisotropy at shorter wavelengths indicate that absorption dipole for shorter wavelength is orthogonal to the emission dipole. (For interpretation of the references to colour in this figure legend, the reader is referred to the web version of this article.)

tral region, above 4 ns makes DyLight 594 probe attractive for energy transfer and rotational dynamics studies. DyLight 594 has also favorable polarization properties. The fluorescence anisotropy remains constant within the entire long wavelength transition, from 470 nm to 610 nm (Fig. 4). When conjugated to IgG, DyLight 594 has significantly higher anisotropy than in free form (Fig. 4) and the anisotropy measured in glycerol at 5 °C is very close to the limiting value of 0.4 (Fig. 4).

Next, we observed fluorescence photo bleaching for DyLight 594 and Alexa 594 dyes (Fig. 5). Both dyes are fairly photostable and degraded in the light in the similar fashion.

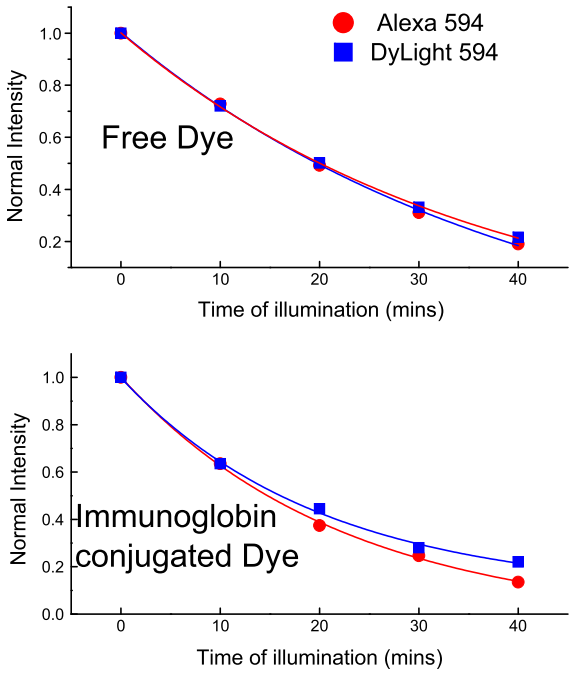

Fig. 5. Comparative study for photostability of free (top panel) and IgG conjugated (bottom panel) Alexa 594 (●) and DyLight 594 (■) dyes. The normalized intensity values were plotted as function of illumination time and the trend was fitted with a mono-exponential decay model.

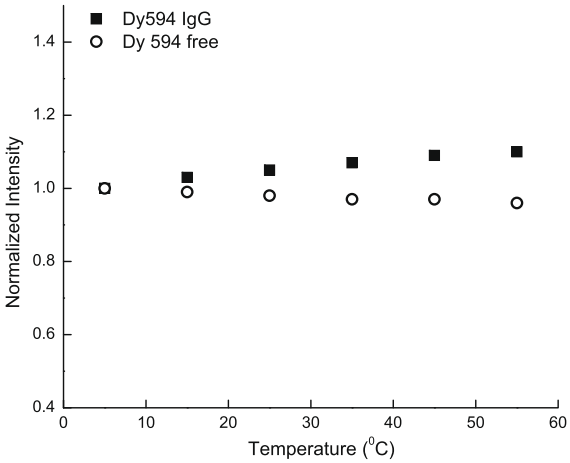

Fig. 6. Temperature dependence of free and immunoglobin conjugated DyLight 594 dye.

Finally, we measured the emission spectra as a function of temperature. The fluorescence intensity of the free dye decreased with temperature slightly, as expected (Fig. 6). However, the DyLight 594 coupled to IgG displays a different behavior. The fluorescence intensity gradually increases with temperature. We suggest that local interaction with protein binding site overcomes a thermal deactivation of excited fluorophore. This could be an additional benefit when using this dye in protein study.

4. Conclusions

We presented spectral properties of a new DyLight dye, DyLight 594, in free and IgG bound form. This dye is fully comparable to Alexa 594 Fluor, however in the bound form DyLight 594 has about 50% higher quantum yield. The dye has relatively long fluorescence lifetime of about 4 ns and favorable polarization properties. Using steady state anisotropy values (Fig. 4) and lifetimes (Fig. 3, Table 1), one can calculate correlation times of free and IgG bound DyLight 594 using Perrin Eq. (3) which is equal 0.28 ns ± 0.03 and 1.95 ns ± 0.06, respectively. The correlation time calculated for DyLight 594 bound to IgG is much shorter than expected for a big protein. It should be considered as an apparent correlation time; an effect of overall correlation time of protein and residual mobility of DyLight 594 molecule. We also cannot exclude a homo-FRET – energy transfer between the same kinds of molecules, because of the presence of few DyLight 594 molecules on one IgG. The calculated value for R_0 of homotransfer is significantly different from that of heterotransfer considering a standard acceptor fluorophore. In conclusion, the new DyLight 594 dye is a bright, photostable probe which can be applied to any fluorescence-based experiments in red region of the spectrum.

Acknowledgements

This research was supported by Texas ETF (CCFT, ZG) and ARP-ATP 000130-0042-2007 (IG) Grants. R. Luchowski is a recipient of a researcher's mobility program from the Polish Ministry of Science and Higher Education.

References

[1] M. Bruchez Jr., M. Moronne, P. Gin, S. Weiss, A.P. Alivisatos, Semiconductor nanocrystals as fluorescent biological labels, Science 281 (1998) 2013.

[2] U. Resch-Genger, M. Grabolle, S. Cavaliere-Jaricot, R. Nitschke, T. Nann, Quantum dots versus organic dyes as fluorescent labels, Nat. Methods 5 (2008) 763–775.
[3] V. Biju, T. Itoh, A. Anas, A. Sujith, M. Ishikawa, Semiconductor quantum dots and metal nanoparticles: syntheses, optical properties, and biological applications, Anal. Bioanal. Chem. 391 (2008) 2469–2495.
[4] A. Crameri, E.A. Whitehorn, E. Tate, W.P. Stemmer, Improved green fluorescent protein by molecular evolution using DNA shuffling, Nat. Biotechnol. 14 (1996) 315–319.
[5] J. Lippincott-Schwartz, E. Snapp, A. Kenworthy, Studying protein dynamics in living cells, Nat. Rev. Mol. Cell Biol. 2 (2001) 444–456.
[6] N.C. Shaner, P.A. Steinbach, R.Y. Tsien, A guide to choosing fluorescent proteins, Nat. Methods 2 (2005) 905–909.
[7] N. Panchuk–Voloshina, R.P. Haugland, J. Bishop-Stewart, M.K. Bhalgat, P.J. Millard, F. Mao, et al., Alexa dyes, a series of new fluorescent dyes that yield exceptionally bright, photostable conjugates, J. Histochem. Cytochem. 47 (1999) 1179.
[8] M. Benchaib, R. Delorme, M. Pluvinage, P.A. Bryon, C. Souchier, Evaluation of five green fluorescence-emitting streptavidin-conjugated fluorochromes for use in immunofluorescence microscopy, Histochem. Cell Biol. 106 (1996) 253–256.
[9] P. Ravdin, D. Axelrod, Fluorescent tetramethyl rhodamine derivatives of alpha-bungarotoxin: preparation, separation, and characterization, Anal. Biochem. 80 (1977) 585–592.
[10] V. Balzani, R. Ballardini, New trends in the design of luminescent metal complexes , Photochem. Photobiol. 52 (1990) 409–416.
[11] F.S. Richardson, Terbium(III) and europium(III) ions as luminescent probes and stains for biomolecular systems, Chem. Rev. 82 (1982) 541–552.
[12] M. Li, P.R. Selvin, Luminescent polyaminocarboxylate chelates of terbium and europium: the effect of chelate structure, Bioconjugate Chem. 5 (1994) 278.
[13] G. Crosby, J. Demas, Quantum efficiencies on transition metal complexes. II. Charge-transfer luminescence, J. Am. Chem. Soc. 93 (1971) 2841–2847.
[14] C.V. Kumar, J.K. Barton, N.J. Turro, Photophysics of ruthenium complexes bound to double helical DNA, J. Am. Chem. Soc. 107 (1985) 5518–5523.
[15] L. Li, H. Szmacinski, J.R. Lakowicz, Long-lifetime lipid probe containing a luminescent metal–ligand complex, Biospectroscopy 3 (1997) 155–159.
[16] J.R. Lakowicz, Principles of Fluorescence Spectroscopy, second ed., Kluwer Academic/Plenum Publisher, New York, 1999.

Photophysical properties of Cerulean and Venus fluorescent proteins

Pabak Sarkar
University of North Texas Health Science Center
Center for Commercialization of Fluorescent Technologies
3500 Camp Bowie Boulevard
Fort Worth, Texas 76107
and
University of North Texas Health Science Center
Department of Molecular Biology and Immunology
3500 Camp Bowie Boulevard
Fort Worth, Texas 76107

Srinagesh V. Koushik
Steven S. Vogel
National Institutes of Health
National Institute on Alcohol Abuse and Alcoholism
Laboratory of Molecular Physiology
5625 Fishers Lane
Rockville, Maryland 20892

Ignacy Gryczynski
University of North Texas Health Science Center
Center for Commercialization of Fluorescent Technologies
3500 Camp Bowie Boulevard
Fort Worth, Texas 76107
and
University of North Texas Health Science Center
Department of Cell Biology and Genetics
3500 Camp Bowie Boulevard
Fort Worth, Texas 76107

Zygmunt Gryczynski
University of North Texas Health Science Center
Center for Commercialization of Fluorescent Technologies
3500 Camp Bowie Boulevard
Fort Worth, Texas 76107
and
University of North Texas Health Science Center
Department of Molecular Biology and Immunology
3500 Camp Bowie Boulevard
Fort Worth, Texas 76107

Abstract. Cerulean and Venus are recently developed fluorescent proteins, often used as a donor-acceptor pair by researchers in Förster resonance energy transfer–based colocalization studies. We characterized the fluorescent properties of these two proteins in a broad spectral range (form ultraviolet to visible region). Excitation spectra, lifetimes, and polarization spectra show significant energy transfer from aromatic amino acids to the fluorescent protein chromophore. High steady-state anisotropy values and the lack of a fast component in anisotropy decays show that the fluorescent protein chromophore is rigidly fixed within the protein structure. Furthermore, we show that the chromophores are not accessible to external quenchers, such as acrylamide or potassium iodide (KI), allowing the removal of "unwanted" background in the environment with external quencher, while leaving the Cerulean/Venus fluorescence unchanged. [DOI: 10.1117/1.3156842]

Keywords: Förster resonance energy transfer; fluorescence timeline; fluorescence anisotropy.

Paper 08429R received Dec. 8, 2008; revised manuscript received Apr. 14, 2009; accepted for publication May 7, 2009; published online Jun. 24, 2009.

1 Introduction

The use of green fluorescent protein (GFP) as a marker to visualize specific proteins inside living cells has revolutionized cell biology.[1,2] The genetic sequence-encoding GFP has been optimized to facilitate both its expression in mammalian cells,[3,4] as well as its photophysics for best use in elucidating the distribution and intracellular trafficking of genetically tagged proteins.[5–9] The advent of spectral variants of GFP has extended the utility of this technology by enabling the detection of protein-protein interactions *in vivo*. Specific proteins can now be tagged with florescent proteins (FPs) that fluoresce in the blue, green, yellow, orange, or red region.[10] In conjunction with basic light microscopy, many molecular interactions can be implied based on simple colocalization studies.[11] This colocalization approach is however limited by the resolution of light microscopy (typically, 0.2 μm). More sophisticated imaging technologies, including spectral imaging,[12] fluorescence lifetime imaging (FLIM),[13–15] and imaging based on changes in fluorescence anisotropy,[16,17] are being applied to detect interactions between FP-tagged proteins at a resolution of 1–10 nm. One such approach is to monitor Förster resonance energy transfer (FRET) between a protein tagged with a donor-FP and a putative binding partner labeled with an acceptor FP. FRET efficiency can be measured by monitoring reciprocal change in the intensity of

Address all correspondence to Zygmunt Gryczynski, Department of Molecular Biology and Immunology, University of North Texas, 3500 Camp Bowie Blvd, Fort Worth, TX 76107; Tel: 817 735 5471; Fax: 817 735 2118; E-mail: zgryczyn@hsc.unt.edu

1083-3668/2009/14(3)/034047/9/$25.00 © 2009 SPIE

emission from donor and acceptor fluorophores. More advanced and precise measurement of FRET efficiencies can be achieved by monitoring the change of fluorescence lifetime of the donor fluorophore. A high transfer efficiency is often interpreted as an indication of close proximity (<10 nm). Another approach, also based on FRET, is emerging as a method for dynamically monitoring the multimeric state of protein assemblies.[17–19] In this method, fluorescence anisotropy is used to measure energy migration between proteins labeled with the same FP. High anisotropy is indicative of low FRET and vice versa. Furthermore, the amplitude of a drop in anisotropy encodes information on the number of fluorophores in a molecular complex that are participating in the energy migration.

The accurate interpretation of biological FRET experiments utilizing complex quantitative imaging modalities, such as anisotropy analysis or FLIM, relies on an in-depth knowledge of the photophysics of the fluorophores being used. Specifically, for FLIM, it is important to know the lifetime of a fluorophore in the absence of acceptors, and it is also essential to appreciate any other factors that might alter its fluorescence lifetime in the course of an experiment.[20–22] For anisotropy analysis, it is important to know the fundamental anisotropy of a fluorophore (primarily a function of the orientation of its absorption and emission dipoles), how rigidly the fluorophore is attached to a protein of interest and it is also useful to understand any other factors that might alter the orientation of its emission relative to its excitation.[20–22] Furthermore, these sophisticated types of imaging experiments are often difficult to interpret if other endogenous fluorophores are present. Under these circumstances, measured fluorescence lifetimes or anisotropies will be a function of both the fluorophores of interest, as well as the contaminating fluorophores. Unfortunately contaminating fluorophores, like flavins, nicotinamides, porphyrins, etc., are almost always present in living biological samples.

Two of the most popular spectral variant of GFP used for biological FRET studies are Cerulean,[23] a blue emitting FP, and Venus,[24] a yellow emitter. The crystal structure of both of these proteins have been reported.[25,26] Although the photophysics of GFP has been extensively studied,[27–30] this knowledge base may not universally apply to these spectral variants. Furthermore, it has long been suggested that in the FP family FRET might occur between an internal tryptophan and the FP fluorophore.[31–33] If true, this could significantly alter fluorescent protein lifetime and anisotropy in a wavelength-dependent manner, and potentially complicate the interpretation of FRET between Cerulean and Venus. In this study, we characterize the lifetime and anisotropy of purified Cerulean and Venus and in so doing reveal: (*i*) Cerulean and to a lesser extent Venus fluorescence both decay as a double exponential, (*ii*) These fluorophores are rigidly fixed within their beta-barrel structure, and (*iii*) they both express efficient energy transfer between an internal tryptophan and their fluorophores upon UV excitation. Because the fluorophore within Cerulean and Venus are sequestered from the solvent/media due to their protein structure, we find they are resistant to dynamic quenching. We demonstrate how this can be exploited to remove the effects of endogenous fluorophores in these types of FRET experiments.

2 Materials and Methods

Tris buffer (Trizma), Acrylamide (electrophoresis grade), flavin mononucleotide (FMN), and KI were from Sigma-Aldrich Inc., St. Louis, Missouri. 20X PBS, pH-7.5 was from AMRESCO®, Solon, Ohio. The water used for the analysis was deionized (from Millipore® deionizer unit). Both Cerulean and Venus were diluted in 0.1 M Tris, pH 8.5. In the iodide quenching studies with FMN PBS pH 7.5 was used as the buffer as fluorescence of FMN is sensitive to alkaline pH.

2.1 *Purification of Cerulean and Venus*

2.1.1 *Expression and purification of Cerulean and Venus proteins*

6x His-tagged Cerulean and Venus cloned into pRSET B (Invitrogen) and the recombinant proteins were expressed in BL21 (DE3) pLysS bacteria (Invitrogen). Bacteria were lysed, and proteins were purified using Ni-NTA Magnetic Agarose beads (Qiagen), according to the manufacturer's instructions. The protein was concentrated by centrifugation using Centricon centrifugal filter devices (Millipore).

To assess protein integrity and purity of samples 1.4 and 0.14 mg of purified Cerulean and Venus were run on a 10% SDS PAGE gel (Bio-Rad) and Coomassie stained. For the Western blots, 25 ng of Cerulean and Venus proteins were separated on a 10% SDS-PAGE gel under denaturing conditions. The proteins in the gel were transferred onto a polyvinylidine flouride (PVDF) membrane (Immobilon P, Millipore) by electrophoresis. The blot was blocked in a solution containing phosphate-buffered saline (pH 7.4, Invitrogen), 0.05% Tween 20 (Sigma) (PBST), and 5% BSA (ICN Biochemicals) for 30 min. The blot was probed with rabbit anti-GFP polyclonal antibody (ab6556, Abcam; 1:1000 dilution) in PBST and 5% BSA for 1 h at room temperature. The blot was washed in PBST and then probed with a mixture of a goat anti-rabbit HRP conjugated antibody (Pierce, 1:5000 dilution) and HRP-Conjugated Biotin antibody (Cell Signaling, 1:5000 dilution; for biotinlyated mass ladder) in PBST for 30 min. The blot was rinsed and washed as described earlier. Protein bands were visualized by chemiluminescence (SuperSignal West Dura Extended Duration Substrate Kit, Pierce) using a Kodak Image Station 4000R. Densitometry analysis of the protein bands were performed using the analysis software in Kodak Image Station 4000R.

2.2 *Fluorescence Studies*

Varian Cary Eclipse fluorescence spectrophotometer (Varian Inc.) was used for steady-state fluorescence measurements. We used broad range (UV-Visual) polarizers (Manual Polarizer Accessory, Varian Inc., Australia) for measurements in both the visible and ultraviolet regions. At 285 nm, the polarization was $>90\%$, whereas in visible region the polarization was $>96\%$. The mathematical expression used to calculate anisotropy was

$$r = \frac{I_{VV} - GI_{VH}}{I_{VV} + 2GI_{VH}}, \tag{1}$$

where I_{VV} and I_{VH} are vertically excited–vertically emitted and vertically excited–horizontally emitted fluorescence components of the proteins and G is the instrumental G factor.[21]

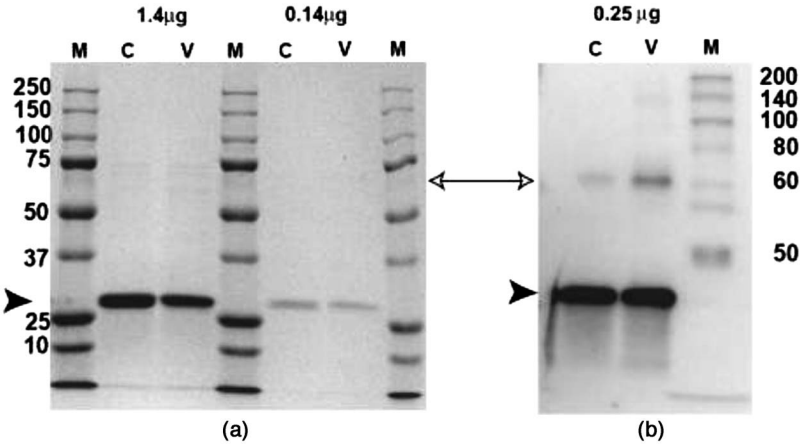

Fig. 1 Characterization of purified proteins. (a) Coomassie staining of a SDS PAGE gel shows 27 kDa (arrow heads) Cerulean (C) and Venus (V) protein bands. There seems to be minor contaminating bands at 60 KDa (double-headed arrow). (b) Western blot of Cerulean and Venus protein, where the Anti GFP antibody strongly cross reacts with the 27 kDa protein.

Time-resolved fluorescence measurements were carried out on FluoTime200 fluorometer (PicoQuant GmbH). This fluorometer is equipped with an ultrafast microchannel plate and is capable to well resolve subnanosecond decays. For studies in the UV region, the samples were excited with a picosecond-pulsed LED light source PLS-280, with bandwidth of 20 nm, manufactured by PicoQuant GmBh. Full width at half maxima (FWHM) of the pulse was ~500 ps, and the repetition rate used for the measurements using the LED was 5 MHz. For visible region studies, 405 nm (for Cerulean) or 470 nm (for Venus) pulsed laser diodes LDH-PC-405 or LDH-PC-470 (PicoQuant GmBh) were used, respectively, in the low-power regime (<70 ps FWHM) with 5 MHz repetition rates. The laser diodes are routinely used to measure fluorescence decays and lifetimes within ±10 ps accuracy. The lifetime data were analyzed by FluoTime software, version 4.0 (PicoQuant GmbH).

For lifetime measurements, a monochromator supported by long wave pass filter on the observation path was used. All the measurements for lifetime decay were performed using magic angle conditions. The decay was fitted with a multiexponential model using the expression

$$I(t) = \sum_i \alpha_i e^{-t/\tau_i}, \tag{2}$$

where $I(t)$ is the intensity at a time t, α_i is the amplitude of i'th component and τ_i is the lifetime of the i'th component.

Time-resolved anisotropy decays were fitted to the multiexponential model using the expression

$$r(t) = \sum r_i e^{(-t/\theta_i)}, \tag{3}$$

where, $r(t)$ is the anisotropy in time t, r_i is the amplitude of the i'th component and θ_i is the correlation time of the i'th component.

All the studies were carried out in room temperature (22°C). The background from the buffer was <1% of the signal, and the background from external quencher KI in buffer was subtracted from all the concerned measurements.

3 Results and Discussion

The purity of Cerulean and Venus were accessed using Coomasie staining of the proteins and Western blot analysis (Fig. 1). The serial dilution of Cerulean and Venus (1.4 and 0.14 mg) reveals a strong band at 27 kDa (FP, arrowheads in Fig 1) and some minor contaminants (double-headed arrows, Fig 1). Densitometry analysis of the Coomassie staining [Fig. 1(a)] revealed that Cerulean was 97% pure and Venus was 90% pure.

3.1 *Steady-State Fluorescence*

Cerulean–Venus is an excellent donor acceptor pair, with selective donor excitation using the 405 or 442-nm laser lines, and observation at 470 nm (no signal from acceptor at this wavelength). This significantly simplifies the FRET measurements and its interpretation. The excitation and emission spectra of both proteins are presented in Fig. 2. There is a significant increase in the excitation intensity in the UV region, at <300 nm. Emission spectra did not change with excitation (data not shown), suggesting either an electronic transition in the chromophore or that excitation energy absorbed by other moieties (such as aromatic amino acids) are efficiently transferred to the chromophore.

To study these possibilities further, we measured polarization spectra. Figure 3 shows steady-state excitation and emission polarization spectra of Cereluan, while Fig. 4 shows the same for Venus protein. Whereas the anisotropy values remain relatively constant within the emission spectra (b), the excitation anisotropies decrease significantly in shorter wavelengths (top panels). Such polarization dependences are common in (*i*) single fluorophore with different excited-state dipoles at higher electronic transition and (*ii*) a donor-acceptor system when excitation anisotropy is observed at acceptor emission. In fact, single-step energy transfer significantly affects anisotropy.

3.2 *Time-Resolved Fluorescence*

Next, we measured fluorescence lifetimes of fluorescent proteins with UV excitation (285 nm) and with direct long-

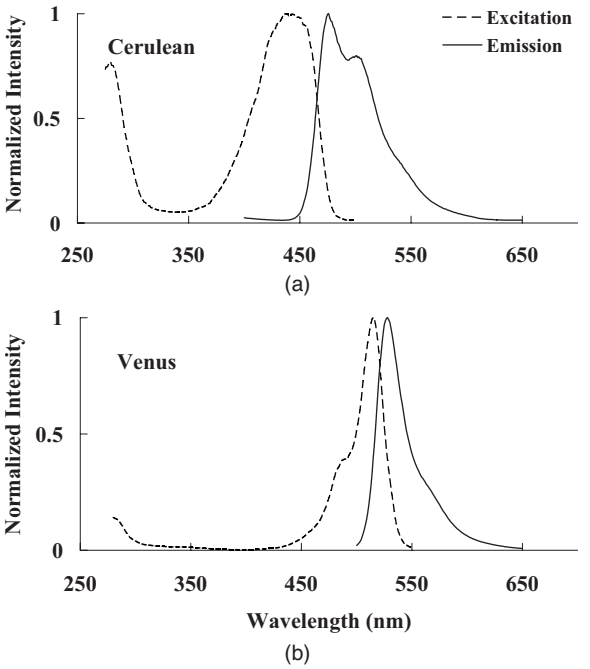

Fig. 2 Excitation and emission spectrum of (a) Cerulean and (b) Venus fluorescent proteins. Fluorescent protein excitation intensity in the UV (280 nm) is thought to be due to FRET from aromatic amino acids to the fluorescent protein chromophore.

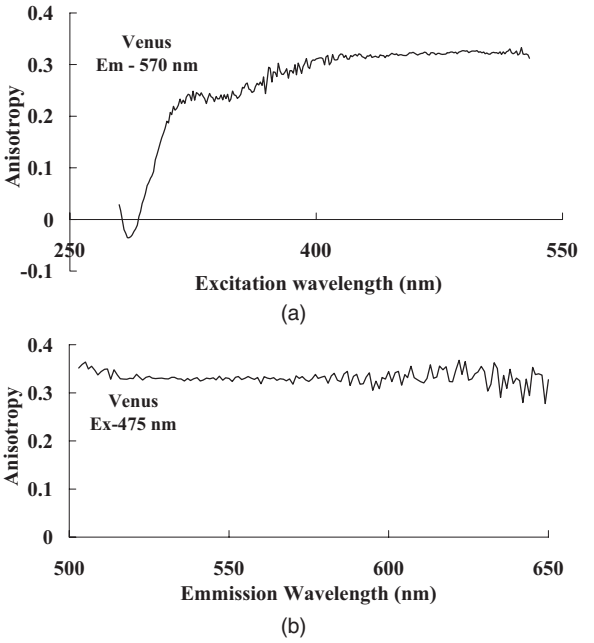

Fig. 4 (a) Excitation and (b) emission steady-state anisotropy of Venus. The high value of steady-state emission anisotropy (b) suggests limited flexibility of the chromophore within the barrel structure of the protein. The negative value of excitation anisotropy in the UV region is consistent with FRET occurring between aromatic amino acids and the fluorescent protein chromophore.

wavelength excitation at 405 and 470 nm for Cerulean and Venus, respectively. The intensity decays of Cereluan and Venus fluorescent proteins with long-wavelength excitation, measured by time-correlated single-photon counting, are presented in Figs. 5 and 6, respectively. One- and two-exponential fits to the experimental data are presented in Table 1. For both proteins, the fluorescence intensity decays were best fitted using a two-exponent decay model, though single exponential fits with lifetimes of 3.18 and 3.03 ns for Cereluan and Venus may in many cases be acceptable. Lifetimes were significantly longer with UV excitation. Furthermore, strong negative lifetime components of ~0.2 ns were

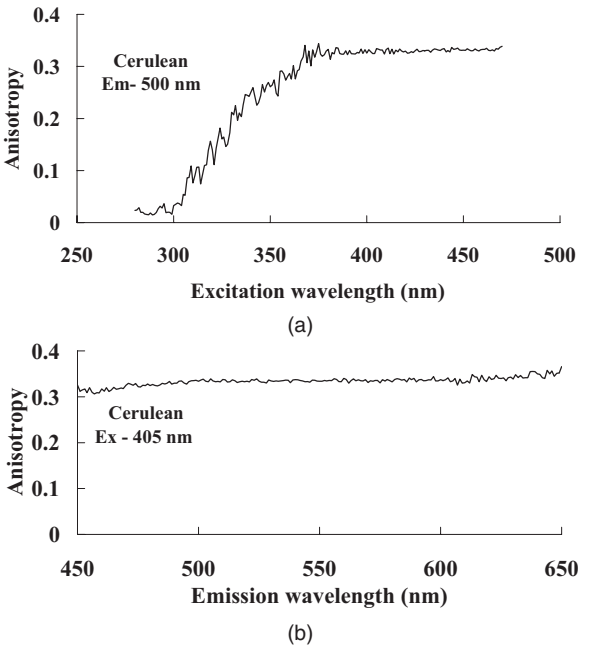

Fig. 3 (a) Excitation and (b) emission steady-state anisotropies of Cerulean. The high value of emission anisotropy, >0.3, suggests limited flexibility of the fluorophore within the protein structure. The rapid decrease of the excitation anisotropy is consistent with FRET between aromatic amino acids and the fluorescent protein chromophore.

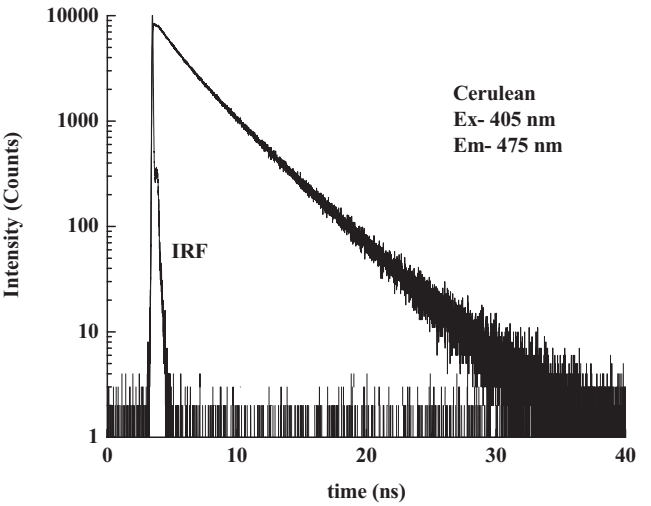

Fig. 5 Time-domain intensity decay of Cerulean. The decay is well approximated with a two exponential decay model (see Table 1). The amplitude and fractional intensity weighted average lifetimes are 2.82 and 3.23 ns respectively.

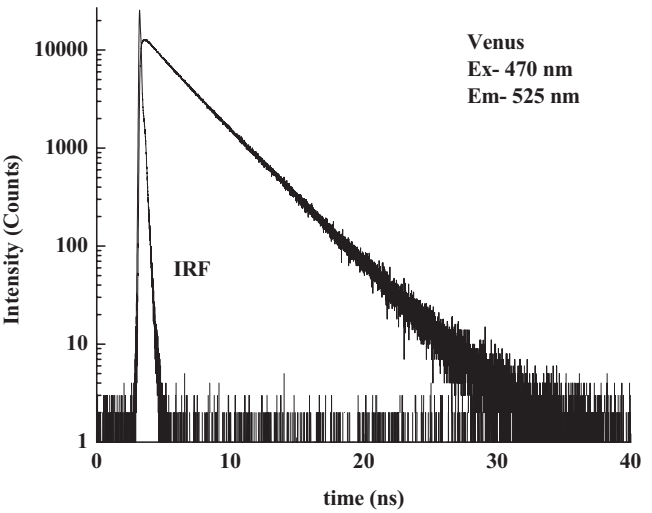

Fig. 6 Time-domain intensity decay of the Venus. The decay is well approximated using a two exponential decay model (see Table 1). The amplitude and fractional intensity weighted average lifetimes are 2.87 and 3.03 ns respectively.

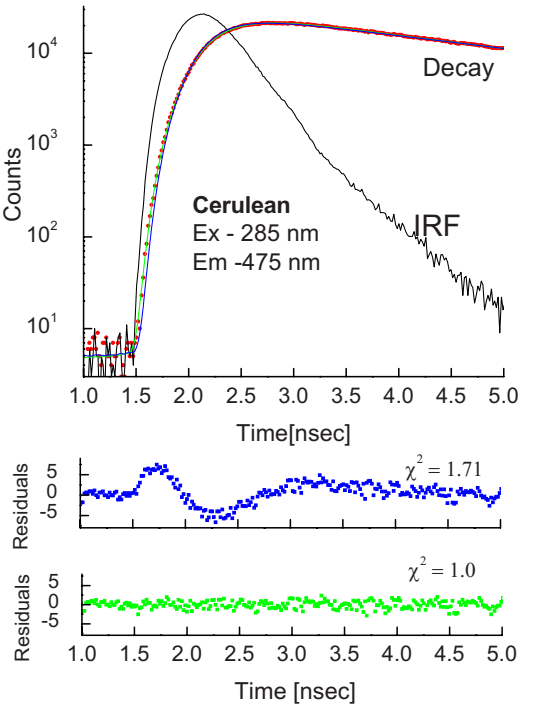

Fig. 7 Initial intensity decay of Cerulean with the excitation in Trp excitation region (285 nm). The blue line and residuals show the fit with positive component only, while the green line and residuals show the fit with one negative component. A negative component is needed to fit the data better. (Color online only.)

observed (Table 1). This is a characteristic property of a process occurring in the excited state. A negative component in the intensity decay indicates that the fluorescent protein chromophore is receiving additional "pumping" after excitation. This is consistent with FRET occurring between the aromatic amino acids and the fluorescent protein chromophore.

This is visualized in Figs. 7 and 8 for Cerulean and Venus respectively. Although the data were fitted for the whole decay, we present the fit only for the initial 5 ns, in order to show the necessity of negative component to fit the decay. The short decay time (0.16 and 0.2 ns for Cerulean and Venus, respectively) associated with the negative decay component shows that the energy transfer process is very efficient ($>90\%$) if we assume that the lifetime of unquenched tryptophan or tyrosine is $\sim$3 ns. This explains the absence of a significant tryptophan emission. The low steady-state excitation anisotropy value for Cerulean (Fig. 3) and negative value for Venus (Fig. 4) observed with excitation of $<$350 nm is consistent with significantly different near-orthogonal orientations for donor (Trp) and acceptor (fluorescent protein chromophore) transition moments. However, characterization of Trp donor profile was not an option due to presence of mild spectroscopic impurities (as seen in SDS-Page and Western Blot).

Anisotropy decays of both proteins (Figs. 9 and 10) are similar, displaying high values of initial anisotropy and corre-

Table 1 Multiexponential analysis of fluorescence intensity decays of Cerulean and Venus.

Protein	Ex (nm)	Em (nm)	α_1	T_1 (ns)	α_2	T_2 (ns)	α_3	T_3 (ns)	X^2
Cerulean	405	475	1.0	3.18±0.03	—	—	—	—	4.7
			0.403	1.52±0.04	0.597	3.70±0.02	—	—	0.9
	285	475	1.0	3.47±0.09	—	—	—	—	3.1
			0.936	2.08±0.03	1.253	4.02±0.02	−1.189	0.16±0.01	1.0
Venus	470	525	1.0	3.03±0.01	—	—	—	—	1.7
			0.160	1.31±0.07	0.840	3.17±0.01	—	—	0.9
	285	525	1.0	3.35±0.09	—	—	—	—	1.2
			1.835	3.31±0.02	−0.835	0.2±0.02	—	—	1.0

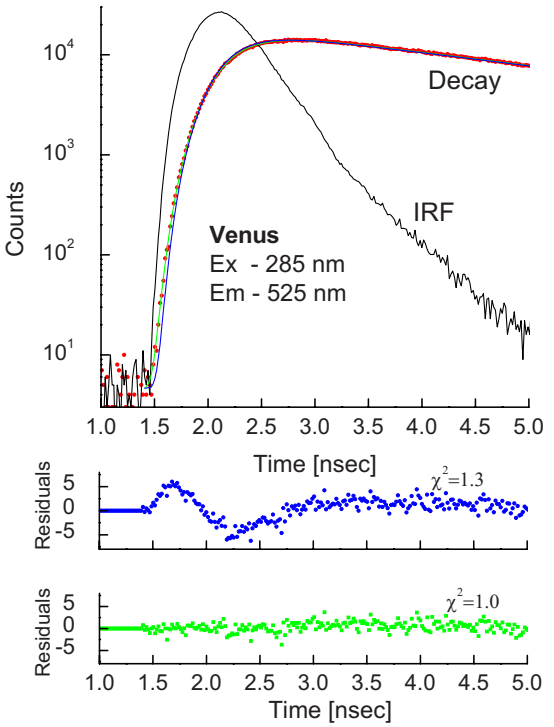

Fig. 8 The initial intensity decay of Venus with the excitation in Trp excitation region (285 nm). The blue colored line and residuals show the fit with positive component only, while green line and residuals show the fit with one negative component. A negative component is needed to fit the data better.

lation times of ~15 ns (Table 2). The fits to these decays can be modestly improved using a decay model with a second correlation time. However, these second correlation times are on the order of a few nanoseconds and are most likely associated with the nonspherical shape of the protein than with chromophore internal mobility. The very high steady-state anisotropies observed as well as the relatively slow anisotropy decays measured indicates that the fluorescent protein chromophores in Cerulean and Venus are rigidly oriented within the protein structure and have little freedom for rotation. This attribute should encourage polarization studies using fluorescent proteins, because the local fluorophore mobility is a bottleneck in many rotational diffusion investigations.

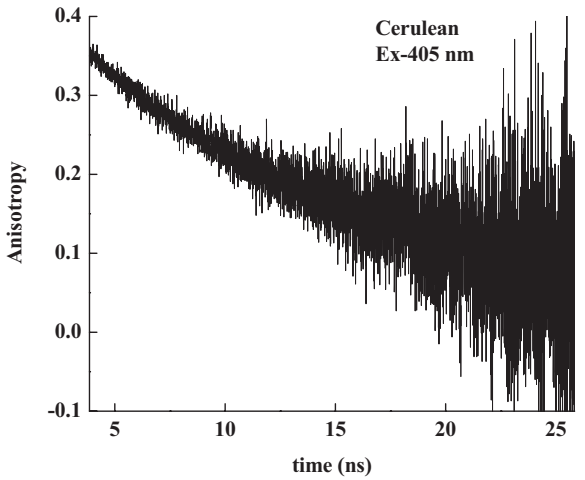

Fig. 9 Anisotropy decay of Cerulean. Two components are needed to fit the data well (See Table 2). The limiting anisotropy (r_0) was 0.4, and the rotational correlation times (θ_a and θ_b) were 6.7 and 19.6 ns.

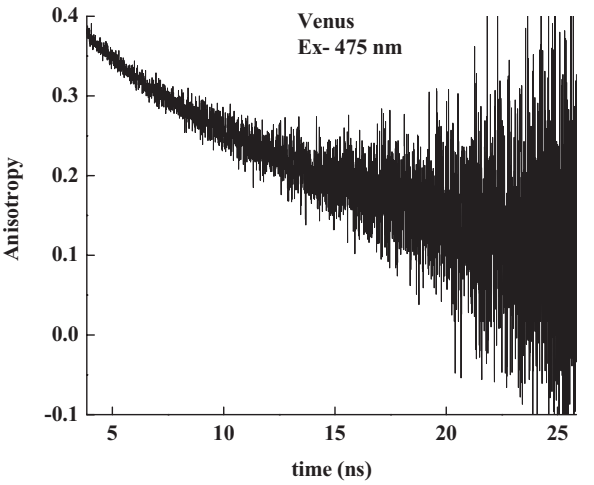

Fig. 10 Anisotropy decay of Venus. Two components are needed to fit the data well (See Table 2). The limiting anisotropy (r_0) was 0.4, and the rotational correlation times (θ_a and θ_b) were 3.7 and 20.3 ns.

3.3 *Fluorescence Quenching Study*

GFP fluorescence is known to be resistant to many quenching reagents. This is thought to arise from the GFP β-barrel protein structure that physically surrounds and sequester the GFP fluorophore from water soluble factors.[25,26] We next wanted to determine if the β-barrel structure of Cerulean and Venus would also protect their fluorophores from quenching reagents. We also wanted to determine if the high-efficiency energy transfer observed with UV excitation was also insensitive to external quenchers. First, we noted that with long-wavelength excitations, even high concentrations of acrylamide or potassium iodide (KI) in the solution do not change the emissions of Cereluan or Venus proteins (data not shown). This indicates that their chromophores are not readily accessible to these quenchers.

Next, we used UV excitation to test if the tryptophan fluorophore is also protected by the β-barrel structure. Figures 11 and 12 show the effect of acrylamide and/or KI presence on the UV-excited Cereluan and Venus proteins. There was little evidence for quenching of either Cerulean or Venus fluorescence. We conclude that the fluorescent protein chromophores as well as the tryptophan residue is effectively shielded from these quenchers. One can note that, in the presence of acrylamide, the emission spectrum of our purified Cerulean (and to a lesser extent Venus) was reduced at 400–450 nm (Fig. 11). Presumably, tryptophan in a small fraction of denatured fluorescent proteins can be quenched.

We decided to test if the unique protective nature of the fluorescent protein β-barrel structure can be exploited to suppress background fluorescence in fluorescent protein experiments. We prepared the mixture of Cereluan or Venus proteins with flavin mononucleotide (FMN). Flavins are an abundant chemical moiety found in cells. A major obstacle to live-cell

Table 2 Anisotropy decay analyses of Cerulean and Venus emission.

Protein	r_1	θ_1 (ns)	r_2	θ_2 (ns)	$\bar{\theta}$ (ns)	X_r^2
Cerulean	0.352±0.002	14.5±0.5	—	—	14.5	1.6
	0.088±0.001	6.7±0.4	0.266±0.002	19.6±0.6	18.3	1.5
Venus	0.374±0.002	16.4±0.6	—	—	16.4	2.0
	0.048±0.001	3.7±0.4	0.331±0.002	21.4±0.7	20.3	1.8

florescence imaging is that flavin fluorescence often masks the fluorescence of less abundant exogenous fluorophores experimentally introduced into cells. To illustrate this, a solution of either Cerulean (Fig. 13) or Venus (Fig. 14) and the flavin FMN were prepared and their emission spectra recorded. As expected, the strong FMN emission masked the fluorescent protein spectra in these mixtures. Addition of 0.35 Molar KI selectively quenched FMN to reveal the previously masked fluorescence protein spectra. To illustrate this effect, we prepared and imaged a microscopy slide with immobilized Venus protein (Fig. 15, star-shaped spot). Next, a drop of FMN solution was applied to the slide, primarily over the immobilized Venus. This led to fluorescence dominated by FMN. The star-shaped Venus spot could not be distinguished. Finally, we progressively added KI solution [Fig. 15(b)]. As FMN was selectively quenched, the fluorescent Venus protein spot was again revealed.

4 Conclusions

In addition to excitation with visible light (400–550 nm) both, Cereluan and Venus fluorescent proteins can be efficiently excited in the UV region at wavelengths (280 nm), where tryptophan and tyrosine are excited. Surprisingly, appreciable emission from these aromatic amino acids was not observed in the emission spectra of fluorescent proteins when excited with UV light (285 nm). UV excitation is thought to be accompanied by a very efficient energy transfer from aromatic amino acids (presumably tryptophan and/or tyrosine) to the fluorescent protein chromophore because, under these conditions, a negative lifetime decay component (pumping) was observed in the fluorescence intensity decay. The lifetime associated with this lifetime decay component was <200 ps. Assuming a nonquenched lifetime of tryptophan/tyrosine species of ~ 3 ns, one can calculate a transfer efficiency of $>90\%$. With such a high-energy-transfer efficiency, it is not surprising that the fluorescence spectra of tryptophan in fluorescent proteins cannot be measured accurately. Also, presence of trace amount of impurities in the sample (Fig. 1) contribute to the signal seen at the Trp emission region, mak-

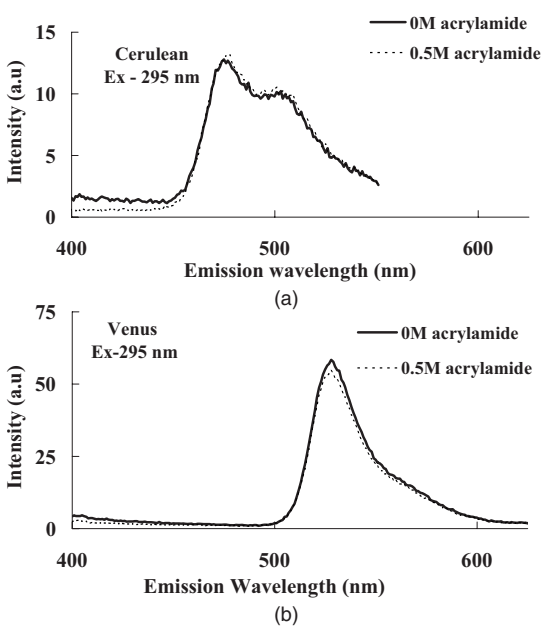

Fig. 11 Effect of acrylamide on (a) the fluorescence of Cerulean and (b) Venus.

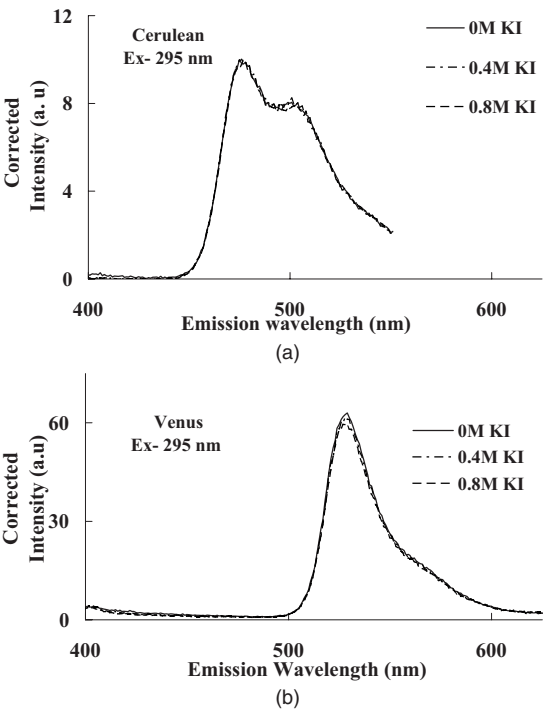

Fig. 12 Effect of KI on the (a) fluorescence spectrum of Cerulean and (b) Venus.

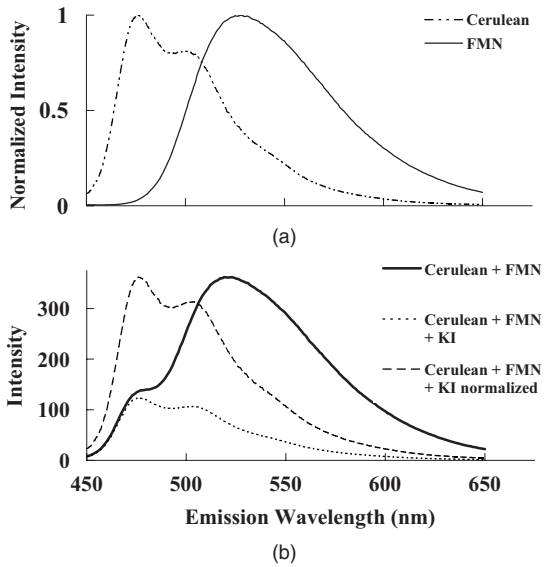

Fig. 13 Effect of KI on the fluorescence mixture of Cerulean and FMN. (a) Normalized emission spectra of Cerulean and FMN. (b) Emission spectrum of mixture in absence (solid thick lines) and presence (dotted lines) of KI. Dashed line represent normalized spectrum of mixture in presence of KI.

ing the interpretation even more complex. Furthermore, steady-state anisotropy measurements of the Cerulean or Venus fluorophore were only low with UV excitation, again indicating energy transfer between an aromatic amino acid and the fluorescent protein chromophore.

Time-resolved fluorescence anisotropy decay analysis also revealed that the emission dipole orientation of the Cereluan and Venus chromophores are rigidly fixed in the protein structure. This conclusion is based on our inability to detect any local, subnanosecond decay component in time-resolved an-

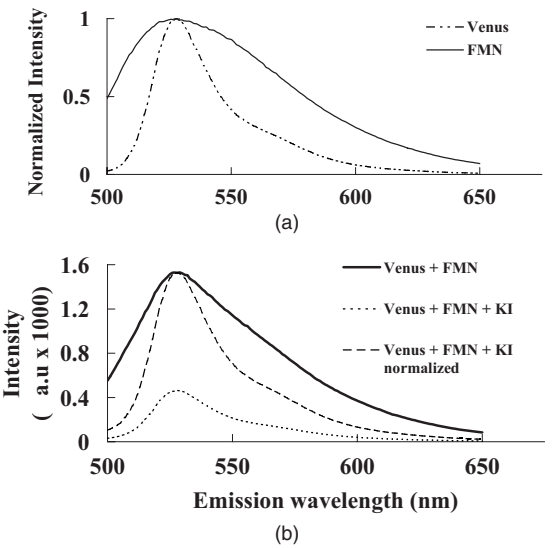

Fig. 14 Effect of KI on the fluorescence mixture of Venus and FMN. (a) Normalized emission spectra of Venus and FMN. (b) Emission spectrum of mixture in absence (solid thick lines) and presence (dotted lines) of KI. Dashed line represent normalized spectrum of mixture in presence of KI.

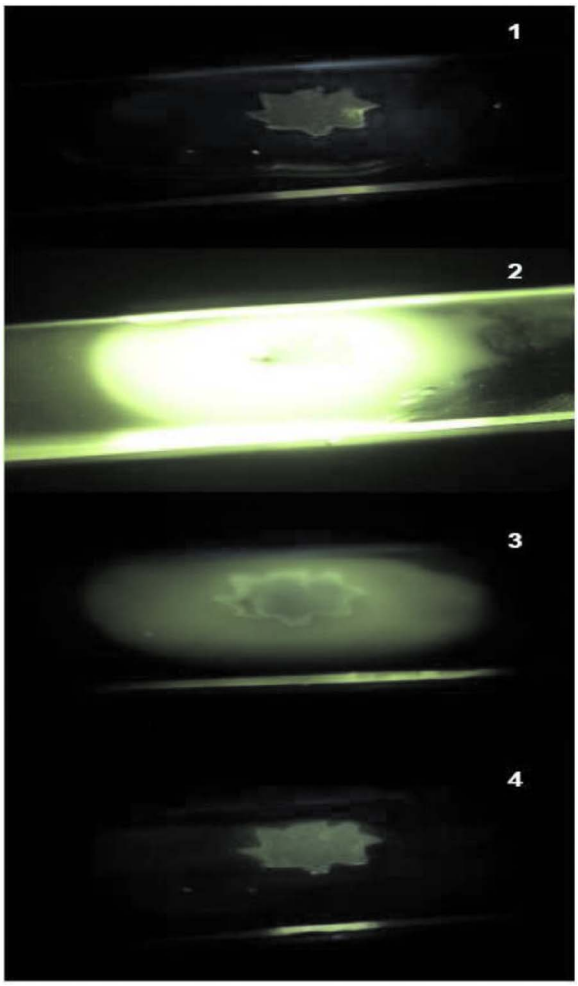

Fig. 15 Photograph of the combination of Venus and FMN emissions. Venus is immobilized at the surface of the glass slide (1). Next the slide was flooded with 500 μM FMN solution (2). Then solution of 2M KI was added drop wise; 2–3 drops (3 and 4). The illumination was from 450 nm LED, Observation was through 495 LWP filter. Canon® EOS 300D camera with an 18–35 mm lens was used to take the photograph using a shutter speed of 3 min. Images were trimmed by Canon ZoomBrowser® software. No additional modifications were made with the photographs.

isotropy measurements. The presence of trace impurities in the sample makes the interpretation of fluorescence decay from the internal tryptophan more complex. This prevented us from determining if the orientation of its emission dipole is also rigidly fixed. Nonetheless, the negative steady-state anisotropy observed with UV excitation of Venus, which contains only one tryptophan residue, strongly indicates energy transfer from tryptophan residues to the chromophore region. The excitation anisotropy (while acceptor emission was observed) value dropped for Cerulean, but still remained positive. This can be due to presence of two tryptophan residues in Cerulean.

Both, tryptophan and the fluorescent protein chromophore are buried in the protein structure and not accessible to the external quenchers, acrylamide and/or KI. This is a unique advantage of fluorescent proteins over other probes. We have shown that quenchers can be used to selectively suppress non-

specific fluorescent background. In biological samples, such as cells or tissue, fluorescent background is a major obstacle in any fluorescence study, especially in those based on FRET. Our observation that the fluorescence of purified Venus is selectively spared while the fluorescence of FMN is almost completely quenched suggests that using KI solution in washing procedures will improve the ratio of fluorescent protein emission to background fluorescence. We understand that high concentrations of iodide will be toxic to the cell itself and thus cannot be used in live-cell imaging instantaneously. But this study proves the concept that using flavin quenchers can be a good strategy of improving signal-to-noise ratio in imaging experiments that use these fluorescent proteins. Use of other known quenchers of flavin, such as oxygen or reducing flavins in the cells, can be a potentially feasible future strategy. These simple experimental manipulations might be the key for allowing quantitative imaging of fluorescent proteins in cells with high background fluorescence (such as neurons) or for readily detecting the fluorescence emission of single fluorescent protein molecules by dramatically increasing the signal-to-noise ratio.

Acknowledgments

This research was supported by the National Institutes of Health Project No. ZO1AA000452-01 to S.S.V., and by the Texas Emerging Technologies Fund Grant to Z. G.

References

1. J. Lippincott-Schwartz, E. Snapp, and A. Kenworthy, "Studying protein dynamics in living cells," *Nat. Rev. Mol. Cell Biol.* **2**(6), 444–456 (2001).
2. J. Zhang, R. E. Campbell, A. Y. Ting, and R. Y. Tsien, "Creating new fluorescent probes for cell biology," *Nat. Rev. Mol. Cell Biol.* **3**(12), 906–918 (2002).
3. A. Crameri, E. A. Whitehorn, E. Tate, and W. P. Stemmer, "Improved green fluorescent protein by molecular evolution using DNA shuffling," *Nat. Biotechnol.* **14**(3), 315–319 (1996).
4. R. Heim, D. C. Prasher, and R. Y. Tsien, "Wavelength mutations and posttranslational autoxidation of green fluorescent protein," *Proc. Natl. Acad. Sci. U.S.A.* **91**(26), 12501–12504 (1994).
5. L. S. Barak, S. S. Ferguson, J. Zhang, C. Martenson, T. Meyer, and M. G. Caron, "Internal trafficking and surface mobility of a functionally intact beta2-adrenergic receptor-green fluorescent protein conjugate," *Mol. Pharmacol.* **51**(2), 177–184 (1997).
6. S. P. Dobson, C. Livingstone, G. W. Gould, and J. M. Tavare, "Dynamics of insulin-stimulated translocation of GLUT4 in single living cells visualised using green fluorescent protein," *FEBS Lett.* **393**(2–3), 179–184 (1996).
7. T. Nakamura, K. Aoki, and M. Matsuda, "Monitoring spatio-temporal regulation of Ras and Rho GTPase with GFP-based FRET probes," *Methods* **37**(2), 146–153 (2005).
8. M. L. Nonet, "Visualization of synaptic specializations in live *C. elegans* with synaptic vesicle protein-GFP fusions," *J. Neurosci. Methods* **89**(1), 33–40 (1999).
9. D. Toomre, P. Keller, J. White, J. C. Olivo, and K. Simons, "Dual-color visualization of trans-Golgi network to plasma membrane traffic along microtubules in living cells," *J. Cell. Sci.* **112**(Pt 1), 21–33 (1999).
10. N. C. Shaner, P. A. Steinbach, and R. Y. Tsien, "A guide to choosing fluorescent proteins," *Nat. Methods* **2**(12), 905–909 (2005).
11. M. M. Falk and U. Lauf, "High resolution, fluorescence deconvolution microscopy and tagging with the autofluorescent tracers CFP, GFP, and YFP to study the structural composition of gap junctions in living cells," *Microsc. Res. Tech.* **52**(3), 251–262 (2001).
12. C. Thaler, S. V. Koushik, P. S. Blank, and S. S. Vogel, "Quantitative multiphoton spectral imaging and its use for measuring resonance energy transfer," *Biophys. J.* **89**(4), 2736–2749 (2005).
13. Y. Chen, J. D. Mills, and A. Periasamy, "Protein localization in living cells and tissues using FRET and FLIM," *Differentiation* **71**(9–10), 528–541 (2003).
14. A. G. Harpur, F. S. Wouters, and P. I. Bastiaens, "Imaging FRET between spectrally similar GFP molecules in single cells," *Nat. Biotechnol.* **19**(2), 167–169 (2001).
15. F. S. Wouters and P. I. Bastiaens, "Fluorescence lifetime imaging of receptor tyrosine kinase activity in cells," *Curr. Biol.* **9**(19), 1127–1130 (1999).
16. A. H. Clayton, Q. S. Hanley, D. J. Arndt-Jovin, V. Subramaniam, and T. M. Jovin, "Dynamic fluorescence anisotropy imaging microscopy in the frequency domain (rFLIM)," *Biophys. J.* **83**(3), 1631–1649 (2002).
17. I. Gautier, "Homo-FRET microscopy in living cells to measure monomer-dimer transition of GFP-tagged proteins," *Biophys. J.* **80**(6), 3000–3008 (2001).
18. D. S. Lidke, "Imaging molecular interactions in cells by dynamic and static fluorescence anisotropy (rFLIM and emFRET)," *Biochem. Soc. Trans.* **31**(Pt 5), 1020–1027 (2003).
19. L. W. Runnels and S. F. Scarlata, "Theory and application of fluorescence homotransfer to melittin oligomerization," *Biophys. J.* **69**(4), 1569–1583 (1995).
20. D. M. Jameson, J. C. Croney, and P. D. Moens, "Fluorescence: basic concepts, practical aspects, and some anecdotes," *Methods Enzymol.* **360**, 1–43 (2003).
21. J. R. Lakowicz, *Principles of Fluorescence Spectroscopy*, Wiley-VCH, Weinheim (1999).
22. B. Valeur, *Molecular Fluorescence*, Plenum, New York (2002).
23. M. A. Rizzo, G. H. Springer, B. Granada, and D. W. Piston, "An improved cyan fluorescent protein variant useful for FRET," *Nat. Biotechnol.* **22**(4), 445–449 (2004).
24. T. Nagai, K. Ibata, E. S. Park, M. Kubota, K. Mikoshiba, and A. Miyawaki, "A variant of yellow fluorescent protein with fast and efficient maturation for cell-biological applications," *Nat. Biotechnol.* **20**(1), 87–90 (2002).
25. A. Rekas, J. R. Alattia, T. Nagai, A. Miyawaki, and M. Ikura, "Crystal structure of venus, a yellow fluorescent protein with improved maturation and reduced environmental sensitivity," *J. Biol. Chem.* **277**(52), 50573–50578 (2002).
26. G. D. Malo, "X-ray structure of Cerulean GFP: a tryptophan-based chromophore useful for fluorescence lifetime imaging," *Biochemistry* **46**(35), 9865–9873 (2007).
27. S. T. Hess, E. D. Sheets, A. Wagenknecht-Wiesner, and A. A. Heikal, "Quantitative analysis of the fluorescence properties of intrinsically fluorescent proteins in living cells," *Biophys. J.* **85**(4), 2566–2580 (2003).
28. S. Inoue, O. Shimomura, M. Goda, M. Shribak, and P. T. Tran, "Fluorescence polarization of green fluorescence protein," *Proc. Natl. Acad. Sci. U.S.A.* **99**(7), 4272–4277 (2002).
29. G. H. Patterson, S. M. Knobel, W. D. Sharif, S. R. Kain, and D. W. Piston, "Use of the green fluorescent protein and its mutants in quantitative fluorescence microscopy," *Biophys. J.* **73**(5), 2782–2790 (1997).
30. K. Suhling, "Imaging the environment of green fluorescent protein," *Biophys. J.* **83**(6), 3589–3595 (2002).
31. A. F. Bell, D. Stoner-Ma, R. M. Wachter, and P. J. Tonge, "Light-driven decarboxylation of wild-type green fluorescent protein," *J. Am. Chem. Soc.* **125**(23), 6919–6926 (2003).
32. J. J. van Thor, A. J. Pierik, I. Nugteren-Roodzant, A. Xie, and K. J. Hellingwerf, "Characterization of the photoconversion of green fluorescent protein with FTIR spectroscopy," *Biochemistry* **37**(48), 16915–16921 (1998).
33. A. Volkmer, V. Subramaniam, D. J. Birch, and T. M. Jovin, "One- and two-photon excited fluorescence lifetimes and anisotropy decays of green fluorescent proteins," *Biophys. J.* **78**(3), 1589–1598 (2000).

Journal of Photochemistry and Photobiology B: Biology 92 (2008) 19–23

Contents lists available at ScienceDirect

Journal of Photochemistry and Photobiology B: Biology

journal homepage: www.elsevier.com/locate/jphotobiol

Binding of 8-anilino-1-naphthalenesulfonate to lecithin:cholesterol acyltransferase studied by fluorescence techniques

Pabak Sarkar [a,b,*], Shashank Bharill [a,b], Ignacy Gryczynski [b,c,*], Zygmunt Gryczynski [a,b], Maya P. Nair [a], Andras G. Lacko [a]

[a] Department of Molecular Biology and Immunology, University of North Texas Health Science Center, 3500 Camp Bowie Boulevard, Fort Worth, TX 76107, United States
[b] Center for Commercialization of Fluorescence Technologies, University of North Texas Health Science Center, 3500 Camp Bowie Boulevard, Fort Worth, TX 76107, United States
[c] Department of Cell Biology and Genetics, University of North Texas Health Science Center, 3500 Camp Bowie Boulevard, Fort Worth, TX 76107, United States

ARTICLE INFO

Article history:
Received 1 February 2008
Received in revised form 31 March 2008
Accepted 31 March 2008
Available online xxxx

Keywords:
Lecithin cholesterol acyltransferase
8-Anilino-1-naphthalene sulfonate
Fluorescence anisotropy
Fluorescence lifetime

ABSTRACT

The solvatochromic fluorescent probe 8-anilino-1-naphthalenesulfonate (ANS) has been used to study the hydrophobicity and conformational dynamics of lecithin:cholesterol acyltransferase (LCAT). The ANS to LCAT binding constant was estimated from titrations with ANS, keeping a constant concentration of LCAT (2 μM). Apparent binding constant was found to be dependent on the excitation. For the direct excitation of ANS at 375 nm the binding constant was 4.7 μM^{-1} and for UV excitation at 295 nm was 3.2 μM^{-1}. In the later case, not only ANS but also tryptophan (Trp) residues of LCAT is being excited. Fluorescence spectra and intensity decays show an efficient energy transfer from tryptophan residues to ANS. The apparent distance from Trp donor to ANS acceptor, estimated from the changes in donor lifetime was about 3 nm and depends on the ANS concentration. Steady-state and time-resolved fluorescence emission and anisotropies have been characterized. The lifetime of ANS bound to LCAT was above 16 ns which is characteristic for it being in a hydrophobic environment. The ANS labeled LCAT fluorescence anisotropy decay revealed the correlation time of 42 ns with a weak residual motion of 2.8 ns. These characteristics of ANS labeled LCAT fluorescence show that ANS is an excellent probe to study conformational changes of LCAT protein and its interactions with other macromolecules.

1. Introduction

Lecithin:cholesterol acyltransferase (LCAT) is a key enzyme in cholesterol transport [1]. It is synthesized in the liver and circulates in the blood, associated with high density lipoproteins [1–3]. The LCAT transfers an acyl group from phosphatidylcholine to cholesterol through a trans-esterification reaction resulting in cholesteryl ester and lysophosphatidylcholine [4]. The formation and accumulation of cholesteryl esters in the core of HDL results in the removal of cholesterol from the lipoprotein surface and simultaneously promotes efflux of cholesterol from cell membranes into HDL [5]. This process has been termed reverse cholesterol transport (RCT) because its ability to promote the flow of cholesterol from peripheral tissues to the liver. RCT begins with the secretion of nascent discoidal HDL by the liver, followed by the build up of its cholesteryl ester core, resulting in spherical shape and growth in diameter with the progressive accumulation of cholesteryl esters [6]. This overall process involving LCAT (RCT) has been linked to protection of the arteries from atherosclerosis via removal of unesterified cholesterol from arterial tissue [7].

Although recent studies identified important structural features of LCAT [1,4–6], the three dimensional structure of the enzyme remains unsolved due to the unavailability of diffraction grade crystals [8]. The studies presented here intend to probe the hydrophobic regions of LCAT and the conformational behavior of tryptophan residues that would allow additional detailed studies on substrate interactions and thus the mechanism of action of LCAT.

Extrinsic fluorescent probes have been used in conformational studies, of macromolecules, including serum albumin [9] and myoglobin [10]. In addition, ANS has recently been used to study its interaction with the antibiotic target *Mur A* [11], to probe apomyoglobin unfolding [12] and to characterize lipid-binding properties of intracellular proteins [13]. The binding of ANS to hydrophobic regions of proteins has been proposed to tighten the macromolecular conformation [14].

Here, we describe the ANS binding to LCAT via studies of intrinsic fluorescence, modulated by the presence of ANS, as well as the extrinsic fluorescence attributable to ANS. Both steady-state and

* Corresponding author. Address: Department of Molecular Biology and Immunology, University of North Texas Health Science Center, 3500 Camp Bowie Boulevard, Fort Worth, TX 76107, United States. Tel.: +1 817 735 0148/5471; fax: +1 817 735 2118 (P. Sarkar).
E-mail addresses: psarkar@hsc.unt.edu (P. Sarkar), igryczyn@hsc.unt.edu (I. Gryczynski).

1011-1344/$ - see front matter © 2008 Elsevier B.V. All rights reserved.
doi:10.1016/j.jphotobiol.2008.03.009

time-resolved techniques have been applied to probe the conformational parameters associated with the binding of ANS to the enzyme.

2. Materials and methods

8-Anilino-1-naphthalenesulfonate (ANS) ammonium salt was acquired from Aldrich, MO. The PBS (pH 7.4) was used to dissolve ANS and in the titrations. Absorption spectra were measured on a Cary 50 spectrophotometer (Varian Inc.).

2.1. LCAT purification

Recombinant LCAT was purified from the conditioned medium of engineered human lung cells, as described previously [15]. Approximately 800 ml conditioned culture medium containing LCAT was loaded on a phenyl-sepharose column (2.5 × 18 cm), that had previously been equilibrated with 0.005 M PO_4, 0.3 M NaCl, pH 7.4. The column was washed with the same buffer until the absorbance at 280 nm decreased below 0.01. Subsequently, the purified LCAT was eluted with deionized water. All the experiments were done in Phosphate buffered saline, pH 7.4 (20× solution purchased from Amresco, OH).

2.2. LCAT–ANS titration and steady-state fluorescence measurement

The steady-state emission was recorded on an Eclipse spectrofluorometer (Varian Inc.). 500 μl of LCAT (2 μM) solution was taken in 4 mm × 10 mm quartz cuvette and predetermined volume of 600 μM ANS stock was added in each step. The steady-state fluorescence emission spectrum was measured after each addition of ANS, with 295 nm excitation (exciting the trp residues of LCAT) and 375 nm excitation (exciting protein bound ANS) light. All other conditions (like slit size, PMT voltage and temperature) were not altered during the recordings. Then emission intensity at 480 nm (emission peak of protein bound ANS fluorescence) of each reading was plotted against the corrected ANS concentration (considering the 'volume effect' upon ANS addition). This plot was fitted with the equation

$$y = \frac{K_d + [\mathrm{ANS}]_c + [\mathrm{LCAT}]_c - \sqrt{(K_d + [\mathrm{ANS}]_c + [\mathrm{LCAT}]_c)^2 - 4[\mathrm{ANS}]_c[\mathrm{LCAT}]_c}}{2[\mathrm{LCAT}]_c} \quad (1)$$

where y is the calculated value of intensity, K_d is the dissociation constant in μM^{-1}, $[ANS]_c$ is the corrected ANS concentration in μM, $[LCAT]_c$ is corrected LCAT concentration in μM. The dissociation constant was calculated from the fit.

2.3. Steady-state anisotropy measurement

For steady-state anisotropies, fluorescence signals were measured using the Cary Eclipse spectrofluorometer equipped with polarizer (Varian Inc.) at excitation and emission window. Measurements were taken with vertically oriented excitation polarizer in combination with either vertically or horizontally oriented emission polarizer. From them anisotropies were calculated using the expression

$$r = \frac{I_{VV} - GI_{VH}}{I_{VV} + 2GI_{VH}} \quad (2)$$

where r is the anisotropy, I_{VV} is the intensity measured with vertically oriented excitation polarizer and vertically oriented emission polarizer, I_{VH} is the intensity measured with vertically oriented excitation polarizer and horizontally oriented emission polarizer and G is the instrumental factor.

2.4. Fluorescence lifetime and anisotropy decay measurements

The intensity decays were measured with FluoTime 200 fluorometer (PicoQuant Inc.). This fluorometer is equipped with ultrafast microchannel plate detector (MCP) from Hamamatsu Inc., and pulsed 375 nm laser diode (70 ps half width), providing sub nanosecond resolution. The UV (285 nm) excitation was obtained from a pulsed LED (500 ps half width). All the samples measured were freshly prepared and the recordings were taken at room temperature (around 20 °C). The fluorescence lifetimes were calculated using FluoFit4 program from PicoQuant Inc., which uses the following non-linear least square expression to fit the measurements:

$$I(t) = \int_{-\infty}^{t} \mathrm{IRF}(t') \sum_{i=1}^{n} A_i \exp^{-\frac{t-t'}{\tau_i}} dt' \quad (3)$$

where $I(t)$ is the intensity at time t, $\mathrm{IRF}(t')$ is the instrument response function at time t (calculated from measuring the scattering from LED or the laser), A_i is the amplitude of a single exponential component i, and τ_i is the lifetime of the component.

Anisotropy decay was measured in the same instrument recording the vertical or horizontal component of the emitted light. The time dependant anisotropy was calculated as

$$r(t) = \frac{I_{\mathrm{parallel}}(t) - GI_{\mathrm{perpendicular}}(t)}{I_{\mathrm{parallel}}(t) + 2GI_{\mathrm{perpendicular}}(t)} \quad (4)$$

where $r(t)$ is the measured anisotropy at time t, $I_{\mathrm{parallel}}(t)$ is the parallel component of emission (in comparison to excitation) at time t and $I_{\mathrm{perpendicular}}(t)$ is the perpendicular component of emission at time t and G is the instrumental G-factor.

The measured anisotropy was then fitted with the expression

$$r(t) = \sum_{i=1}^{n} R_i \exp^{-(t/\phi_i)} \quad (5)$$

where $r(t)$ is the fitted anisotropy at time t, R_i is the single anisotropy component and ϕ_i is the correlation time of the single component.

From the fit expression, the correlation time was used to estimate the molecular weight of the fluorescent complex using Perrin's equation.

3. Results and discussion

3.1. ANS binding to LCAT studied via tryptophan emission

First, we observed the fluorescence from LCAT protein in the absence and presence of ANS using UV excitation at 295 nm. At this wavelength, tryptophan (Trp) residues in LCAT are excited, resulting in a broad fluorescence peak with the maximum near 340 nm. Because Trp residues are relatively sensitive to the polar environment [16–18], they tend to display a red shift with the emission maximum at 360 nm or longer. However, in a less polar environment (buried deeply inside the protein), Trp fluorescence is shifted towards shorter wavelengths. In the case of LCAT protein, most of the Trp residues are apparently buried and are shielded from the water molecules.

Progressive addition of ANS in titration experiment resulted in a decrease of Trp emission with a simultaneous increase of ANS fluorescence (Fig. 1). Because the competing ANS absorption and reabsorption do not account for the magnitude of the quenching, we performed time-resolved measurements of ANS-labeled LCAT to elucidate the nature of this effect. The decay of Trp fluorescence intensity was shorter in the presence of ANS than in the control, as shown in Fig. 2 and Table 1. The quenching of Trp residues by ANS was thus likely to be due to Foerster resonance energy transfer (FRET) mechanism. Similar FRET has been reported for ANS labeled

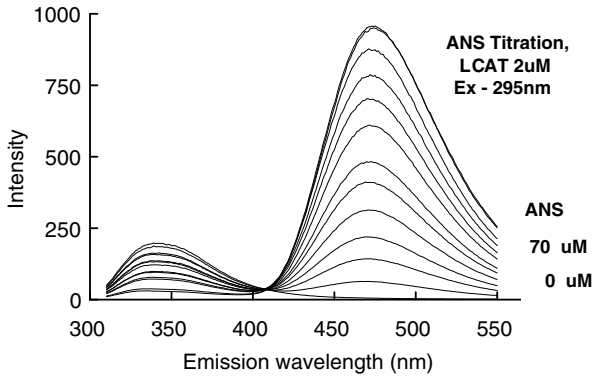

Fig. 1. Emission spectra of LCAT protein in absence and presence of ANS at 295 nm excitation. Progressive increase of ANS concentration results in a decrease of tryptophan fluorescence (340 nm) with a simultaneous increase of ANS fluorescence (480 nm).

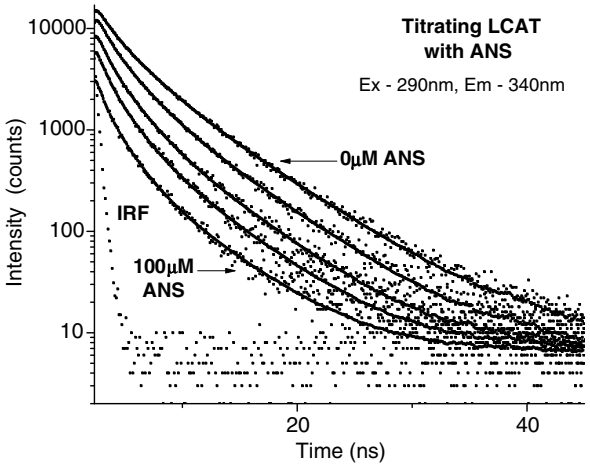

Fig. 2. Fluorescence intensity decays of LCAT protein (tryptophan emission at) in absence and presence of ANS. The excitation was 285 nm from a pulsed LED, and the observation was at 340 nm. The decrease of tryptophan lifetime is due energy transfer from tryptophan to ANS.

bovine serum albumin (BSA) [19] and other proteins. Using the energy transfer efficiencies calculated from measured lifetimes, and critical Foerster distance for Trp–ANS of 28.6 Å [19], we estimated the apparent transfer efficiencies and Trp to ANS distances (Table 2). These distances were found to become shorter with increasing concentration of ANS.

Shorter Foerster's distance at higher ANS concentration might reflect the presence of more than one ANS binding site in LCAT or it might be due to unbound LCAT molecules at lower concentration. To find out the basis of the phenomenon we assumed that only one molecule of ANS is bound to each molecule of LCAT and calculated the hypothetical energy transfer considering that at high concentrations of ANS in the solution all the LCAT molecules are bound with one ANS molecule. We compared the calculated values with the experimental result (Table 2). The calculated values are not comparable with the experimental value, suggesting there is more than one ANS binding site in LCAT that can result in energy transfer from Trp residues from LCAT.

Table 2
Efficiency of energy transfer (E_T) and the apparent distance (r) between tryptophan and ANS molecules in LCAT

[ANS] (μM)	Fraction of LCAT–ANS complex[a]	Expected E_T[b]	Observed E_T	r (Å)
3.29	4.34	0.243	0.190	36.4
12.59	0.777	0.437	0.365	31.4
35.92	0.977	0.549	0.445	29.7
85.93	1	0.562	0.562	27.4

[a] Assuming that at high concentration of ANS, all LCAT molecules are bound with ANS.
[b] Assuming that there is only one type of binding, ANS binding site in LCAT.

The changes in fluorescence intensities of ANS (at 480 nm) were used to study kinetics of the ANS binding to LCAT. The fit to one component kinetic model is presented in Fig. 3. The data can be fitted with the binding constant $K_d = 3.2\ \mu M^{-1}$. Two component model did not improve the quality of the fit.

3.2. ANS binding to LCAT studied with ANS fluorescence

Upon selective excitation of the ANS probe at 375 nm, the Trp residues are not excited, and only ANS emission is observed (Fig. 4). From Fig. 4, it is clear that there was no background emission from the 2 μM solution of LCAT in the absence of ANS. Fig. 5 shows the titration of LCAT with ANS at 375 nm excitation. In this case one component model provides satisfactory fit to the data with the binding constant $K_d = 4.7\ \mu M^{-1}$.

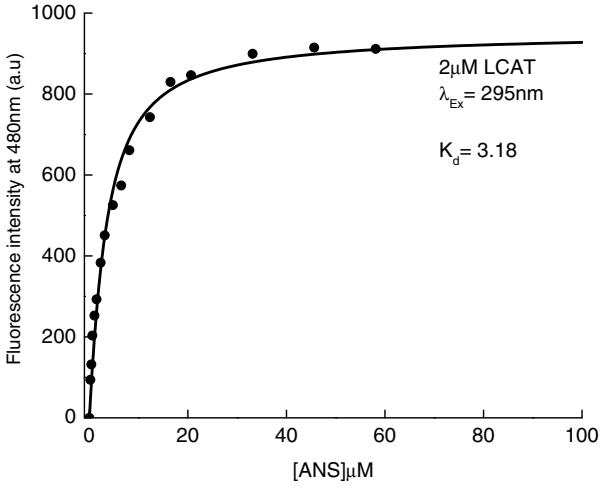

Fig. 3. Kinetics of ANS binding to LCAT protein observed for ANS emissions with 295 nm excitation.

Table 1
Individual and average lifetimes calculated from lifetime decay curves with given concentrations of ANS bound to 2 μM LCAT solution in PBS

[ANS] (μM)	$\bar{\tau}$ (ns)	$\langle\tau\rangle$ (ns)	τ_1 (ns)	α_1	τ_2 (ns)	α_2	τ_3 (ns)	α_3	χ^2
0	4.22	2.74	0.657	0.350	2.734	0.437	6.184	0.213	1.087
4	3.62	2.22	0.645	0.414	2.422	0.435	5.915	0.151	1.032
15	3.14	1.74	0.487	0.456	2.036	0.424	5.466	0.121	1.041
40	2.94	1.52	0.439	0.507	1.910	0.393	5.383	0.101	1.033
100	2.77	1.20	0.299	0.560	1.621	0.349	5.077	0.091	1.008

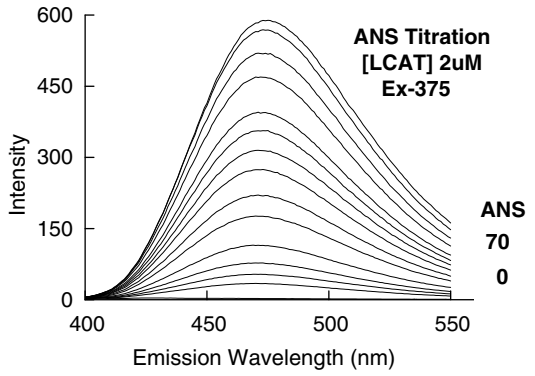

Fig. 4. The ANS titration spectra of ANS-labeled LCAT protein. The excitation was 375 nm.

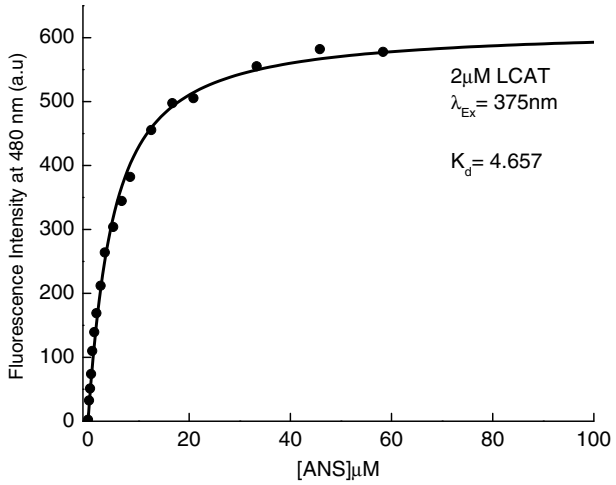

Fig. 5. Kinetics of ANS binding to LCAT protein observed for ANS with 375 nm excitation.

The fluorescence intensity decay of the ANS labeled LCAT is presented in Fig. 6. The average lifetime of 16.12 ns suggests that the ANS molecules were tightly bound in the hydrophobic pockets of the protein, and is thus shielded from water molecules.

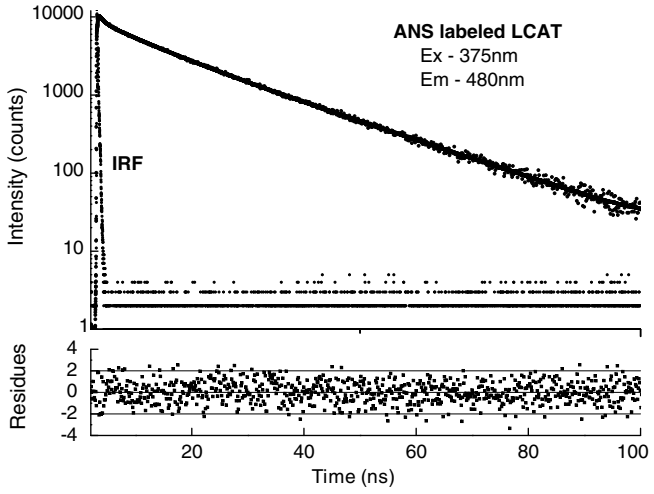

Fig. 6. The intensity decay of ANS–labeled LCAT protein. The excitation was 375 nm from a pulsed laser diode and the observation was 480 nm.

The relatively long fluorescence lifetime is convenient for studying dynamic changes in protein conformation. The time-resolved anisotropy measurements are presented in Fig. 7. The recovered correlation time of 42 ns is in a good agreement with the calculated value obtained from a hydrodynamic model for a 62 kDa protein [20]. The steady-state anisotropies depend on both, lifetimes and correlation times of macromolecules. The anisotropy measurements, as ratio-metric are very precise and relatively simple to apply in the absence of time-resolved instrumentation. The excitation and emission anisotropies of ANS-labeled LCAT are presented in Fig. 8. Across the emission spectrum, the ANS anisotropy remained constant at the value of about 0.23. The complete immobilization of ANS fluorophores would result in the limiting value of anisotropy of 0.4. We believe that partial immobilization of LCAT protein will be observed from the anisotropy measurements.

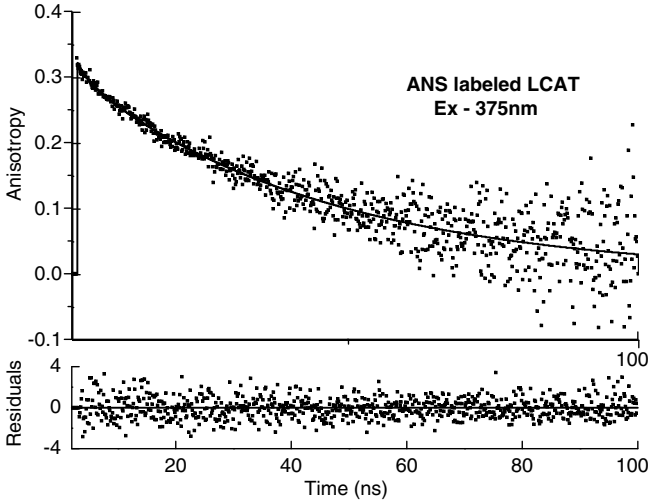

Fig. 7. The anisotropy decay of ANS–labeled LCAT protein. The excitation was 375 nm from a pulsed laser diode and the observation was 480 nm.

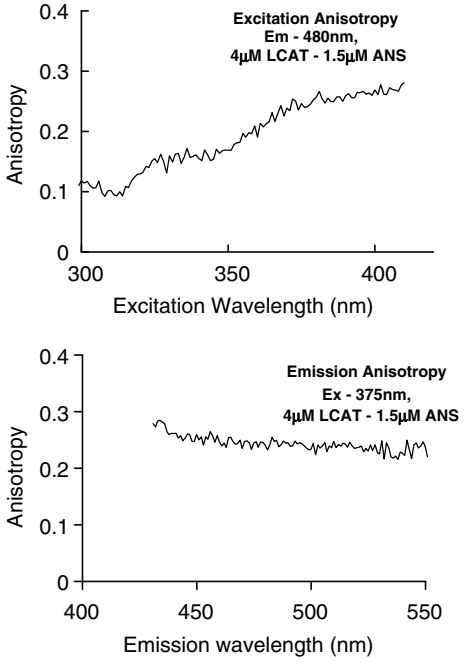

Fig. 8. Steady-state anisotropy spectra of ANS–labeled LCAT protein. Top: the excitation anisotropy spectrum. Bottom: the emission anisotropy spectrum.

4. Conclusions

The ANS chromophore known to be non-fluorescent in the water and other polar solvents, bind to the hydrophobic regions of LCAT protein and displays fluorescence emission.

The binding constants recovered from ANS titrations are different for 295 nm and 375 nm excitations. In the case of 295 nm excitation there is an additional pathway for ANS excitation via FRET from Trp residues. This is reflected in smaller K_d value for ANS binding. ANS is also able to quench the Trp fluorescence emitted by proteins, due to a FRET mechanism. The fluorescence of ANS-labeled LCAT can be used in future studies to study the rotational mobility of the enzyme while the interaction of LCAT with other macromolecules may be studied via anisotropy measurements.

Acknowledgements

This research was supported by Texas Emerging Technologies Fund Grant. Additional support (for S.B.) was provided by Public Health Service Grant P20 MD001633.

References

[1] S. Santamarina-Fojo, G. Lambert, J.M. Hoeg, H.B. Brewer Jr., Lecithin-cholesterol acyltransferase: role in lipoprotein metabolism, reverse cholesterol transport and atherosclerosis, Curr. Opin. Lipidol. 11 (3) (2000) 267–275.
[2] A. Jonas, Lecithin cholesterol acyltransferase, review, Biochim. Biophys. Acta 1529 (2000) 245–256.
[3] P.J. Barter, Hugh sinclair lecture: the regulation and remodelling of HDL by plasma factors, Atheroscler Suppl. (4) (2002) 39–47.
[4] M. Jauhiainen, P.J. Dolphin, Human plasma lecithin:cholesterol acyltransferase (LCAT). On the role of essential carboxyl groups in catalysis, Adv. Exp. Med. Biol. 285 (1991) 71–75.
[5] V.I. Zannis, A. Chroni, M. Krieger, Role of apoA-I, ABCA1, LCAT, and SR-BI in the biogenesis of HDL, J. Mol. Med. 84 (4) (2006) 276–294.
[6] G. Schmitz, G. Assmann, B. Melnik, The role of lecithin: cholesterol acyltransferase in high density lipoprotein3/high density lipoprotein2 interconversion, Clin. Chim. Acta 119 (3) (1982) 225–236.
[7] M. Cucuianu, M. Coca, N. Hâncu, Reverse cholesterol transport and atherosclerosis. A mini review, Rom. J. Intern. Med. 45 (1) (2007) 17–27.
[8] K.R. Murray, M.P. Nair, A.F. Ayyobi, J.S. Hill, P.H. Pritchard, A.G. Lacko, Probing the 121–136 domain of lecithin:cholesterol acyltransferase using antibodies, Arch. Biochem. Biophys. 385 (2) (2001) 267–275.
[9] J.R. Lakowicz, Principles of Fluorescence Spectroscopy, third ed., Springer, New York, 2006.
[10] D.W. Pierce, S.G. Boxer, Dielectric relaxation in a protein matrix, J. Phys. Chem. 96 (1992) 5560–5566.
[11] E. Schönbrunn, S. Eschenburg, K. Luger, W. Kabsch, N. Amrhein, Structural basis of interaction of fluorescence probe 8-anilino-1-naphthalene sulfonate (ANS) with antibiotic target MurA, PNAS 97 (12) (2000) 6345–6349.
[12] G. Wang, Y. Gao, M.L. Geng, Analysis of heterogenous fluorescence decays in proteins using fluorescence lifetime of 8-anilino-1-naphthalene sulfonate to probe apomyoglobin unfolding at equilibrium, Biochem. Biophys. Acta 1760 (2006) 1125–1137.
[13] C.D. Kane, D. Bernlohr, A simple assay for intracellular lipid-binding proteins using displacement of 1-anilinonaphthalene-8-sulfonic acid, Anal. Biochem. 233 (1996) 197–204.
[14] D. Matulis, C.G. Baumann, V.A. Bloomfield, R.E. Lovrien, 1-Anilino-8-naphthalene sulfonate as a protein conformational tightening agent, Biopolymers 49 (1999) 451–458.
[15] S.B. Lane, K.T. Tchedre, M.P. Nair, A.E. Thigpen, A.G. Lacko, Characterization of lecithin:cholesterol acyltransferase expressed in a human lung cell line, Protein Expr. Purif. 36 (2) (2004) 157–164.
[16] A.P. Demchenko, Ultraviolet Spectroscopy of Proteins, Springer-Verlag, New York, 1981.
[17] J.R. Lakowicz, Principles of Fluorescence Spectroscopy, second ed., Plenum Press, New York, 1999.
[18] B. Valeur, Molecular Fluorescence, Principles and Applications, Wiley–VCH, New York, 2002.
[19] J. Malicka, I. Gryczynski, J. Kusba, Y. Shen, J.R. Lackowicz, Effects of metallic silver particles on resonance energy transfer in labeled bovine serum albumin, Biochem. Biophys. Res. Commun. 294 (2002) 886–892.
[20] J.R. Lakowicz, Principles of Fluorescence Spectroscopy, Plenum Press, New York and London, 1983.

BIBLIOGRAPHY

1. Nelson DL, Cox MM, Lehninger AL. *Principles of Biochemistry*. Freeman New York; 2008.

2. Alberts, B., Bray,D., Lewis, J., Raff, M., Roberts K., Watson, J.D.,. *Molecular Biology of the Cell.* ; 1994.

3. Bagatolli LA, Ipsen JH, Simonsen AC, Mouritsen OG. An outlook on organization of lipids in membranes: Searching for a realistic connection with the organization of biological membranes. *Prog Lipid Res*. 2010.

4. Demchenko AP, Mély Y, Duportail G, Klymchenko AS. Monitoring biophysical properties of lipid membranes by environment-sensitive fluorescent probes *Biophys J*. 2009;96:3461-3470.

5. Demchenko AP, Yesylevskyy SO. Nanoscopic description of biomembrane electrostatics: Results of molecular dynamics simulations and fluorescence probing. *Chem Phys Lipids*. 2009;160:63-84.

6. Singer SJ, Nicolson GL. The fluid mosaic model of the structure of cell membranes. *Science*. 1972;175:720-731.

7. Vereb G, Szöllősi J, Matko J, et al. Dynamic, yet structured: The cell membrane three decades after the Singer–Nicolson model. *Proc Natl Acad Sci U S A*. 2003;100:8053.

8. Engelman DM. Membranes are more mosaic than fluid. *Nature*. 2005;438:578-580.

9. Nag K. *Structure and Dynamics of Membranous Interfaces*. Wiley; 2008.

10. Leventis PA, Grinstein S. The distribution and function of phosphatidylserine in cellular membranes. *Annual review of biophysics*. 2010;39:407-427.

11. Lindner R, Naim HY. Domains in biological membranes. *Exp Cell Res*. 2009;315:2871-2878.

12. Cohen LB, Salzberg BM. Optical measurement of membrane potential. *Ergeb Physiol*. 1978;83:35-88.

13. Xu C, Loew LM. The effect of asymmetric surface potentials on the intramembrane electric field measured with voltage-sensitive dyes *Biophys J*. 2003;84:2768-2780.

14. Nakano Y, Makino K, Ohshima H, Kondo T. Analysis of electrophoretic mobility data for human erythrocytes according to sublayer models. *Biophys Chem*. 1994;50:249-254.

15. Makino K, Taki T, Ogura M, et al. Measurements and analyses of electrophoretic mobilities of RAW 117 lymphosarcoma cells and their variant cells. *Biophys Chem*. 1993;47:261-265.

16. Vassar PS, Levy EM, Brooks DE. Studies on the electrophoretic separability of B and T human lymphocytes. *Cell Immunol*. 1976;21:257-271.

17. Smith J. Potential-sensitive molecular probes in membranes of bioenergetic relevance. *Biochim Biophys Acta*. 1990;1016:1-28.

18. Solaini G, Sgarbi G, Lenaz G, Baracca A. Evaluating mitochondrial membrane potential in cells. *Biosci Rep*. 2007;27:11-21.

19. Shakibaei M, Schulze-Tanzil G, Takada Y, Aggarwal BB. Redox regulation of apoptosis by members of the TNF superfamily. *Antioxidants & Redox Signaling*. 2005;7:482-496.

20. Chen LB. Mitochondrial membrane potential in living cells. *Annu Rev Cell Biol*. 1988;4:155-181.

21. Rottenberg H. Membrane potential and surface potential in mitochondria: Uptake and binding of lipophilic cations. *J Membr Biol*. 1984;81:127-138.

22. Rottenberg H. The measurement of membrane potential and deltapH in cells, organelles, and vesicles. *Methods Enzymol*. 1979;55:547-569.

23. Lakowicz JR. *Principless of Fluorescence Spectroscopy.* 2nd ed. New York: Kluwer Academic / Plenum Publisher; 1999.

24. Kasha M. Characterization of electronic transitions in complex molecules. *Discuss Faraday Soc*. 1950;9:14-18.

25. Lakowicz J. Fluorescence spectroscopy of biomolecules, in encyclopaedia of molecular biology and molecular medicine. . 1995.

26. Stokes G. On the change of refrangibility of light.--no. II. *Philosophical Transactions of the Royal Society of London*. 1853;143:385-396.

27. Lippert E. Spektroskopische bestimmung des dipolmomentes aromatischer verbindungen im ersten angeregten singulettzustand. *Zeitschrift für Elektrochemie, Berichte der Bunsengesellschaft für physikalische Chemie*. 1957;61:962-975.

28. Slavik J. Anilinonaphthalene sulfonate as a probe of membrane composition and function. *Biochim Biophys Acta*. 1982;694:1-25.

29. McRae E. Theory of solvent effects on molecular electronic spectra. frequency shifts. *J Phys Chem*. 1957;61:562-572.

30. Suppan P. Invited review solvatochromic shifts: The influence of the medium on the energy of electronic states. *J Photochem Photobiol A*. 1990;50:293-330.

31. Mataga N, Kaifu Y, Koizumi M. Solvent effects upon fluorescence spectra and the dipolemoments of excited molecules. *Bull Chem Soc Jpn*. 1956;29:465-470.

32. Kawski A. On the estimation of excited-state dipole moments from solvatochromic shifts of absorption and fluorescence spectra. *ZEITSCHRIFT FUR NATURFORSCHUNG A*. 2002;57:255-262.

33. Rettig W. Charge separation in excited states of decoupled systems-TICT compounds and implications regarding the development of new laser dyes and the primary process of vision and photosynthesis. *Angewandte Chemie International Edition in English*. 1986;25:971-988.

34. Cohen LB, Salzberg BM, Davila HV, et al. Changes in axon fluorescence during activity: Molecular probes of membrane potential. *J Membr Biol*. 1974;19:1-36.

35. Ross WN, Salzberg BM, Cohen LB, et al. Changes in absorption, fluorescence, dichroism, and birefringence in stained giant axons: Optical measurement of membrane potential. *J Membr Biol*. 1977;33:141-183.

36. Gupta RK, Salzberg BM, Grinvald A, et al. Improvements in optical methods for measuring rapid changes in membrane potential. *J Membr Biol*. 1981;58:123-137.

37. Loew LM. Characterization of potentiometric membrane dyes. *Adv Chem Ser*. 1994;235:151.

38. Bublitz GU, Boxer SG. Stark spectroscopy: Applications in chemistry, biology, and materials science. *Annu Rev Phys Chem*. 1997;48:213-242.

39. Clarke RJ, Kane DJ. Optical detection of membrane dipole potential: Avoidance of fluidity and dye-induced effects. *Biochimica et Biophysica Acta (BBA)-Biomembranes*. 1997;1323:223-239.

40. Loew L, Simpson L. Charge-shift probes of membrane potential: A probable electrochromic mechanism for p-aminostyrylpyridinium probes on a hemispherical lipid bilayer. *Biophys J*. 1981;34:353-365.

41. Gross E, Bedlack Jr RS, Loew LM. Dual-wavelength ratiometric fluorescence measurement of the membrane dipole potential. *Biophys J*. 1994;67:208-216.

42. Betz WJ, Mao F, Smith CB. Imaging exocytosis and endocytosis. *Curr Opin Neurobiol*. 1996;6:365-371.

43. Fluhler E, Burnham VG, Loew LM. Spectra, membrane binding, and potentiometric responses of new charge shift probes *Biochemistry (N Y)*. 1985;24:5749-5755.

44. Brackmann U, ed. *Lambdachrome Laser Dyes Data Sheets*; 1994.

45. Berezin MY, Lee H, Akers W, Achilefu S. Near infrared dyes as lifetime solvatochromic probes for micropolarity measurements of biological systems. *Biophys J*. 2007;93:2892-2899.

46. Luchowski R, Kapusta P, Szabelski M, et al. FRET-based picosecond lifetime reference for instrument response evaluation *Measurement Science and Technology*. 2009;20:095601.

47. Luchowski R, Gryczynski Z, Sarkar P, et al. Instrument response standard in time-resolved fluorescence *Rev Sci Instrum*. 2009;80:033109.

48. Jędrzejewska B, Pietrzak M, Pączkowski J. Solvent effects on the spectroscopic properties of styrylquinolinium dyes series *J Fluoresc*. 2010;20:73-86.

49. Scheffler IE. A century of mitochondrial research: Achievements and perspectives. *Mitochondrion*. 2001;1:3-31.

50. Nicholls DG, Ward MW. Mitochondrial membrane potential and neuronal glutamate excitotoxicity: Mortality and millivolts. *Trends Neurosci*. 2000;23:166-174.

51. Mammucari C, Rizzuto R. Signaling pathways in mitochondrial dysfunction and aging. *Mech Ageing Dev*. 2010.

52. Lu D, Huang J, Basu A. Protein kinase Cϵ activates protein kinase B/Akt via DNA-PK to protect against tumor necrosis factor-α-induced cell death. *J Biol Chem*. 2006;281:22799.

53. Narendra D, Tanaka A, Suen DF, Youle RJ. Parkin is recruited selectively to impaired mitochondria and promotes their autophagy. *Science's STKE*. 2008;183:795.

54. Johnson LV, Walsh ML, Chen LB. Localization of mitochondria in living cells with rhodamine 123. *Proc Natl Acad Sci U S A*. 1980;77:990.

55. Dykens JA, Stout AK. Assessment of mitochondrial membrane potential in situ using single potentiometric dyes and a novel fluorescence resonance energy transfer technique. *Methods Cell Biol*. 2001;65:285-309.

56. Emaus RK, Grunwald R, Lemasters JJ. Rhodamine 123 as a probe of transmembrane potential in isolated rat-liver mitochondria: Spectral and metabolic properties. *Biochimica et Biophysica Acta (BBA)-Bioenergetics*. 1986;850:436-448.

57. Juan G, Cavazzoni M, Sáez GT, O'Connor JE. A fast kinetic method for assessing mitochondrial membrane potential in isolated hepatocytes with rhodamine 123 and flow cytometry. *Cytometry*. 1994;15:335-342.

58. Nakayama S, Sakuyama T, Mitaku S, Ohta Y. Fluorescence imaging of metabolic responses in single mitochondria. *Biochem Biophys Res Commun*. 2002;290:23-28.

59. Mitra K, Lippincott-Schwartz J. Analysis of mitochondrial dynamics and functions using imaging approaches. .

60. Jester JV, Andrews PM, Matthew Petroll W, Lemp MA, Dwight Cavanagh H. In vivo, real-time confocal imaging. *J Electron Microsc Tech*. 1991;18:50-60.

61. Mitra K, Lippincott-Schwartz J. Analysis of mitochondrial dynamics and functions using imaging approaches *Curr Protoc Cell Biol*. 2010;Chapter 4:Unit 4.25.1-21.

62. Rottenberg H, Wu S. Quantitative assay by flow cytometry of the mitochondrial membrane potential in intact cells. *Biochimica et Biophysica Acta (BBA)-Molecular Cell Research*. 1998;1404:393-404.

63. Cossarizza A, Baccaranicontri M, Kalashnikova G, Franceschi C. A new method for the cytofluorometric analysis of mitochondrial membrane potential using the J-aggregate forming lipophilic cation 5, 5', 6, 6'-tetrachloro-1, 1', 3, 3'-tetraethylbenzimidazolcarbocyanine iodide (JC-1). *Biochem Biophys Res Commun*. 1993;197:40-45.

64. Plasek J, Vojtiskova A, Houstek J. Flow-cytometric monitoring of mitochondrial depolarisation: From fluorescence intensities to millivolts. *Journal of Photochemistry and Photobiology B: Biology*. 2005;78:99-108.

65. Schmidt R, Wurm CA, Jakobs S, Engelhardt J, Egner A, Hell SW. Spherical nanosized focal spot unravels the interior of cells. *Nature Methods*. 2008;5:539-544.

66. Celli A, Gratton E. Dynamics of lipid domain formation: Fluctuation analysis. *Biochim Biophys Acta*. 2009.

67. Lacko AG, Nair M, Paranjape S, Mooberry L, McConathy WJ. Trojan horse meets magic bullet to spawn a novel, highly effective drug delivery model *CHEMOTHERAPY-BASEL-*. 2006;52:171.

68. Matz C, Jonas A. Micellar complexes of human apolipoprotein AI with phosphatidylcholines and cholesterol prepared from cholate-lipid dispersions. *J Biol Chem*. 1982;257:4535.

69. Jonas A. Reconstitution of high-density lipoproteins *Methods Enzymol*. 1986;128:553-582.

70. Short J, Roberts J, Roberts D, Hodges G, Gutsell S, Ward R. Practical methods for the measurement of log P for surfactants *Ecotoxicol Environ Saf*. 2010.

71. Magde D, Elson E, Webb W. Thermodynamic fluctuations in a reacting system—measurement by fluorescence correlation spectroscopy *Phys Rev Lett*. 1972;29:705-708.

72. Magde D, Elson EL, Webb WW. Fluorescence correlation spectroscopy. II. an experimental realization *Biopolymers*. 2004;13:29-61.

73. Betz WJ, Mao F, Bewick GS. Activity-dependent fluorescent staining and destaining of living vertebrate motor nerve terminals. *J Neurosci*. 1992;12:363-375.

74. Luchowski R, Sarkar P, Bharill S, et al. Fluorescence polarization standard for near infrared spectroscopy and microscopy *Appl Opt*. 2008;47:6257-6265.

75. Jensen KHR, Rekling JC. Development of a no-wash assay for mitochondrial membrane potential using the styryl dye DASPEI. *Journal of Biomolecular Screening*. 2010.

76. Hranjec M, Kralj M, Piantanida I, et al. Novel cyano-and amidino-substituted derivatives of styryl-2-benzimidazoles and benzimidazo (1, 2-a quinolines. synthesis, photochemical synthesis, DNA binding, and antitumor evaluation, part 3 *J Med Chem*. 2007;50:5696-5711.

77. Jameson DM, Croney JC, Moens PD. Fluorescence: Basic concepts, practical aspects, and some anecdotes. *Methods Enzymol*. 2003;360:1-43.

78. Fang Z, Takizawa N, Wilson KA, et al. The Membrane-Associated protein, supervillin, accelerates F-Actin-Dependent rapid integrin recycling and cell motility. *Traffic*. 2010;11:782-799.

79. Mills JW, Falsig Pedersen S, Walmod PS, Hoffmann EK. Effect of cytochalasins on F-actin and morphology of ehrlich ascites tumor cells. *Exp Cell Res*. 2000;261:209-219.

80. Chen Y, Mills JD, Periasamy A. Protein localization in living cells and tissues using FRET and FLIM. *Differentiation*. 2003;71:528-541.

81. Gautier I, Tramier M, Durieux C, et al. Homo-FRET microscopy in living cells to measure monomer-dimer transition of GFP-tagged proteins. *Biophys J*. 2001;80:3000-3008.

82. Harpur AG, Wouters FS, Bastiaens PI. Imaging FRET between spectrally similar GFP molecules in single cells. *Nat Biotechnol*. 2001;19:167-169.

83. Kinnally KW, Tedeschi H, Maloff BL. Use of dyes to estimate the electrical potential of the mitochondrial membrane. *Biochemistry*. 1978;17:3419-3428.

84. Celli A, Gratton E. Dynamics of lipid domain formation: Fluctuation analysis. *Biochim Biophys Acta*. 2009.

85. Soltoff SP. Rottlerin: An inappropriate and ineffective inhibitor of PKC [delta]. *Trends Pharmacol Sci*. 2007;28:453-458.

86. Soltoff SP. Rottlerin is a mitochondrial uncoupler that decreases cellular ATP levels and indirectly blocks protein kinase Cδ tyrosine phosphorylation. *J Biol Chem*. 2001;276:37986.